ご 挨 拶

平成３０年（2018 年）は、おかげさまで第３７回日本糖質学会年会を仙台で無事開催できましたこと、これもひとえに皆様からのご助力・ご支援をいただいた賜物と、改めて感謝申し上げます。翌年の平成３１年は、５月１日に元号が令和となり、希望を持って新たな時代の幕開けを迎えました。その約半年後の 11 月に発生した新型コロナウイルス(COVID-19)は、あっという間に世界中を覆い尽くし、医療崩壊や経済活動への甚大な被害のみならず、大学の教育・研究活動も大きな影響を受けて、現在に至っています。COVID-19 は、少なくとも今後数年にわたって人間社会から消えることはないでしょう。人間と野生動物が接触する機会が増え、このような全く予期できないパンデミックが起こりやすくなっているそうです。臨床症状の予測や治療法が無い感染症の前に、地球における我々自身の生活のあり方の変革が迫られています。世界中の人々が、この時だからこそ地球上のありとあらゆる生物のために人類がなすべきことは何かを自分自身に問いかけ、求めて行動することで、より良い未来の地球が創造されていくと信じています。

令和元年の 2019 年度には、理化学研究所から新たに山口芳樹博士が分子生体膜研究所の教授(薬品物理化学教室)として着任され、喜ばしいことに現在の４部門から５部門体制となりました。東北医科薬科大学の分子生体膜研究所が、日本の糖鎖生物学研究の発展に、これまで以上に貢献できることを、仙台の地から所員一同願って、研究に勤しんでおります。

今回の年報では、各研究部門の研究活動報告および第 3 回箱守仙一郎賞の奨励賞および優秀論文賞のご紹介をいたします。皆様からのなお一層のご指導、ご鞭撻のほど衷心よりお願い申しあげます。

令和２年３月吉日

東北医科薬科大学分子生体膜研究所・所長

東北糖鎖研究会会長

井ノ口　仁一

目 次

東北医科薬科大学分子生体膜研究所
「箱守仙一郎賞」（Sen-itiroh Hakomori Glycoscience Award）規約

平成 30 年 9 月 22 日
東北医科薬科大学分子生体膜研究所
井ノ口　仁一

名称　　箱守仙一郎賞

授与機関　　東北医科薬科大学分子生体膜研究所

目的　　生物系化学系を問わず広く糖鎖科学を専攻し、日夜努力を続けている東北エリアの研究者を顕彰することにより、日本の糖鎖科学研究の増進を図る。

賞の種別　　奨励賞　　1 名　　顕彰楯および副賞
優秀論文賞　1～2 名　　顕彰楯および副賞

対象
1）奨励賞：東北エリア（新潟県および群馬県を含む）で研究に従事する応募時 45 歳までの研究者
2）優秀論文賞：同地域で研究に従事し，申請時点で大学院生もしくは博士研究員である者
＊いずれも指定された期間内に発表（accepted でも可）された学術論文に対して審査・授与する。

選考方法　　自薦および他薦によるものとし、東北糖鎖研究会世話人が審査する。評価を点数化（次項参照）して決する。

授賞方法　　東北糖鎖研究会開催時に授賞および受賞講演を行う。

運用方法　　顕彰楯および副賞の購入費は、箱守賞基金を原資とし、分子生体膜研究所がこれを支弁する。

その他　　事務局は分子生体膜研究所内に置く。

審査

（1）応募資格および応募方法

東北 6 県、新潟県および群馬県（東北糖鎖研究会エリア）で研究を行っている 45 歳以下の糖鎖科学研究者（大学院生、博士研究員は自動的に優秀論文賞へのノミネートとなる)。対象論文は、その年度内（ただし応募締切以前）に Impact factor が付与されている英文学術雑誌（査読有）に出版、または掲載が決定されている原著論文（accepted でも可）とし、応募者が筆頭著者となっているものとする。要旨和訳と論文 PDF を添えて既定のエントリーフォームに記入してメールにて応募する。化学系・生物系は問わない。自薦および他薦どちらでも受け付ける。応募期間等についてはその都度決定し、周知する。

書類送付先：東北医科薬科大学 分子生体膜研究所　所長 井ノ口 仁一
メールアドレス：jin@tohoku-mpu.ac.jp

（2）エントリーフォーム（別添）

（3）審査委員および審査方法

1）分子生体膜研究所所長が審査員長を務める。

2）東北糖鎖研究会世話人が審査員となる。ただし、世話人が推薦者または自薦者の所属責任者あるいは論文の共著者である場合は審査に参加しない。

3）期限内に提出された論文について事務局が一次審査（下記基礎点による）を行い、奨励賞および優秀論文賞それぞれ上位 3 報を選定する。

4）上位 3 報について審査員が下記評価項目を採点し、全員（その都度人数は異なる）の評価平均点＋基礎点（100 点満点、1 点未満は四捨五入）から最上位者を受賞者として決定する。

5）最高点が複数出た場合は審査員長の判断に委ねる。

基礎点		評価最高点	
Impact factor	2.0 未満 10 点	独創性	10 点
	4.0 未満 20 点	インパクト（重要性）	10 点
	6.0 未満 30 点	論文構成	10 点
	8.0 未満 40 点	将来性	10 点
	10 未満 50 点		
	10 以上 60 点		

令和元年度　箱守仙一郎賞
(Sen-itiroh Hakomori Glycoscience Award)

米国ワシントン大学名誉教授の箱守仙一郎博士は，本学分子生体膜研究所の名誉所長・顧問を長年務められております。2017 年に箱守先生が８８歳を迎えられたことを記念して，また先生の糖鎖生命科学研究分野における世界的なご功績を長く後世に伝承すべく，分子生体膜研究所では後進研究者の育成を目的とした「箱守仙一郎賞」(Sen-itiroh Hakomori Glycoscience Award) を創設致しました。対象を本学内に留めず広く東北エリアの糖鎖科学の振興を目的とし，東北糖鎖研究会（http://tohokut-tousa.strikingly.com）の世話人による厳正な審査の結果，第３回箱守仙一郎賞の研究奨励賞及び優秀論文賞の受賞者が決定し，新潟で行われた第１３回東北糖鎖研究会で授賞式及び奨励賞受賞講演が行われました。

第 3 回箱守仙一郎賞

奨励賞

伊左治 知弥

東北医科薬科大学 分子生体膜研究所 細胞制御学教室

A complex between phosphatidylinositol 4 kinase IIα and integrin α3β1 is required for *N*-glycan sialylation in cancer cells

優秀論文賞

佐野 加苗

群馬大学理工学府 物質・生命理工学領域 博士後期課程二年

Fluorescence quenching-based assay for measuring Golgi endo-α-mannosidase

二瓶 渉

大阪大学大学院 理学研究科 化学専攻 特任研究員

NPC1L1-dependent intestinal cholesterol absorption requires ganglioside GM3 in membrane microdomains

左より，伊左治知弥博士，東秀好教授（分子生体膜研究所）

佐野加苗さん（D2）

二瓶渉博士

奨励賞

A complex between phosphatidylinositol 4 kinase IIα and integrin α3β1 is required for *N*-glycan sialylation in cancer cells.

伊左治 知弥（東北医科薬科大学 分子生体膜研究所 細胞制御学・講師）

我々のグループはがん細胞で生じる異常な糖鎖変化のメカニズムに注目している。これまでに、がんの予後と相関する遺伝子 Golgi phosphoprotein 3（GOLPH3）GOLPH3 がシアル酸転移酵素と結合することが効率的な *N*-型糖鎖のシアリル化に重要であることを報告した（Isaji, et. al., JBC. 2014）。GOLPH3 の上流として小胞輸送の調節因子であるホスファチジルイノシトール 4 キナーゼ IIα（PI4KIIα）が予想された。しかし、PI4KIIα がシアリル化をどのように調節されるのかは不明であった。シアリル化 *N*-型糖鎖や細胞移動の調節を解析するために、PI4KIIα の発現を抑制できる誘導型ノックダウン(KD)の乳癌細胞を樹立した。予想通り、KD 細胞では PI4P 量が著しく抑制されていた。また、KD 細胞の細胞表面においてシアリル化糖鎖を認識するレクチンの反応性が低下し、さらに、HPLC で定量すると、複合型糖鎖と比べ、シアリル化糖鎖が著しく減少していた。また、インテグリン β1 のシアリル化糖鎖も同様に低下していた。AKT のリン酸化とインテグリン α3 依存的な細胞移動は KD 細胞において低下したものの、細胞表面のインテグリン分子種の発現量は control 細胞と変わらなかった。興味深いことに、インテグリン α3β 1 および PI4KIIα は共局在し、さらに、インテグリン α3β1 および PI4KIIα の両方の過剰発現は、高シアリル化を誘導した。一方で、インテグリン α3 遺伝子の欠損によって、細胞全体のシアリル化が有意に低下した。以上から、乳癌細胞の転移・浸潤といった悪性表現型は、PI4KIIα とインテグリン α3β 1 との間の複合体によってシアリル化が増加することによって、促進されるという全く新規な分子機構を提示した。

参考文献

Isaji T, Im S, Kameyama A, Wang Y, Fukuda T, Gu J.
J Biol Chem. 294, 4425-4436 (2019)

【経歴】

平成 12 年：岐阜薬科大学薬学部卒業，平成 14 年：岐阜薬科大学大学院薬学研究科博士前期課程修了，平成 18 年：大阪大学大学院医学系研究科博士後期課程修了（博士・医学），同年東北薬科大学細胞制御学助手，平成 20 年：同　助教，平成 28 年: 同　講師（平成 28 年 大学名が東北医科薬科大学に改称)。現在、糖鎖の制御機構に関する研究に従事。

【受賞の感想と抱負】

この度、令和元年箱守仙一郎賞奨励賞を頂きました。箱守先生はじめ東北糖鎖研究会の先生方に深く感謝申し上げます。糖鎖研究を始めたきっかけは、細胞の研究がしたいと、博士課程で大阪大学・谷口直之先生の教室の門を叩いたことでした。修士課程までは、岐阜薬科大学の原明先生のもと、糖代謝酵素の速度論解析をしていました。谷口研では現在の上司でもある顧建国先生の下、接着分子インテグリンの GnT-III による修飾を見いだしました。精製したインテグリンの性質を比べて糖鎖構造の違いによってリガンド結合能が変化することを明らかにしました。現所属に移ってからは、インテグリンの付加部位の同定と機能解析を行ってきました。糖鎖の発現機構に興味があって、GOLPH3 によるシアル酸転移酵素の制御機構や PI4KIIα による糖鎖制御の研究にシフトしてきました。まだまだ、糖転移酵素には不明な部分が多いですが、ひとつひとつ明らかにしていきたいと考えています。この研究を行うにあたり、最後に学生の頃からの指導教員であり現所属の上司でもある顧建国先生をはじめ、ご指導・ご協力いただきました共著者の先生方・大学院生、ご支援くださった研究室のメンバーに心より感謝申し上げます。高名な箱守先生の名を冠した賞の受賞を励みに、糖鎖の制御について、乳癌以外のがんにおいても機能しているか明らかにしていきたいと考えています。糖鎖科学のさらなる発展に少しでも貢献できるように引き続き精進してゆきます。今後ともご指導ご鞭撻のほどよろしくお願い申し上げます。

伊左治　知弥

優秀論文賞

Fluorescence quenching-based assay for measuring Golgi endo-α-mannosidase

Kanae Sano, Taiki Kuribara, Nozomi Ishii, Ayumi Kuroiwa,
Toshitada Yoshihara, Seiji Tobita, Kiichiro Totani, and Ichiro Matsuo
Chemistry an Asian Journal, 2019, *14*, 1965-1969.
DOI: 10.1002/asia.201900240

佐野 加苗（群馬大学理工学府 物質・生命理工学領域　博士後期課程二年）

Golgi endo-α-mannosidase（G-EM）はシスゴルジに局在するエンド型の糖加水分解酵素で、アスパラギン結合型糖鎖 A-arm 構造中の $Glc_{1\sim3}Man_1$ 残基を切断する。この基質特異性から、G-EM は正常な糖鎖プロセシングを受けていないまま小胞体からゴルジ体へ誤って輸送された糖タンパク質上の糖鎖を正常な糖鎖プロセシング過程へと戻す役割を担うことが示唆されている。本研究では細胞内の G-EM 活性をリアルタイムで検出することを志向し、FRET 消光の解消を作動原理とした糖鎖プローブをデザインした。すなわち G-EM が認識する Glc_1Man_3 構造を合成後、FRET ペアとして非還元末端側に蛍光性置換基、還元末端側に消光性置換基を導入した。得られたプローブにより G-EM 活性検出を行ったところ、酵素反応の進行に伴い蛍光強度が増加、G-EM 活性を測定できることを確認した。さらに、プローブの非還元末端側に蛍光性置換基を導入したことで α-glucosidase 耐性を付与することもできた。本研究は、Chemistry an Asian Journal の very important paper に選出された。

【受賞感想と抱負】
この度は令和元年度箱守仙一郎優秀論文賞を賜り光栄に存じます。選考委員の先生方に厚く御礼申し上げます。今回の学術論文は、私が第一著者として出版された人生初の論文で、私にとって記念すべき本論文を受賞対象として選出していただけたことは誠に幸運なことと思っています。
私は、群馬大学 松尾一郎教授のご指導のもと、糖鎖の化学合成を基盤とし、糖加水分解酵素の活性測定プローブの合成やアスパラギン結合型糖鎖の全合成研究を行なっています。糖鎖合成では必要な単糖誘導体を数百グラムスケールで大胆に合成する一方で、何段階にもわたって目的物までようやくたどり着き、わずかな量のオリゴ糖を慎重に扱う場面にも直面します。糖鎖誘導体の保護基を除去する工程においては、化合物の親水性・疎水性が大きく変化するため、時には誘導体の性状の変化に対応しきれず、せっかく合成した誘導体を消失するということも起きます。私はそのような苦い思いも経験しつつ、自分の最終目的物へとたどり

着くためには、反応の種類とスケールなど状況に応じた柔軟性が必要なのだと常々感じ、楽しみながら日々奮闘しております。今回の受賞内容の研究は、期待した通りにプローブが切断されて蛍光強度が増加する様子を観察することができましたが、細胞内での活性検出には至っていません。今後も新たな糖鎖プローブの合成研究に挑戦しながら、細胞内での活性検出など、自分にとって新たな領域を精力的に広げていきたいと思います。

私は、昨年 11 月より約 1 年間の予定で海外留学の機会を得て、ニュージーランドカンタベリー大学の Antony Fairbanks 先生のもとで新しい研究テーマに取り組んでいます。ニュージーランドはゆったりとした気風が魅力的な国で、私が所属する大学の研究環境においても同様の雰囲気が感じられます。国外で研究生活を過ごしている現在、日本において多くの先生方や仲間、恵まれた糖質科学の環境に支えられ研究を行なっていたことを身に沁みて感じております。帰国後は、これまで以上に研究に対して真摯に取り組み、日本の糖鎖科学研究に貢献できるよう、ニュージーランドでの研究留学を存分に楽しみながら成長して参りたいと思っております。最後に、日々熱心にご指導くださいました松尾一郎先生はじめ研究室の皆様、関係者の皆様に深く感謝申し上げます。

佐野　加苗

優秀論文賞

NPC1L1 依存的な腸管からのコレステロール吸収は 膜マイクロドメイン のガングリオシド GM3 を必要とする

NPC1L1-dependent intestinal cholesterol absorption requires ganglioside GM3 in membrane microdomains

Wataru Nihei, Masakazu Nagafuku, Hirotaka Hayamizu, Yuta Odagiri, Yumi Tamura, Yui Kikuchi, Lucas Veillon, Hirotaka Kanoh, Kei-ichiro Inamori, Kenta Arai, Kazuya Kabayama, Koichi Fukase, Jin-ichi Inokuchi
J Lipid Res, 2018, 59:2181-2187.

二瓶　渉　（大阪大学大学院　理学研究科　化学専攻　特任研究員）

13 回膜貫通タンパク質 NPC1L1(Niemann-pick C1 Like 1)は脂質ラフトとよばれる膜マイクロドメインに局在し、コレステロールに富む細胞膜領域と共に取り込まれることで腸管からのコレステロール吸収を担う。しかし、NPC1L1 によるコレステロール輸送の詳細な分子機序には不明な点が多い。本研究では新たに、NPC1L1 はその機能に酸性スフィンゴ糖脂質であるガングリオシド GM3 を必要とする事を見出した。
HEK293T 細胞において GM3 合成酵素(GM3S)を欠失させた HEK293T GM3SKO 細胞ではコントロール細胞と比較して、コレステロール依存的な NPC1L1 の細胞内取り込みが抑制され、コレステロール取り込み能が低下していた。さらに、脂質異常症モデルマウスである ApoE 変異（$ApoE^{shl}$)マウスの GM3S を欠失させた $ApoE^{shl}$/GM3SKO マウスでは、高コレステロール血症が著明に改善されていた。次にリポタンパク質中のコレステロール含量について検討を行ったところ、$ApoE^{shl}$ マウスと比較して $ApoE^{shl}$/GM3SKO マウスではキロミクロン画分中のコレステロール含量が大幅に低下していた。これらは GM3S 欠損による腸管からのコレステロール吸収の低下を示唆し、細胞を用いた検討と同様に GM3S 欠損による NPC1L1 の機能低下を支持する結果である。そこで、腸管からのコレステロール吸収率を検討したところ、$ApoE^{shl}$ マウスと比較して $ApoE^{shl}$/GM3SKO マウスでは腸管からのコレステロール吸収率が低下し、コレステロールの経口投与に伴う NPC1L1 の絨毛内部への取り込みが抑制されていた。これらの結果は NPC1L1 を介した腸管からのコレステロール吸収においてガングリオシドが重要な役割を果たす事を示唆している。

【受賞の感想と抱負】

この度は令和元年度第 3 回箱守仙一郎賞優秀論文賞を賜り大変光栄に存じます。東北糖鎖研究会の審査委員の先生方に厚く御礼申し上げます。

本研究の遂行にあたり、ご指導・ご助言を頂きました井ノ口先生をはじめ多くの先生方、研究室の皆様に心より感謝申し上げます。今後とも何卒ご指導ご鞭撻のほどよろしくお願い申し上げます。

二瓶　渉

研究報告

＜機能病態分子部門＞
特任教授　井ノ口 仁一
准教授　稲森 啓一郎
講師　永福 正和
助教　狩野 裕考
博士研究員　新田 昂大

糖尿病性腎症におけるグロボ系糖脂質の病態生理学的役割

糖尿病性腎症は，糖尿病の主要な合併症の一つであり，透析導入の主な原因疾患として問題となっている．糖尿病性腎症は，腎機能が一端低下･進行すると治療を行っても完全には回復せず，進行を遅らせることしかできない．したがって，早期発見と新規治療のための病態生理学的解析が重要となる．スフィンゴ糖脂質は，スフィンゴ脂質であるセラミドとグルコースやガラクトース，シアル酸などの糖で構成されている．セラミドは，スフィンゴシン塩基に脂肪酸(アシル基)がアミド結合で結合しており，多くの分子種が存在している．セラミド分子種の多様性は，アシル鎖長[長鎖脂肪酸(C16-20)と極長鎖脂肪酸(C22-26)]や修飾(2-水酸化・二重結合)が異なる脂肪酸によって，セラミドが構成されるため生じる．スフィンゴ糖脂質は，がん，糖尿病，神経変性疾患など，さまざまな疾患において病態生理学的役割を担っていることが知られている．しかし，糖尿病性腎症におけるスフィンゴ糖脂質の病態生理的役割については，未だ不明である．本研究では，糖尿病性腎症おけるスフィンゴ糖脂質の病態生理学的な意義を明らかにするために，腎臓のスフィンゴ糖脂質を解析した．

糖尿病モデルマウスや高脂肪食負荷マウス，ストレプトゾトシン誘導性 1 型糖尿病マウスの腎臓で発現変化するスフィンゴ糖脂質が異なることが判明した．食欲抑制に関与するレプチン受容体が変異した *db/db* マウスでは，グルコシルセラミドやラクトシルセラミドの発現が増加することが報告されているが，本研究でグロボ系スフィンゴ糖脂質(Gb3Cer)の発現が，コントロールマウスと比較して低いことを見いだした．糖尿病は複数の遺伝因子と環境因子の両方が発症に関与することから，糖尿病発症に複数の疾患感受性遺伝子が関与する KK マウスに高脂肪食負荷することで，スフィンゴ糖脂質の病態生理学的意義を検討した．腎臓のスフィンゴ糖脂質発現を解析した結果，*db/db* マウスとは対象的にグロボ系スフィンゴ糖脂質が発現増加していた．*db/db* と KK マウスの腎臓で，発現変化するスフィンゴ糖脂質が対照的な理由を明らかにするために，レプチン遺伝子が変異した *ob/ob* 及びストレプトゾトシン誘導性 1 型糖尿病マウスの解析を行った．*ob/ob* マウスは，*db/db* マウスと類似の発現変化パターンを示し，*ob/ob* マウスへのレプチン投与は腎 Gb3Cer の発現量を，コントロールマウスと同レベルまで回復させ

た．興味深いことに，ストレプトゾトシン誘導性 1 型糖尿病マウスも，*ob/ob*, *db/db* マウスと同様に腎 Gb3Cer の発現が低下していた．ストレプトゾトシン誘導性糖尿病マウスは，インスリンの欠乏によりレプチンが合成・分泌される脂肪組織の激減，それに伴う低レプチン血症を呈する．また，KK マウスの場合，過食や高脂肪食負荷の結果，脂肪組織が肥大し高レプチン血症を呈する．これらの事実を踏まえると，上記の結果は，レプチンが腎臓のグロボ系糖脂質の発現に関与していることを示唆している．

最近の研究では，スフィンゴ糖脂質の構成脂肪酸が異なる分子種が,生理活性に大きな影響を与えることが示されつつある．したがって，糖尿病性腎症に関連して発現変化するスフィンゴ糖脂質の分子種を解析することは，病態生理学的に重要である．本研究では，高脂肪食を 8 週間負荷した KK マウスの腎臓で，増加が確認されたグロボ系糖脂質の分子種解析を，液体クロマトグラフ-タンデム質量分析計を用いて行った．その結果，飽和の極長鎖分子種(C22, C23, C24)が特に増加していた．糖尿病抵抗性の C3H/HeN マウスの腎臓では, KK マウスの腎臓で発現の低い 2-水酸化脂肪酸が結合した分子種が高発現していた．

上記の結果より，グロボ系糖脂質の病態形成への関与が示唆されることから，糖尿病性腎症の病態形成に重要な炎症反応における，グロボ系糖脂質の炎症惹起活性の有無をヒト単球やマウス骨髄由来マクロファージを用いて評価した．その結果，極長鎖グロボ系糖脂質は，Toll-like receptor 4 (TLR4)リガンド(LPS, HMGB1)の存在下，TLR4 選択的なポジティブモジュレーターとして炎症促進活性を持つことが示唆された (Fig. 1)．高血糖状態の慢性な持続により，終末糖化産物(AGEs)の産生や酸化ストレスが誘起され，腎臓への活性化マクロファージの浸潤やメサンギウム細胞の TLR4 発現が上昇する．加えて，糖尿病では LPS や HMGB1 などの血中濃度も上昇することから，腎臓は炎症が惹起されやすい状態に陥っている．レプチンは視床下部に作用し食欲抑制やエネルギー消費亢進に関わるだけでなく，免疫細胞に作用することで炎症性サイトカインの分泌を促進し，炎症反応に関与する．炎症性サイトカインは，腎糸球体細胞のグロボ系糖脂質の発現を増加させる．したがって，高脂肪食負荷により肥大した脂肪組織から分泌促進されたレプチンが，腎臓のグロボ系糖脂質の発現を増加させ，増加したグロボ系糖脂質が, TLR4 リガンド存在下, TLR4 に作用することで炎症反応を促進し，糖尿病性腎症の病態形成に関与していることが本研究より示唆される．レプチンによる腎臓のグロボ系糖脂質の発現変化メカニズムのさらなる解明により，糖尿病性腎症の新たな診断法や治療薬開発の進展につながることが予想される．

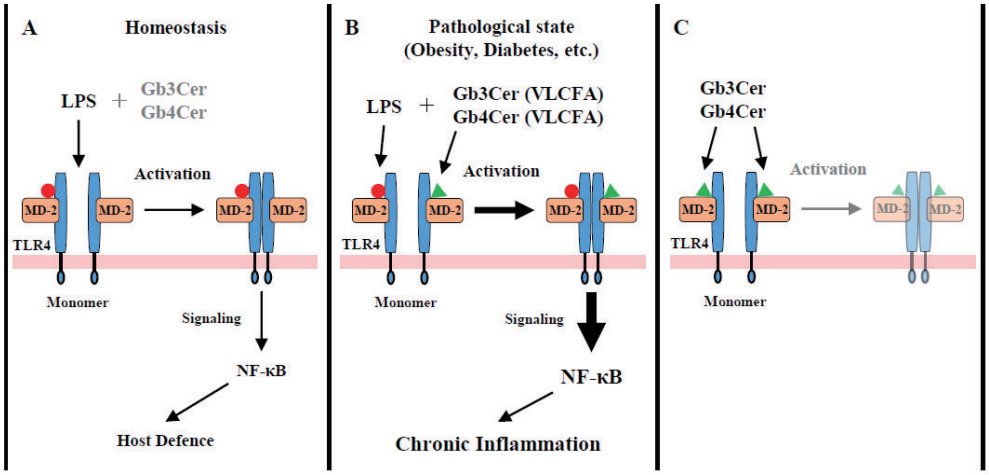

Fig. 1. Gb3Cer and Gb4Cer の TLR4 シグナルにおける作業仮説

A: TLR4 signaling by LPS. Dimerization of TLR4/MD-2 units required, at least, one molecule of LPS. B: Synergistic activation of TLR4/MD-2 by LPS and Gb3Cer/Gb4Cer. Gb3Cer/Gb4Cer associate with TLR4/MD-2 complex as modulator in presence of LPS, and enhance inflammatory response through trans-interaction. C: Gb3Cer/Gb4Cer alone could not induce activation of TLR4/MD-2 complex.

＜発表論文＞

1. Overexpression of HexCer and LacCer containing 2-hydroxylated fatty acids in cholangiocarcinoma and the association of the increase of LacCer (d18:1-h23:0) with shorter survival of the patients. Silsirivanit A, Phoomak C, Teeravirot K, Wattanavises S, Seubwai W, Saengboonmee C, Zhan Z, Inokuchi J, Suzuki A, Wongkham S (2019) ***Glycoconj. J.*** 36, 103-111.
2. Visual Function in Mice Lacking GM3 Synthase. Hiraoka M, Ohkawa E, Abe A, Murata M, Go S, Inokuchi J, Ohguro H (2019) ***Curr. Eye Res.*** 44, 664-670.
3. Serum GM3(d18:1-16:0) and GM3(d18:1-24:1) levels may be associated with lymphoma: An exploratory study with haematological diseases. Nishikawa M, Kurano M, Nitta T, Kanoh H, Inokuchi J, Yatomi Y (2019) ***Sci. Rep.*** 9, 6308.
4. Globo-series glycosphingolipids enhance lipopolysaccharide-induced inflammation and play a pathophysiological role in diabetic nephropathy. Nitta T, Kanoh H, Inamori K, Suzuki A, Takahashi T, Inokuchi J (2019) ***Glycobiology*** 29, 260-268.
5. スフィンゴ糖脂質の生合成とその制御.
   井ノ口仁一、岩渕和久
   セラミド研究の新展開　セラミド研究会編　P44-50 食品化学新聞社
6. スフィンゴ糖脂質の脂肪酸鎖を介した自然免疫応答の制御機構.
   狩野裕考、井ノ口仁一
   セラミド研究の新展開　セラミド研究会編　P145-150 食品化学新聞社

＜学会発表＞

・**糖脂質ガングリオシドの欠損による肥満モデルマウスの病態改善および受容体シグナルへの影響**

稲森啓一郎

第 7 回 AAA (Academy of Aging and CArdiovascular-Diabetes Research), 東京，2019 年 1 月，演題番号 2

・**Homeostatic and pathogenic roles of GM3 ganglioside molecular species in TLR4 signaling in obesity**

Hirotaka Kanoh, Takahiro Nitta, Akemi Suzuki, Jin-ichi Inokuchi

Keystone symposia: Innate Immune Receptors: Roles in Immunology and Beyond, Taipei, Taiwan, Mar/2019, Poster No. 2009

・**Homeostatic and Pathogenic Roles of Ganglioside GM3 Molecular Species in TLR4 Signaling**

Jin-ichi Inokuchi

FEBS Special Meeting 2019 Sphingolipid Biology: Sphingolipids in Physiology and Pathology May 6-10 Cascais, Portugal. Program book page14

・**極長鎖ガングリオシドによる TLR4 制御メカニズムと Halo-tag によるメカニズム解析の試み**

狩野裕考

大阪大学 Halo-tag セミナー，大阪大学・理学研究科, 2019 年 5 月

・**糖尿病性腎症における腎 Gb3Cer 発現誘導機構に関する解析**

新田昂大

2019 年度（令和元年度）日本薬学会東北支部主催 第 18 回 生物化学若手研究者セミナー，仙台, 2019 年 7 月

・**糖鎖による生活習慣病・慢性炎症性疾患等の新規診断・治療法の開発**

井ノ口仁一、狩野裕考

第 51 回 日本臨床検査医学会/東北支部総会 特別講演，仙台, 2019 年 7 月

・**高脂肪食負荷に伴う視床下部炎症におけるガングリオシドの機能的役割**

稲森啓一郎，狩野　裕考，新田　昂大，井ノ口仁一

第 38 回日本糖質学会年会，名古屋，2019 年 8 月，演題番号 P-155

・**糖尿病性腎症における腎 Gb3Cer 発現誘導機構に関する解析**

新田昂大，狩野裕考，稲森啓一郎，鈴木明身，井ノ口仁一

第 38 回 日本糖質学会年会，名古屋, 2019 年 8 月，要旨集 p.105

・**ガングリオシドのアシル鎖構造に基づいた自然免疫応答の調節機構**

狩野裕考，新田昂大，鈴木明身，井ノ口仁一

第 38 回 日本糖質学会年会，名古屋, 2019 年 8 月，要旨集 p.77

・**Homeostatic and Pathogenic Roles of GM3 Ganglioside Molecular Species in TLR4 Signaling in Metabolic Disorders**

Jin-ichi Inokuchi, Hirotaka Kanoh
Glyco25 (25th International symposium on Glycoconjugates),
Milan, Italy, Aug/2019, Program p.26

・**糖尿病性腎症における腎 Gb3Cer 発現誘導機構に関する解析**
新田昂大, 狩野裕考, 稲森啓一郎, 鈴木明身, 井ノ口仁一
第 13 回 東北糖鎖研究会, 新潟, 2019 年 9 月, 要旨集 p.51

・**ガングリオシドのアシル鎖構造による TLR4 制御メカニズム**
狩野裕考, 新田昂大,鈴木明身, 井ノ口仁一
第 13 回 東北糖鎖研究会, 新潟, 2019 年 9 月, 要旨集 p.52

・**レプチンによる腎スフィンゴ糖脂質 Gb3Cer の発現誘導**
新田昂大, 狩野裕考, 稲森啓一郎, 鈴木明身, 井ノ口仁一
第 92 回 日本生化学会大会, 横浜, 2019 年 9 月, 要旨集 p.133

・**肥満に伴う視床下部炎症におけるガングリオシドの役割**
稲森啓一郎，狩野　裕考，新田　昂大，井ノ口仁一
第 92 回日本生化学会大会，横浜，2019 年 9 月，演題番号 1P-371

・**糖脂質による慢性炎症疾患の新たな診断・治療法の開発**
井ノ口仁一, 狩野裕考
第17回 糖質科学コンソーシアム（JCGG）シンポジウム
グライコサイエンス＆エンジニアリングの未来 -糖鎖の多様性と普遍性：
糖鎖暗号の解明と制御に向けて-, 京都, 2019年10月, 要旨集 p.24

・**糖脂質による慢性炎症疾患の新たな診断・治療法の開発**
井ノ口仁一
第２６０回日本泌尿器科学会東北地方会共催セミナー
令和元年１１月９日　東北医科薬科大学、仙台

・**Glycosphingolipids and leptin signaling**
Kei-ichiro Inamori, Hirotaka Kanoh, Takahiro Nitta, Jin-ichi Inokuchi
11th Asian Community of Glycoscience and Glycotechnology (ACGG) Conference,
Busan, Korea, Nov/2019, Abstract p.62

・**Homeostatic and pathogenic roles of GM3 ganglioside molecular species in TLR4 signaling in metabolic disorders**
Hirotaka Kanoh, Takahiro Nitta, Akemi Suzuki, Jin-ichi Inokuchi
11th Asian Community of Glycoscience and Glycotechnology (ACGG) Conference,
Busan, Korea, Nov/2019, Abstract p.83

・**GM3 species in metainflammation**
Asia Zonca, Hirotaka Kanoh, Takahiro Nitta, Wataru Nihei, Satomi Kudoh, Maria Ciampa, Laura Mauri, Sandro Sonnino, Jin-ichi Inokuchi, Alessandro Prinetti
11th Asian Community of Glycoscience and Glycotechnology (ACGG) Conference,
Busan, Korea, Nov/2019, Abstract p.168

・**高脂肪食誘導性の視床下部炎症におけるガングリオシドの役割**

稲森啓一郎，狩野　裕考，新田　昴大，井ノ口仁一
第 42 回日本分子生物学会年会，福岡，2019 年 12 月，演題番号 4LBA-092

・**Homeostatic and pathogenic roles of GM3 ganglioside molecular species in TLR4 signaling in obesity**
Jin-ichi Inokuchi
The first Academia Sinica-Tohoku Medical and Pharmaceutical University (TMPU) Joint Symposium. December 19-20, 2019, Academia Sinica Campusm Taipei, Taiwan.

Glycobiology, 2019, vol. 29, no. 3, 260–268
doi: 10.1093/glycob/cwy105
Advance Access Publication Date: 20 December 2018
Original Article

Immunology

Globo-series glycosphingolipids enhance Toll-like receptor 4-mediated inflammation and play a pathophysiological role in diabetic nephropathy

Takahiro Nitta[2,3], Hirotaka Kanoh[2], Kei-ichiro Inamori[2], Akemi Suzuki[2], Tomoko Takahashi[3], and Jin-ichi Inokuchi[2,1]

[2]Division of Glycopathology, Institute of Molecular Biomembrane and Glycobiology and [3]Division of Pathophysiology, Department of Pharmaceutical Sciences, Faculty of Pharmaceutical Sciences, Tohoku Medical and Pharmaceutical University, Sendai 981-8558, Japan

[1]To whom correspondence should be addressed: Tel: +81-22-727-0117; Fax: +81-22-727-0076; e-mail: jin@tohoku-mpu.ac.jp

Received 4 October 2018; Revised 14 November 2018; Editorial decision 20 November 2018; Accepted 21 November 2018

Abstract

Alteration of glycosphingolipid (GSL) expression plays key roles in the pathogenesis and pathophysiology of many important human diseases, including cancer, diabetes and glycosphingolipidosis. Inflammatory processes are involved in development and progression of diabetic nephropathy, a major complication of type 2 diabetes mellitus. GSLs are known to play roles in inflammatory responses in various diseases, and levels of renal GSLs are elevated in mouse models of diabetic nephropathy; however, little is known regarding the pathophysiological role of these GSLs in this disease process. We studied proinflammatory activity of GSLs in diabetic nephropathy using spontaneously diabetic mouse strain KK. Mice were fed a high-fat diet (HFD) (60% kcal from fat) or normal diet (ND) (4.6% kcal from fat) for a period of 8 wk. HFD-feeding resulted in quantitative and qualitative changes of renal globo-series GSLs (particularly Gb3Cer), upregulation of TNF-α, and induction of renal inflammation. Gb3Cer/Gb4Cer treatment enhanced inflammatory responses via TLR4 in TLR4/MD-2 complex expressing cells, including HEK293T, mouse bone marrow-derived macrophages (BMDMs) and human monocytes. Our findings suggest that HFD-induced increase of Gb3Cer/Gb4Cer positively modulate TLR4-mediated inflammatory response, and that such GSLs play an important pathophysiological role in diabetic nephropathy.

Key words: diabetic nephropathy, Globo-series GSLs, renal inflammation, TLR4 ligands, Toll-like receptor 4

Introduction

Diabetic nephropathy, a major complication of type 2 diabetes mellitus (T2DM), is defined histologically by renal changes such as diffuse mesangial cell proliferation, mesangial matrix expansion, diffuse or nodular glomerulosclerosis, podocyte loss, glomerular basement membrane thickening, tubulointerstitial fibrosis and atrophy, hyaline arteriolosclerosis, and arterial sclerosis, and is associated with (micro)albuminuria and reduced glomerular filtration rate (Alsaad and Herzenberg 2007; Fioretto and Mauer 2007). Morphological changes as above involve genetic factors, and are based on biochemical and hemodynamic changes (Vardarli et al. 2002; Lee et al. 2005; Freedman et al. 2007; Kanwar et al. 2011).

Biochemical changes arise from immune cell-mediated inflammation, a key causative factor in pathogenesis of diabetic nephropathy. Inflammatory cytokines (e.g., TNF-α, IL-6, IL-1β) are secreted from infiltrated and activated macrophages, and are enhanced by oxidative stress through increased levels of reactive oxygen species (ROS) (Pai et al. 1996; Das and Elbein 2006; Yoshida and Tsunawaki 2008; Elmarakby and Sullivan 2012; Badal and Danesh 2014).

Glycosphingolipids (GSLs) consist of hydrophilic oligosaccharides and hydrophobic ceramide (Figure 1A). Ceramide species are composed of sphingosine linked to a particular fatty acyl chain by amide bond (Figure 1B). Ceramide acyl chains vary in chain length, degree of saturation and presence/absence of α-hydroxylation (Figure 1B). GSLs containing a variety of ceramide structures are crucial components of plasma membranes. GSLs play key roles in fundamental biological processes such as development, cell adhesion, and signaling (Hakomori and Igarashi 1995; Hakomori et al. 1998; Tagami et al. 2002; Yu et al. 2009). Numerous previous reports have demonstrated pathophysiological involvement of GSLs in kidney diseases, including lupus nephritis, polycystic kidney disease, Fabry disease, renal cancer, hemolytic uremic syndrome and diabetic nephropathy (Obrig et al. 1993; Zador et al. 1993; Deshmukh et al. 1994; Biswas et al. 2006; Biancini et al. 2012; Grove et al. 2014; Nowling et al. 2015; Subathra et al. 2015). A 2015 study showed involvement of glucosylceramide (GlcCer) and lactosylceramide (LacCer) in fibrosis, extracellular matrix production, and hypertrophy of kidney cells (Subathra et al. 2015). Aside from this, little is known regarding roles of GSLs in pathophysiology of diabetic nephropathy. GSLs evidently play important roles in inflammatory responses contributing to various diseases (Kim et al. 2002; Ohmi et al. 2011; De Francesco et al. 2013), but no study to date has focused on such role of GSLs in diabetic nephropathy.

To test the hypothesis that GSLs play a pathophysiological role in inflammatory responses contributing to diabetic nephropathy, we used a mouse model of T2DM with high-fat diet (HFD). T2DM and diabetic nephropathy in humans are complex diseases that involve polygenic factors and environmental factors, such as obesity and sedentary lifestyle (Vardarli et al. 2002; Lee et al. 2005; Freedman et al. 2007; Kanwar et al. 2011; Wu et al. 2014). We analyzed associations between renal GSLs and renal inflammation using KK mice. This strain is a useful model for studies of T2DM and diabetic nephropathy because it displays correlations between polygenic factors and susceptibility to these disease processes (Shike et al. 2001; Fan et al. 2003). We fed KK mice with HFD to more closely simulate pathological conditions associated with human T2DM and diabetic nephropathy, and observed for the first time increased levels of renal globo-series GSLs under such condition. Globo-series GSLs enhanced TLR4-mediated inflammation in both mouse bone marrow-derived macrophages (BMDMs) and human monocytes. Our findings indicate that globo-series GSLs act as a positive modulator on TLR4-mediated inflammatory response, and play a role in pathophysiology of diabetic nephropathy.

Results

HFD feeding induces obesity, hyperglycemia and renal inflammation in KK mice

Inbred mouse strain KK was established in 1957 from an inbred strain of native Japanese mice that spontaneously developed diabetes of polygenic origin. Many diabetic characteristics (glucose intolerance, insulin resistance, hyperinsulinemia, moderate hyperglycemia, hyperlipidemia, hypercholesterolemia, hyperleptinemia, histological changes of renal glomerulus) are associated with obesity in KK mice (Makino et al. 1985; Igel et al. 1998; Suto et al. 1998; Okazaki et al. 2002), and these mice are often used in studies of diabetes and diabetic complications. To elucidate the pathophysiological role of GSLs in diet-induced diabetic nephropathy, we introduced HFD at age 8 wk in one group of KK mice, while another group was maintained on normal diet (ND) as a control. Initial body weight (at age 8 wk) and final weight (at age 16 wk) for the two groups are shown in Figure 2A. Comparative values of three parameters at 16 wk in the two groups (hereafter referred to simply as "HFD" and "ND" for convenience) were: final body weight (ND, 35.4 ± 2.5 g; HFD, 45.9 ± 2.4 g; $P < 0.001$) (Figure 2A), weight gain (ND, 127 ± 8.5%; HFD, 163 ± 8.5%; $P < 0.001$) (Figure 2B), non-fasting blood glucose (ND, 214 ± 51 mg/dL; HFD, 328 ± 126 mg/dL; $P < 0.01$) (Figure 2C). Each of these parameters was significantly increased in HFD relative to ND. Blood glucose level in HFD was indicative of hyperglycemia. Renal inflammation was assessed by measuring TNF-α gene expression level by quantitative PCR. TNF-α level was significantly higher in HFD than in ND (Figure 2D). These findings indicate that HFD feeding induced nephritis in KK mice.

Increased levels of renal GSLs in HFD-fed KK mice

GSL levels are elevated in kidneys of mice with various renal diseases (diabetic nephropathy, lupus nephritis, polycystic kidney disease) (Deshmukh et al. 1994; Nowling et al. 2015; Subathra et al. 2015). We examined quantitative and qualitative changes of GSLs in kidneys of ND and HFD. HPTLC analysis revealed that levels of

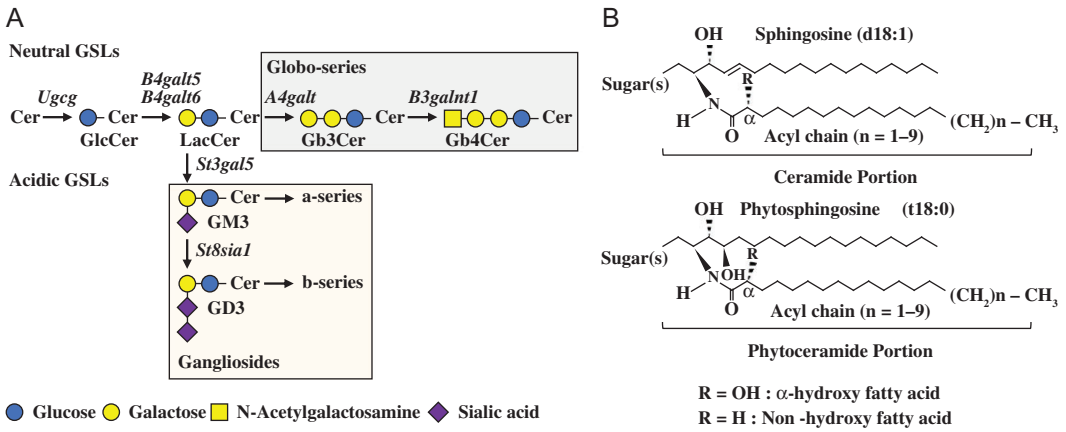

Fig. 1. Biosynthetic pathways and structural diversity of glycosphingolipids. (**A**) GSL biosynthetic pathways. (**B**) Structures of GSL molecular species.

neutral GSLs were significantly higher in HFD, whereas acidic GSL levels did not differ notably between the two groups (Figure 3A, B). Increase in HFD was particularly notable for globo-series GSLs (Gb3Cer and Gb4Cer) (Figure 3A). We further analyzed Gb3Cer level, which showed the greatest increase. Densitometric analysis of HPTLC data showed a 4.7-fold increase of Gb3Cer level in HFD (Figure 3C). Gb3Cer is synthesized from LacCer by A4GALT, and is then converted to Gb4Cer by B3GALNT1 (Figure 1A). In a search for possible causes of Gb3Cer metabolism abnormalities in HFD, we assessed renal expression levels of *A4galt* (Gb3Cer synthase gene) in HFD vs. ND. *A4galt* expression level was significantly higher in HFD (Figure 3D). The higher contents of Gb3Cer/Gb4Cer in HFD can therefore be explained, at least in part, by increased Gb3Cer synthase expression level. LC-ESI-MS/MS analysis detected 26 molecular species of Gb3Cer and 18 molecular species of Gb4Cer carrying ceramide (Figure 4A, B) or phytoceramide (phyto-Gb3Cer, phyto-Gb4Cer) (Figure S1). These species were increased significantly in HFD compared to ND. In particular, there were elevated levels of three species, d18:1-16:0, d18:1-22:0 and d18:1-24:0, in Gb3Cer/Gb4Cer species (Figure 4A, B). Total Gb3Cer level (calculated as sum of values from the 26 molecular species) was 6.2-fold higher for HFD than for ND (Figure 4C), consistently with results from HPTLC/densitometry (Figure 3C). Total Gb4Cer level (calculated as sum of values from the 18 molecular species) was 2.8-fold higher for HFD than for ND (Figure 4D).

For our analyses, we define fatty acids (FAs) with chain length ≤20 carbons as long chain fatty acids (LCFAs) and those with chain length >20 carbons as very long chain fatty acids (VLCFAs) according to previous report (Kihara 2012). In KK mouse kidney, the three most abundant species, d18:1-16:0, d18:1-22:0 and d18:1-24:0, accounted for more than half of the total in Gb3Cer (Figure S1E) or Gb4Cer (Figure S1F) species. Among these species, the proportion of d18:1-22:0 species, VLCFA, was increased markedly in HFD (Figure S1E, F). The elevated levels of renal Gb3Cer/Gb4Cer carrying VLCFAs (saturated FAs: 22:0, 23:0, 24:0; monounsaturated FAs: 24:1; α-hydroxy FAs: h22:0, h23:0, h24:0; monounsaturated and α-hydroxy FAs: h24:1) were higher than the elevated levels of Gb3Cer/Gb4Cer carrying LCFAs (saturated FAs: 16:0, 18:0, 20:0;

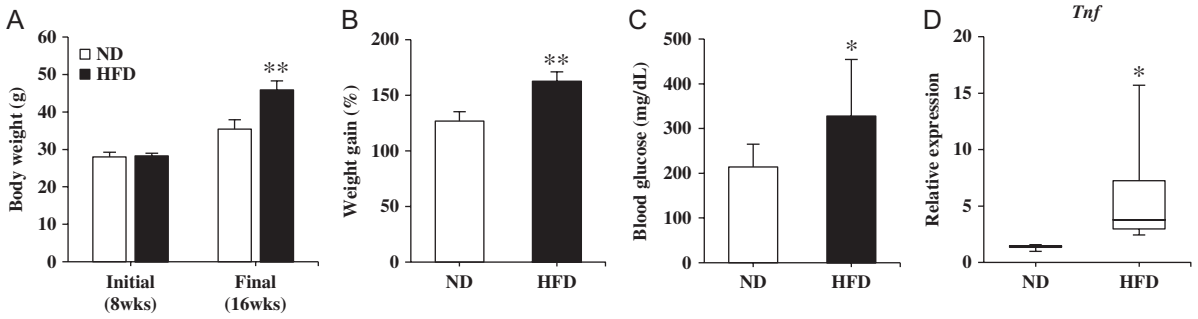

Fig. 2. Obesity, hyperglycemia, and renal inflammation in HFD-fed KK mice (hereafter referred to as "HFD"). (**A**) initial (age 8 wk) and final (age 16 wk) body weight ($n = 8$ for each group). (**B**) Weight gain ($n = 8$ for each group). (**C**) Non-fasting blood glucose of ND and HFD fed for 8 wk ($n = 13$ for each group). Data shown are mean ± SD. $^*P < 0.01$, $^{**}P < 0.001$ for comparison with ND (by Student's *t*-test in A, B; Welch's *t*-test in C). (**D**) mRNA expression level of TNF-α shown as box plot ($n = 4$ for each group). $^*P < 0.05$ vs. ND, by Mann–Whitney unpaired test.

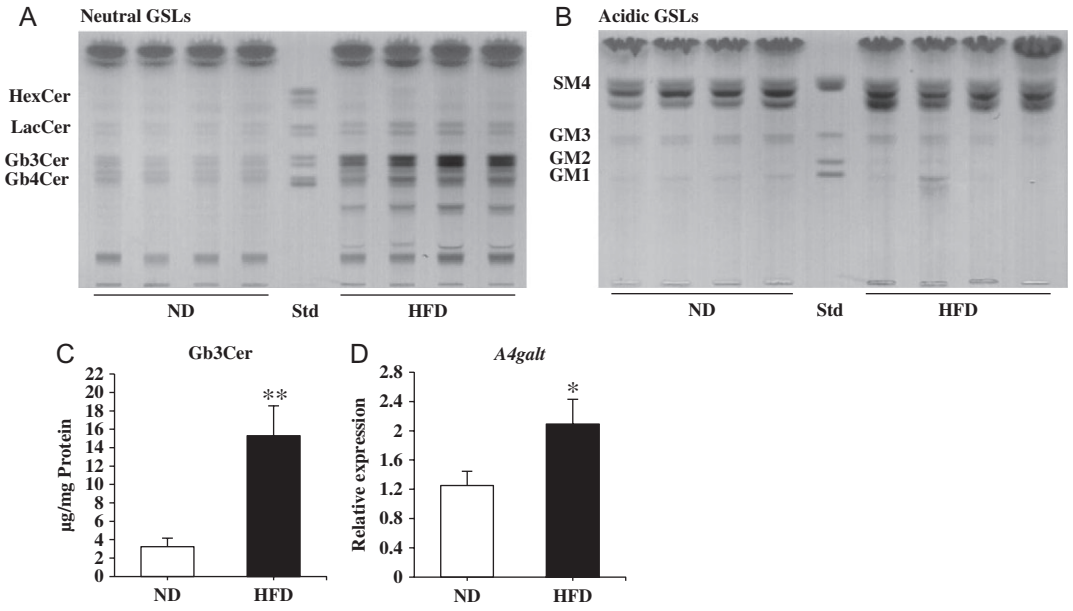

Fig. 3. Strong increase in renal globo-series GSL levels in HFD. (**A, B**) Neutral (**A**) and acidic (**B**) GSLs extracted from ND and HFD kidneys were spotted on HPTLC plates and developed as described in Materials and methods. (**C**) Comparison of kidney Gb3Cer levels under ND and HFD. (**D**) Quantitative RT-PCR analysis of Gb3Cer synthase gene *A4galt* in kidney. $n = 4$ for each group. $^*P < 0.01$, $^{**}P < 0.001$ vs. ND, by Student's *t*-test. Data shown are mean ± SD.

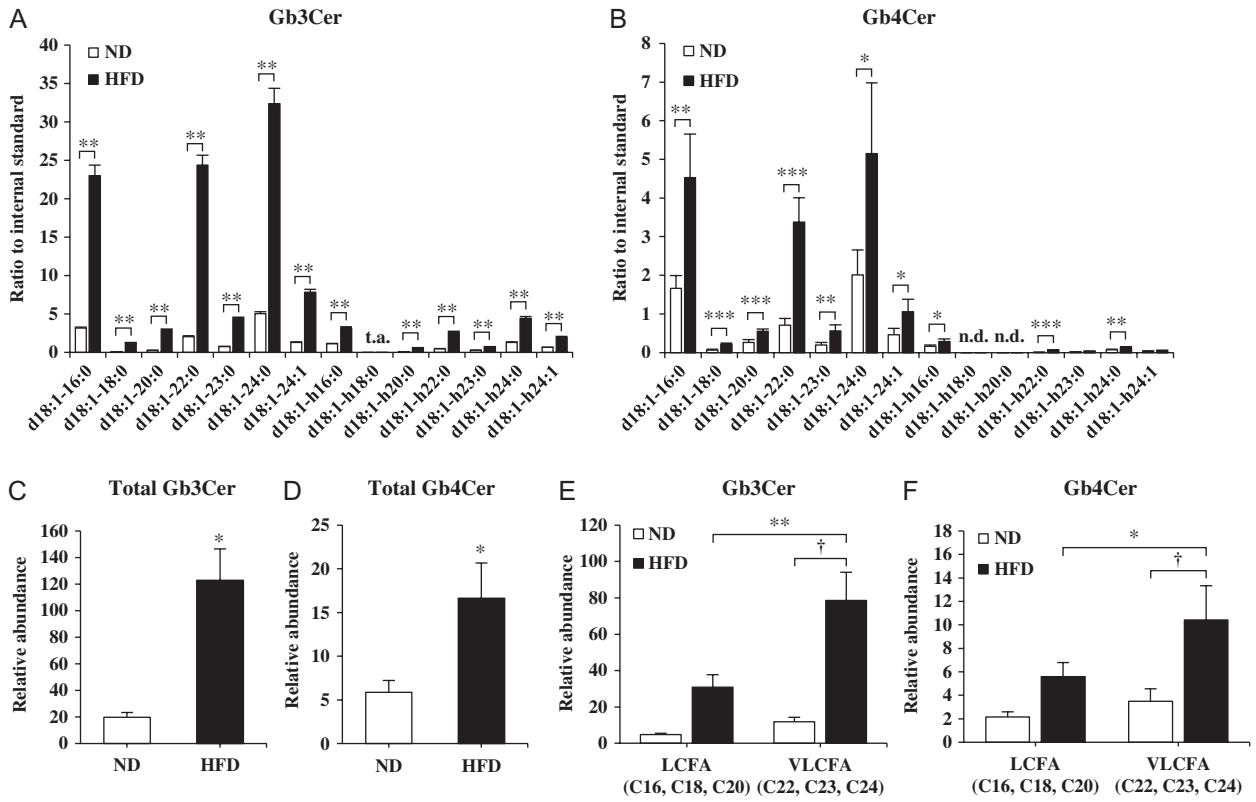

Fig. 4. LC-ESI-MS/MS analysis of renal Gb3Cer and Gb4Cer molecular species showing increased levels in HFD relative to ND. (**A**, **B**) 14 ceramide-carrying Gb3Cer species (A) and 12 ceramide- carrying Gb4Cer species (B) were detected, and are shown as relative abundance in bar graphs. $n = 4$ for each group. $^{*}P < 0.05$, $^{**}P < 0.01$, $^{***}P < 0.001$ vs. ND, by Welch's *t*-test and Student's *t*-test. t.a., trace amount; n.d., not detected. (**C**, **D**) Total levels of Gb3Cer (C) and Gb4Cer (D), calculated as described in Materials and Methods, were compared in HFD vs. ND ($n = 4$ for each group). $^{*}P < 0.01$ vs. ND, by Welch's *t*-test (C) and Student's *t*-test (D). (**E**, **F**) The levels of globo-series GSL molecular species (E, Gb3Cer; F, Gb4Cer) carrying VLCFAs (C22-C24) and LCFAs (C16-C20) and comparison between HFD and ND. $n = 4$ for each group. $^{*}P < 0.05$, $^{**}P < 0.01$ vs. LCFAs, by Student's t-test; $^{\dagger}P < 0.01$ vs. ND (VLCFAs), by Welch's *t*-test (E) and Student's *t*-test (F). Data shown are mean ± SD.

α-hydroxy FAs: h16:0, h18:0, h20:0) in comparison between ND and HFD (Figure 4E, F). These findings indicate that HFD feeding produces quantitative and qualitative changes of renal Gb3Cer and Gb4Cer, and suggest that these alterations of Gb3Cer and Gb4Cer molecular species plays a pathophysiological role in diet-induced diabetic nephropathy.

Involvement of globo-series GSLs in renal inflammatory responses

In view of the greatly altered renal Gb3Cer/Gb4Cer levels in HFD-induced diabetic nephropathy, we examined the roles of globo-series GSLs in inflammatory responses associated with diabetic nephropathy. Enzyme-linked immunosorbent assay (ELISA) was used to measure production of TNF-α by mouse BMDMs or human monocytes stimulated with LPS (0.25 ng/mL and 0.1 ng/mL, respectively) plus Gb3Cer or Gb4Cer (each 0, 2.5, 5, 10 μM) (Figure 5A, B). We used commercially available Gb3Cer/Gb4Cer carrying VLCFAs (C22, C24) as major molecular species (Figure S2), and these molecular species were selectively increased in kidney by HFD feeding (Figure 4A, B). A higher TNF-α level was produced by co-stimulation with LPS and Gb3Cer/Gb4Cer than by stimulation with LPS alone (Figure 5A, B), but the degree of this effect declined as Gb3Cer/Gb4Cer concentration increased (Figure 5A). Human IL-6 and IL-12/23 levels also higher by co-stimulation with LPS and these GSLs than by stimulation with LPS alone (Fig. S4).

To determine the selectivity of Gb3Cer/Gb4Cer for TLR4, we assessed specificity of these GSLs for TLRs using TLR4/MD-2-over-expressing HEK293T cells or TLR ligands for TLR4, 1/2, 5, 7/8 and 2/6. We observed that a higher NF-κB activity was induced in response to co-stimulation with LPS (20 ng/mL) and Gb3Cer/Gb4Cer (each 3, 10, 30 ng/mL) than by stimulation with LPS alone in TLR4/MD-2 overexpressing HEK293T (Figure 5C). The degree of NF-κB activity declined as these GSLs increased, consistent with the result of co-stimulation of mouse BMDMs as shown in figure 5A. Gb3Cer/Gb4Cer also selectively enhanced human IL-6 (hIL-6) production induced by TLR4 ligands, LPS and HMGB1, but not by ligands for TLR1/2, 5, 7/8 and 2/6 (Figure 5D). However, these GSLs alone did not have the ability to produce hIL-6 via TLR4. These results indicated that Gb3Cer/Gb4Cer selectively and positively modulates TLR4-mediated inflammatory response in human and mouse monocytes/macrophages.

Discussion

Diabetic nephropathy is a major complication of T2DM arising from genetic factors and environmental factors. Associations between renal GSLs and diabetic nephropathy have been reported in several animal models (Masson et al. 2005; Grove et al. 2014; Subathra et al. 2015). The *db/db* mouse model used in the above studies has a diabetic phenotype resulting from a single gene

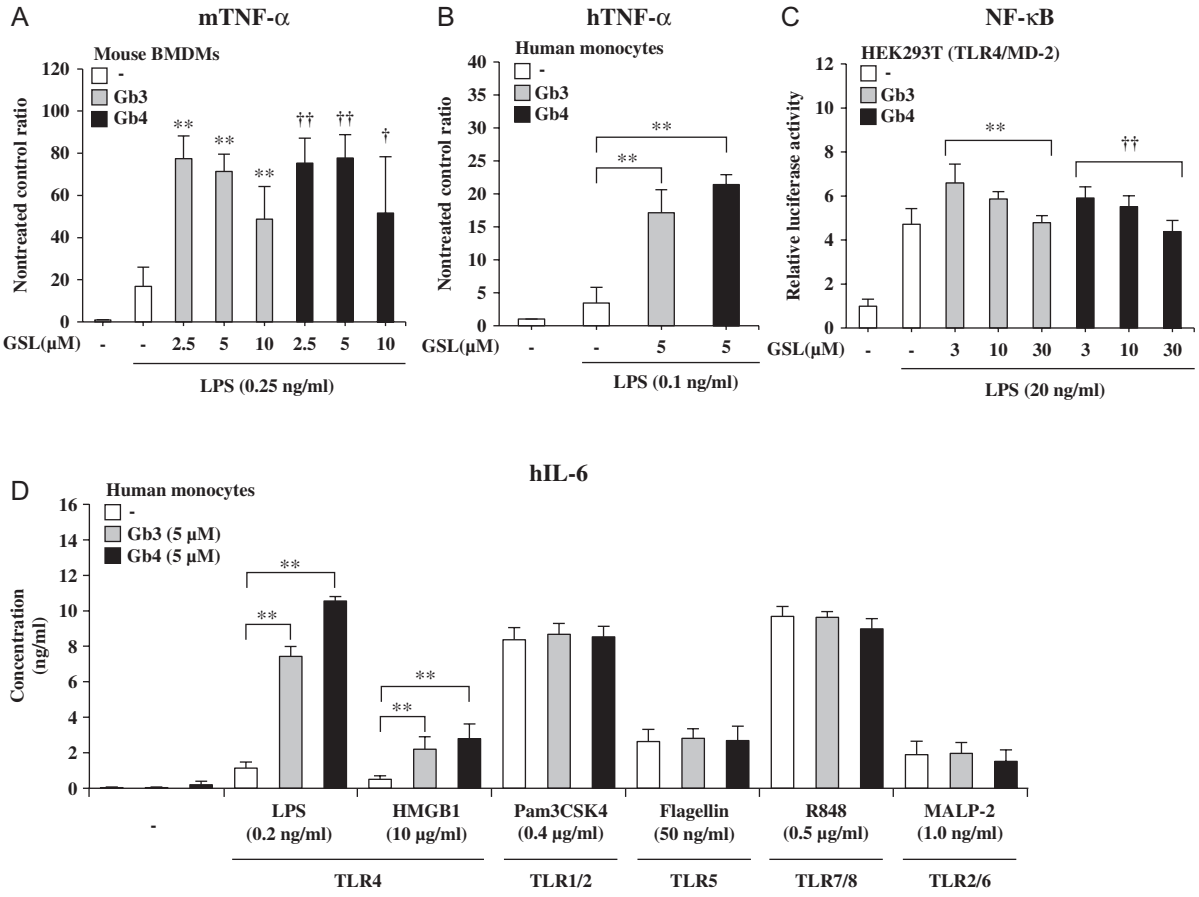

Fig. 5. Globo-series GSLs selectively affect inflammatory responses via TLR4. **A:** ELISAs for murine TNF-α in BMDM culture supernatant following treatment with LPS (0, 0.25 ng/mL) plus Gb3Cer or Gb4Cer (0, 2.5, 5, 10 μM). TNF-α amount was normalized to nontreated control and expressed as ratio. $n = 4$ for each group. $^{**}p < 0.01$ vs. group treated with LPS only; $^{\dagger}p < 0.05$, $^{\dagger\dagger}p < 0.01$ vs. group treated with LPS only, by Dunnett's test. **B:** ELISAs for human TNF-α in human monocyte culture supernatant following treatment with LPS (0, 0.1 ng/mL) plus 5 μM Gb3Cer or Gb4Cer. TNF-α amount was normalized to nontreated control and expressed as ratio. $n = 3$ for each group. $^{**}p < 0.01$, by Dunnett's test. **C:** TLR4/MD-2-overexpressing HEK293T cells were transfected with NF-κB luciferase construct and stimulated with LPS (0, 20 ng/mL) plus Gb3Cer or Gb4Cer (0, 3, 10, 30 μM). Luciferase activity was normalized to nontreated control and expressed as relative luciferase activity. $n = 4$ for each group. $^{**}p < 0.01$ vs. group treated with LPS only; $^{\dagger\dagger}p < 0.01$ vs. group treated with LPS only, by one-way ANOVA. **D:** ELISAs for human IL-6 in human monocyte culture supernatant following treatment with TLR ligands (TLR4: LPS, human recombinant HMGB1; TLR1/2: Pam3CSK4; TLR5: Flagellin; TLR7/8: R848; TLR2/6: MALP-2) plus 5 μM Gb3Cer or Gb4Cer. $n = 4$ for each group. $^{**}p < 0.01$, by Dunnett's test. Data are shown as mean ± SD.

mutation for leptin receptor. However, obesity, T2DM, and diabetic nephropathy in humans are polygenic diseases. We therefore used mouse strain KK, a polygenic disease model, for analysis of diabetic nephropathy. Levels of renal globo-series GSLs (Gb3Cer, Gb4Cer) were strikingly increased in HFD (Figure 3A). These GSLs were also increased by HFD feeding in nondiabetic C3H/HeN mice (Figure S3). L.J. Siskind's group (Subathra et al. 2015) and J.A. Shayman's group (Zador et al. 1993) reported increased levels of renal GSLs (HexCer, LacCer, GM3) in *db/db* mice with diabetic nephropathy and in Sprague-Dawley rats with streptozotocin-induced diabetes. Our findings and previous reports implicated the GSL species in pathophysiology of diabetic nephropathy.

In the present study, enhanced levels of globo-series GSLs resulted, at least in part, from increased gene expression of Gb3Cer synthase (Figure 3D). Increased Gb3Cer synthase expression has been observed in response to LPS and inflammatory cytokines such as IL-1 and TNF-α (van Setten et al. 1997; Hughes et al. 2000; Okuda et al. 2010; Kondo et al. 2013). Indeed, renal expression of TNF-α gene was higher in HFD than in ND in the present study (Figure 2D).

We used LC-ESI-MS/MS to evaluate differential levels of renal Gb3Cer/Gb4Cer molecular species in HFD vs. ND. Contents of d18:1-16:0, 22:0, 24:0 species were significantly higher in HFD than in ND (Figure 4A, B). The proportion of d18:1-22:0, VLCFA, to the total Gb3Cer/Gb4Cer species was increased markedly in HFD compared to ND (Figure S1E, F). These results suggest that these species, specifically VLCFA species, are involved in pathophysiology of diabetic nephropathy. Hyperglycemia typically results in renal macrophage infiltration and renal inflammation, both of which contribute to pathogenesis and pathophysiology of diabetic nephropathy (Chow et al. 2004; Navarro-Gonzalez et al. 2011). Therefore, we assessed proinflammatory activity of Gb3Cer/Gb4Cer in TLR4/MD-2-overexpressing HEK293T cells, mouse BMDMs and human monocytes (Figure 5A–D). Gb3Cer/Gb4Cer enhanced inflammatory response in the presence of TLR4 ligands, LPS and HMGB1, but neither in the absence of the ligands nor in the presence of the other ligands (Figure 5D). The effects of Gb3Cer/Gb4Cer on TLR4-

mediated inflammatory response declined as concentration increased (Figure 5A, C). Furukawa's group has reported that Gb4Cer is an endogenous ligand of TLR4/MD-2, and that Gb4Cer negatively regulated TLR4/MD-2 complex at a dosage higher than the one we used for immune cells (Kondo et al. 2013). Therefore, Gb4Cer appears to be capable of enhancing inflammatory response at lower concentrations, and suppressing inflammatory response at higher concentrations (Figure 5A, C). These results indicated that Gb3Cer/Gb4Cer alone would not be able to induce inflammatory response via TLRs but selectively and positively modulate TLR4-mediated inflammatory response in presence of TLR4 ligands. However, the mechanism how Gb3Cer/Gb4Cer enhances TLR4-mediated inflammatory response remains unclear. Previous studies have been demonstrated that GSLs implicated in TLR4 signaling on the microdomain (Cai et al. 2013; Nikolaeva et al. 2015; Mobarak et al. 2018). However, our results support that Gb3Cer/Gb4Cer associates with TLR4 as a modulator, and induces TLR4 signaling through trans-interaction rather than *cis*-interaction between these GSLs and TLR4 on the microdomain because Gb3Cer/Gb4Cer did not enhance inflammatory response via TLR1/2, TLR5, and TLR2/6 that located on the plasma membranes. In addition, Furukawa's group has reported recently that Gb4Cer bind to MD-2 by binding assay using radiolabeled Gb4Cer (Kondo et al. 2013). Therefore, we propose the current model (Figure 6) whereby Gb3Cer/Gb4Cer modulates TLR4-mediated inflammatory response in the presence of TLR4 ligands by binding to TLR4/MD-2 complex. It is known that TLR4 signaling is required for the homo-dimerization composed of two units of TLR4/MD-2/LPS complex after LPS binding to TLR4/MD-2 units (Park et al. 2009). Interestingly, Saitoh et al. reported that, at least, a single TLR4 ligand could induce TLR4 dimerization (Figure 6A) (Saitoh et al. 2004), suggesting that there is still room for one more ligand to interact with dimeric TLR4/MD-2 complex. Therefore, Gb3Cer/Gb4Cer might bind to the empty side of TLR4/MD-2 units, and enhances TLR4 signaling mediated by LPS which binds to the other side of TLR4/MD-2 units (Figure 6B). However, Gb3Cer/Gb4Cer alone would not be able to induce activation of TLR4/MD-2 complex (Figure 6C).

Previous reports (van Setten et al. 1997; Legros et al. 2017) showed that Gb3Cer and Gb4Cer are abundant in human renal glomerular cells, and that these cells and KK mouse kidney cells have similar expression patterns of certain molecular species. Gb3Cer in human renal glomerular cells is increased in response to proinflammatory cytokines (van Setten et al. 1997). Circulating endotoxin and HMGB1 levels, TLR4 ligands, are elevated in both humans and mice with T2DM (Brun et al. 2007; Creely et al. 2007; Al-Attas et al. 2009; Wang et al. 2015). HMGB1 is also up-regulated in mouse mesangial cells under high glucose levels (Chen et al. 2015). Given that Gb3Cer and Gb4Cer are up-regulated by proinflammatory cytokines and affect TLR4-expressing cells, such as macrophage and mesangial cells (Kaur et al. 2012), these GSLs might exacerbate and prolong renal inflammation in diabetic nephropathy.

Taken together, our findings suggest that the effect of Gb3Cer/Gb4Cer via TLR4 play an important role in the pathophysiology of diet-induced diabetic nephropathy.

Materials and methods

Animals and feeding conditions

Eight-week-old male KK/Ta mice (CLEA Japan; Tokyo, Japan) were divided randomly into two groups. The control group was fed normal diet (ND) (CE-2; CLEA Japan), while the HFD group was fed high-fat diet (HFD) (D12492; Research Diet; New Brunswick, NJ) ad lib for 8 wk. Kidneys and blood (from right ventricle) were harvested after sacrificing animals. Non-fasting blood glucose was measured using Accu-Chek Aviva strips (Roche DC; Japan).

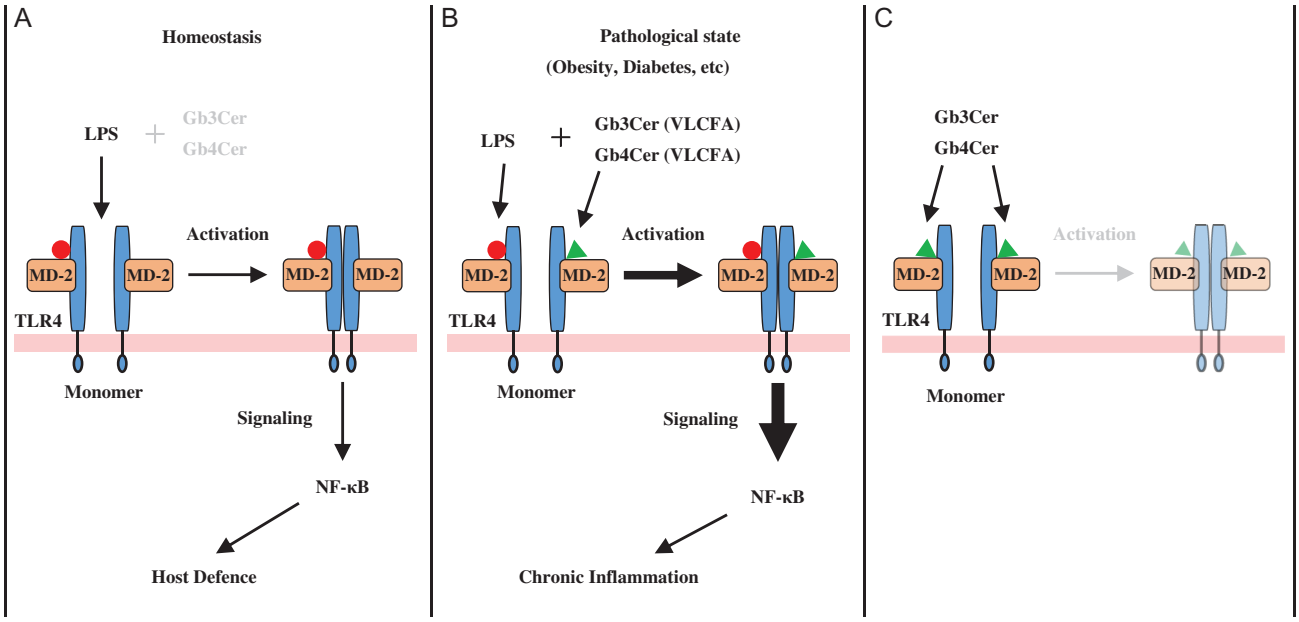

Fig. 6. Working hypothesis for the action of Gb3Cer/Gb4Cer on TLR4 signaling. (**A**) TLR4 signaling by LPS. Dimerization of TLR4/MD-2 units requires, at least, one molecule of LPS (Saitoh et al. 2004). (**B**) Synergistic activation of TLR4/MD-2 by LPS and Gb3Cer/Gb4Cer. Gb3Cer/Gb4Cer associates with TLR4/MD-2 complex as a modulator in presence of LPS, and enhances inflammatory response through trans-interaction. (**C**) Gb3Cer/Gb4Cer alone would not induce activation of TLR4/MD-2 complex.

Analysis of GSLs

Lyophilized kidney tissue was extracted with chloroform/methanol (2:1 and 1:1, v/v). Total lipids were separated into acidic and neutral fractions on DEAE-Sephadex A-25 anion-exchange columns (GE Healthcare Life Sciences). Acidic and neutral lipids were de-esterified by mild alkaline hydrolysis and desalted using a Sep-Pak C18 cartridge (Waters; Milford, MA). Acidic and neutral GSLs (respective protein equivalent 1000 μg and 200 μg) were spotted on HPTLC plates, developed respectively with chloroform/methanol/0.2% $CaCl_2$ (55:45:10, v/v/v) and chloroform/methanol/water (60:25:4, v/v/v), and visualized by orcinol/sulfuric acid staining.

RNA isolation, reverse transcription and quantitative PCR

Total RNA was extracted using Sepasol-RNA I super G (Nacalai Tesque; Kyoto, Japan) and Fast Gene RNA Premium Kit (Nippon Genetics; Tokyo). cDNA was generated from 500 ng total RNA using PrimeScript RT Reagent kit (Takara Bio). Primer-probe sets for mouse *A4galt* (Mm01307145_m1) and *Tnf* (Mm00443258_m1) were from Applied Biosystems (Foster City, CA) and mouse *Gapdh* (Mm.PT.39a.1) was from Integrated DNA Technologies (Coralville, IA). Quantitative PCR was performed on StepOnePlus Real-Time PCR System (Applied Biosystems) using these primer-probe sets and THUNDERBIRD Probe qPCR Mix (Toyobo Co.; Osaka, Japan). Relative mRNA levels were calculated from a standard curve and normalized to GAPDH expression.

Mass spectrometric (MS) analysis

Gb3Cer and Gb4Cer molecular species were quantified by HPLC coupled with electrospray ionization tandem MS (LC-ESI-MS/MS) in multiple reaction monitoring (MRM) positive ionization mode (Supplementary Table 1). A triple stage quadrupole (TSQ) Vantage AM instrument (Thermo Fisher; Waltham, MA) was calibrated by directly infusing a neutral GSL mixture containing Gb3Cer and Gb4Cer species. All ion source parameters and ionization conditions were optimized to improve sensitivity. Neutral GSLs from mouse kidney extract were dissolved in 100 μL methanol, and 5 μL of the solution was injected into an HPLC pump (model Accela 1250, Thermo Fisher) and separated on a Develosil C30 column (C30-UG-3-1 × 50 mm; Nomura Chemical Co.; Japan).

Gradient program and parameters were as follow: start with 100% solvent A (20% H_2O/50% 2-propanol/30% methanol containing 0.1% acetic acid and 0.1% ammonia) for 5 min; ramp up to 100% solvent B (2% H_2O/50% 2-propanol/48% methanol containing 0.1% acetic acid and 0.1% ammonia) over 30 min; maintain 100% solvent B for 5 min; return to 100% solvent A over 1 min, hold there for 9 min; flow rate throughout chromatographic run: 60 μL/min; +3000 V potential applied between ion source, electrospray needle, and nitrogen gas; collision energy 60 eV for Gb3Cer molecular species, 52 eV for Gb4Cer molecular species. Gb3Cer (d18:1-17:0) (Matreya, LLC; State College, PA) was added to neutral GSL samples from mouse kidney extract as internal standard and relative abundance of each Gb3Cer/Gb4Cer molecular species was determined based on ratio to internal standard. Total Gb3Cer/Gb4Cer value was calculated as sums of relative abundance for the 26 and 18 (respectively) molecular species detected. A caveat regarding interpretation of these MS data is that ionization efficiencies are not the same for all molecular species. In view of the limited availability of pure molecular species standards, we assumed that all species have ionization efficiencies comparable to those of the internal standards used.

Purification of human monocytes

Heparinized fresh human peripheral blood was diluted to double the volume with cold PBS (4°C; endotoxin-free; Nacalai Tesque) containing 1 μg/mL polymyxin B (Sigma-Aldrich; St. Louis, MO). Diluted blood was overlaid on cold lymphocyte separation solution (4°C, Nacalai Tesque) containing 1 μg/mL polymyxin B, and centrifuged for 25 min at 4°C, 800 × *g*. Peripheral blood mononuclear cell (PBMC) fraction was collected and diluted to double the volume of wash solution (PBS, 1% heat-inactivated FCS (Biosera), 5 mM EDTA, pH 7.5 (Nacalai Tesque), 1 μg/mL polymyxin B). PBMCs were separated by centrifugation for 10 min at 4°C, 600 × *g*, and washed twice. PBMCs were resuspended in 750 μL wash solution and incubated with 120 μL anti-human CD14 magnetic particles (BD Biosciences) for 30 min at room temperature. CD14-positive cells (monocytes) were separated by magnetic field and washed three times with wash solution. Purified cells were resuspended in cold low-glucose DMEM (Nacalai Tesque) with 0.75% FCS, left on ice for 45 min, counted, diluted to 2.0 × 10^5/mL with culture medium (low-glucose DMEM, 0.75% FCS, 40 ng/mL recombinant human granulocyte-macrophage colony-stimulating factor (GM-CSF) (BioLegend; San Diego, CA), and cultured in 96-well plates (100 μL/well) overnight at 37°C in 5% CO_2 atmosphere.

Differentiation of mouse bone marrow-derived macrophages (BMDMs)

Femoral and tibial bone marrows of 12- to 16-wk-old nondiabetic C3H/HeN mice (Japan SLC, Inc.) were collected in 1% FCS-supplemented low-glucose DMEM, and erythrocytes were lysed in RBC lysis buffer. Bone marrow cells were washed in 1% FCS DMEM, and then cultured for 5–7 days in 10% FCS DMEM supplemented with 40 ng/mL recombinant human macrophage colony- stimulating factor (M-CSF) (BioLegend). Non-adhesive cells were washed out with PBS. Differentiated macrophages were collected in ice-cold PBS (with 1% FCS, 5 mM EDTA) by scraping, washed, counted, diluted to 2.0 × 10^5/mL in 1% FCS DMEM, and cultured in 96-well plates (100 μL/well) overnight at 37°C in 5% CO_2 atmosphere.

Vector construction

Vector carrying murine MD-2 and TLR4 cDNA (pDUO-mMD2/TLR4) was from InvivoGen (San Diego, CA). cDNA fragments, fused with a KpnI site and one Kozak sequence (ACC) at 5'-end and a SalI site at 3'-end, were amplified by PCR (KOD-Plus-Neo; Toyobo), and inserted separately into pCDNA3 at KpnI and XhoI site (Invitrogen). A set of vectors for dual luciferase assay, NF-κB reporter gene (pGL3-ELAM; a Firefly luciferase gene controlled by NF-κB-dependent promoter of ELAM-1), and control reporter gene (pRL-TK; a Renilla luciferase gene controlled by constitutive active promoter of thymidine kinase) were gifts from Dr. Takayuki Kuraishi (Kanazawa University, Japan).

Cell culture and transfection

HEK293T cells were obtained from RIKEN Bioresource Center (Japan) and maintained in 10% FCS low-glucose DMEM at 37°C in 5% CO_2 atmosphere. Prior to transfection, cells were diluted to 2.0 × 10^5/mL in 1% FCS DMEM and cultured in 96-well plates (100 μL/well) overnight. Cells in each well were transfected with vectors

(20 ng pCDNA3-mMD-2, 0.1 ng pCDNA3-mTLR4, 40 ng pGL3-ELAM, 20 ng pRL-TK), complexed with 0.5 μL Lipofectamine LTX and 0.25 μL Plus reagent in 20 μL Opti-MEM (Invitrogen), and subjected to stimulation 24 h after transfection.

Cell stimulation, enzyme-linked immunosorbent assay (ELISA) and luciferase assay

Gb3Cer (from pig RBCs; Nacalai Tesque) and Gb4Cer (from pig RBCs; Fuji-film Wako, Japan) were dissolved (1 mM) in DMSO, and diluted with low-glucose DMEM to 100 μM just before experiments. Cells were incubated with Gb3Cer/Gb4Cer, and stimulated after 30 min with TLR ligands: LPS from *E. coli* O111:B4 (Sigma-Aldrich); human recombinant HMGB1 (Biolegend, San Diego, CA); Pam3CSK4 (Novus Biologicals, Littleton, CO); Flagellin from *S. Typhmurium* (ENZO Life science, Farmingdale, NY); R848 (Fuji-film wako, Japan); MALP-2 (Novus Biologicals, Littleton, CO). After 18 h culture, media were collected and subjected to ELISA. ELISA kits for human IL-6, human TNF-alpha, human IL-12/23 (p40), and murine TNF-alpha were from BioLegend. Firefly and Renilla luciferase activities were measured using Dual-Glo Luciferase Assay System (Promega; Australia) on a microplate reader (model Infinite 200 PRO; Tecan; Switzerland).

Statistical analysis

Data were analyzed by Student's *t*-test, Welch's *t*-test, Dunnett's multiple comparison test, one-way ANOVA, or Mann Whitney unpaired test as appropriate, using the Microsoft Excel.

Supplementary data

Supplementary data is available at *Glycobiology* online.

Funding

This study was supported by JSPS KAKENHI Grants-in-Aid for Scientific Research (B) (JP16H04767 to J.I.), Grants-in-Aid for Exploratory Research (JP17K19569 to J.I.), and Grants-in-Aid for Young Scientist (B) (JP17K15450 to H.K.), Takeda Science Foundation (J.I.), Fugaku Trust for Medicinal Research (J.I.), and Mizutani Foundation for Glycoscience (J.I.).

Acknowledgements

The authors are grateful to the Center for Laboratory Animal Science, Tohoku Medical and Pharmaceutical University, for their services, to Prof. Koichi Fukase at Osaka university for helpful suggestions, to K. Miyahara, N. Okajima, and M. Goto at Inokuchi laboratory for their skillful technical support, and to Dr. S. Anderson for English editing of the manuscript.

Conflict of interest statement

The authors declare that they have no conflict of interest.

Abbreviations

BMDMs, bone marrow-derived macrophages; ELISA, enzyme-linked immunosorbent assay; FAs, fatty acids; Gb3Cer, globotriaosylceramide; Gb4Cer, globotetraosylceramide; GlcCer, glucosylceramide; GSL(s), glycosphingolipid(s); HFD, high-fat diet; LacCer, lactosylceramide; LC-ESI-MS/MS, HPLC coupled with electrospray ionization tandem mass spectrometry; LCFAs, long chain fatty acids; LPS, lipopolysaccharide; ND, normal diet; PBMC, peripheral blood mononuclear cell; T2DM, type 2 diabetes mellitus; TLR4, Toll-like receptor 4; TNF-α, tumor necrosis factor α; VLCFAs, very long chain fatty acids.

References

Al-Attas O, Al-Daghri N, Al-Rubeaan K, da Silva N, Sabico S, Kumar S, McTernan P, Harte A. 2009. Changes in endotoxin levels in T2DM subjects on anti-diabetic therapies. *Cardiovasc Diabetol*. 8:20.

Alsaad K, Herzenberg A. 2007. Distinguishing diabetic nephropathy from other causes of glomerulosclerosis: an update. *J Clin Pathol*. 60:18–26.

Badal S, Danesh F. 2014. New insights into molecular mechanisms of diabetic kidney disease. *Am J Kidney Dis*. 63:S63–S83.

Biancini G, Vanzin C, Rodrigues D, Deon M, Ribas G, Barschak A, Manfredini V, Netto C, Jardim L, Giugliani R et al. 2012. Globotriaosylceramide is correlated with oxidative stress and inflammation in Fabry patients treated with enzyme replacement therapy. *Biochim Biophys Acta*. 1822:226–232.

Biswas K, Richmond A, Rayman P, Biswas S, Thornton M, Sa G, Das T, Zhang R, Chahlavi A, Tannenbaum C et al. 2006. GM2 expression in renal cell carcinoma: potential role in tumor-induced T-cell dysfunction. *Cancer Res*. 66:6816–6825.

Brun P, Castagliuolo I, Di Leo V, Buda A, Pinzani M, Palu G, Martines D. 2007. Increased intestinal permeability in obese mice: new evidence in the pathogenesis of nonalcoholic steatohepatitis. *Am J Physiol Gastrointest Liver Physiol*. 292:G518–G525.

Cai W, Du A, Feng K, Zhao X, Qian L, Ostrom SR, Xu C. 2013. Adenylyl cyclase 6 activation negatively regulates TLR4 Signaling through lipid raft–mediated endocytosis. *J Immunol*. 191(12):6093–6100.

Chen Y, Qiao F, Zhao Y, Wang Y, Liu G. 2015. HMGB1 is activated in type 2 diabetes mellitus patients and in mesangial cells in response to high glucose. *Int J Clin Exp Pathol*. 8(6):6683–6691.

Chow F, Ozols E, Nikolic-Paterson D, Atkins R, Tesch G. 2004. Macrophages in mouse type 2 diabetic nephropathy: correlation with diabetic state and progressive renal injury. *Kidney Int*. 65:116–128.

Creely S, McTernan P, Kusminski C, Fisher fM, Da Silva N, Khanolkar M, Evans M, Harte A, Kumar S. 2007. Lipopolysaccharide activates an innate immune system response in human adipose tissue in obesity and type 2 diabetes. *Am J Physiol Endocrinol Metab*. 292:E740–E747.

Das SK, Elbein SC. 2006. The genetic basis of type 2 diabetes. *Cell Sci*. 2(4): 100–131.

De Francesco PN, Mucci JM, Ceci R, Fossati CA, Rozenfeld PA. 2013. Fabry disease peripheral blood immune cells release inflammatory cytokines: role of globotriaosylceramide. *Mol Genet Metab*. 109:93–99.

Deshmukh GD, Radin NS, Gattone VH, Shaymanl JA. 1994. Abnormalities of glycosphingolipid, sulfatide, and ceramide in the polycystic (cpwcpk) mouse. *J Lipid Res*. 35:1611–1618.

Elmarakby A, Sullivan J. 2012. Relationship between oxidative stress and inflammatory cytokines in diabetic nephropathy. *Cardiovasc Ther*. 30:49–59.

Fan Q, Shike T, Shigihara T, Tanimoto M, Gohda T, Makita Y, Wang L, Horikoshi S, Tomino Y. 2003. Gene expression profile in diabetic KK/Ta mice. *Kidney Int*. 64:1978–1985.

Fioretto P, Mauer M. 2007. Histopathology of diabetic nephropathy. *Semin Nephrol*. 27:195–207.

Freedman B, Bostrom M, Daeihagh P, Bowden D. 2007. Genetic factors in diabetic nephropathy. *Clin J Am Soc Nephrol*. 2:1306–1316.

Grove K, Voziyan P, Spraggins J, Wang S, Paueksakon P, Harris R, Hudson B, Caprioli R. 2014. Diabetic nephropathy induces alterations in the glomerular and tubule lipid profiles. *J Lipid Res*. 55:1375–1385.

Hakomori S, Handa K, Iwabuchi K, Yamamura S, Prinetti A. 1998. New insights in glycosphingolipid function glycosignaling domain a cell surface assembly of glycosphingolipids with signal transducer molecules, involved in cell adhesion coupled with signaling. *Glycobiology*. 8:xi–xix.

Hakomori S, Igarashi Y. 1995. Functional role of glycosphingolipids and gangliosides in control of cell adhesion, motility, and growth, through glycosynaptic microdomains. *Biochim Biophys Acta*. 1780:421–433.

Hughes A, Stricklett P, Schmid D, Kohan D. 2000. Cytotoxic effect of Shiga toxin-1 on human glomerular epithelial cells. *Kidney Int*. 57:2350–2359.

Igel M, Taylor BA, Phillips SJ, Becker W, Herberg L, Joost H-G. 1998. Hyperleptinemia and leptin receptor variant Asp600Asn in the obese, hyperinsulinemic KK mouse strain. *J Mol Endocrinol*. 21:337–345.

Kanwar Y, Sun L, Xie P, Liu F, Chen S. 2011. A glimpse of various pathogenetic mechanisms of diabetic nephropathy. *Annu Rev Pathol*. 6:395–423.

Kaur H, Chien A, Jialal I. 2012. Hyperglycemia induces Toll like receptor 4 expression and activity in mouse mesangial cells: relevance to diabetic nephropathy. *Am J Physiol Renal Physiol*. 303:F1145–F1150.

Kihara A. 2012. Very long-chain fatty acids: elongation, physiology and related disorders. *J Biochem*. 152:387–395.

Kim OS, Park EJ, Joe E-h, Jou I. 2002. JAK-STAT signaling mediates gangliosides-induced inflammatory responses in brain microglial cells. *J Biol Chem*. 227:40594–40601.

Kondo Y, Ikeda K, Tokuda N, Nishitani C, Ohto U, Akashi-Takamura S, Ito Y, Uchikawa M, Kuroki Y, Taguchi R et al. 2013. TLR4-MD-2 complex is negatively regulated by an endogenous ligand, globotetraosylceramide. *Proc Natl Acad Sci USA*. 110:4714–4719.

Lee S, Lee T, Ihm C, Kim M, Woo J, Chung J. 2005. Genetics of diabetic nephropathy in type 2 DM: candidate gene analysis for the pathogenic role of inflammation. *Nephrology (Carlton)*. 10(Suppl):S32–S36.

Legros N, Pohlentz G, Runde J, Dusny S, Humpf H, Karch H, Muthing J. 2017. Colocalization of receptors for Shiga toxins with lipid rafts in primary human renal glomerular endothelial cells and influence of D-PDMP on synthesis and distribution of glycosphingolipid receptors. *Glycobiology*. 27:947–965.

Makino H, Kanatsuka A, Suzuki T, Kuribayashi S, Hashimoto N, Yishida S, Nishimura M. 1985. Insulin resistance of fat cells from spontaneously diabetic KK mice. *Diabetes*. 34:844–849.

Masson E, Troncy L, Ruggiero D, Wiernsperger N, Lagarde M, Bawab SE. 2005. a-series gangliosides mediate the effects of advanced glycation end products on pericyte and mesangial cell proliferation. *Diabetes*. 54: 220–227.

Mobarak E, Håversen L, Manna M, Rutberg M, Levin M, Perkins R, Rog T, Vattulainen I, Borén J. 2018. Glucosylceramide modifies the LPS-induced inflammatory response in macrophages and the orientation of the LPS/TLR4 complex in silico. *Sci Rep*. 8:1–11.

Navarro-Gonzalez J, Mora-Fernandez C, Muros de Fuentes M, Garcia-Perez J. 2011. Inflammatory molecules and pathways in the pathogenesis of diabetic nephropathy. *Nat Rev Nephrol*. 7:327–340.

Nikolaeva S, Bayunova L, Sokolova T, Vlasova Y, Bachteeva V, Avrova N, Parnova R. 2015. GM1 and GD1a gangliosides modulate toxic and inflammatory effects of E. coli lipopolysaccharide by preventing TLR4 translocation into lipid rafts. *Biochim Biophys Acta*. 1851(3):239–247.

Nowling T, Mather A, Thiyagarajan T, Hernandez-Corbacho M, Powers T, Jones E, Snider A, Oates J, Drake R, Siskind L. 2015. Renal glycosphingolipid metabolism is dysfunctional in lupus nephritis. *J Am Soc Nephrol*. 26:1402–1413.

Obrig TG, Louise CB, Lingwood CA, Boyd B, Barley-Maloney L, Daniel TO. 1993. Endothelial heterogeneity in Shiga toxin receptors and responses. *J Biol Chem*. 268:15484–15488.

Ohmi Y, Tajima O, Ohkawa Y, Yamauchi Y, Sugiura Y, Furukawa K, Furukawa K. 2011. Gangliosides are essential in the protection of inflammation and neurodegeneration via maintenance of lipid rafts: elucidation by a series of ganglioside-deficient mutant mice. *J Neurochem*. 116: 926–935.

Okazaki M, Saito Y, Udaka Y, Maruyama M, Murakami H, Ota S, Kikuchi T, Oguchi K. 2002. Diabetic nephropathy in KK and KK-Ay mice. *Exp Anim*. 51(2):191–196.

Okuda T, Nakakita S, Nakayama K. 2010. Structural characterization and dynamics of globotetraosylceramide in vascular endothelial cells under TNF-alpha stimulation. *Glycoconj J*. 27:287–296.

Pai R, Bassa B, Kirschenbaum MA, Kamanna VS. 1996. TNF-a stimulates monocyte adhesion to glomerular mesangial cells. *J Immunol*. 156:2571–2579.

Park SB, Song HD, Kim MH, Choi BS, Lee H, Lee JO. 2009. The structural basis of lipopolysaccharide recognition by the TLR4–MD-2 complex. *Nature*. 458:1191–1195.

Saitoh S, Akashi S, Yamada T, Tanimura N, Kobayashi M, Konno K, Matsumoto F, Fukase K, Kusumoto S, Nagai Y et al. 2004. Lipid A antagonist, lipid IVa, is distinct from lipid A in interaction with Toll-like receptor 4 (TLR4)-MD-2 and ligand-induced TLR4 oligomerization. *Int Immunol*. 16(7):961–969.

Shike T, Hirose S, Tomino Y, Kobayashi M, Funabiki K, Shirai T. 2001. Susceptibility and negative epistatic loci contributing to type 2 diabetes and related phenotypes in a KK/Ta mouse model. *Diabetes*. 50:1943–1948.

Sonnino S, Prinetti A, Nakayama H, Yangida M, Ogawa H, Iwabuchi K. 2009. Role of very long fatty acid- containing glycosphingolipids in membrane organization and cell signaling: the model of lactosylceramide in neutrophils. *Glycoconj J*. 26:615–621.

Subathra M, Korrapati M, Howell L, Arthur J, Shayman J, Schnellmann R, Siskind LJ. 2015. Kidney glycosphingolipids are elevated early in diabetic nephropathy and mediate hypertrophy of mesangial cells. *Am J Physiol Renal Physiol*. 309:F204–F215.

Suto J, Matsuura S, Imamura K, Yamanaka H, Sekikawa K. 1998. Genetic analysis of non-insulin-dependent diabetes mellitus in KK and KKAy mice. *Eur J Endocrinol*. 139:654–661.

Tagami S, Inokuchi J, Kabayama K, Yoshimura H, Kitamura F, Uemura S, Ogawa C, Ishii A, Saito M, Ohtsuka Y et al. 2002. Ganglioside GM3 participates in the pathological conditions of insulin resistance. *J Biol Chem*. 277:3085–3092.

van Setten PA, van Hinsbergh VW, van der Velden TJ, van de Kar NC, Vermeer M, Mahan JD, Assmann KJ, van den Heuvel LP, Monnens LA. 1997. Effects of TNF-α on verocytotoxin cytotoxicity in purified human glomerular microvascular endothelial cells. *Kidney Int*. 51:1245–1256.

Vardarli I, Baier L, Hanson R, Akkoyun I, Fischer C, Rohmeiss P, Basci A, Bartram C, Van Der Woude F, Janssen B. 2002. Gene for susceptibility to diabetic nephropathy in type 2 diabetes maps to 18q22.3-23. *Kidney Int*. 62:2176–2183.

Wang H, Qu H, Deng H. 2015. Plasma HMGB-1 levels in subjects with obesity and Type 2 diabetes: a cross-sectional study in China. *PLoS One*. 10 (8):1–10.

Wu Y, Ding Y, Tanaka Y, Zhang W. 2014. Risk factors contributing to type 2 diabetes and recent advances in the treatment and prevention. *Int J Med Sci*. 11:1185–1200.

Yoshida L, Tsunawaki S. 2008. Expression of NADPH oxidases and enhanced H_2O_2-generating activity in human coronary artery endothelial cells upon induction with tumor necrosis factor-alpha. *Int Immunopharmacol*. 8:1377–1385.

Yu RK, Nakatani Y, Yanagisawa M. 2009. The role of glycosphingolipid metabolism in the developing brain. *J Lipid Res*. 50:S440–S445.

Zador IZ, Deshmukh GD, Kunkel R, Johnson K, Radin NS, Shayman JA. 1993. A role for glycosphingolipid accumulation in the renal hypertrophy of streptozotocin-induced diabetes mellitus. *J Clin Invest*. 91:797–803.

総論編 4

スフィンゴ糖脂質の生合成とその制御

井ノ口　仁一*1、岩渕　和久*2

はじめに

ドイツ生まれの神経化学者であるJ.L.W Thudichum（1829-1901）は、ヒトの脳の両親媒性の不思議な脳物質に対して、謎を問いかけるスフィンクスに因んで、「スフィンゴシン」と名づけた[1)]。長鎖アミノアルコールであるスフィンゴシン（スフィンゴイド塩基）に脂肪酸が酸アミド結合した化合物をセラミド、セラミドに更にリン酸基を有するものをスフィンゴリン脂質と呼び、その代表的な脂質はスフィンゴミエリンであり、動物細胞膜のスフィンゴ脂質グループの主要成分である。一方、糖が結合したものをスフィンゴ糖脂質（GSL）と呼ぶ。本稿では、GSL生合成・代謝とその制御機構、ヒトのGSL合成異常およびGM3合成酵素ノックアウトマウスの表現型について述べる。

1 スフィンゴ糖脂質（GSL）の生合成

GSLは、セラミドにグルコース、ガラクトース、N-アセチルガラクトサミン、N-アセチルグルコサミン、シアル酸などの糖や硫酸の段階的な酵素反応によって、多様な分子が生合成され、細胞膜脂質二重層の外側半葉に局在して非対称構造

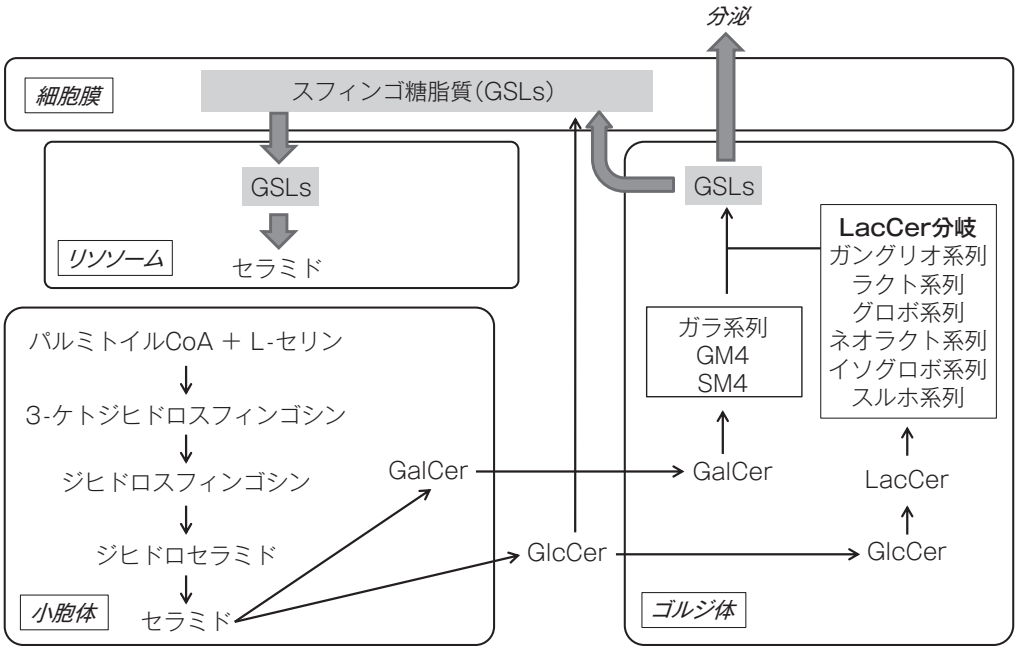

図1A　スフィンゴ糖脂質の生合成と代謝（A：細胞内小器官におけるGSLs代謝）

＊1 東北医科薬科大学 分子生体膜研究所長、＊2 順天堂大学大学院医療看護学研究科 教授

を形成している。GSLの生合成は、ラクトシルセラミド（LacCer）を分岐点としてガングリオ系列、ラクト系列、グロボ系列、ネオラクト系列、イソグロボ系列、スルホ系列の多様なGSLが生合成され、また、ガラ系列はガラクトシルセラミド（GalCer）にシアル酸および硫酸基が付加され、それぞれGM4とSM4が生成する（**図１A, B**）。シアル酸を含むスフィンゴ糖脂質をガングリオシドと呼び、細胞膜マイクロドメインの構成分子として、様々な細胞膜上におけるシグナル伝達を制御している。ガングリオシドファミリー生合成の最初の分子は、ラクトシルセラミドにシアル酸が転移して生成するGM3である。GM3は末梢組織の主要なガングリオシドである。GM3は、糖脂質研究の草分けである山川民夫博士がウマ赤血球からヘマトシドとして同定されたものである[1)]。ヒトGM3合成酵素（GM3S、ST3GAL5；以降GM3Sと略）は、斎藤らにより1998年に遺伝子クローニングされた[2)]。図１Bに示すように、GM3からは多様なガングリオシドが生合成されるが、それらは、細胞や組織において特徴的な発現特異性を示す。GM2/GD2合成酵素（β-1,4 *N*-acetylgalactosaminyltransferase：B4GalNAcT1；以下GM2Sと略）は、主に脊椎動物の脳神経系に発現し複合型ガングリオシド生合成の鍵となる酵素で、GM3、GD3、LacCerに*N*-アセチルガラクトサミン（*N*-acetylgalactosamine：GalNAc）を転移して、それぞれからGM2、GD2、GA2（asialo-GM2）が生合成される（図１B）。一方、GalCerにシアル酸が付加しGM4が生合成される（図１B）。その生合成に関わるシアル酸転移酵素は近年まで不明であったが、GM3Sノックアウトマウスでは、赤血球やミエリンのGM4が消失することから、GM3合成酵素がGM4の生合成も担っていることが明らかになった[3、4)]。

2 スフィンゴ糖脂質生合成制御機構

細胞内におけるスフィンゴ（糖）脂質の生合成制御機構について、現時点での作業仮説も含めて**図２**に示した。国立感染研の花田は、CERTとよ

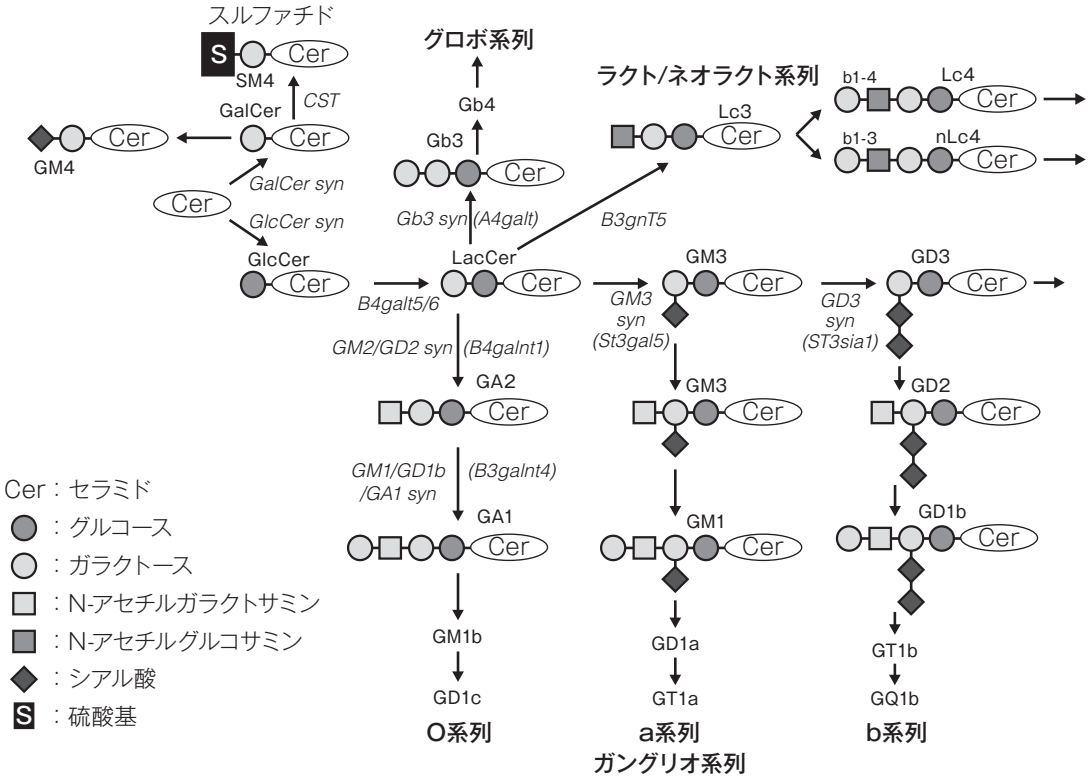

図１B　ガングリオシド系列、グロボ系列、ラクト・ネオラクト系列及びスルファチドの生合成経路

ばれる小胞体からゴルジ体へ特異的にセラミドを運ぶ分子を発見した[5]。CERTに結合したセラミドは、CERTのPHドメインとゴルジ膜局所に濃縮されたホスファチジルイノシトール-4-一リン酸（PI4P）と複合体を形成し、主としてスフィンゴミエリン（SM）の生合成に利用される。また、小胞体膜の細胞質側で合成されたセラミドの一部は、小胞体、シス/メディアゴルジ膜の細胞質側でグルコシルセラミド（GlcCer）になる[6]。また、最近の林らの研究に依れば、GlcCer合成酵素とSM合成酵素1はゴルジのトランス側で複合体を形成することが分かっている[7]。この事実は、GlcCer合成酵素は、ゴルジ膜のトランス側に局在していることを示唆している。ただし、その合成活性に関しては、まだ証拠が不十分であると考えられる. 生成したGlcCerは非ゴルジ経路を通って細胞膜に輸送されるか[8]、糖脂質転移（glycolipid-transter）ドメインを持つFAPP2でトランスゴルジに輸送され、ゴルジ体膜の内側にフリップした後、ラクトシルセラミド（LacCer）に変換されることが示された[9、10]。おそらく、LacCer合成酵素はゴルジ体で局在が異なる２種類が存在し、FAPP2と結合したGlcCer はグロボ系などの中性糖脂質（Gb3など）の生合成に利用されるのであろう。一方、LacCer合成酵素とGM3合成酵素（GM3S）は、複合体を形成してガングリオシドファミリーの合成を制御している可能性が報告されている[11]。従って、細胞特異的なスフィンゴ糖脂質分子種の発現機構の包括的な理解には種々の生合成酵素の細胞内局在および動態を徹底的に解明していくことが不可欠である。第２章には、現時点までに報告されているスフィンゴ糖脂質合成酵素の細胞内局在について詳細にまとめられているので、参照されたい。

GM3SはII型の膜タンパク質であり複数のアスパラギン結合型糖鎖が付加される。これらの糖鎖はGM3Sの酵素活性に必須である[12]。GM3Sには、N末端側の細胞質領域の長さが異なる３種類のアイソフォーム（M1-、M2-、M3-GM3S）が存在し、それぞれの細胞内動態が大きく異なって

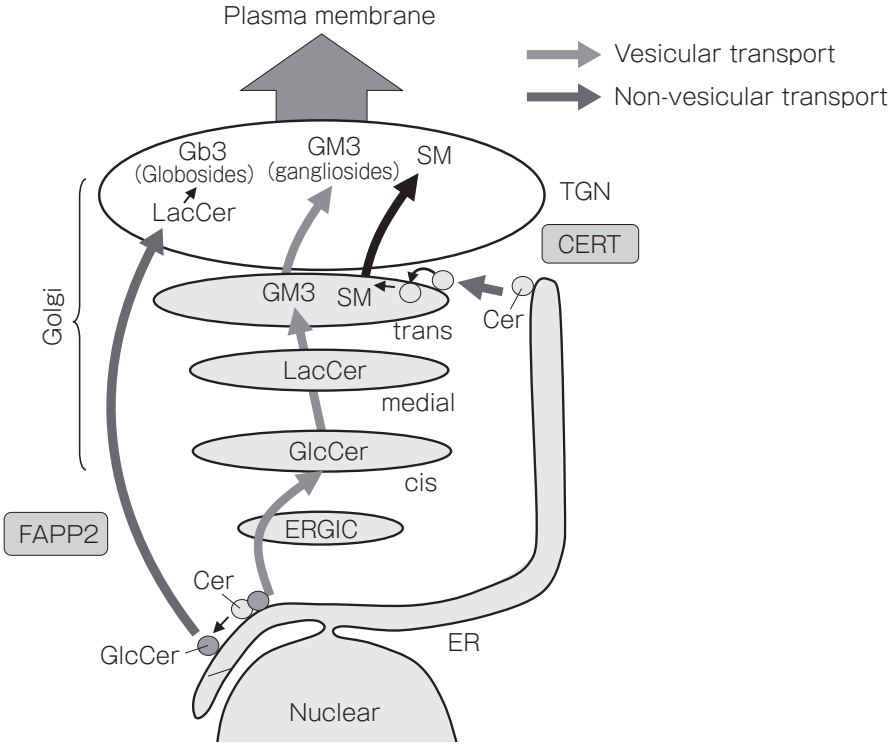

図２ スフィンゴ糖脂質生合成制御機構
スフィンゴミエリン、グロボシド、ガングリオシドの糖脂質生合成の最近の局面（作業仮説を含む）

いる[13]。シアル酸転移酵素ファミリーのなかでも最も長い68アミノ酸の細胞外領域を有するM1-GM3Sは、N末側に逆行輸送シグナルR-basedモチーフを持ち、小胞体に局在している（**図３**）。M1-GM3Sの逆行輸送は不完全であり、一部のM1-GM3Sは逆行輸送を逃れ、ゴルジ体まで運ばれた後、GM3を合成する。つまり、M1-GM3Sは安定して小胞体に局在しながら、ゆっくりとゴルジ体へGM3Sを供給していることが示唆される。また、M2-GM3SとM3-GM3Sはどちらもゴルジ体に局在しているが、M2-GM3Sは速やかにリソソームへ運ばれて分解されるのに対し、M3-GM3Sは安定してゴルジ体に繋留する。３種類のアイソフォームの量的バランスと局在のバランスがGM3合成の制御に重要であると推測される（図３）[13、14]。今後、ラクトシルセラミドに作用する６種の酵素（図１A）の細胞内動態が解明され、スフィンゴ糖脂質生合成制御機構の全貌が解明されることが期待される。

3 *GM3S*ノックアウトマウスの表現型

種々のスフィンゴ糖脂質合成酵素のノックアウトマウスの解析から、細胞種特異的に発現するスフィンゴ糖脂質分子種の機能が見いだされつつある（**図４**）。詳しくは総説を参照されたい[15]。ここでは、*GM3S*ノックアウトマウスの解析により見えて来たガングリオシドの機能について述べる。

GM3の分子レベルでの作用機序が明らかとなった代表例としては、インスリン受容体の機能制御である。肥満モデル動物のZucker fa/faラットとob/obマウスの脂肪組織において*GM3S*遺伝子の発現増加に伴いGM3発現量が著しく増加するという発見を契機に[16]、*GM3S* KOマウスでインスリン感受性の亢進することが証明された[17]。また、グルコシルセラミド合成酵素阻害剤を処理することで、肥満モデル動物のインスリン抵抗性[18]や多発性嚢胞腎（polycystic kidney disease, PKD）などを改善する[19]などの報告が相次ぎ、GM3と２型糖尿病との関わりが注目されている。現在で

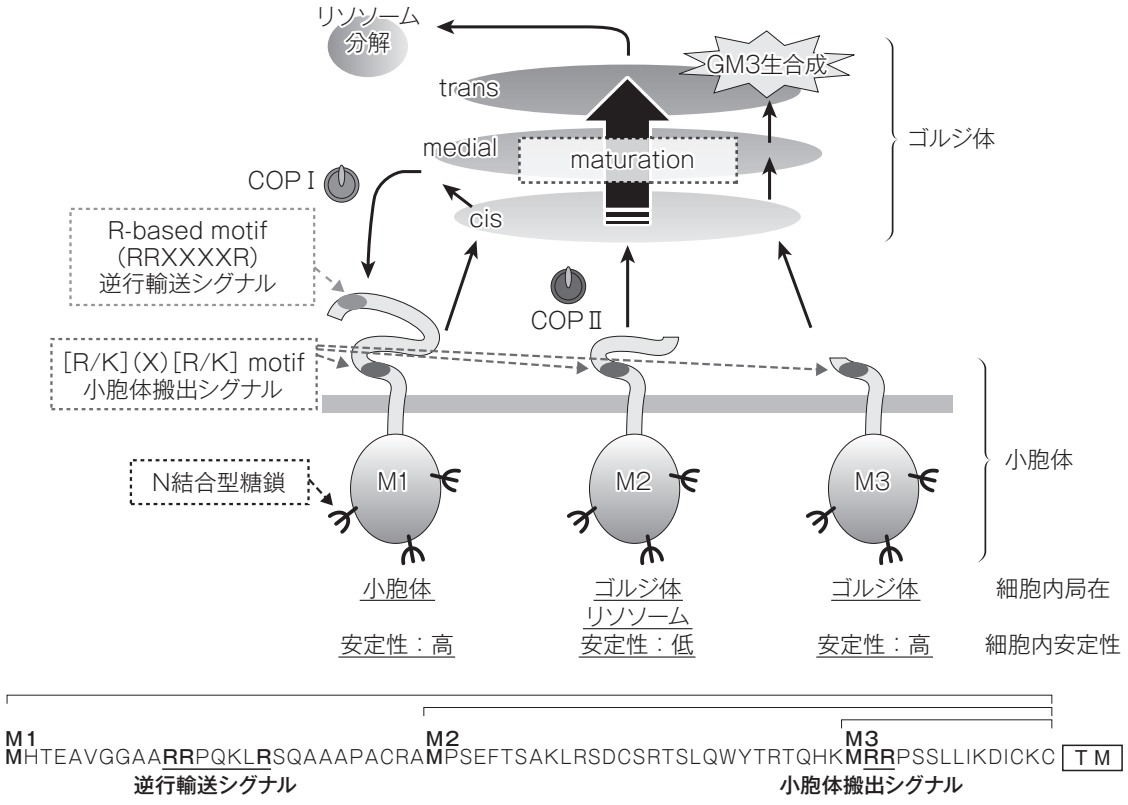

図３　GM3合成酵素アイソフォームの細胞内動態[7-9]

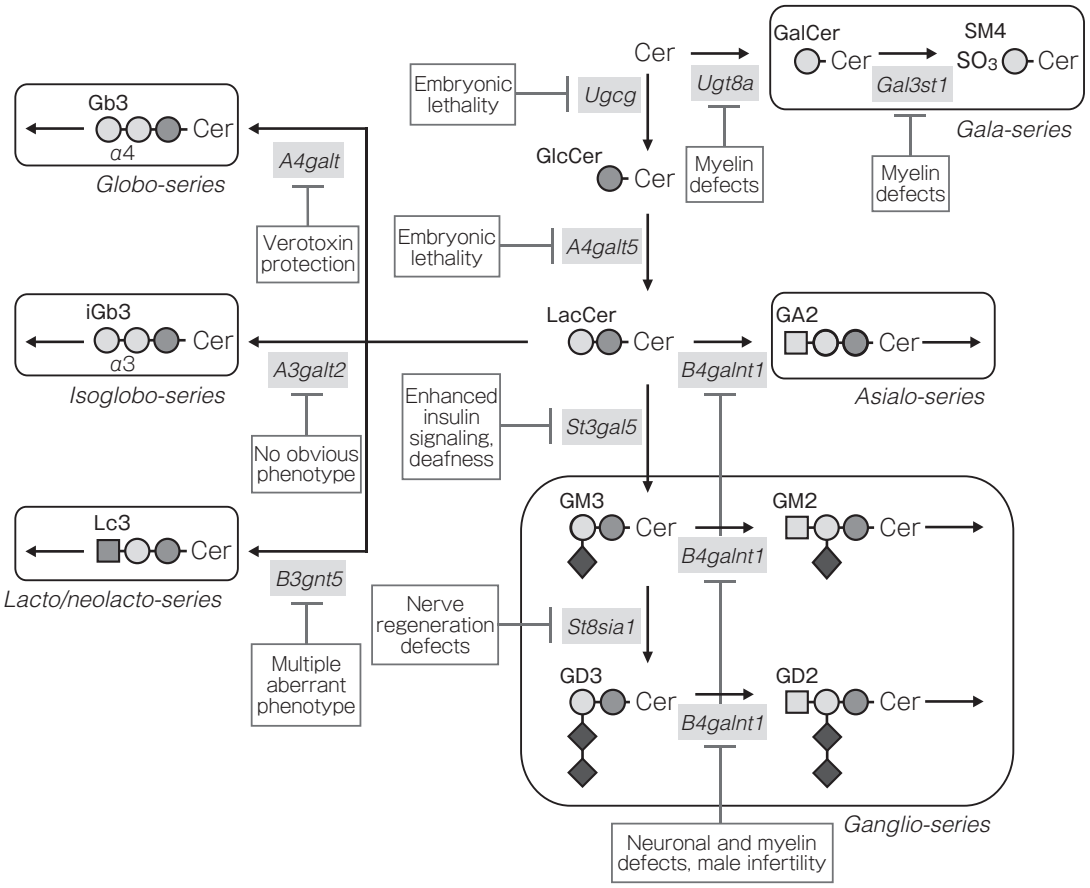

図４　種々のスフィンゴ糖脂質合成酵素ノックアウトマウスの表現型（引用文献14より改変）

は、このようなGM3発現量の増加によるインスリンシグナル抑制の効果は、インスリン受容体はカベオラと呼ばれる細胞膜上のくぼみ構造に存在することでインスリンによるシグナル伝達を行うが、肥満に伴いカベオラとは別のマイクロドメインを形成しているGM3が膜上に増加することでインスリン受容体の膜直上のリシン残基とGM3の静電気的相互作用が生じ、インスリン受容体がカベオラから解離すると考えられている[20]。

GM3S KOマウスはメンデルの法則に従う比率で産まれ、聴覚異常[21]を呈するもののほぼ正常に成長し、寿命も野生型と比較して大きな差は見られない。*GM3S* KOマウスのほぼすべての臓器では、a, b系列のガングリオシドが消失し、通常ほとんど発現が見られない０系列 のガングリオシドが発現する（図１B）。ガングリオシドを完全に欠損したマウスである*GM3S*と*GM2S*遺伝子の二重欠損（*GM2S/GM3S* DKO）マウスは、生後すぐに重篤な中枢神経障害を示し、大多数が早期に死亡する[22]。従って、*GM3S* KOマウスでは、GAIの末端ガラクトースにシアル酸が付加されて生成するGM1b、さらにシアル酸が付加されたGD1cなどの「０系列」ガングリオシドが生命維持に重要な「a, b系列」ガングリオシドの機能を代償していると考えられる（図１B）。

4　ヒトにおけるガングリオシド合成異常

ヒトでスフィンゴ糖脂質合成酵素の遺伝子変異は、*GM3S*と*GM2S*で見出されている。現在までの報告を**図５**にまとめた。最初に見出された*GM3S*遺伝子変異は、アーミッシュ家系（７世紀に米国ペンシルバニア州に移住した保守派アーミッシュ家系）で見出されたナンセンス変異（288STOP）である[23]。この*GM3S*欠損は幼児期

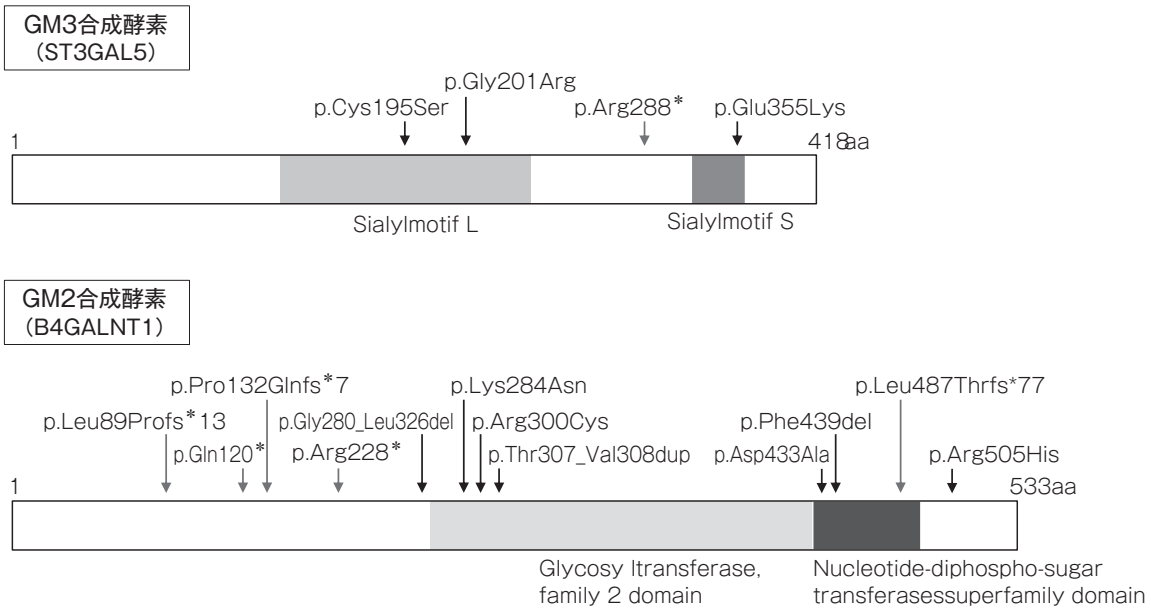

図５　GM3及びGM2合成酵素で見出された遺伝子変異

ST3GAL5 and B4GNT1 遺伝子配列は、それぞれ NM_003896.3 および NM_001478.4にもとずいている。
遺伝子変異の箇所の記載は、Sequence Variant Nomenclature（http://varnomen.hgvs.org/）に従って記載した。

に発症する重篤なてんかん症状、重度の知的障害、舞踏病アテトーゼ（choreoathetosis)、脊柱側弯症、脊椎麻痺、顔面形成異常、視覚異常等の症状を呈し、20歳前後で死亡する。その後同じ*GM3S*変異では、上記の症状に加えフランスでは難聴[24]、米国では皮膚の色素沈着異常[25]などの多彩な異常が報告されている。また、E355Kのミスセンス変異では皮膚の色素沈着異常を呈するSalt-and-pepper症候群[26]、C195S、G201Rでは神経系の発達障害を呈するレット症候群（Rett syndrome）様の症状などが報告されている[27]。

*GM2S*のミスセンス変異はクウェート、イタリア、オールド・オーダー・アーミッシュの家系において、複合型遺伝性痙攣性対麻痺（ニューロパチー、小脳失調、脳梁の菲薄化、精神発達遅延、痙攣、難聴、網膜色素変性症、魚鱗癬などをともなう疾患）様の症状がある患者で同定されている[28-30]。

*GM3S*ノックアウトマウスとヒトの*GM3S*遺伝子異常を比較すると、ヒトの表現型がより重篤であることがわかる。ヒトとマウスの表現型の違いを解明するには、ガングリオシド生合成制御機構や関連遺伝子発現の相違等を比較検討していく必要があり、今後の課題である。

【引用文献】

1）山川民夫（1981）　糖脂質物語　講談社学術文庫.
2）Ishii, A. *et al*. Expression Cloning and Functional Characterization of Human cDNA for Ganglioside GM3 Synthase. *J. Biol. Chem*. **273**, 31652-31655（1998）
3）Chisada, S. *et al*, Zebrafish and mouse alpha2,3-sialyltransferases responsible for synthesizing GM4 ganglioside. *J.Biol. Chem*., **284**, 30534-30546（2009）
4）Uemura S. *et al*. Expression machinery of GM4: The excess amounts of GM3/GM4S synthase（ST3GAL5）are necessary for GM4 synthesis in mammalian cells. *Glycoconj. J*. **31**, 101-108（2014）
5）Hanada, K. *et al*. Molecular machinery for non-vesicular trafficking of ceramide. *Nature*, **426**, 803-809,（2003）
6）Halter D, *et al*.: Pre- and post-Golgi translocation of glucosylceramide in glycosphingolipid synthesis. *J Cell Biol*, **179**, 101-115（2007）
7）Hayashi, Y. *et al*. Complex formation of sphingomyelin synthase 1 with glucosylceramide synthase increases sphingomyelin and decreases glucosylceramide levels. *J. Biol. Chem*., **293**, 17505-17522（2018）
8）Marcus D. My career as an immunoglycobiologist. Proc. Jpn. Acad., Ser. B 89,（2013）doi: 10. 2183/pjab. 89. 257
9）D'Angelo G. *et al*. Glycosphingolipid synthesis requires FAPP2 transfer of glucosylceramide. *Nature*, **449**, 62-67（2007）

10) D'Angelo G, *et al*. Vesicular and non-vesicular transport feed distinct glycosylation pathways in the Golgi. *Nature*, **501**, 116-120(2013)
11) Giraudo, C.G., & Maccioni, H.J. Ganglioside Glycosyltransferases Organize in Distinct Multienzyme Complexes in CHO-K1 Cells. *J. Biol. Chem*., **278**, 40262-40271(2003)
12) Uemura, S. *et al*. Substitution of the N-glycan function in glycosyltransferases by specific amino acids: ST3Gal-V as a model enzyme. *Glycobiology*, **16**, 258-270(2006)
13) Uemura, S. *et al*. The Cytoplasmic Tail of GM3 Synthase Defines Its Subcellular Localization, Stability, and In Vivo Activity. *Mol. Biol. Cell*, **20**, 3088-3100(2009)
14) Uemura, S. *et al*. The regulation of ER export and Golgi retention of ST3Gal5 (GM3/GM4 synthase) and B4GalNAcT1(GM2/GD2/GA2 synthase) by arginine/lysine-based motif adjacent to the transmembrane domain. *Glycobiology*, **25**, 1410-422 (2015)
15) Allende, M.L. and Rroia, R.L. Simplifying complexity: genetically resculpting glycosphingolipid synthesis pathways in mice to reveal function. *Glycoconj J*. **31**, 613-622(2014).
16) Tagami, S., Inokuchi, J. *et al*., Ganglioside GM3 participates in the pathological conditions of insulin resistance. *J. Biol. Chem*., **277**, 3085-3092(2002)
17) Yamashita, T. *et al*. Enhanced insulin sensitivity in mice lacking ganglioside GM3. *Proc Natl Acad Sci USA*, **100**, 3445-3449(2003)
18) Zhao, H. *et al*. Inhibiting glycosphingolipid synthesis improves glycemic control and insulin sensitivity in animal models of type 2 diabetes. *Diabetes*, **56**, 1210-1218(2007)
19) Natoli, T.A., *et al*., Inhibition of glucosylceramide accumulation results in effective blockade of polycystic kidney disease in mouse models. *Nature Med*. **16**, 788-793(2010)
20) Kabayama, K. *et al*. Dissociation of the insulin receptor and caveolin-1 complex by ganglioside GM3 in the state of insulin resistance. *Proc Natl Acad Sci. USA*, **104**, 13678-13683(2007)
21) Yoshikawa, M. *et al*. Mice lacking ganglioside GM3 synthase exhibit complete hearing loss due to selective degeneration of the organ of Corti. *Proc. Natl. Acad. Sci. USA*, **106**, 9483-9488(2009)
22) Yamashita, T. *et al*. Interruption of ganglioside synthesis produces central nervous system degeneration and altered axon-glial interactions. *Proc Natl Acad Sci USA*, **102**, 2725-2730(2005)
23) Simpson, M.A. *et al*. Infantile-onset symptomatic epilepsy syndrome caused by a homozygous loss-of-function mutation of GM3 synthase. *Nat. Genet*., **36**, 1225-1229(2004)
24) Fragaki, K. *et al*. Refractory epilepsy and mitochondrial dysfunction due to GM3 synthase deficiency. *European journal of human genetics*. **21**, 528-534(2013)
25) Wang, H. *et al*. Cutaneous dyspigmentation in patients with ganglioside GM3 synthase deficiency. *Am J Med Genet*. **A161a**, 875-879(2013)
26) Boccuto, L. *et al*. A mutation in a ganglioside biosynthetic enzyme, ST3GAL5, results in salt & pepper syndrome, a neurocutaneous disorder with altered glycolipid and glycoprotein glycosylation. *Hum Mol Genet*. **23**, 418-433(2014)
27) Lee, J.S. *et al*. GM3 synthase deficiency due to ST3GAL5 variants in two Korean female siblings: Masquerading as Rett syndrome-like phenotype. *Am J Med Genet*. **A161a**, 875-879(2013)
28) Boukhris, A. *et al*. Alteration of ganglioside biosynthesis responsible for complex hereditary spastic paraplegia. *Am J Human Genet*. **93**, 118-123 (2013)
29) Harlalka, G.V. *et al*. Mutations in B4GALNT1 (GM2 synthase) underlie a new disorder of ganglioside biosynthesis. *Brain*. **136**, 3618-3624(2013)
30) Wakil, S.M. *et al*. Novel B4GALNT1 mutations in a complicated form of hereditary spastic paraplegia. *Clinical Genetics*. **86**, 500-501(2014)

＜生体膜情報部門＞
教授　東 秀好
助教　中川 哲人
助教　黒田 喜幸

Gタンパク質共役受容体（GPCR）による糖鎖合成制御と糖鎖によるGPCRの活性制御

1. β2 アドレナリン受容体シグナルによるヒアルロン酸合成の上昇

ヒアルロン酸（HA）は、N-アセチルグルコサミンとグルクロン酸の２糖繰り返し構造から成る直鎖の高分子多糖である。HA は細胞外マトリックスの構成分子として、組織の弾性や物性維持に関わる他、創傷治癒や細胞増殖を制御する。また、HA 産生の増減や HA のサイズが、炎症反応や癌、血管疾患などの病態を制御する。HA は細胞膜上に存在し、３種類のイソ型が知られるヒアルロン酸合成酵素（HAS1、HAS2、HAS3）によって産生される。HAS は多種の増殖因子やサイトカイン、ホルモンなどで遺伝子の発現が制御されており、翻訳後修飾により HA 産生能が変化する。近年、G タンパク質共役型受容体（GPCR）である UDP-グルコース受容体の $P2Y_{14}$ や ATP/UTP 受容体の $P2Y_2$ のシグナルにより、HAS2 遺伝子発現が上昇し HA 産生が亢進することが報告され、組織損傷部位での HA 産生の増加に GPCR シグナルが関与していることが示唆された（*1, 2*）。$P2Y_{14}$ は Gαi と共役し、$P2Y_2$ は Gαq と共役することから、GPCR シグナルでの HA 産生は単一シグナルによる制御ではないと考えられる。

β2 アドレナリン受容体（β2AR）はカテコラミンをリガンドとする GPCR であり、その活性化は血管や気管支などの平滑筋を弛緩させる作用を現す。気管支喘息の治療で使用される β 作動薬は、β2AR と Gαs が共役することで生じるシグナルを介して気管支平滑筋を弛緩させることを目的としている。また、気管支喘息では気管支の炎症反応をともない、気管支喘息患者の肺胞洗浄液中の HA 量が増加している（*3*）。さらに、β 作動薬の長期連用は、β2AR と相互作用したアレスチンによるシグナルにより、炎症反応の増悪やムチンの産生亢進といった副作用が生じる。このことから我々は、β2AR によるシグナルが平滑筋の収縮だけでなく、HA 産生にも影響しうるのではないかと考えた。

そこで、HEK293T（ヒト胎児腎臓由来細胞）に β2AR を発現させ、非選択的 β 作動薬であるイソプロテレノール（ISO）や β2 選択的作動薬のサルブタモール（Sal）で刺激した。培養液中に分泌された HA 量を測定すると、β 作動薬で刺激した細胞では HA 量が増加することが分かった。次に、β 作動薬刺激による HA 量の増加が、HAS の発現亢進によるものかを検討するため、リアルタイム PCR により HAS 遺伝子の発現量を調べた。ISO で 2 時間、β2AR 発現細胞を刺激す

ると、HAS2 遺伝子の発現が亢進した。HAS2 遺伝子の発現増加は Sal での刺激でも同様に生じたことから、β2AR の活性化が HAS2 遺伝子の発現を亢進させると考えられた。さらに、β2AR シグナルが HAS2 遺伝子発現を亢進させるシグナル伝達経路を明らかにするため、各種阻害剤で前処理を行い、Sal 刺激による HAS2 遺伝子発現への影響を調べた。その結果、β2AR の活性化は Gαs - cAMP - PKA - JNK - STAT3 シグナルを介して HAS2 遺伝子の転写を亢進していることが分かった。

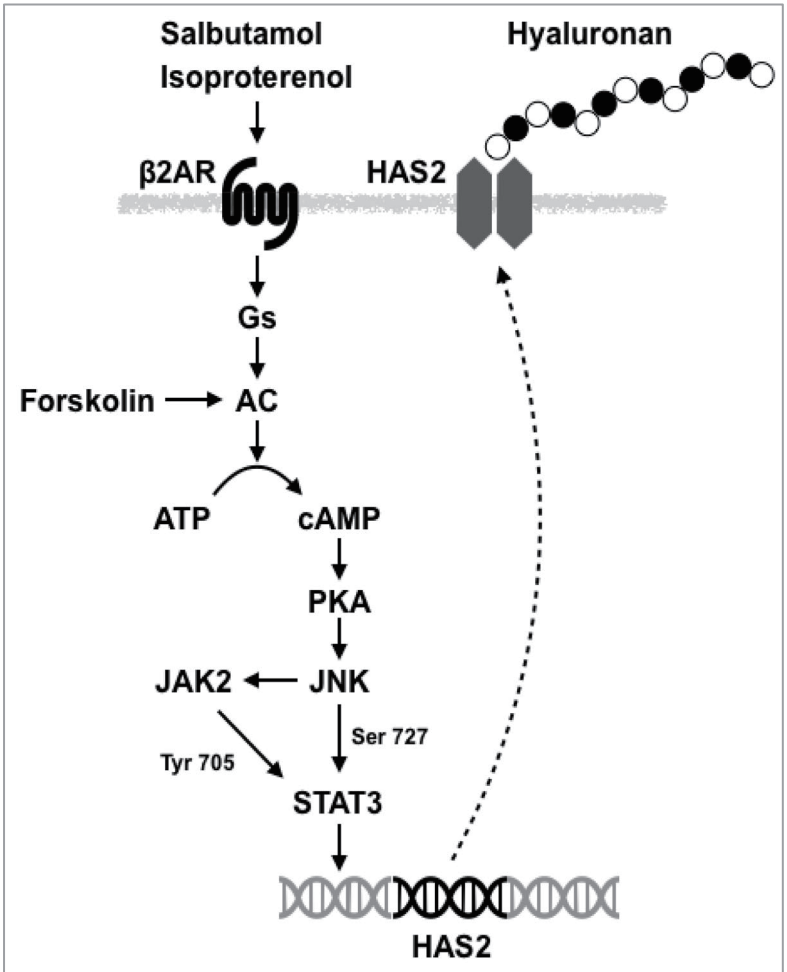

β2 アドレナリン受容体の活性化が HA 産生を 増加させるシグナル

β 作動薬による β2AR の活性化は、三量体 G タンパク質（Gαs）を介して、cAMP - PKA シグナルを活性化させる。PKA は JNK を活性化させ、STAT3 の Ser727 をリン酸化する。さらに、JNK が JAK2 を活性化することで、STAT3 の Tyr705 をリン酸化し、STAT3 の転写活性化を引き起こす。活性化した STAT3 が HAS2 のプロモーター領域に結合し、HAS2 遺伝子の転写を亢進させ、HAS2 タンパク質の発現が増加することにより HA 産生が上昇すると考えられる。

HAS2 遺伝子のプロモーター領域には STAT3 結合部位が存在し、STAT3 活性化によって HAS2 遺伝子発現が上昇する(*4*)。また、Gαs 恒常的活性化変異体発現細胞では cAMP - PKA シグナルによって STAT3 の活性化が生じる (*5*)。このことから、β2AR による HA 産生の上昇は、β2AR のシグナルが STAT3 を活性化し、HAS2 遺伝子の転写が亢進することで生じると考えられる。HAS2 遺伝子のプロモーター領域には CREB 結合部位も存在し、cAMP - PKA シグナルが CREB を活性化するとされるが、我々の実験結果からは β2AR のシグナルが CREB により HAS2 遺伝子の発現を制御することは確認できなか

った。

また、β2AR のシグナルには、アレスチンとの相互作用を介したシグナルも存在する。アレスチンのシグナルは主に MAP キナーゼ（MEK1/2 - ERK1/2）を介するが、β2AR による HAS2 遺伝子の発現増加は、MEK1/2 阻害剤では抑制されなかった。気管支喘息においては、アレスチンのシグナルが炎症反応の増悪などを引き起こすことが知られているが、β2AR による HA 産生の増加は炎症反応の抑制や組織修復の促進といった有益な効果のみを示すのかもしれない。β2AR の活性化により産生された HA が細胞や組織にどのような作用を及ぼしているのかは今後の検討課題である。

2. ガングリオシドとコンドロイチン硫酸刺激によるブラジキニン B2 受容体の不応化・内在化の機構

ブラジキニン B2 受容体（B2R）は、血管平滑筋や神経組織をはじめとする多くの組織に恒常的に発現しており、炎症や疼痛、血管拡張に関与する GPCR である。以前我々は、B2R 発現 CHO-K1 細胞のガングリオシド GT1b とコンドロイチン硫酸 C（CSC）での順次刺激により、B2R のアゴニストであるブラジキニン（BK）による細胞内 Ca^{2+}上昇が抑制されることを報告している（*6*）。GPCR をアゴニストに長時間あるいは繰り返し暴露すると、アレスチンが結合して G タンパク質との結合が阻害され（不応化）、さらにはエンドサイトーシスされる（内在化）。このことから、GT1b と CSC による順次刺激はアゴニスト非依存的な不応化・内在化を誘導したと考えられたので、この不応化機構を解析した。

まず、B2R 発現 HEK293 細胞を GT1b と CSC により順次刺激し、抽出した

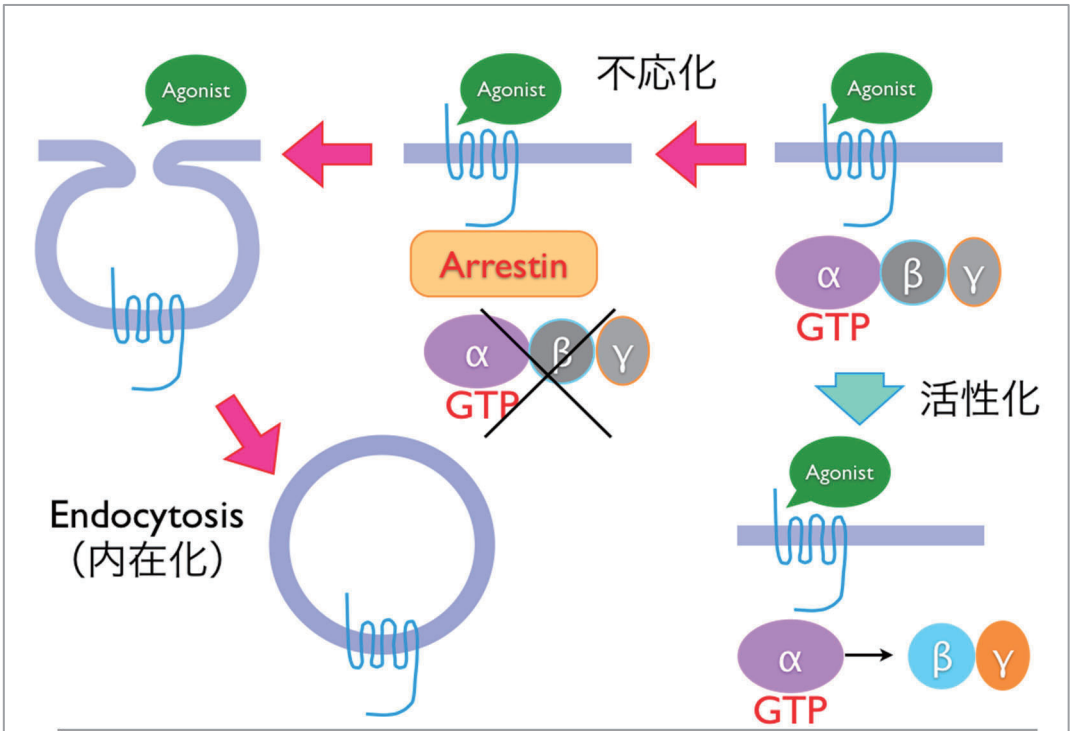

GPCR の活性化と不応化（desensitization）、内在化(internalization)

膜画分に含まれる B2R をウエスタンブロッティングで検出した。その結果、GT1b と CSC の順次刺激により細胞膜上から分子質量の小さい、未熟な N 型糖鎖を有する B2R が減少することが分かった。細胞膜からの B2R 消失は、GT1b および CSC の単独刺激や同時刺激ではほとんど起こらなかった。次に、細胞上の B2R 減少が不応化によるものかを明らかにするため、共免疫沈降法を用いて B2R とアレスチンの相互作用を調べた。GT1b と CSC の順次刺激後には、無刺激と比較してアレスチンと相互作用している B2R が多いことが分かった。また、B2R の糖鎖の成熟度とは無関係にアレスチンは相互作用していた。さらに、GPCR がアレスチンと相互作用するために重要である GPCR キナーゼ（GRK）を阻害すると、GT1b と CSC の順次刺激による B2R の細胞膜上からの減少も阻害された。これらのことから、GT1b と CSC の順次刺激は、B2R に対して立体構造上の変化を引き起こし、B2R が GRK によるリン酸化を受けやすくなり、アゴニスト非依存的にアレスチンと相互作用することで不応化し、内在化することが示唆された。また、B2R の糖鎖の成熟は、内在化されやすさに影響することも示唆された。

References

1. Jokela, T.A., Karna, R., Makkonen, K.M., Laitinen, J.T., Tammi, R.H., and Tammi, M.I. (2014) Extracellular UDP-glucose activates P2Y14 Receptor and Induces Signal Transducer and Activator of Transcription 3 (STAT3) Tyr705 phosphorylation and binding to hyaluronan synthase 2 (HAS2) promoter, stimulating hyaluronan synthesis of keratinocytes. J Biol Chem. 289, 18569-18581
2. Rauhala, L., Jokela, T., Karna, R., Bart, G., Takabe, P., Oikari, S., Tammi, M. I., Pasonen-Seppanen, S., and Tammi, R.H. (2018) Extracellular ATP activates hyaluronan synthase 2 (HAS2) in epidermal keratinocytes via $P2Y_2$, Ca^{2+} signaling, and MAPK pathways. Biochem J. 475, 1755-1772
3. Garantziotis, S., Brezina, M., Castelnuovo, P., and Drago, L. (2016) The role of hyaluronan in the pathobiology and treatment of respiratory disease. Am J Physiol Lung Cell Mol Physiol. 310, L785-795
4. Tammi, R.H., Passi, A.G., Rilla, K., Karousou, E., Vigetti, D., Makkonen, K., and Tammi, M.I. (2011) Transcriptional and post-translational regulation of hyaluronan synthesis. Febs j. 278, 1419-1428
5. Liu, A.M., Lo, R.K., Wong, C.S., Morris, C., Wise, H., and Wong, Y.H. (2006) Activation of STAT3 by G αs distinctively requires protein kinase A, JNK, and phosphatidylinositol 3-kinase. J Biol Chem. 281, 35812-35825
6. Shimazaki, A., Nakagawa, T., Mitoma, J., and Higashi, H. (2012) Gangliosides and chondroitin sulfate desensitize and internalize B2 bradykinin receptors. Biochem. Biophys. Res. Commun. 420, 193-198.

＜学会発表＞

・**β2 アドレナリン受容体シグナルによるヒアルロン酸合成の上昇**

黒田喜幸、中川哲人、東 秀好

第 38 回日本糖質学会年会，名古屋，2019 年 8 月，要旨集 p.154

・**ガングリオシドとコンドロイチン硫酸刺激によるブラジキニン B2 受容体の不応化制御機構**

石井孝和，黒田喜幸，中川哲人，東 秀好

第 13 回 東北糖鎖研究会，新潟，2019 年 9 月，要旨集 p.53

＜細胞制御学部門＞
教授　　顧 建国
准教授　福田 友彦
講師　　伊左治 知弥

糖鎖修飾の特異性と受容体の機能制御

一般的に、糖タンパク質は小胞体やゴルジ体のオルガネラにおいて糖鎖で修飾され、適切な場所に運ばれ機能するとよく知られているが、その詳細な分子機序は必ずしも明らかになっていない。インテグリンはα鎖とβ鎖から成るヘテロ二量体で、主に細胞外マトリックス（ECM）への細胞接着を媒介する膜貫通型糖タンパク質で、細胞内タンパク質のチロシンリン酸化や低分子量 GTP 結合タンパク質の活性化を通じて細胞内骨格系の再編成や増殖･分化のシグナル伝達に深く関わる。また、インテグリンと細胞増殖因子受容体との相互作用は、細胞の増殖・移動・生存などの生理的な過程のみならず、がん細胞の増殖・転移･浸潤など病理的な過程にも重要な役割を担っている。これまで、私達は代表的な細胞接着分子であるインテグリン α5β1 に付加された N-型糖鎖の機能解析を行い、N-型糖鎖が α5β1 のヘテロ二量体の形成や細胞膜上での発現に必須であり、またインテグリンを介する細胞移動･増殖などの機能を特異的に制御することを明らかにした。しかし、その特異性を生じる分子機構に関してはまだ不明である。我々は、シアル酸転移酵素や α1,6 フコース(コアフコース)転移酵素 (Fut8)などの機能に注目し、インテグリン α5β1 やクラス III 受容体チロシンキナーである Fms-Like Tyrosine Kinase 3（FLT3）がモデル分子として、糖鎖修飾の特異性および糖鎖による受容体の機能制御に関して主に以下の 3 点について研究した。

I. N-型糖鎖の α2,3 シアリル化の特異性に関する研究

シアル酸など糖鎖末端に位置する構造は、糖鎖と糖鎖認識分子との直接的な接触の場を形成するため、病態変化や感染･免疫作用において果たす役割が大きい。シアル酸を付加するシアル酸転移酵素はスーパーファミリーを形成しているが、N 型糖鎖に付加されるのは α2,3 と α2,6 結合である。α2,6 結合で付加するのは ST6GAL1 遺伝子 1 種類だが、同じ α2,3 結合を触媒する α2,3 シアル酸転移酵素は ST3GAL3、ST3GAL4 および ST3GAL6 の 3 種の酵素が存在している。このため、α2,3 シアル酸が生体に重要であることは多くの報告から明らかであるにもかかわらず、3 種存在することに意味や、その機能解析は未解明なまま残されている。

この問題にアプローチするため、CRISPER/Cas9 システムを用いて、それぞれ酵素欠損（KO）細胞株を作成した。細胞増殖、コロニー形成能や ERK・AKT な

どシグナル伝達に関わる分子のリン酸化を指標に検討したところ、ST3GAL4-KO は ST3GAL3-KO や ST3GAL6-KO 細胞とは異なる表現型を示した(1)。これは、異なる α2,3 シアル酸転移酵素が同じ細胞内に存在していても、相補していないことを示している。β1 インテグリンや EGFR をモデル標的分子としてより詳細に検討した。興味深いことに、β1 インテグリンの α2,3 シアリル化は ST3GAL4-KO 細胞で低下するのに対して、EGFR の α2,3 シアリル化は ST3GAL6-KO 細胞で低下した（右図)。さらに、ST3GAL6-KO 細胞に 3 つの遺伝子をそれぞれ過剰発現したところ、ST3GAL6 の過剰発現のみが EGFR の α2,3 シアリル化と細胞形態を回復させることができた。同様に、ST3GAL4-KO 細胞に ST3GAL4 を過剰発現させた時のみ β1 のシアリル化が回復した。

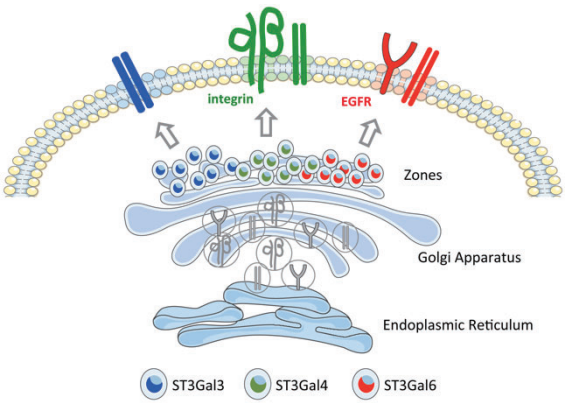

これらの結果は、3 種の α2,3 シアル酸転移酵素がそれぞれ固有の役割をもち、異なる標的タンパク質を修飾していることを明確に示している。哺乳類の複雑な生体システム制御のために、多様なシアル酸転移酵素が必要な理由の解明に繋がる可能性がある。

II. EpCAM がインテグリン β1 と相互作用し癌細胞の接着と移動を制御する

インテグリンやカドヘリンなどの細胞接着分子は細胞の機能や細胞間コミュニケーションに深く関わる。上皮特異的な細胞間接着分子に EpCAM（Epithelial cell adhesion molecule）がある。EpCAM は、多くのがんにおいて高い発現が認められるため、治療標的・診断および予後のマーカーとして注目されている分子であるが、その機能について不明な点が多い。

がん研究のモデル細胞株 7 種(MiaPaCa-2, A431, CW2, 293T, HeLa, MDA-MB-231 および HepG2)の EpCAM 発現を調べたところ、大腸癌細胞株 CW-2 および類上皮癌細胞株 A431 で特に高い発現をみいだした(2)。高発現している細胞における EpCAM の機能を明らかにするため、CRISPER/Cas9 システムを用いて、EpCAM 欠失細胞を作成した。CW-2 細胞や A431 細胞ともに、EpCAM の発現が無くなると、細胞の形態が長く伸びた細胞から丸い形態に変化した。この変化は、EpCAM が細胞接着・伸展を制御することを示している。また、細胞増殖・移動・コロニー形成能の低下と、インテグリンの下流の中心分子である focal adhesion kinase(FAK)や、AKT、ERK など細胞内のシグナル分子のリン酸化も低下した。インテグインと EpCAM の生理的相互作用を調べるため、共免疫沈降法を用いて検討したところ、EpCAM はインテグリン β1 鎖と複合体を形成してい

ることが分かった。さらに、インテグリン β1 鎖とヘテロ二量体を形成しているインテグリン α 鎖の発現を検討したところ、インテグリン α5 鎖の発現が EpCAM 欠損により低下することが分かった。このことは、安定的なインテグリン α5β1 の発現に EpCAM が重要であることを示唆している。以上から、EpCAM の発現と正に相関するがんの治療抵抗性獲得は、EpCAM-インテグリン複合体による細胞機能の制御に関連する可能性が強く示唆された。これは、今後 EpCAM-インテグリン複合体を標的とした新しい抗腫瘍戦略を提案するものであろう。

また、最近、我々はインテグリン α5 鎖のみならず、β1 鎖上の EGFR と結合する糖鎖付加部位の同定に成功した(3)。これらの結果は、膜上のインテグリンを介する複合体の形成機序の解明に役に立つと考えられる。

III. FLT3 を介したシグナル伝達経路活性化における Fut8 の機能

Fms-Like Tyrosine Kinase 3（FLT3）はクラス III 受容体チロシンキナーゼファミリーのメンバーに属する糖タンパク質で、急性骨髄性白血病（AML）患者の約 3 分の 1 に活性化変異が認められる。FLT3 はリガンドの結合により、二量体化・自己リン酸化が生じるが、活性化変異ではリガンド非存在下でも恒常的に活性化される。細胞は病的状態に陥ると、正常とは異なった構造を持つ糖鎖が生成することが知られているので、本研究では FLT3 の細胞外ドメインに付加された N 型糖鎖に焦点を当てた解析を行った。野生型（WT）、膜貫通ドメインの近傍に見られる内部タンデム重複（ITD）、および FLT3 のチロシンキナーゼドメイン（TKD）の活性化変異体の N 結合型糖鎖の構造が異なることを見出した(4)。興味深いことに、IL-3 依存性 pro-B 細胞株 Ba/F3 に WT または変異体 FLT3 遺伝子を導入したところ、細胞のコアフコシル化を大きく誘導した。 FLT3 を介したシグナル伝達におけるコアフコシル化の機能を解明するために、CRISPR / Cas9 システムを使用して、コアフコシル化酵素である Fut8 を欠損させたノックアウト（KO）Ba/F3 細胞を確立し FLT3 遺伝子を導入したところ、驚くべきことに、FLT3-WT を発現させた KO 細胞は IL-3 非依存的に細胞増殖を引き起こした（右図）。IL-3 非存在下での Ba/F3 細胞の増殖は FLT3 の活性化と明確な相関を示すことから、この増殖は発現させた野生型 FLT3 がコアフコシルされていないことによることを示唆している。Fut8KO 細胞に発現させた野生型 FLT-3(FLT3-WT)は、下流である STAT5、AKT および ERK シグナル伝達経路を活性化させ、細胞のチロシンリン酸化レベルを大幅に増

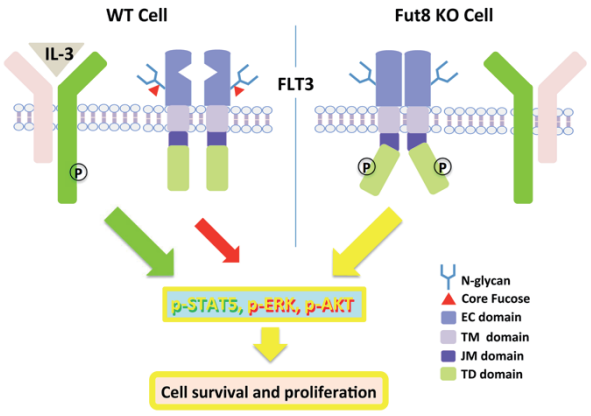

加させた。これらの活性化は、Fut8 の発現を回復させることで消失した。さらに、チロシンキナーゼ阻害剤を添加したところ、Fut8KO またはフコシル化阻害剤によって誘導される細胞増殖が阻害された。コアフコシル化による FLT3 の活性化の機構を明らかにするため、抗 FLT3 抗体を用いて発現部位を検討したところ、FLT3-WT 細胞と同じ発現パターン、すなわち主に細胞表面に発現していて、発現部位に変化は認められなかった。そこで、FLT3 のリガンド非存在下でも FLT3 が二量体化・自己リン酸化にできるか検討したところ、Fut8KO 細胞ではリガンド刺激なしで FLT3 の二量体形成が誘導されていることを明らかにした。

本研究は、コアフコシル化が FLT3 の活性化の調節機能に深くかかわっていることを示した。この知見はコアフコシル化の制御による AML の治療に有効な薬剤の開発に価値ある方向性を提供するものであろう。

＜発表論文＞

1. ST3GAL3, ST3GAL4, and ST3GAL6 differ in their regulation of biological functions via the specificities for the α2,3-sialylation of target proteins. Qi, F., Isaji, T., Duan, C., Yang, J., Wang, Y., Fukuda, T. and Gu, J. ***FASEB J***., 34: 881-879. 2020
2. EpCAM associates with integrin and regulates cell adhesion in cancer cells. Yang, J., Isaji, T., Zhang, G., Qi, F., Duan, C., Fukuda, T. and Gu, J. ***Biochem Biophys Res Commun.*** doi: 10.1016/j.bbrc.2019.11.152., 2019
3. Identification of the minimal N-glycosylation on integrin α5β1 required for its inhibitory effect on EGFR signaling and cell proliferation. Hou, S., Hang, Q., Isaji, T., Fukuda, T. and Gu, J. ***Biochem Biophys Res Commun.*** doi: 10.1016/j.bbrc.2019.11.188., 2019
4. Deficiency of core fucosylation activates cellular signaling dependent on FLT3 expression in a Ba/F3 cell system. Duan, C., Fukuda, T., Isaji, T., Qi, F., Yang, J., Wang, Y., Takahashi, S. and Gu, J. ***FASEB J***., doi: 10.1096/fj.201902313RR. 2020
5. Core Fucosylation of Maternal Milk N-glycan Evokes B Cell Activation by Selectively Promoting the L-fucose Metabolism of Gut Bifidobacterium spp. and Lactobacillus spp. li, M., Bai, Y., Zhou, J., Huang, W., Yan, J., Tao, J., Fan, Q., Liu, Y., Mei, D., Yan, Q., Yuan, J., Malard, P., Wang, Z., Gu, J., Taniguchi, N. and Li, W. ***MBio.*** doi: 10.1128/mBio.00128-19, 2019
6. Establishment and characterization of a fucosylated protein-specific mAb for fucosylated α-fetoprotein: a potential application for clinical research. Egashira1, Y., Suganuma, M., Kataoka, Y., Higa, Y., Ide, N., Kamada, Y., Gu, J., Fukagawa1, K. and Miyoshi, E. *Sci Rep.* 9:12359. doi: 10.1038/s41598-019-48821-x. 2019
7. Ablation of core fucosylation attenuates the signal transduction via T cell receptor to suppress the T cell development. Liang, W., Mao, S., Li, M., Zhang, N., Sun, S., Fang, H., Zhang, J., Gu, J., Wang, J. and Li, W. Mol Immunol. 112:312-321. doi: 10.1016/j.molimm.2019.06.011., 2019

＜学会発表＞

- **Functions of glycosylation in cell adhesion and EMT of cancer cells**
  顧建国,中国科学院過程工程研究所・生化工程国家重点実験拠点研究講座，北京市，2019 年 3 月
- **PTM of glycosylation in cell adhesion and EMT of cancer cells and diseases**
  顧建国,北京大学・生命科学学院学術セミナー，北京市，2019 年 3 月
- **Glycosylation in cancer cells and diseases**
  顧建国,天津医科大学・基礎医学院学術セミナー，天津市，2019 年 3 月
- **Significance of core fucosylation in brain and its relationship with diseases**
  顧建国
  2019 International Academic Forum on Neuroinflammation and Psychopharmacology, 南通市, 2019 年 5 月，要旨集 p.6
- **糖鎖修飾によるインテグリンの選別輸送ゾーンの制御とその分子機序の解明**
  顧建国
  第 2 回オルガネラゾーン 研究会，東京, 2019 年 5 月
- **Glycosylation in cell adhesion and EMT of cancer cells and diseases**
  顧建国
  International Brain Workshop 2019 in Sendai: Molecular Basis and Therapeutics for Intractable Neuropsychiatry Diseases，仙台市, 2019 年 8 月，要旨集 p.14
- **細胞内外の糖鎖発現とインテグリン機能とその制御**
  顧建国，伊左治知弥，福田友彦
  第 38 回日本糖質学会年会，名古屋，2019 年 8 月，要旨集 p.131
- **PI4KIIα とインテグリン α3β1 の複合体形成による *N*-型糖鎖調節**
  伊左治知弥，任翔壎，亀山昭彦[a]，福田友彦，顧建国
  (国立研究開発法人産業技術総合研究所 生命工学領域[a])
  第 38 回日本糖質学会年会，名古屋，2019 年 8 月，要旨集 p.132
- **α1,6 フコシルトランスフェラーゼ(Fut8)欠損によるグリア細胞の活性化**
  福田友彦、庄子隼人、陸需、張冬梅、伊左治知弥、顧建国
  第 38 回日本糖質学会年会，名古屋，2019 年 8 月，要旨集 p.210
- **癌細胞における PI4KIIα とインテグリン α3β1 の複合体形成による *N*-型糖鎖の調節**
  伊左治知弥，任翔壎，亀山昭彦[a]，福田友彦，顧建国
  (国立研究開発法人産業技術総合研究所 生命工学領域[a])
  第 13 回東北糖鎖研究会，新潟, 2019 年 9 月，要旨集 p.20
- **ST3GAL3, ST3GAL4, and ST3GAL6 differ in their regulation of biological functions via the specificities for the α2,3-sialylation of target proteins**
  Feng Qi, Tomoya Isaji, Chengwei Duan, Jie Yang, Yuqin Wang,
  Tomohiko Fukuda and Jianguo Gu

第 13 回東北糖鎖研究会, 新潟, 2019 年 9 月, 要旨集 p.58

・**PI4KIIα とインテグリン α3β1 の複合体形成による癌細胞における N-型糖鎖の調節**

伊左治知弥, 任 翔壎, 亀山昭彦 [a], 福田友彦, 顧建国

（国立研究開発法人産業技術総合研究所 生命工学領域 [a]）

第 92 回日本生化学会大会，横浜，2019 年 9 月，演題番号 P-0191，T10m-02

・**コアフコースによるグリア細胞過活性化の抑制**

福田友彦, 庄子隼人, 陸需, 張冬梅, 伊左治知弥, 顧建国

第 92 回日本生化学会大会，横浜，2019 年 9 月，演題番号 3P-008

・**Functional N-glycosylation in cell adhesions**

顧建国

The 5th China-Australia conference on Immunity in Tuberculosis & Wuhan University Famous Medical Scientists Forum，武漢市，2019 年 11 月，要旨集 p13

・**A novel regulatory mechanism of N-glycan sialylation by the GOLPH3-PI4K-Integrin complex in cancer cells**

顧建国

The 11th International Symposium of Tumor Biological Diagnosis and Therapy in Nanjing，南京市，2019 年 11 月，要旨集 p90

・**PI4KIIα とインテグリン α3β1 の複合体形成による新たな N-糖鎖制御メカニズム**

伊左治知弥, 福田友彦, 顧建国

第２回オルガネラゾーン 若手の会, 東京, 2019 年 11 月, 要旨集 P17

・**糖鎖修飾によるインテグリンの選別輸送ゾーンの制御について**

顧建国, 伊左治知弥, 福田友彦, 戸島拓郎 [a], 中野明彦 [a]

(理化学研究所 光量子工学研究センター[a])

第 3 回オルガネラゾーン 研究会, 東京, 2019 年 11 月, 要旨集 P2

・**Regulation of integrin functions by N-glycosylation**

顧建国

第４２回日本分子生物学会年会， 福岡, 2019 年 12 月, 要旨集 P175

・**A novel regulatory mechanism of N-glycan sialylation by the GOLPH3-PI4K-Integrin complex in cancer cells**

顧建国

The first Academia Sinica-Tohoku Medical and Pharmaceutical University (TPMU) Joint Symposium on Glycoscience, Academia Sinica, Taipei, 2019 年 12 月

Received: 16 July 2019 | Revised: 23 September 2019 | Accepted: 30 September 2019

DOI: 10.1096/fj.201901793R

RESEARCH ARTICLE

THE FASEB JOURNAL

ST3GAL3, ST3GAL4, and ST3GAL6 differ in their regulation of biological functions via the specificities for the α2,3-sialylation of target proteins

Feng Qi[1,2] | **Tomoya Isaji**[1] | **Chengwei Duan**[1] | **Jie Yang**[1] | **Yuqin Wang**[3] | **Tomohiko Fukuda**[1] | **Jianguo Gu**[1]

[1]Division of Regulatory Glycobiology, Institute of Molecular Biomembrane and Glycobiology, Tohoku Medical and Pharmaceutical University, Sendai, Japan

[2]Department of Pharmacy, The Fourth Affiliated Hospital of Nantong University, Yancheng, China

[3]Department of Pharmacology, Pharmacy College, Nantong University, Nantong, China

Correspondence
Jianguo Gu, Division of Regulatory Glycobiology, Institute of Molecular Biomembrane and Glycobiology, Tohoku Medical and Pharmaceutical University, 4-4-1 Komatsushima, Aoba-ku, Sendai, Miyagi 981-8558, Japan.
Email: jgu@tohoku-mpu.ac.jp

Funding information
MEXT | Japan Society for the Promotion of Science (JSPS), Grant/Award Number: 15H04354, 19H03184 and 19K07049; National Natural Science Foundation of China (NSFC), Grant/Award Number: 31670807; Science and Technology Project from Jiangsu Traditional Chinese Medicine Bureau, Grant/Award Number: YB2017072; Ministry of Education, Culture, Sports, Science and Technology (MEXT), Grant/Award Number: 18H04868

Abstract

The α2,3-sialylation of N-glycans is considered important but complicated because the functions of the three β-galactoside α2,3-sialyltransferases, ST3GAL3, ST3GAL4, and ST3GAL6, could be compensating for one another. To distinguish their specific functions, we established each individual knockout (KO) cell line. Loss of either the ST3GAL3 or ST3GAL6 genes decreased cell proliferation and colony formation, as opposed to the effect in the ST3GAL4 KO cells. The phosphorylation levels of ERK and AKT were significantly suppressed in the ST3GAL6 KO and ST3GAL3 KO cells, respectively. The cell aggregations were clearly observed in the KO cells, particularly the ST3GAL3 KO and ST3GAL6 KO cells, and the expression levels of E-cadherin and claudin-1 were enhanced in both those cell lines, but were suppressed in the ST3GAL4 KO cells. Those alterations were reversed with an overexpression of each corresponding gene in rescued cells. Of particular interest, the α2,3-sialylation levels of β1 integrin were clearly suppressed in the ST3GAL4 KO cells, but these were increased in the ST3GAL3 KO and ST3GAL6 KO cells, whereas the α2,3-sialylation levels of EGFR were significantly decreased in the ST3GAL6 KO cells. The decrease in α2,3-sialylation increased the α2,6-sialylation on β1, but not EGFR. Furthermore, a cross-restoration of each of the three genes in ST3GAL6 KO cells showed that overexpression of ST3GAL6 sufficiently rescued the total α2,3-sialylation levels, cell morphology, and α2,3-sialylation of EGFR, whereas the α2,3-sialylation levels of β1 were greatly enhanced by an overexpression of ST3GAL4. These results clearly demonstrate that the three α2,3-sialyltransferases modify characteristic target proteins and regulate cell biological functions in different ways.

KEYWORDS

EGFR, glycoproteins, N-glycan, integrin β1, α2,3-sialyltransferase

Abbreviations: BSA, bovine serum albumin; ConA, concanavalin A; CRISPR/Cas-9, clustered regularly interspaced short palindromic repeats/caspase-9; DMEM, Dulbecco's modified Eagle's medium; DOX, doxycycline; EGFR, epidermal growth factor receptor; FBS, fetal bovine serum; KO, knockout; MAM, Maackia amurensis lectin; RES, rescued cell; SSA, Sambucus sieboldiana agglutinin; ST3GAL3, β-galactoside α2,3-sialyltransferase 3; ST3GAL4, β-galactoside α2,3-sialyltransferase 4; ST3GAL6, β-galactoside α2,3-sialyltransferase 6; ST6GAL1, β-galactoside α2,6-sialyltranferase 1; WT, wild type.

1 | INTRODUCTION

N-Glycan biosynthesis is complex and involves many enzymes in the endoplasmic reticulum (ER) and the Golgi apparatus, but small numbers of enzymes found in the Golgi apparatus are responsible for branching and extending, as well as for sialylation.[1] In mammals, sialic acids usually serve as the terminal monosaccharides of the glycans in glycoproteins and glycolipids.[2,3] β-Galactoside α2,3-sialyltransferase1 (ST3GAL1) and ST3GAL2-6 and β-galactoside α2,6-sialyltransferase 1 (ST6GAL1) and ST6GAL2 in the Golgi apparatus are responsible for the syntheses of Neu5Ac(α2,3)Gal and Neu5Ac(α2,6)Gal.[4] ST3GAL1 and ST3GAL2 are almost exclusively used in the type III disaccharide Galβ1-3GalNAc that is found in O-glycans and glycolipids.[5] ST3GAL5 is almost exclusively used in lactosyl-ceramide as an acceptor substrate for GM3 production, which is also known as GM3-synthase.[6] In particular, ST3GAL3, ST3GAL4, and ST3GAL6 are known to be involved in the synthesis of N-glycans terminated with Neu5Ac(α2,3)Gal.[7] On the other hand, ST6GAL1 appears to play an important role in the synthesis of N-glycans terminated with Neu5Ac(α2,6)Gal in many kinds of cells and tissues.[8-10] There is ample evidence that sialic acids are important bioinformatic molecules, which play pivotal roles in biological, pathological, and immunological processes through modifying glycoproteins and glycolipids on the cell surface, including nervous system embryogenesis,[11] cell-cell interactions,[12,13] signal transduction,[14] bacterial and viral infection,[15,16] etc

In addition, sialic acids on cell membranes are closely related to tumor invasion and metastasis.[17,18] Many studies have shown that the expression of ST6GAL1 is increased in diverse carcinomas, which may highly correlate with tumor progression. For example, ST6GAL1 regulates macrophage apoptosis by controlling the α2,6-sialylation of tumor necrosis factor receptor-1.[19] ST6GAL1 is up-regulated in colon carcinoma, and its metastasis and poor prognosis is ascribed to sialylation of the Fas death receptor by ST6GAL1 that provides protection against Fas-mediated apoptosis.[20] Moreover, differentiation of human dendritic cells is accompanied by an increased expression of sialylated glycans, mainly through the activities of ST3GAL1 and ST6GAL1.[21] However, among the six enzymes of α2,3-sialyltransferases, ST3GAL3, ST3GAL4, and ST3GAL6 participate mainly in the generation of NeuAcα2,3Galβ3/4GlcNAc, which is the precursor of sLe^a or sLe^x,[22,23] two important tumor-associated sialylated glycoconjugates.[24-26] In fact, the increased sialylation and expressions of these sialyltransferases genes in cervical cancer were also reported.[27-31] Therefore, study of the expression and biological functions of ST3GAL3, ST3GAL4, and ST3GAL6 in tumors is of great importance.

Until now, several reports have chronicled the functions of these cells in various types of tumors. For example, the expression of ST3GAL3 has been associated with tumor progression, differentiation, and metastasis in extrahepatic cholangiocarcinoma,[32] and secondary tumor recurrence in gastric cancer.[33] ST3GAL6 is known to promote cell adhesion and migration of multiple myeloma cells by increasing the synthesis of selectin ligands, and a knockdown of ST3GAL6 has reduced the ability of multiple myeloma cells to home in the bone marrow, which prolonged the rate of survival in a xenograft mouse model.[34] On the other hand, there has been no consensus on the clinical significance of ST3GAL4. Some researchers reported a decrease in ST3GAL4 mRNA expression in gastrointestinal and ovarian cancer,[35,36] while others have shown significant increases in cervical intraepithelial neoplasia, colorectal cancer, and pancreatic adenocarcinoma tissues.[37-39] These different phenomena are yet to be clearly explained. ST3GAL3, ST3GAL4, and ST3GAL6 show a similar enzymatic substrate specificity in catalyzing the transfer of sialic acid on the terminal Gal residue of the disaccharide Galβ1-3/4GlcNAc of glycoproteins,[40] which makes it plausible that the α2,3-sialylation modification of glycoproteins represents a co-involvement and/or a compensation. As mentioned above, the tissue and tumor-specific expressions of these enzymes have been extensively reported either by comparing their contents in cancer tissues, as well as in the tissues adjacent to cancers,[41-43] or by investigating their overexpressions or the knockdown of a single gene.[34,39,44] Such approaches, however, are insufficient to explain the biological functions of α2,3-sialylation, and its underlying molecular mechanisms.

To distinguish the respective functions of ST3GAL3, ST3GAL4, and ST3GAL6, we used the clustered, regularly interspaced, short palindromic repeats/caspase-9 (CRISPR/Cas-9) system[45] to establish individual gene knockout (KO) HeLa cell lines, and restored the KO cells with the same or different genes to compare their functions. We found that the three enzymes differed in their modification of the α2,3-sialylation of target proteins and in the distinct biological functions each plays in cell adhesion, cell growth, and colony formation.

2 | MATERIALS AND METHODS

2.1 | Antibodies and reagents

The experiments were performed with the following antibodies: rabbit mAbs against Claudin-1 (#13255T), epidermal growth factor receptor (EGFR) (#3777), ERK1/2 (#4695S), phospho-ERK1/2 (#4370S), AKT (#9272), and phospho-AKT (#4060) were obtained from Cell Signaling Technology; mouse mAbs against E-cadherin (#610182), N-cadherin (#610920) and β1 integrin (#610468) were from BD Biosciences; mouse mAbs against α-tubulin (#T6199)

and FLAG (#F1804) was from MilliporSigma; rabbit mAbs against GAPDH (FL-335, #SC-25778) were from Santa Cruz Biotechnology, Inc Alexa Fluor 647 goat anti-mouse IgG and streptavidin were obtained from Thermo Fisher Scientific; Alexa Fluor 488 conjugated anti-mouse (#A11029) was from Invitrogen; Alexa Fluor 568 phalloidin (#A12380) and TO-PRO-3 (#T3605) was from Molecular Probes. The peroxidase-conjugated secondary antibody against rabbit (#7074S) was obtained from Cell Signaling Technology; peroxidase-conjugated secondary antibodies against mouse (#AP124P) were from MilliporeSigma; Maackia amurensis (MAM) lectin (#BA-s7801-2) was from EY Laboratories, Inc; Concanavalin A (ConA) lectin (#B-1005) from Seikagaku Corporation; MAM-Agarose (J310) and SSA-Agarose (J318) were from J-OIL MILLS, Inc An ABC kit was acquired from Vector Laboratories; doxycycline hyclate (DOX) (#D9891) was from Sigma-Aldrich; PrimeScript RT reagent Kit with gDNA Eraser (Perfect Real Time) (#RR047A) was from Takara, Japan; Quick Taq HS DyeMix (DTM-101) was from TOYOBO, Japan.

2.2 | Cell lines and cell culture

The HeLa and 293T cell lines (RIKEN Cell Bank, Tsukuba, Japan) were cultured at 37°C in Dulbecco's modified Eagle's medium (DMEM) with 10% fetal bovine serum (FBS), in a humidified atmosphere containing 5% CO2, except for the virus production.

2.3 | Genomic deletion of ST3GAL3, ST3GAL4, or ST3GAL6 in HeLa cells

The pSpCas9(BB)-2A-GFP (PX458) plasmid and pSpCas9(BB)-2A-Puro (PX459) V2.0 plasmid were purchased from Addgene (PX458:Addgene plasmid #48138, PX459:Addgene plasmid #62988) and were deposited by Dr Feng Zhang.[45] The target site on human ST3GAL4 exon 8 (TTGAACAATGCCCCAGTGGC), as previously described,[46] was cloned into PX458. The target site on human ST3GAL3 exon 8 (TGCCGCCGCTGCATCATCGT) and ST3GAL6 exon 5 (CTATGGGATGAGAACATCAG), which were designed by guide design tool (https://zlab.bio/guide-design-resources/), were cloned into PX459. The three kinds of KO cell lines were created by electroporating cells with the vectors containing the target sequences, according to the manufacturer's recommendations (Amaxa cell line Nucleofector kit; Lonza, Basel, Switzerland). One day post-transfection, the cells transfected with ST3GAL3 KO or ST3GAL6 KO plasmid and were selected with 1 μg/mL puromycin for 48 hours. After further incubation for 5 days, the cells were subjected to fluorescence-activated cell sorting (FACS) to isolate low MAM-binding transfectants. Stable KO cells were cloned by a limiting dilution. For isolation of ST3GAL4 KO cells, 3 days post-transfection, the cells were subjected to FACS to isolate cells that highly expressed GFP. Stable clones were isolated by a limiting dilution. The α2,3-sialylation levels were confirmed by flow cytometry and Western blotting using MAM lectin.

2.4 | ST3GAL3, ST3GAL6, and GFP-tagged E-cadherin expression vectors

We used the Gateway cloning system from Invitrogen for all overexpression experiments. The cDNAs of human ST3GAL3 and ST3GAL6 were kindly provided by Dr H. Narimatsu (National Institute of Advanced Industrial Science and Technology, Japan). The Gateway entry vectors were constructed as described previously.[47] In brief, using LR clonase (Invitrogen), the sub-cloned cDNAs in entry vectors were transferred into CSIV-TRE-RfA-CMV-KT for the doxycycline hyclate inducible overexpression. To express GFP-tagged E-cadherin, expression vector pEGFP-N1-E-cadherin-GFP was transfected using PEI MAX (molecular mass, 40 kDa; Polysciences Inc) as previously described.[48]

2.5 | Virus production and infection

The virus production and infection was performed as described previously.[47,49,50] Briefly, ST3GAL4 overexpression viruses were prepared as previously described.[47] To prepare the ST3GAL3 and ST3GAL6 overexpression viruses, the lentivirus vectors (CSIV-TRE-RfA-CMV-KT) were transfected into 293T cells with packaging plasmids via PEI MAX. The target cells were cultured for 24 hours to obtain virus media for infection. After infection for 72 hours, cells were selected using FACSAria II (BD bioscience) to obtain Kusabira Orange-positive cells (CSIV-TRE-RfA-CMV-KT). Stable clones were also isolated using a limiting dilution. The stable cells that expressed Kusabira Orange-positive in fluorescence microscopy were chosen and used in subsequent studies.

2.6 | Western blot and immunoprecipitation

Western blot and immunoprecipitation were performed as described previously with minor modifications.[47,48] In brief, the indicated cells were rinsed twice with ice-cold PBS and then lysed in a cell lysate buffer (20 mM Tris-HCl, pH 7.4, 150 mM NaCl, 1% Triton X-100) that included protease and phosphatase inhibitors (Nacalai Tesque, Kyoto, Japan) for 30 min. The protein concentrations of lysates were

determined via BCA assay (Pierce). Equal amounts of cell lysates from each sample were resolved by SDS-PAGE. Then, the proteins were transferred to PVDF membranes (MilliporeSigma) and detected with primary and secondary antibodies, and visualized by the Immobilon Western Chemiluminescent HRP Substrate (MilliporeSigma), according to the manufacturer's instructions. For immunoprecipitates, equal amounts of protein lysates from each sample were immunoprecipitated with MAM-agarose or Sambucus sieboldiana Agglutinin (SSA)-agarose, which specifically recognizes α2,3 or α2,6 sialylation, respectively, for 1 hour at 4°C with rotation, and then the immunoprecipitates were washed twice with lysis buffer and subjected to SDS-PAGE. The precipitated glycoproteins were detected using different antibodies.

2.7 | Cell growth and colony formation analysis

The cell growth curves and colony formation assays were performed as described previously with minor modifications.[51,52] In brief, to assay cell growth, the cells (5×10^4) were seeded in six-well culture dishes overnight and then serum starved for 24 hours. After starvation, the cells were supplied with DMEM containing 10% FBS. Cells in the same areas on the cultured dishes were photographed and counted at the indicated times (0, 24, 48, and 72 hours), the folds of change in cell numbers were normalized to those at 0 hour and statistically analyzed. To assay the colony formation, cells (500/per well) were seeded in 6-cm dishes in DMEM containing 10% FBS, incubated at 37°C and the cultured media were changed twice weekly. After incubation for 14 days, the formed colonies were stained with 0.25% crystal violet, and images were taken. Colonies containing more than 50 cells were counted and analyzed statistically from three independent wells of each sample.

2.8 | Flow cytometry analysis

Flow cytometric analysis was performed as described previously with minor modifications.[53,54] Briefly, the indicated semi-confluent cells were detached from the culture dishes using trypsin containing 1 mM EDTA and were subsequently stained with or without the primary biotinylated MAM, followed by incubation with Alexa Fluor 647-conjugated streptavidin. After washing three times with PBS, flow cytometric analysis was performed using a FACSCalibur flow cytometer and Cell Quest Pro software (BD Biosciences).

2.9 | Immunofluorescence

Immunofluorescence staining was performed as described previously with minor modifications.[51,52] In brief, cells were cultured on glass-bottom dishes, rinsed twice with PBS and fixed with 4% paraformaldehyde for 20 min. A nonspecific blocking solution was applied (PBS, 0.1% Triton X-100, 10% BSA) at room temperature for 1 hour. N-cadherin antibodies were used and followed by incubation with anti-mouse Alexa Fluor 488 secondary antibodies (Invitrogen) and Alexa Fluor 568 phalloidin (Invitrogen), and then incubated with TO-PRO-3 for 20 min in the dark. After transfection for 48 hours, those cells overexpressed GFP-tagged E-cadherin were rinsed twice with PBS and fixed with 4% paraformaldehyde for 20 min, and incubated with TO-PRO-3 for 20 min in the dark. Fluorescence images were observed via confocal microscopy using a FluoView FV1000 (Olympus, Tokyo, Japan).

2.10 | RT-PCR for detection of mRNA expression levels

Total RNAs of all cell lines listed in Figure 1A were prepared with TRI reagent (Invitrogen), and 1 μg of total RNA was reverse-transcribed using a PrimeScript RT reagent kit with gDNA Eraser according to the manufacturer's instructions. The primers for KO confirmation were designed around the KO regions. The sequences of those primers are shown in Table 1. The glyceraldehyde-3-phosphate dehydrogenase (GAPDH) mRNA was used as a control in PCR runs, and the reaction products obtained were subjected to electrophoresis using 2% agarose gels containing ethidium bromide.

2.11 | Cell aggregation assay

Cell aggregation assay was performed as described previously.[55] Briefly, cells (2×10^5 cells/mL) were resuspended in DMEM containing 1% BSA with or without 2 mM EDTA. For each condition, 1 mL of the cell suspension was added to a 15-mL tube, which was followed by incubation in a rotator (MACSmixTube Rotator; Miltenyi Biotec, Bergisch-Gladbach, Germany) at 12 rpm for 6 hours at 37°C. The cell suspensions were placed in six-well plates and the field of vision was randomly selected for photography. Cell aggregation assays were performed using three independent wells for each sample.

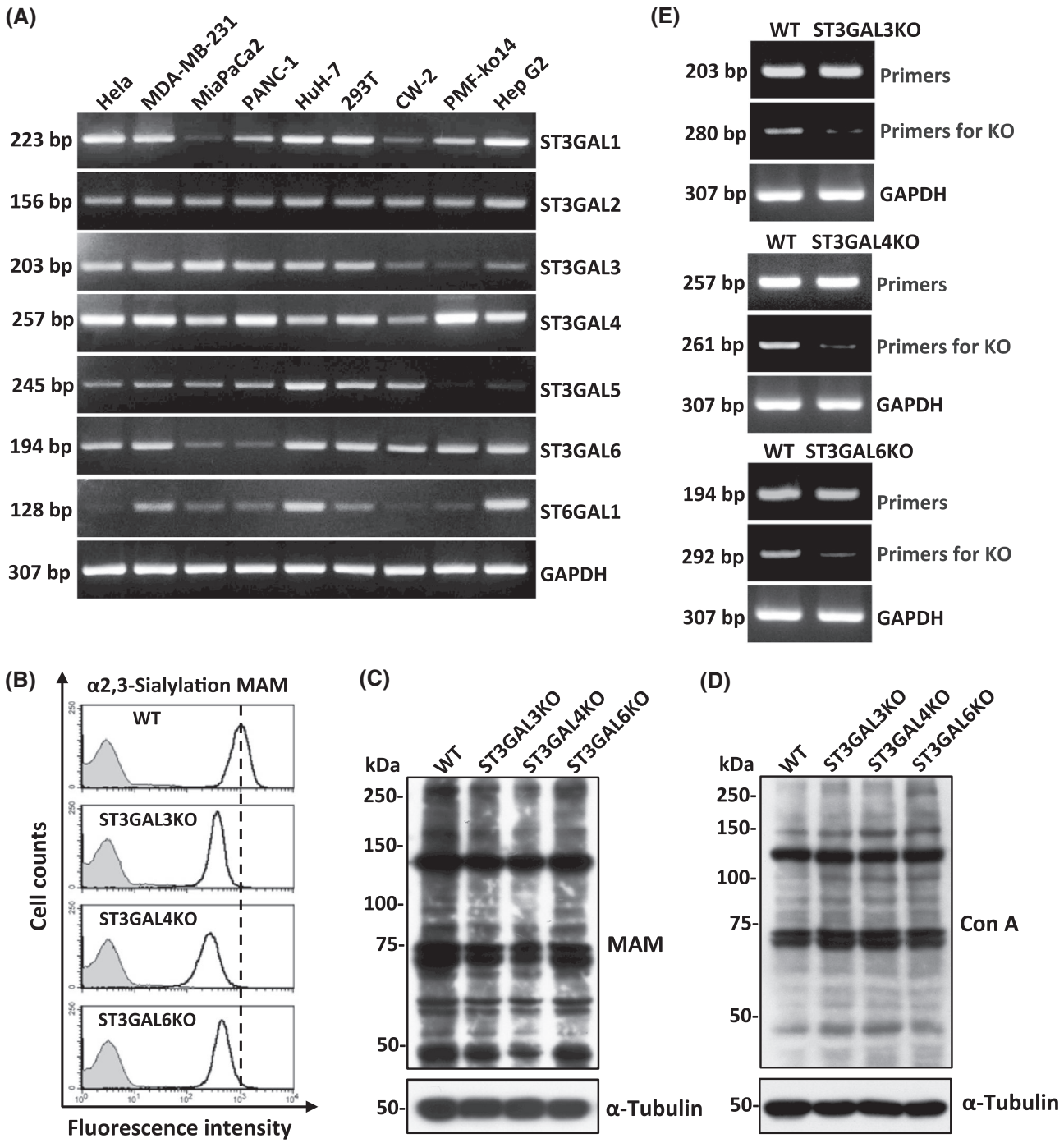

FIGURE 1 Abatement of α2,3-sialylation in ST3GAL3, ST3GAL4, or ST3GAL6 KO cells. A, The mRNA expression levels of α2,3-sialyltransferases (1-6) and α2,6-sialyltransferase (ST6GAL1) in nine cell lines were detected by RT-PCR. GAPDH was used as a control. B, WT and three kinds of KO HeLa cells were collected and incubated with (bold line) or without (grey shadow) MAM lectin, which specifically recognizes sialic acid α2,3 galactose, followed by incubation with Alexa Fluor 647 streptavidin subjected to flow cytometric analysis. The vertical dashed line indicates the peak reacted with MAM lectin in WT cells. Equal amounts of cell lysates from WT and the three types of KO cells were immunoblotted with MAM lectin (C) and ConA lectin (D), which preferentially recognizes high-mannose N-glycans. α-Tubulin was used as a loading control. E, Comparison of the mRNA expression levels using RT-PCR between WT and KO cells. The results obtained from using the normal primers and GAPDH were used as controls

2.12 | Statistical analysis

All data are expressed as the mean ± standard derivation. Statistical analyses were performed using either a Student's *t* test or one-way analysis of variance (ANOVA) by GraphPad Prism version 5 (GraphPad Software, La Jolla, CA, USA). Statistical significance was defined as $P < .05$ (*$P < .05$; **$P < .01$; ***$P < .001$).

TABLE 1 Primer sequences and annealing temperatures for RT-PCR

Gene names	Sense primer (5′–3′)	Antisense primer (5′–3′)	Annealing temperature (°C)
I. Primers for detection of expression levels			
ST3GAL1	GACTTGGAGTGGGTGGTGAG	ACAAGTCCACCTCATCGCAG	57
ST3GAL2	CTCTCGGGCAAGAGCTGTG	CTGCAGCATCATCCACCACC	59
ST3GAL3	CTATGACATTGTGGTGAGACTGA	CTCTCTCCTTGTAGACGATGTATTT	51
ST3GAL4	TGAGGGTGGCCCGAGG	CCGGGAGTAGTTGCCAAAGA	59
ST3GAL5	CCAATGCCAAGTGAGTACACC	TGAGCTCTCTTTACATGGTCAGG	57
ST3GAL6	AGGTGGCTGTTGGAATTGT	GTTGTTGGGTGTTTAGGTTTCTG	51
ST6GAL1	GAAAAATGGGCCTTGGCCTG	GAGCAGGAAAACAAGCCTGC	57
E-cadherin	CGTAGCAGTGACGAATGTGGTAC	AACTGGAGAACCATTGTCTGTAGC	59
GAPDH	CGGAGTCAACGGATTTGGTCGTA	AGCCTTCTCCATGGTGGTGAAGAC	57
II. Primers for KO confirmation			
ST3GAL3	CCGCCGCTGCATCATCGT	TGCACTCACTCTCTCCTTGTAGAC	68
ST3GAL4	GAACAATGCCCCAGTGGC	GGGTTGAGAATCCGAATCTGTTTAG	66
ST3GAL6	CCCTATGGGATGAGAACATCAG	TAGGGTCATTGTGAATAGGATCTG	66

3 | RESULTS

3.1 | KOs of the ST3GAL3, ST3GAL4, or ST3GAL6 genes reduced α2,3-sialylation

To investigate the roles of α2,3-sialylation on N-glycans, first we screened nine cell lines that included HeLa, MDA-MB-231, MiaPaCa2, PANC-1, HuH-7, 293T, CW-2, PMF-ko14, and Hep G2 cells based on RT-PCR (Figure 1A), to determine a suitable cell line highly expresses α2,3-sialyltransferases (ST3GAL3, ST3GAL4, and ST3GAL6), and marginally expresses ST6GAL1. Using primer sequences (Table 1), we found that the expression levels of mRNA for those three α2,3-sialyltransferases in HeLa cells were relatively higher, whereas α2,6-sialyltransferase (ST6GAL1) was relatively lower than those in the other eight cell lines (Figure 1A). So, we chose the HeLa cell line as a suitable cell model to study. And then to distinguish the specific functions of the three α2,3-sialyltransferases of ST3GAL3, ST3GAL4, and ST3GAL6, we established each single KO cell line using the CRISPR/Cas9 system. As expected, flow cytometric analysis using MAM lectin, which specifically recognizes α2,3-sialylated galactose, showed that the α2,3-sialylation levels were decreased in the ST3GAL3 KO, ST3GAL4 KO, and ST3GAL6 KO cells, compared with that in the wild type (WT) cells. The degree of decrease in α2,3-sialylation seemed to be as follows: ST3GAL4 KO > ST3GAL3 KO > ST3GAL6 KO (Figure 1B). The MAM lectin blot showed a similar tendency (Figure 1C). There were no significant differences in the reactive abilities of ConA lectin, which preferentially recognizes high-mannose types of N-glycans, for either the three KO cells or WT cells (Figure 1D). To further confirm the KO results, we designed these primers for KO confirmation in the KO regions (Table 1). As shown in Figure 1E, compared with using normal primers or GAPDH, the RT-PCR results obtained from using the primers for KO confirmation were clearly lower in three KO cells than those in each of the corresponding WT cells, suggesting that the base sequences in the KO regions of three enzymes were changed. These results suggested that the KOs of the ST3GAL3, ST3GAL4, and ST3GAL6 genes were successful.

3.2 | Comparing cell proliferation and cellular signaling among the ST3GAL3 KO, ST3GAL4 KO, and ST3GAL6 KO cells

We used these KO cell lines to compare cell biological functions. First, we investigated the effects of α2,3-sialyltransferase KO on cell proliferation and found that cell growth was significantly suppressed in the ST3GAL3 KO and ST3GAL6 KO cells, but not in the ST3GAL4 KO cells, compared with the WT cells (Figure 2A). It is notable that the cell growth for ST3GAL4 KO cells seemed to demonstrate a cell density-dependent manner, that is, when cells were cultured at a much lower density, the growth rate of ST3GAL4 KO cells was lower than that of the WT cells, but once cells reached a certain density the growth rate of ST3GAL4 KO cells was significantly increased at a rate that was even faster than that of the WT cells (Figure 2A). To confirm those phenomena, a clonogenic assay was conducted to test the single-cell potential for survival and "unlimited" cell division.[52,56] The ST3GAL3 and ST3GAL6 KO cells consistently formed smaller and fewer

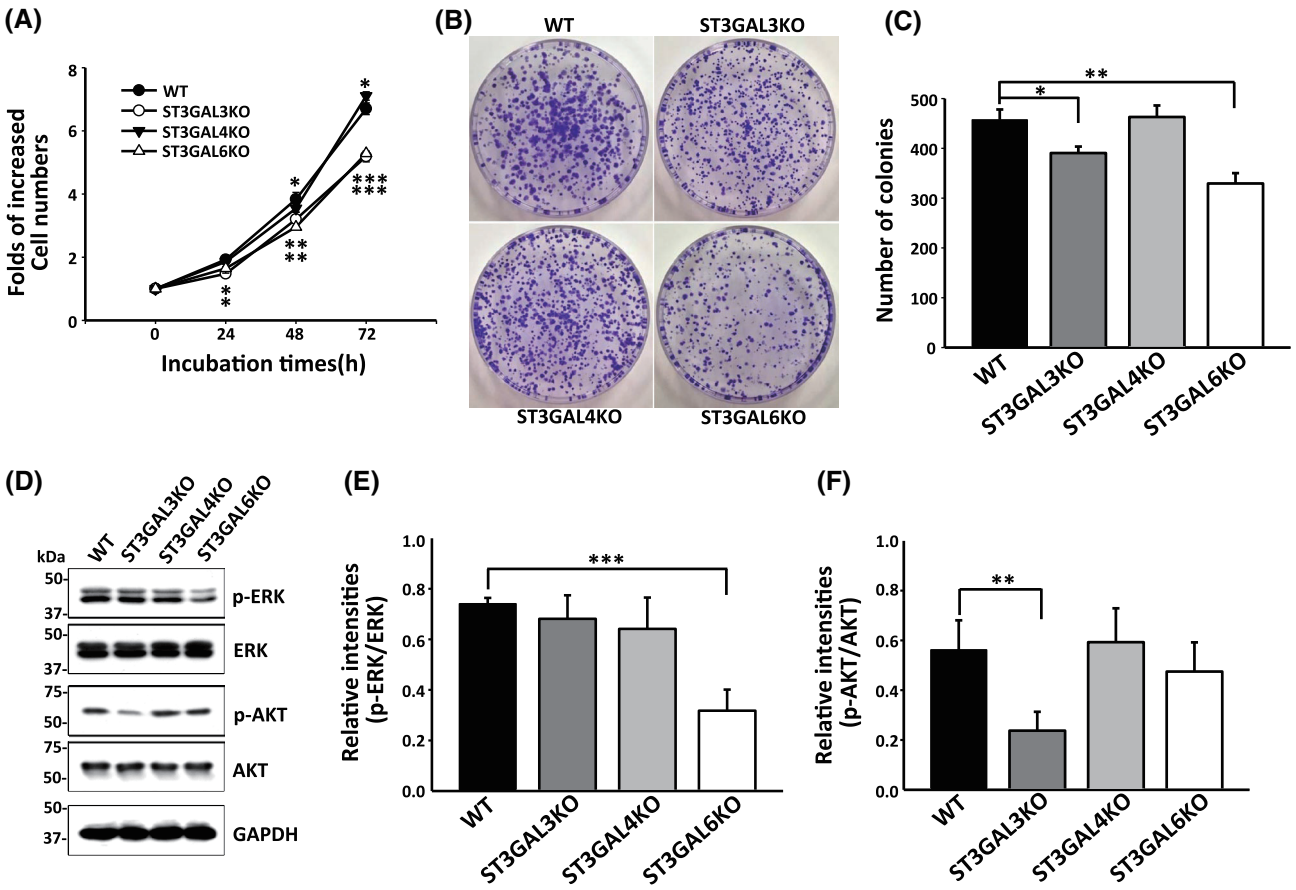

FIGURE 2 Effects of ST3GAL3 KO, ST3GAL4 KO, and ST3GAL6 KO on cell proliferation and cellular signaling. A, WT and the three kinds of KO cells were seeded in six-well culture dishes overnight and then serum starved for 24 hours. After starvation, the cells were supplied with DMEM containing 10% FBS, which was taken as the 0 point (0 hour), and further incubated for 72 hours. The cells in the same areas on the cultured dishes were photographed and counted at the indicated times (0, 24, 48, and 72 hours), the fold changes in the cell numbers were normalized to those at 0 hour. Data are represented as the mean ± standard derivation (n = 3 individual experiments). B, C, WT and the three kinds of cells (500/per well, suspended in a single cell) were grown for 14 days, and then stained with crystal violet and the foci in each well were counted. B, Representative images for colony formation. C, The stained colonies were counted, and quantitative data are presented as the means ± standard derivation from three independent experiments. D, The expression levels of phosphorylated and total ERK and AKT in the four cells were examined by Western blotting with the indicated antibodies. GAPDH was used as a loading control. E, Relative ratios of pERK/ERK in these four cells were quantified (n = 3 independent experiments). F, Relative ratios of pAKT/AKT in these four cells were quantified (n = 3 independent experiments). All values are the means ± standard derivation, one-way ANOVA; *$P < .05$; **$P < .01$; ***$P < .001$

foci, compared with those in the WT cells (Figure 2B,C). Interestingly, the numbers of foci in ST3GAL4 KO cells were similar to those in the WT cells, but the foci seemed smaller than those in the WT cells (Figure 2B,C), which may support the notion again that cell growth exists in a cell density-dependent manner in the ST3GAL4 KO cells. Western blotting was used to detect the activation of ERK and AKT that is related to cell proliferation and survival, we found that the phosphorylation levels of ERK were decreased significantly in ST3GAL6 KO cells (Figure 2D,E), whereas the phosphorylation levels of AKT were significantly decreased in ST3GAL3 KO cells (Figure 2D,F), compared with WT or ST3GAL4 KO cells. Together, these results clearly indicated that ST3GAL3, ST3GAL4, and ST3GAL6 differ in their effect on cell functions via distinct mechanisms.

3.3 | Deletion of ST3GAL3, ST3GAL4, or ST3GAL6 genes altered cell morphology and induced cell aggregation

Next, we noticed cell morphological changes after deletion of the three genes. The KO cells all tended to form islands, which were never observed in the WT cells. Among them, ST3GAL3 KO cells were the most obvious, followed by ST3GAL6 KO cells, while the effect in ST3GAL4 KO cells was much weaker. Immunofluorescent staining of

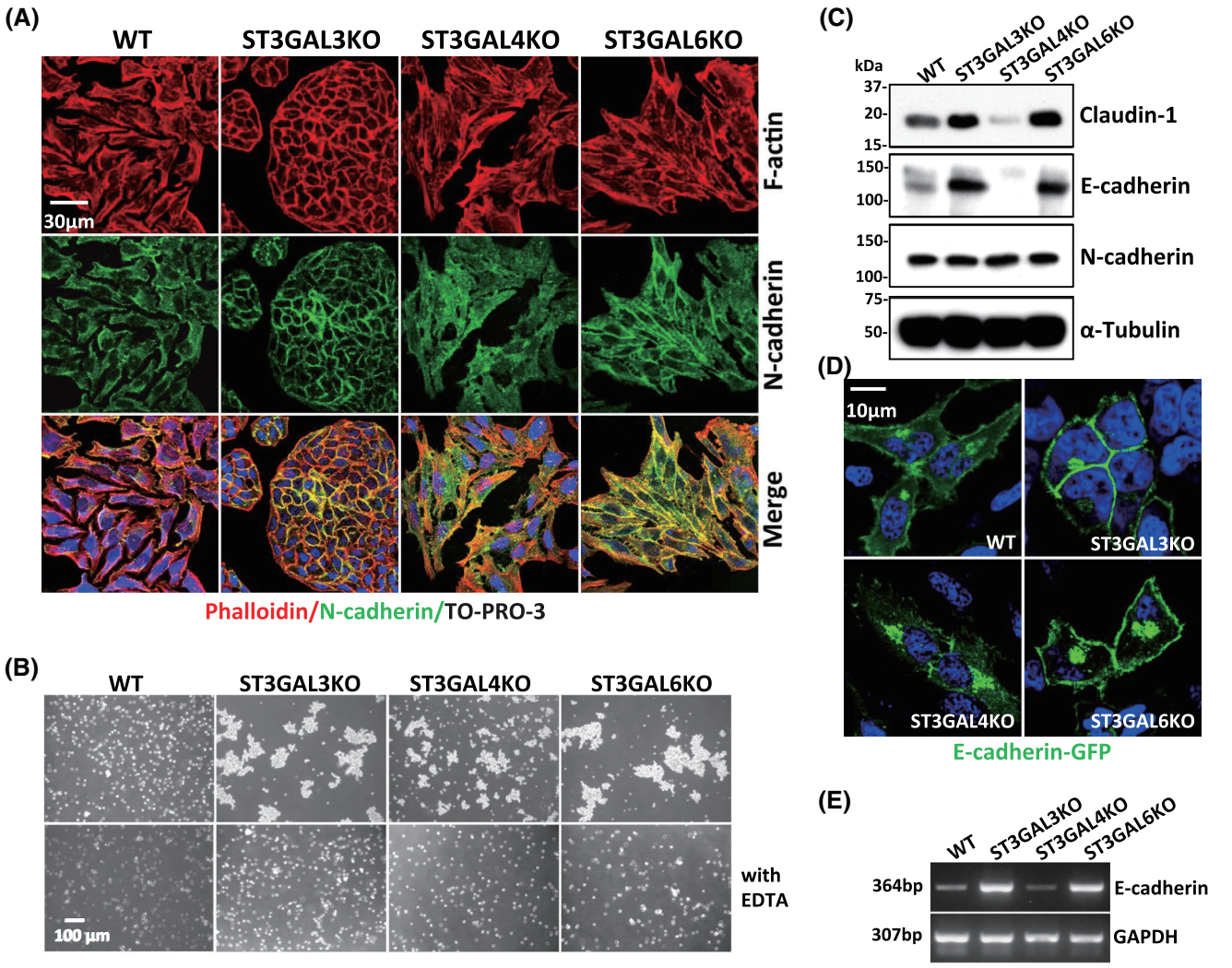

FIGURE 3 Knockout of ST3GAL3, ST3GAL4, or ST3GAL6 in HeLa cells, altered cell morphologies, and induced cell aggregation. A, WT and the three kinds of KO cells were stained with anti-N-cadherin antibody, followed by incubation with fluorescent secondary antibody. Localization of F-actin was examined by staining with Alexa Fluor 568 phalloidin, and the nucleus by TO-PRO-3. B, The four kinds of cells were detached from culture dishes and suspended at 2×10^5 cells/mL in 10% FBS culture medium with or without EDTA, followed by constant rotation (12 rpm) for 6 hours at 37°C. An aliquot of each of these cell suspensions was photographed with a phase-contrast microscope. C, The same amounts of cell lysates from the four cells were examined by Western blotting with the indicated antibodies, and α-tubulin was used as a loading control. D, Fluorescence images of WT and the three kinds of KO cells overexpressed with E-cadherin-GFP, and the nucleus stained by TO-PRO-3. E, The mRNA levels of E-cadherin in WT and three KO cells were detected by RT-PCR. GAPDH was used as a control

F-actin showed that the ST3GAL3 KO cells and ST3GAL6 KO cells exhibited cortical actin around the cell surface, whereas ST3GAL4 KO cells did not (Figure 3A). We attempted to perform immunostaining with E-cadherin antibody, but failed. Instead of E-cadherin, immunostaining with N-cadherin was carried out. N-cadherin was highly expressed in the cell-cell contacts in ST3GAL3 KO and ST3GAL6 KO cells, which existed in a diffuse state in the cytoplasm and in the cell surface in ST3GAL4 KO and WT cells (Figure 3A). Furthermore, we performed a cell aggregation assay in the suspension. The three KO cells all tended to form many aggregates, whereas the WT cells remained as either single cells or as much smaller aggregates (Figure 3B). Those cell aggregates disappeared in the presence of EDTA, suggesting that the cell-cell adhesion had proceeded in a calcium-dependent manner. To better understand the underlying molecular mechanisms, we compared the expression levels of some adhesive molecules, which affect cell-cell adhesion, such as claudin-1, E-cadherin, and N-cadherin. It was interesting that the expressions of claudin-1 and E-cadherin, which promote cell-cell adhesion, were greatly increased in ST3GAL3 KO and ST3GAL6 KO cells, but were decreased in ST3GAL4 KO cells (Figure 3C). On the other hand, the expression levels of N-cadherin were similar in all cells (Figure 3C). To further determine the changes of E-cadherin expression in four groups of cells, we performed an overexpression

system with GFP-tagged human E-cadherin. The ST3GAL3 KO and ST3GAL6 KO cells expressed more E-cadherin on the cell surface, compared to the WT cells and ST3GAL4 KO cells (Figure 3D). In addition, E-cadherin proteins seemed to be internalized in the ST3GAL4 KO cells. We also performed a RT-PCR to examine E-cadherin expression levels in those cells, and found that the pattern of E-cadherin expression at mRNA levels (Figure 3E) was similar to that at the protein levels (Figure 3C). These results again indicated that ST3GAL3, ST3GAL4, and ST3GAL6 differ in their effect on cell morphology via different pathways.

3.4 | Restoration of ST3GAL3, ST3GAL4, or ST3GAL6 genes in each of the corresponding KO cells rescued α2,3-sialylation, cell morphology, and expression of E-cadherin

Given the observations described in Figures 2 and 3, we attempted to determine whether the phenotypes could be rescued by the restoration of each gene in the corresponding KO cells (RES). The α2,3-sialylation levels were compared between the KO and RES cells using flow cytometry and Western blotting. As expected, increased α2,3-sialylation was observed in each of the RES cells by either flow cytometric analysis (Figure 4A) or Western blotting with MAM lectin (Figure 4B). The cell morphologies that tended to form aggregations in the KO cells were reversed to separated or small aggregation morphologies in each of the RES cells, particularly in the ST3GAL3 RES or ST3GAL6 RES cells (Figure 4C). Although the restoration of ST3GAL4 did not signal a significant change in E-cadherin expression, the enhanced E-cadherin expression levels observed in the ST3GAL3 KO and ST3GAL6 KO cells shown in Figure 3C were greatly suppressed in the ST3GAL3 RES and ST3GAL6 RES cells (Figure 4D). These results further supported the notion that ST3GAL3, ST3GAL4, and ST3GAL6 differ in their effect on cell morphology.

3.5 | ST3GAL3, ST3GAL4, or ST3GAL6 modified target glycoproteins differently

Sialylation is well known to play an important role in cancer cell invasion and metastasis, as well as in cell growth. Here, we chose three representative transmembrane glycoproteins, β1 integrin, EGFR, and N-cadherin to detect the changes in α2,3-sialylation and α2,6-sialylation levels in the KO cells. Of particular interest, the α2,3-sialylation levels of β1 integrin were only decreased in the ST3GAL4 KO cells, compared with those in the WT cells. Conversely, the α2,3-sialylation levels were increased in the ST3GAL3 KO and ST3GAL6 KO cells (Figure 5A,D). The underlying mechanisms for the enhancement remain unclear, but it is reasonable that the KOs of ST3GAL3 and ST3GAL6 genes would decrease a competitor for a common donor substrate, CMP-NANA, which could relatively increase the amounts of CMP-NANA available for ST3GAL4 to catalyze the α2,3-sialylation of β1 integrin. However, the α2,3-sialylation levels of EGFR were only decreased in the ST3GAL6 KO cells, but not in the other two KO cells (Figure 5B,E). Curiously, the changes in the α2,3-sialylation of N-cadherin were similar among the three KO cells (Figure 5C,F). On the other hand, the changes in the α2,6-sialylation of the target proteins, with the exception of EGFR in the ST3GAL6 KO cells, were the opposite (Figure 5), suggesting that these α2,3-sialyltransferases may compete with ST6GAL1 for the same substrates. These results strongly suggest that ST3GAL3, ST3GAL4, and ST3GAL6 differ in their regulation of biological functions via the modification of different target glycoproteins, that is, each enzyme has preferential target proteins.

3.6 | Cross-restoration using ST3GAL3, ST3GAL4, or ST3GAL6 genes in ST3GAL6 KO cells differed in the rescued α2,3-sialylation and cell morphology

To further confirm the specificities of the three α2,3-sialyltransferases, we performed a cross-restoration with ST3GAL3, ST3GAL4, or ST3GAL6 genes in the ST3GAL6 KO cells. The efficiencies for rescuing the α2,3-sialylation levels in the ST3GAL6 RES cells, examined using flow cytometry, were clearly higher than those in the cells expressed with ST3GAL3 or ST3GAL4 (Figure 6A), which was further confirmed by lectin blotting with MAM lectin (Figure 6B). The expression levels of each α2,3-sialyltransferase were similar among these cells, as confirmed by Western blotting with anti-Flag antibody (Figure 6B). In addition, the cell aggregations induced by ST3GAL6 deficiency were efficiently rescued to normal cell morphology, as with WT cells, by overexpression of ST3GAL6, but neither ST3GAL3 nor ST3GAL4 overexpression had the same effect (Figure 6C). These results clearly indicated that the overexpressions of ST3GAL3 or ST3GAL4 could not completely rescue the decreased α2,3-sialylation levels and functions caused by ST3GAL6 deletion, further suggesting that these three enzymes have preferential target proteins.

3.7 | Cross-restoration with ST3GAL3, ST3GAL4, or ST3GAL6 genes in the ST3GAL6 KO cells differ in the rescue levels of α2,3-sialylation and α2,6-sialylation on target glycoproteins

Again, the α2,3-sialylation and α2,6-sialylation levels of β1 integrin, EGFR, and N-cadherin were tested following

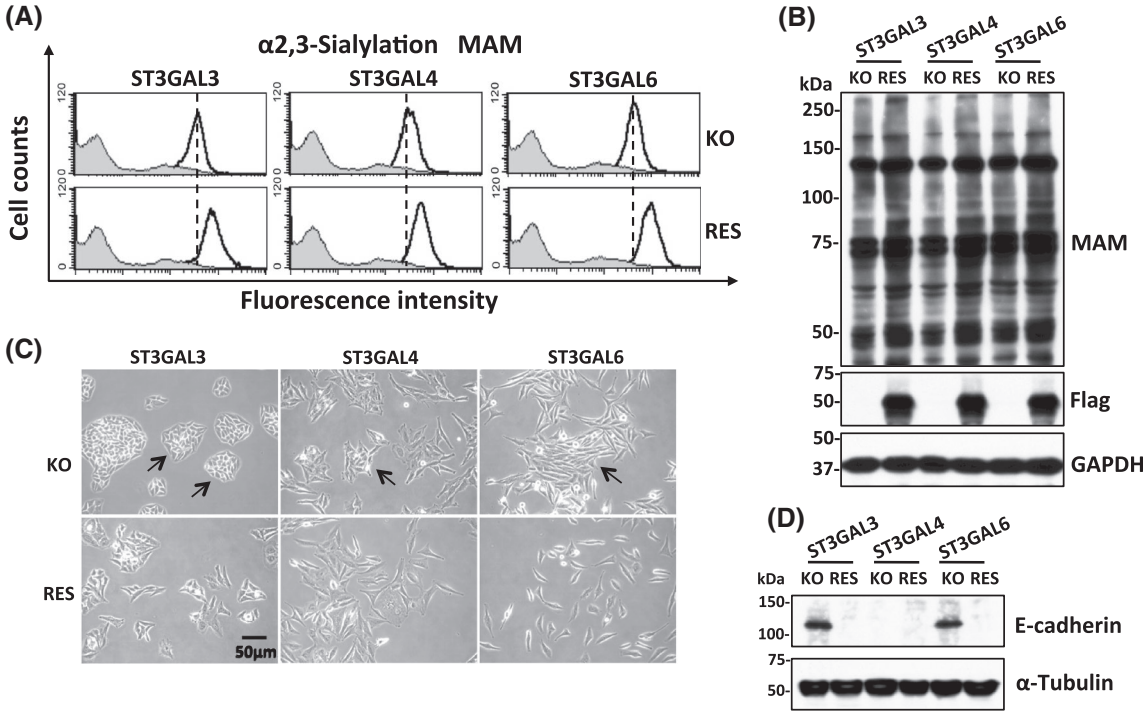

FIGURE 4 Forced expression of ST3GAL3, ST3GAL4, or ST3GAL6 KO genes in each of the corresponding KO cells, and the rescued cell morphologies and E-cadherin expressions. Each KO cells and restoration of each gene in the corresponding KO (RES) cells were cultured in the presence of DOX at 1 μg/mL for 72 hours before the following experiments were performed. A, The KO and RES cells were collected and incubated with (bold line) or without (gray shadow) MAM lectin, followed by incubation with Alexa Fluor 647 streptavidin and subjected to flow cytometric analysis. The vertical dashed lines indicate the peaks reacted with MAM lectin in KO cells. B, Equal amounts of cell lysates from these KO and RES cells were examined by immunoblot with MAM lectin and anti-Flag antibodies. GAPDH was used as a loading control. C, Representative cell morphologies of each KO and RES cells were taken with a phase-contrast microscope. Arrows indicated cell aggregation. D, The same amounts of cell lysates from each KO and RES cells were analyzed by Western blotting with the E-cadherin antibody, and α-tubulin was used as a loading control

cross-restoration with ST3GAL3, ST3GAL4, or ST3GAL6 genes in ST3GAL6 KO cells. The increases in α2,3-sialylation and decreases in α2,6-sialylation of β1 integrin were much more obvious in the cells restored with the ST3GAL4 gene compared with those restored using the other versions (Figure 7A,D) while both the α2,3-sialylation and α2,6-sialylation of EGFR that were down-regulated in the KO of the ST3GAL6 gene were preferentially rescued by an overexpression of ST3GAL6, but not by overexpressions of either ST3GAL3 or ST3GAL4 (Figure 7B,E). Curiously, consistent with the data shown in Figure 5B, the expression of ST3GAL6 seemed correlated with both α2,3- and α2,6-sialylation of EGFR. Compared with the other two genes, restoration with the ST3GAL6 gene in the ST3GAL6 KO cells efficiently increased α2,3-sialylation levels and decreased the α2,6-sialylation levels of N-cadherin (Figure 7C). These results further clearly demonstrated that the three enzymes have individual specific target proteins, and that ST3GAL4 is the most critical for the α2,3-sialylation of β1 integrin while ST3GAL6 is the most important for the α2,3-sialylation of EGFR.

4 | DISCUSSION

In the present study, we used the same HeLa cell line to investigate the functions of three α2,3-sialyltransferases, ST3GAL3, ST3GAL4, and ST3GAL6, which are the most important sialyltransferases for the α2,3-sialylation of N-glycans. We found that (i) the three α2,3-sialyltransferases had different functions in cell proliferation and cell adhesion, as well as in cellular signaling; (ii) the three α2,3-sialyltransferases individually promote specific modifications for different target proteins (Figure 8), for example, ST3GAL4 modifies β1 integrin, while ST3GAL6 modifies EGFR; and (iii) the three α2,3-sialyltransferases show negligible levels of compensation for α2,3-sialylation, and may compete with ST6GAL1 for sialylation of the same target protein. Our studies are the first to characterize the α2,3-sialylation of the three enzymes in the same cell line, which may help us to understand their functional expressions, and explain some previous results or interpret some controversial observations obtained from different cells or tumor tissues.[35,38,57]

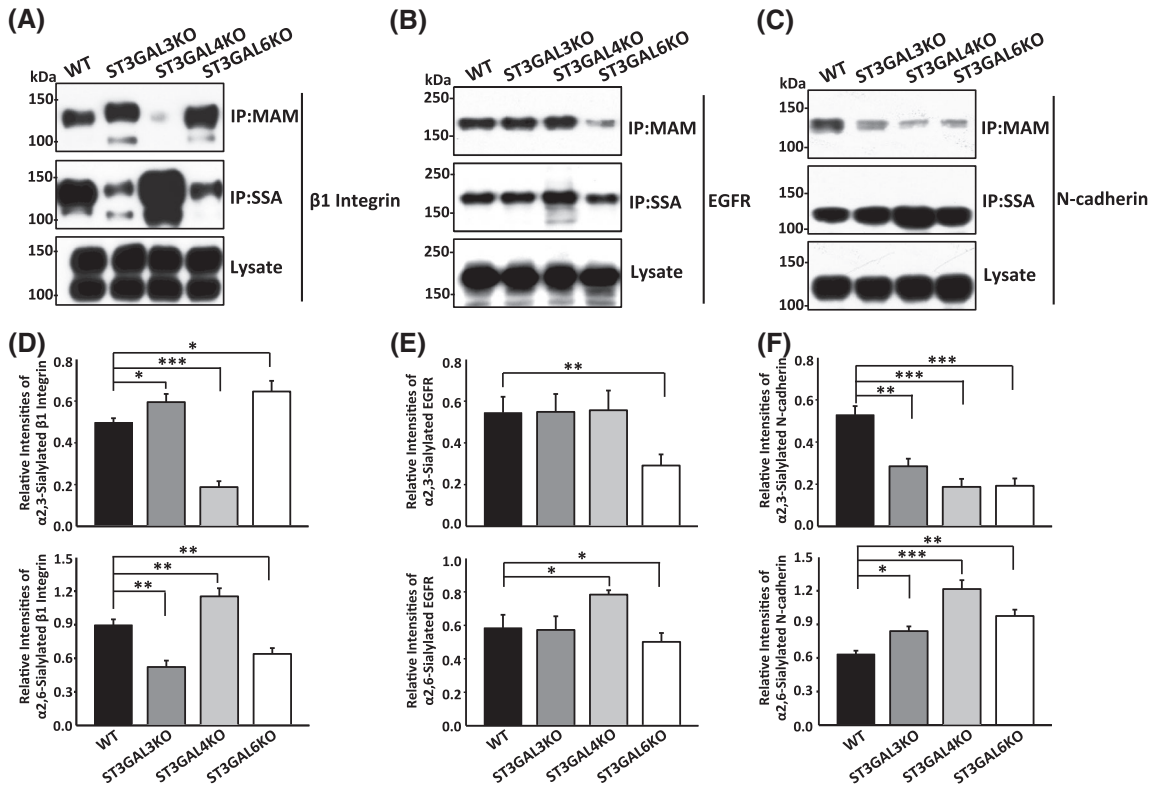

FIGURE 5 Knockout of ST3GAL3, ST3GAL4, or ST3GAL6 in HeLa cells differed in the alteration of the levels of α2,3-sialylation and α2,6-sialylation of specific glycoproteins. Equal amounts of cell lysates were immunoprecipitated with MAM-agarose or Sambucus sieboldiana Agglutinin (SSA)-agarose which specifically recognizes α2,6-sialylation, for 1 hour at 4°C with rotation, and then the immunoprecipitates were washed twice with lysis buffer and subjected to SDS-PAGE. The precipitated glycoproteins and cell lysates were immunoblotted for β1 integrin (A), EGFR antibody (B), and N-cadherin (C) antibodies. The relative levels of α2,3 and α2,6 sialylation on β1 integrin (D), EGFR (E), and N-cadherin (F) in these four kinds of cells were quantified (n = 3 independent experiments). All values are the means ± standard derivation, one-way ANOVA; *$P < .05$; **$P < .01$; ***$P < .001$

Glycan structures expressed on glycoproteins and glycolipids of cells are essential for regulating normal cell functions.[58] Altered tumor-associated carbohydrate antigens have been identified in many solid tumors, and the changes in terminal sialylation are very important in malignant transformation and cancer progression.[59,60] Until now, most studies have focused on either the effects of three kinds of sialylation linkages (α2,3, α2,6, and α2,8) in tumors or on the expression levels of certain sialyltransferases in tumors. Examples of these studies include the following: α2,3-sialylation of α2 integrin has been related to the bone metastatic behavior of prostate cancer cells[60]; malignant transformation of oral epithelium was found to be accompanied by α2,3-sialylation, wherein α2,6-sialylation was related to disease progression and metastatic potentials[61]; melanoma progression has been associated with a significant increase in α2,3-sialylation on the surface[57]; several sialyltransferase genes were found to be highly expressed in human colon and gastric tumor tissues[62,63]; and important functions of a single sialyltransferase have been observed by manipulation of the gene expression in a cell line.[39,44,64] However, very little is known about which sialyltransferase(s) is/are specifically responsible for the synthesis of these altered glycans on defined glycoproteins. The main function of these three enzymes is to modify the α2,3-sialylation of glycoproteins. As far as we could ascertain, few studies have compared the functions of these genes in the same cell line. The present study clearly demonstrated that ST3GAL4 in HeLa cells significantly contributes to total α2,3-sialylation levels, compared with the effect from either ST3GAL3 or ST3GAL6, but each sialyltransferase has its own specific target glycoproteins, which subsequently affects cellular signaling. ST3GAL4 KO significantly decreases the α2,3-sialylation of integrin β1, but not that of EGFR; ST3GAL6 KO, however, greatly decreases the α2,3-sialylation of EGFR, but not that of integrin β1. Consistently, the levels of p-ERK and cell proliferation were down-regulated in ST3GAL6 KO cells, not in ST3GAL4 KO cells, compared with WT cells. Curiously, the levels of p-AKT were only suppressed in the ST3GAL3 KO cells, suggesting that ST3GAL3 might specifically modify some glycoproteins that promote AKT activation to regulate cell proliferation. Thus, we speculated that the ranges for the α2,3-sialylation of glycoproteins affected by ST3GAL3, ST3GAL4, and ST3GAL6 are different. In fact, the present results were supported by a

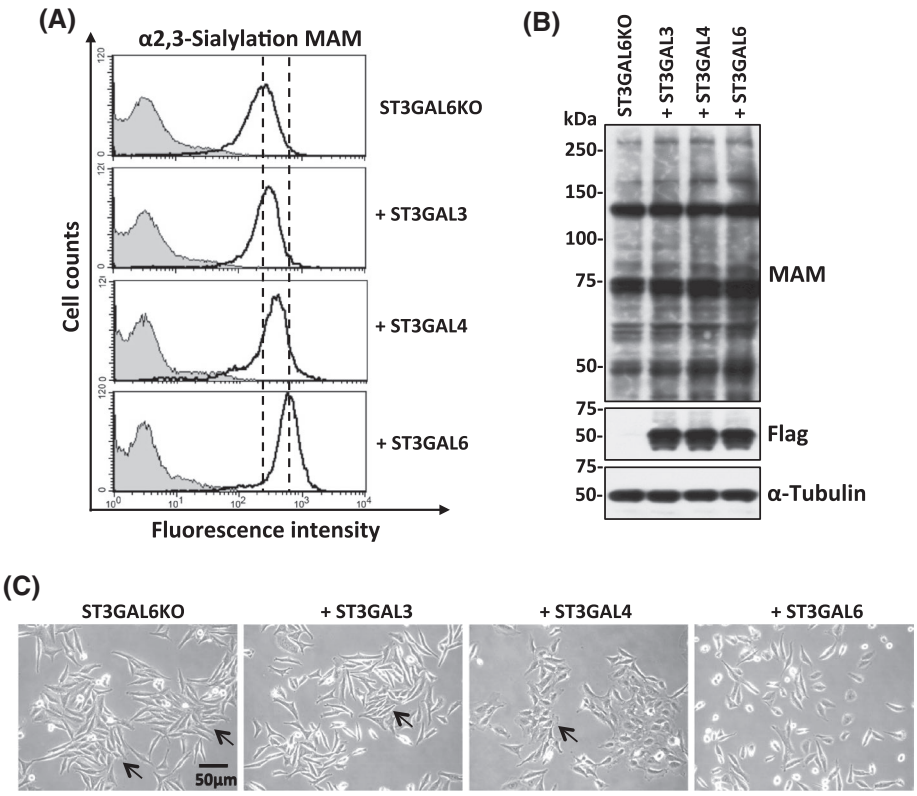

FIGURE 6 Restoration of either ST3GAL3 or ST3GAL4 genes could not completely rescue the α2,3-sialylation levels and cell morphologies of impaired ST3GAL6 KO cells. The ST3GAL6 KO cells transfected with or without ST3GAL3, ST3GAL4, or ST3GAL6 genes were cultured in the presence of DOX at 1 μg/mL for 72 hours before the following experiments were performed. A, These four kinds of cells were collected and incubated with (bold line) or without (gray shadow) MAM lectin, followed by incubation with Alexa Fluor 647 streptavidin and subjected to flow cytometric analysis. The vertical dashed lines indicate the peaks of the reaction abilities with MAM lectin in the ST3GAL6 KO cells rescued with or without ST3GAL6 genes. B, Equal amounts of cell lysates were examined by immunoblotting with MAM lectin and anti-flag antibody. α-Tubulin was used as a loading control. C, Representative cell morphologies of these four kinds of cells were taken with a phase-contrast microscope. Arrows indicated cell aggregation

previous study, which found that the sialylation of a recombinant glycoprotein, erythropoietin, was specifically modified by ST3GAL4, and not by either ST3GAL3 or ST3GAL6 in Chinese Hamster Ovary cells.[7] An observation made in the present study whereby the α2,3-sialylation of integrin β1 was conversely increased in both the ST3GAL3 and ST3GAL6 KO cells could also be very important (Figure 5A). Although the exact underlying mechanism in this novel result will require further studies, it would be plausible to speculate that a KO of either the ST3GAL3 or ST3GAL6 gene may relatively increase the amounts of a common donor substrate, CMP-NANA, which would allow ST3GAL4 to modify integrin β1, which further suggests that the KO effect of a glycogene may be expressed as both a loss-of-function and a gain-of-function.

The specificities of the three enzymes for their own target proteins were also proved by the cross-restoration experiments. Overexpression of either ST3GAL3 or ST3GAL4 in the ST3GAL6 KO cells increased the levels of α2,3-sialylation to some extent, but the recovery level observed in ST3GAL6 RES cells was never reached (Figure 6), suggesting ST3GAL6 has its own intrinsic target proteins, as described above. In fact, the restorative ability with respect to the α2,3-sialylation of integrin β1 was the highest in the ST3GAL4 RES cells, while that of the α2,3-sialylation of both EGFR and N-cadherin was the highest in the ST3GAL6 RES cells (Figure 7). Furthermore, cell morphology differed among the three cross-restoration cells, and only the overexpression of ST3GAL6 could rescue it to the level of WT cells. When the important functions of integrin β1,[65,66] EGFR,[67] and N-cadherin[68] are considered, there can be little doubt that the three sialyltransferases differentially regulate cell biological functions, cancer progression, and tumor resistance. Of course, the specificities of the three enzymes give them a relative approach rather than an all-or-nothing effect. The overexpression of ST3GAL4 in the ST3GAL6 KO cells also slightly increased the α2,3-sialylation levels of EGFR, as ST3GAL6 did.

Changes in the α2,6-sialylation levels of these KO cells merit recognition, since α2,3- and α2,6-sialyltranfserases may compete with common substrates to a certain extent, and this competition is manifested in specific glycoproteins

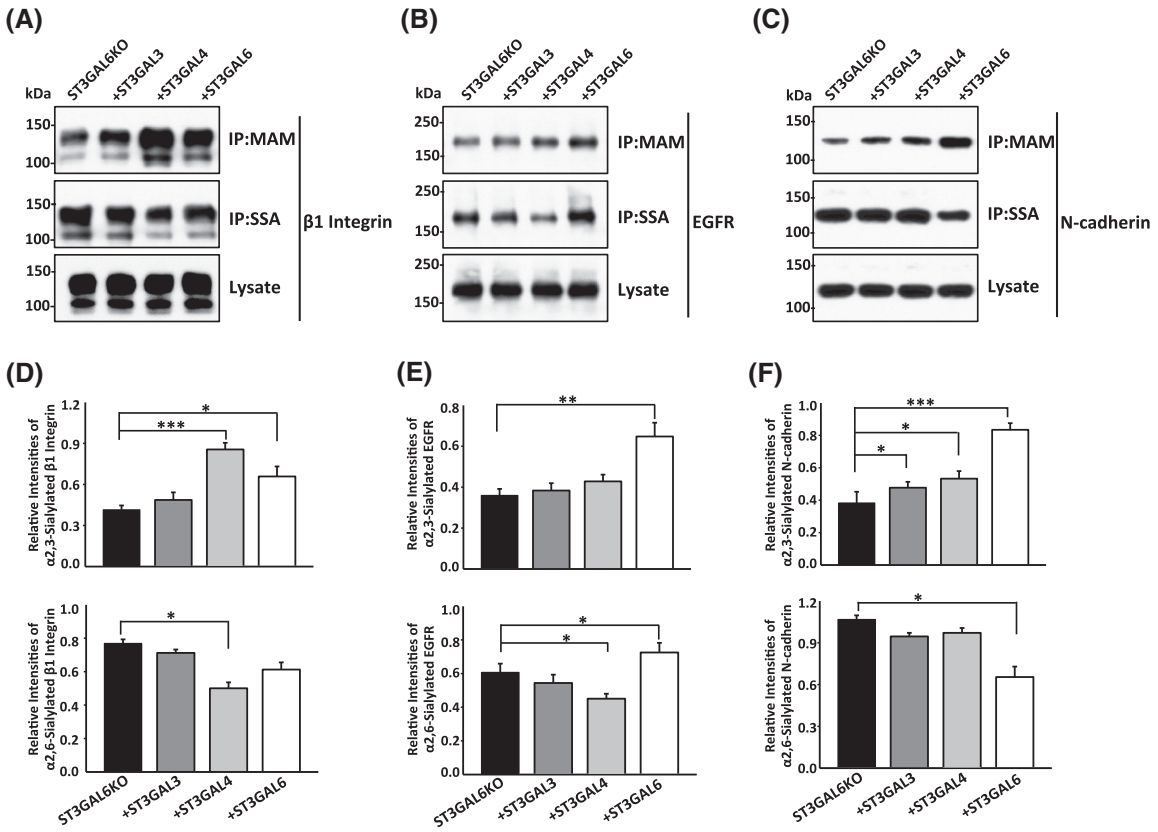

FIGURE 7 The cross-restoration of ST3GAL3, ST3GAL4, or ST3GAL6 in ST3GAL6 KO cells differed in the alteration of sialylation in target proteins. As described in Figure 6, the ST3GAL6 KO cells transfected with or without ST3GAL3, ST3GAL4, or ST3GAL6 genes, were cultured in complete medium with 1 μg/mL DOX for 72 hours before the following experiments were performed. Equal amounts of cell lysates as indicated were immunoprecipitated with MAM-agarose or SSA-agarose for 1 hour at 4°C with rotation, and then the immunoprecipitates were washed twice with lysis buffer and subjected to SDS-PAGE. The precipitated glycoproteins and cell lysates were immunoblotted for β1 integrin (A), EGFR (B), or N-cadherin (C) antibodies. The relative levels of α2,3- and α2,6-sialylation on β1 integrin (D), EGFR (E), and N-cadherin (F) in these four kinds of cells were quantified (n = 3 independent experiments). All values are reported the means ± standard derivation (error bars), one-way ANOVA; *$P < .05$; **$P < .01$; ***$P < .001$

such as β1 integrin. Interestingly, among all three genes, ST3GAL4 deficiency alone reciprocally increased the levels of α2,6-sialylation (Figure 5), while the overexpression of ST3GAL4 conversely decreased the α2,6-sialylation levels of β1 integrin (Figure 7). Therefore, when evaluating the effect of α2,3-sialylation, the influences of α2,6-sialylation could not be neglected, since the α2,6-sialylation of β1 plays important roles in cell adhesion and cell proliferation.[52,69] These results could also partly explain the observation of different phenotypes in these three KO cells. Although the decrease in the α2,3-sialylation of β1 integrin was more obvious in the ST3GAL4 KO cells, the phenomena of cell-cell aggregation and cell proliferation were much weaker than that observed in the ST3GAL3 KO cells, which might have been due to the significant increase in the α2,6-sialylation of β1 integrin in the ST3GAL4 KO cells. In fact, the expression of ST6GAL1 is important for not only β1-mediated cell adhesion but also for cellular signaling such as that seen in the PI3K-AKT signaling pathway.[52,70] Our previous results showed that the up-regulation of α2,6-sialylation inhibited E-cadherin expression,[71] which might partly explain why the expression levels of E-cadherin were increased in ST3GAL3 or ST3GAL6 KO cells, whereas it was decreased in the ST3GAL4 KO cells in the present study, although we could not identify whether the levels of sialylated E-cadherin changed after a KO of the three enzymes. Nevertheless, we did not exclude other possibilities that could affect E-cadherin expression.

It is noteworthy that the down-regulation of α2,3-sialylation decreased the α2,6-sialylation of EGFR in the ST3GAL6 KO cells (Figure 5) while up-regulation of α2,3-sialylation increased it (Figure 7). Thus far, the details of this molecular mechanism remain unclear, but α2,3-sialylation could affect EGFR conformation changes, which could result in the promotion of ST6GAL1 accessibility to some glycosylation sites for α2,6-sialylation. In fact, EGFR contains 12 potential N-glycosylation sites, and the N-glycans on EGFR have been reported to play important roles in receptor functions that include ligand binding and tyrosine kinase activity.[72] For example, the Asn-420-Gln mutant EGFR did not bind to the EGF ligand, but spontaneously induced oligomerization, resulting

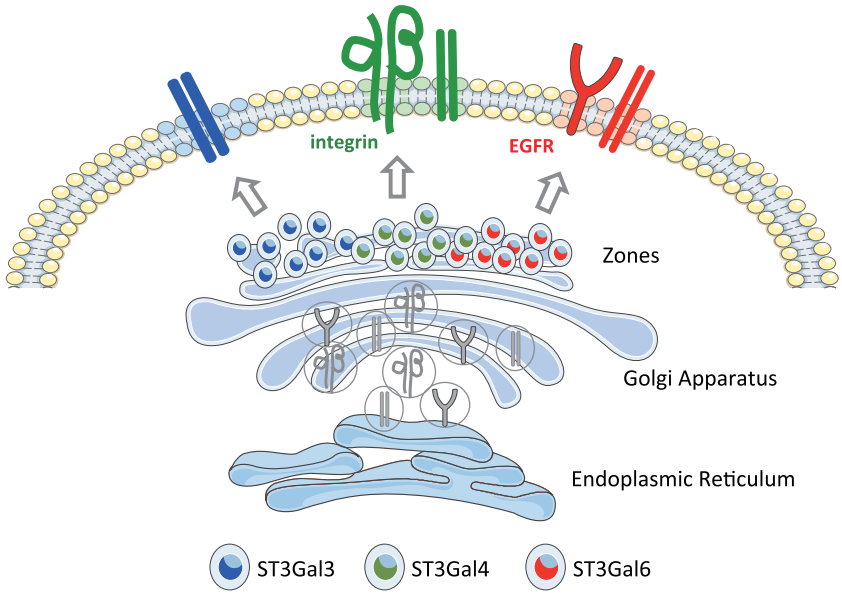

FIGURE 8 The proposed mechanisms for the modification of α2,3-sialylation by ST3GAL3, ST3GAL4, and ST3GAL6 in glycoproteins expressed on the cell surface in different domains. All membrane glycoproteins such as β1 integrin, EGFR, and N-cadherin were synthesized in ribosomes and then transferred from the ER to the Golgi apparatus for oligosaccharide assembly, and then finally transported to the cell surface in different domains. The present study clearly supported the notion that there are distinct functional units (80), referred to as "zones," in the Golgi apparatus (78, 79), that is, the α2,3-sialylation of β1 integrin was mainly catalyzed in zones containing ST3GAL4, whereas the α2,3-sialylation of EGFR occurred in zones containing ST3GAL6. On the other hand, the α2,3-sialylation of N-cadherin was accomplished in zones containing ST3GAL3, ST3GAL4, and ST3GAL6. Furthermore, it is worth noting that ST6GAL1 could be ubiquitously distributed in all of those zones. These results clearly demonstrate that the three α2,3-sialyltransferases of ST3GAL3, ST3GAL4, and ST3GAL6 differed in their modification of target proteins and in their regulation of cell biological functions

in phosphorylation of the receptor in the absence of a ligand, further supporting the notion that glycans may be involved in maintaining the proper structure of target proteins.[73] Of course, we could not exclude the effects from glycolipids or/and O-glycosylated proteins, since the sialyltransferases in this study were also involved in the modification of glycolipids and/or O-glycoproteins.[23,34,74-76]

Most sialytransferases modify proteins in the Golgi apparatus. Based on our results, we speculated that three α2,3-sialytransferases modify glycoproteins (β1, EGFR, and N-cadherin) through different pathways or functional distinct Golgi units (Figure 8), which can also be referred to as the "zones" of mitochondria[77] or Golgi apparatus.[78,79] Hiroyuki et al agreed with our observations and reported that functional distinct Golgi units exist in Drosophila cells[80] to selectively modify target proteins such as Notch and GAG core proteins. Therefore, it is reasonable to postulate that distinct Golgi zones containing different kinds of sialyltransferases exist in HeLa cells, and that the majority of β1 integrin or EGFR might be modified with α2,3-sialylation in the zones containing ST3GAL4 or ST3GAL6, respectively. ST6GAL1 might ubiquitously exist in those zones together with ST3GAL3, ST3GAL4, or ST3GAL6. In addition, the specificities for target protein modification might also depend on the acceptor structures, it is known that ST3GAL3 seems to prefer the Galβ1-3GlcNAc disaccharide, whereas ST3GAL4 and ST3GAL6 appear to prefer the Galβ1-4GlcNAc linkage.[22,81,82] The detailed mechanisms will require further study.

In conclusion, using KO and cross-restoration techniques, we clearly demonstrated that ST3GAL3, ST3GAL4, and ST3GAL6 differ in their modification of target proteins and in their regulation of cell biological functions. Clarifying the specificities of the three sialyltransferases and the underlying molecular mechanisms will shed light on the biological functions of ST3GAL3, ST3GAL4, and ST3GAL6 in various tissues and cells, and could also provide insight into drug developments for cancer and infection therapies.

ACKNOWLEDGMENTS

This work was supported in part by a Grant-in-Aid for Scientific Research (15H04354 and 19H03184 to JG and 19K07049 to TI) from the Japan Society for the Promotion of Science, grant from National Natural Science Foundation of China (No. 31670807) and Science and Technology Project from Jiangsu Traditional Chinese Medicine Bureau (YB2017072); and by a Grant-in-Aid for Scientific Research on Innovative Areas (18H04868 to JG) from the Ministry of Education, Culture, Sports, Science, and Technology of Japan.

CONFLICT OF INTEREST

The authors declare no conflicts of interest and no competing financial interests.

AUTHOR CONTRIBUTIONS

F. Qi, T. Isaji, and J. Gu designed the research; F. Qi performed all experiments; F. Qi and T. Isaji performed flow cytometric analysis; C. Duan, J. Yang, Y. Wang, and T. Fukuda assisted with experiments; T. Isaji, Y. Wang, T. Fukuda, and J. Gu analyzed and interpreted the data; F. Qi, T. Isaji, and J. Gu wrote and revised the manuscript; and all authors approved the final version of the manuscript.

REFERENCES

1. Bhide GP, Colley KJ. Sialylation of N-glycans: mechanism, cellular compartmentalization and function. *Histochem Cell Biol*. 2017;147:149-174.
2. Li Y, Chen X. Sialic acid metabolism and sialyltransferases: natural functions and applications. *Appl Microbiol Biotechnol*. 2012;94:887-905.
3. Varki NM, Strobert E, Dick EJ Jr, Benirschke K, Varki A. Biomedical differences between human and nonhuman hominids: potential roles for uniquely human aspects of sialic acid biology. *Annu Rev Pathol*. 2011;6:365-393.
4. El-Battari A, Prorok M, Angata K, et al. Different glycosyltransferases are differentially processed for secretion, dimerization, and autoglycosylation. *Glycobiology*. 2003;13:941-953.
5. Kitagawa H, Paulson JC. Differential expression of five sialyltransferase genes in human tissues. *J Biol Chem*. 1994;269:17872-17878.
6. Inokuchi JI, Inamori KI, Kabayama K, et al. Biology of GM3 Ganglioside. *Prog Mol Biol Transl Sci*. 2018;156:151-195.
7. Chung CY, Yin B, Wang Q, Chuang KY, Chu JH, Betenbaugh MJ. Assessment of the coordinated role of ST3GAL3, ST3GAL4 and ST3GAL6 on the alpha2,3 sialylation linkage of mammalian glycoproteins. *Biochem Biophys Res Commun*. 2015;463:211-215.
8. Suzuki O, Abe M, Hashimoto Y. Sialylation by beta-galactoside alpha-2,6-sialyltransferase and N-glycans regulate cell adhesion and invasion in human anaplastic large cell lymphoma. *Int J Oncol*. 2015;46:973-980.
9. Takahashi T, Naka T, Fujimoto M, et al. Aberrant expression of glycosylation in juvenile gastrointestinal stromal tumors. *Proteomics Clin Appl*. 2008;2:1246-1254.
10. Zhou X, Kinlough CL, Hughey RP, et al. Sialylation of MUC4beta N-glycans by ST6GAL1 orchestrates human airway epithelial cell differentiation associated with type-2 inflammation. *JCI Insight*. 2019;4:e122475.
11. Schnaar RL, Gerardy-Schahn R, Hildebrandt H. Sialic acids in the brain: gangliosides and polysialic acid in nervous system development, stability, disease, and regeneration. *Physiol Rev*. 2014;94:461-518.
12. Teppa RE, Petit D, Plechakova O, Cogez V, Harduin-Lepers A. Phylogenetic-derived insights into the evolution of sialylation in eukaryotes: comprehensive analysis of vertebrate beta-galactoside alpha2,3/6-sialyltransferases (ST3Gal and ST6Gal). *Int J Mol Sci*. 2016;17:e1286.
13. Yuan Y, Wu L, Shen S, Wu S, Burdick MM. Effect of alpha 2,6 sialylation on integrin-mediated adhesion of breast cancer cells to fibronectin and collagen IV. *Life Sci*. 2016;149:138-145.
14. Bate C, Nolan W, Williams A. Sialic acid on the glycosylphosphatidylinositol anchor regulates PrP-mediated cell signaling and prion formation. *J Biol Chem*. 2016;291:160-170.
15. Hatcher BL, Hale JY, Briles DE. Free sialic acid acts as a signal that promotes streptococcus pneumoniae invasion of nasal tissue and nonhematogenous invasion of the central nervous system. *Infect Immun*. 2016;84:2607-2615.
16. Jia N, Barclay WS, Roberts K, et al. Glycomic characterization of respiratory tract tissues of ferrets: implications for its use in influenza virus infection studies. *J Biol Chem*. 2014;289:28489-28504.
17. Schauer R. Sialic acids: fascinating sugars in higher animals and man. *Zoology (Jena)*. 2004;107:49-64.
18. Miyagi T, Wada T, Yamaguchi K, Hata K. Sialidase and malignancy: a minireview. *Glycoconj J*. 2004;20:189-198.
19. Liu Z, Swindall AF, Kesterson RA, Schoeb TR, Bullard DC, Bellis SL. ST6Gal-I regulates macrophage apoptosis via alpha2-6 sialylation of the TNFR1 death receptor. *J Biol Chem*. 2011;286:39654-39662.
20. Swindall AF, Bellis SL. Sialylation of the Fas death receptor by ST6Gal-I provides protection against Fas-mediated apoptosis in colon carcinoma cells. *J Biol Chem*. 2011;286:22982-22990.
21. Crespo HJ, Cabral MG, Teixeira AV, Lau JT, Trindade H, Videira PA. Effect of sialic acid loss on dendritic cell maturation. *Immunology*. 2009;128:e621-e631.
22. Okajima T, Fukumoto S, Miyazaki H, et al. Molecular cloning of a novel alpha2,3-sialyltransferase (ST3Gal VI) that sialylates type II lactosamine structures on glycoproteins and glycolipids. *J Biol Chem*. 1999;274:11479-11486.
23. Chachadi VB, Bhat G, Cheng PW. Glycosyltransferases involved in the synthesis of MUC-associated metastasis-promoting selectin ligands. *Glycobiology*. 2015;25:963-975.
24. Kim YJ, Varki A. Perspectives on the significance of altered glycosylation of glycoproteins in cancer. *Glycoconj J*. 1997;14:569-576.
25. Kawamura YI, Adachi Y, Curiel DT, et al. Therapeutic adenoviral gene transfer of a glycosyltransferase for prevention of peritoneal dissemination and metastasis of gastric cancer. *Cancer Gene Ther*. 2014;21:427-433.
26. Dewald JH, Colomb F, Bobowski-Gerard M, Groux-Degroote S, Delannoy P. Role of cytokine-induced glycosylation changes in regulating cell interactions and cell signaling in inflammatory diseases and cancer. *Cells*. 2016;5:e43.
27. Engelstaedter V, Fluegel B, Kunze S, et al. Expression of the carbohydrate tumour marker Sialyl Lewis A, Sialyl Lewis X, Lewis Y and Thomsen-Friedenreich antigen in normal squamous epithelium of the uterine cervix, cervical dysplasia and cervical cancer. *Histol Histopathol*. 2012;27:507-514.
28. Velazquez-Marquez N, Santos-Lopez G, Jimenez-Aranda L, Reyes-Leyva J, Vallejo-Ruiz V. Sialyl Lewis x expression in cervical scrapes of premalignant lesions. *J Biosci*. 2012;37:999-1004.
29. Aco-Tlachi M, Carreno-Lopez R, Martinez-Morales PL, et al. Glycogene expression profiles based on microarray data from cervical carcinoma HeLa cells with partially silenced E6 and E7 HPV oncogenes. *Infect Agent Cancer*. 2018;13:25.
30. Jin Y, Kim SC, Kim HJ, Ju W, Kim YH, Kim HJ. Increased sialylation and reduced fucosylation of exfoliated cervical cells are potential markers of carcinogenesis in the cervix. *Clin Chem Lab Med*. 2016;54:1811-1819.

31. Wang PH, Li YF, Juang CM, et al. Expression of sialyltransferase family members in cervix squamous cell carcinoma correlates with lymph node metastasis. *Gynecol Oncol*. 2002;86:45-52.
32. Jin XL, Zheng SS, Wang BS, Chen HL. Correlation of glycosyltransferases mRNA expression in extrahepatic bile duct carcinoma with clinical pathological characteristics. *Hepatobiliary Pancreat Dis Int*. 2004;3:292-295.
33. Gretschel S, Haensch W, Schlag PM, Kemmner W. Clinical relevance of sialyltransferases ST6GAL-I and ST3GAL-III in gastric cancer. *Oncology*. 2003;65:139-145.
34. Glavey SV, Manier S, Natoni A, et al. The sialyltransferase ST3GAL6 influences homing and survival in multiple myeloma. *Blood*. 2014;124:1765-1776.
35. Zhang L, Zhou W, Velculescu VE, et al. Gene expression profiles in normal and cancer cells. *Science*. 1997;276:1268-1272.
36. Wang PH, Lee WL, Juang CM, et al. Altered mRNA expressions of sialyltransferases in ovarian cancers. *Gynecol Oncol*. 2005;99:631-639.
37. Kudo T, Ikehara Y, Togayachi A, et al. Up-regulation of a set of glycosyltransferase genes in human colorectal cancer. *Lab Invest*. 1998;78:797-811.
38. Lopez-Morales D, Velazquez-Marquez N, Valenzuela O, Santos-Lopez G, Reyes-Leyva J, Vallejo-Ruiz V. Enhanced sialyltransferases transcription in cervical intraepithelial neoplasia. *Invest Clin*. 2009;50:45-53.
39. Perez-Garay M, Arteta B, Llop E, et al. alpha2,3-Sialyltransferase ST3Gal IV promotes migration and metastasis in pancreatic adenocarcinoma cells and tends to be highly expressed in pancreatic adenocarcinoma tissues. *Int J Biochem Cell Biol*. 2013;45:1748-1757.
40. Harduin-Lepers A, Krzewinski-Recchi MA, Colomb F, Foulquier F, Groux-Degroote S, Delannoy P. Sialyltransferases functions in cancers. *Front Biosci (Elite Ed)*. 2012;4:499-515.
41. Carvalho AS, Harduin-Lepers A, Magalhaes A, et al. Differential expression of alpha-2,3-sialyltransferases and alpha-1,3/4-fucosyltransferases regulates the levels of sialyl Lewis a and sialyl Lewis x in gastrointestinal carcinoma cells. *Int J Biochem Cell Biol*. 2010;42:80-89.
42. Cazet A, Julien S, Bobowski M, et al. Consequences of the expression of sialylated antigens in breast cancer. *Carbohydr Res*. 2010;345:1377-1383.
43. Recchi MA, Hebbar M, Hornez L, Harduin-Lepers A, Peyrat JP, Delannoy P. Multiplex reverse transcription polymerase chain reaction assessment of sialyltransferase expression in human breast cancer. *Cancer Res*. 1998;58:4066-4070.
44. Sun M, Zhao X, Liang L, Pan X, Lv H, Zhao Y. Sialyltransferase ST3GAL6 mediates the effect of microRNA-26a on cell growth, migration, and invasion in hepatocellular carcinoma through the protein kinase B/mammalian target of rapamycin pathway. *Cancer Sci*. 2017;108:267-276.
45. Ran FA, Hsu PD, Wright J, Agarwala V, Scott DA, Zhang F. Genome engineering using the CRISPR-Cas9 system. *Nat Protoc*. 2013;8:2281-2308.
46. Kim HS, Lee K, Bae S, et al. CRISPR/Cas9-mediated gene knockout screens and target identification via whole-genome sequencing uncover host genes required for picornavirus infection. *J Biol Chem*. 2017;292:10664-10671.
47. Isaji T, Im S, Gu W, et al. An oncogenic protein Golgi phosphoprotein 3 up-regulates cell migration via sialylation. *J Biol Chem*. 2014;289:20694-20705.
48. Xu Z, Isaji T, Fukuda T, Wang Y, Gu J. O-GlcNAcylation regulates integrin-mediated cell adhesion and migration via formation of focal adhesion complexes. *J Biol Chem*. 2019;294:3117-3124.
49. Isaji T, Sato Y, Fukuda T, Gu J. N-glycosylation of the I-like domain of beta1 integrin is essential for beta1 integrin expression and biological function: identification of the minimal N-glycosylation requirement for alpha5beta1. *J Biol Chem*. 2009;284:12207-12216.
50. Sato Y, Isaji T, Tajiri M, et al. An N-glycosylation site on the beta-propeller domain of the integrin alpha5 subunit plays key roles in both its function and site-specific modification by beta1,4-N-acetylglucosaminyltransferase III. *J Biol Chem*. 2009;284:11873-11881.
51. Hang Q, Isaji T, Hou S, Im S, Fukuda T, Gu J. Integrin alpha5 suppresses the phosphorylation of epidermal growth factor receptor and its cellular signaling of cell proliferation via N-glycosylation. *J Biol Chem*. 2015;290:29345-29360.
52. Hou S, Isaji T, Hang Q, Im S, Fukuda T, Gu J. Distinct effects of beta1 integrin on cell proliferation and cellular signaling in MDA-MB-231 breast cancer cells. *Sci Rep*. 2016;6:18430.
53. Isaji T, Gu J, Nishiuchi R, et al. Introduction of bisecting GlcNAc into integrin alpha5beta1 reduces ligand binding and down-regulates cell adhesion and cell migration. *J Biol Chem*. 2004;279:19747-19754.
54. Isaji T, Sato Y, Zhao Y, et al. N-glycosylation of the beta-propeller domain of the integrin alpha5 subunit is essential for alpha5beta1 heterodimerization, expression on the cell surface, and its biological function. *J Biol Chem*. 2006;281:33258-33267.
55. Zhang G, Isaji T, Xu Z, Lu X, Fukuda T, Gu J. N-acetylglucosaminyltransferase-I as a novel regulator of epithelial-mesenchymal transition. *FASEB J*. 2019;33:2823-2835.
56. Franken NA, Rodermond HM, Stap J, Haveman J, van Bree C. Clonogenic assay of cells in vitro. *Nat Protoc*. 2006;1:2315-2319.
57. Kolasinska E, Przybylo M, Janik M, Litynska A. Towards understanding the role of sialylation in melanoma progression. *Acta Biochim Pol*. 2016;63:533-541.
58. Ohtsubo K, Marth JD. Glycosylation in cellular mechanisms of health and disease. *Cell*. 2006;126:855-867.
59. Cazet A, Julien S, Bobowski M, Burchell J, Delannoy P. Tumour-associated carbohydrate antigens in breast cancer. *Breast Cancer Res*. 2010;12:204.
60. Van Slambrouck S, Groux-Degroote S, Krzewinski-Recchi MA, Cazet A, Delannoy P, Steelant WF. Carbohydrate-to-carbohydrate interactions between alpha2,3-linked sialic acids on alpha2 integrin subunits and asialo-GM1 underlie the bone metastatic behaviour of LNCAP-derivative C4–2B prostate cancer cells. *Biosci Rep*. 2014;34:e00138.
61. Shah MH, Telang SD, Shah PM, Patel PS. Tissue and serum alpha 2-3- and alpha 2-6-linkage specific sialylation changes in oral carcinogenesis. *Glycoconj J*. 2008;25:279-290.
62. Tsuji S. Molecular cloning and functional analysis of sialyltransferases. *J Biochem*. 1996;120:1-13.
63. Jun L, Yuanshu W, Yanying X, et al. Altered mRNA expressions of sialyltransferases in human gastric cancer tissues. *Med Oncol*. 2012;29:84-90.
64. Perez-Garay M, Arteta B, Pages L, et al. alpha2,3-sialyltransferase ST3Gal III modulates pancreatic cancer cell motility and adhesion in vitro and enhances its metastatic potential in vivo. *PLoS One*. 2010;5:e12524.

65. Hynes RO. Integrins: bidirectional, allosteric signaling machines. *Cell*. 2002;110:673-687.
66. Jahangiri A, Aghi MK, Carbonell WS. beta1 integrin: critical path to antiangiogenic therapy resistance and beyond. *Cancer Res*. 2014;74:3-7.
67. Kovacs E, Zorn JA, Huang Y, Barros T, Kuriyan J. A structural perspective on the regulation of the epidermal growth factor receptor. *Annu Rev Biochem*. 2015;84:739-764.
68. Mariotti A, Perotti A, Sessa C, Ruegg C. N-cadherin as a therapeutic target in cancer. *Expert Opin Investig Drugs*. 2007;16:451-465.
69. Hou S, Hang Q, Isaji T, Lu J, Fukuda T, Gu J. Importance of membrane-proximal N-glycosylation on integrin beta1 in its activation and complex formation. *FASEB J*. 2016;30:4120-4131.
70. Ma H, Cheng L, Hao K, et al. Reversal effect of ST6GAL 1 on multidrug resistance in human leukemia by regulating the PI3K/Akt pathway and the expression of P-gp and MRP1. *PLoS ONE*. 2014;9:e85113.
71. Lu J, Isaji T, Im S, et al. beta-Galactoside alpha2,6-sialyltranferase 1 promotes transforming growth factor-beta-mediated epithelial-mesenchymal transition. *J Biol Chem*. 2014;289:34627-34641.
72. Takahashi M, Tsuda T, Ikeda Y, Honke K, Taniguchi N. Role of N-glycans in growth factor signaling. *Glycoconj J*. 2004;20:207-212.
73. Tsuda T, Ikeda Y, Taniguchi N. The Asn-420-linked sugar chain in human epidermal growth factor receptor suppresses ligand-independent spontaneous oligomerization. Possible role of a specific sugar chain in controllable receptor activation. *J Biol Chem*. 2000;275:21988-21994.
74. Vasconcelos-Dos-Santos A, Oliveira IA, Lucena MC, et al. Biosynthetic machinery involved in aberrant glycosylation: promising targets for developing of drugs against cancer. *Front Oncol*. 2015;5:138.
75. Dall'Olio F, Trinchera M. Epigenetic bases of aberrant glycosylation in cancer. *Int J Mol Sci*. 2017;18:998.
76. Arike L, Holmen-Larsson J, Hansson GC. Intestinal Muc2 mucin O-glycosylation is affected by microbiota and regulated by differential expression of glycosyltranferases. *Glycobiology*. 2017;27:318-328.
77. Shimizu S. Organelle zones in mitochondria. *J Biochem*. 2019;165:101-107.
78. Kurokawa K, Osakada H, Kojidani T, et al. Visualization of secretory cargo transport within the Golgi apparatus. *J Cell Biol*. 2019;218:1602-1618.
79. Sasaki K, Yoshida H. Organelle zones. *Cell Struct Funct*. 2019;44:85-94.
80. Yano H, Yamamoto-Hino M, Abe M, et al. Distinct functional units of the Golgi complex in Drosophila cells. *Proc Natl Acad Sci U S A*. 2005;102:13467-13472.
81. Kitagawa H, Paulson JC. Cloning and expression of human Gal beta 1,3(4)GlcNAc alpha 2,3-sialyltransferase. *Biochem Biophys Res Commun*. 1993;194:375-382.
82. Sasaki K, Watanabe E, Kawashima K, et al. Expression cloning of a novel Gal beta (1–3/1-4) GlcNAc alpha 2,3-sialyltransferase using lectin resistance selection. *J Biol Chem*. 1993;268:22782-22787.

How to cite this article: Qi F, Isaji T, Duan C, et al. ST3GAL3, ST3GAL4, and ST3GAL6 differ in their regulation of biological functions via the specificities for the α2,3-sialylation of target proteins. *FASEB BioAdvances*. 2020;34:881–897. https://doi.org/10.1096/fj.201901793R

Received: 10 September 2019 | Revised: 16 December 2019 | Accepted: 23 December 2019

DOI: 10.1096/fj.201902313RR

RESEARCH ARTICLE

THE FASEB JOURNAL

Deficiency of core fucosylation activates cellular signaling dependent on FLT3 expression in a Ba/F3 cell system

Chengwei Duan[1] | **Tomohiko Fukuda**[1] | **Tomoya Isaji**[1] | **Feng Qi**[1] | **Jie Yang**[1] | **Yuqin Wang**[2] | **Shinichiro Takahashi**[3] | **Jianguo Gu**[1]

[1]Division of Regulatory Glycobiology, Institute of Molecular Biomembrane and Glycobiology, Tohoku Medical and Pharmaceutical University, Sendai, Japan

[2]Department of Pharmacology, Pharmacy College, Nantong University, Nantong, China

[3]Division of Laboratory Medicine, Faculty of Medicine, Tohoku Medical and Pharmaceutical University, Sendai, Japan

Correspondence
Jianguo Gu, Division of Regulatory Glycobiology, Institute of Molecular Biomembrane and Glycobiology, Tohoku Medical and Pharmaceutical University, 4-4-1 Komatsushima, Aoba-ku, Sendai, Miyagi 981-8558, Japan.
Email: jgu@tohoku-mpu.ac.jp

Shinichiro Takahashi, Division of Laboratory Medicine, Faculty of Medicine, Tohoku Medical and Pharmaceutical University, 1-15-1 Fukumuro, Miyagino-ku, Sendai, Miyagi 983-8536, Japan.
Email: shintakahashi@tohoku-mpu.ac.jp

Funding information
Japan Society for the Promotion of Science, Grant/Award Number: 19H03184, 17K09019 and 17K08284; National Natural Science Foundation of China, Grant/Award Number: 31670807; Ministry of Education, Culture, Sports, Science, and Technology of Japan, Grant/Award Number: 18H04868

Abstract

Fms-like tyrosine kinase 3 (FLT3) is a glycoprotein, that is a member of the class III receptor tyrosine kinase family. Approximately one-third of acute myeloid leukemia (AML) patients have mutations of this gene, and activation of the FLT3 downstream pathway plays an important role in both normal and malignant hematopoiesis. However, the role of *N*-glycosylation for FLT3 activation remains unclear. In this study, we showed that the N-glycan structures on wild type (WT), internal tandem duplication (ITD), and tyrosine kinase domain (TKD) mutants of FLT3 were different. Interestingly, expression of either WT or mutant FLT3 in Ba/F3 cells, an interleukin-3 (IL-3)-dependent hematopoietic progenitor cell, greatly induced core fucosylation. To elucidate the function of core fucosylation in FLT3-mediated signaling, we used a CRISPR/Cas9 system to establish α1,6-fucosyltransferase (Fut8) knockout (KO) cells. Surprisingly, the Fut8KO resulted in cell proliferation in an IL-3-independent manner in FLT3-WT cells, which was not observed in the parental cells, and suggested that this proliferation is dependent on FLT3 expression. Fut8KO greatly increased cellular tyrosine phosphorylation levels, together with an activation of STAT5, AKT, and ERK signaling, which could be completely neutralized by restoration with Fut8 in the KO cells. Consistently, a tyrosine kinase inhibitor efficiently inhibited cell proliferation induced by Fut8KO or specific fucosylation inhibitor. Additionally, immunostaining with FLT3 showed that the proteins were mainly expressed on the cell surface in the KO cells, which is similar to FLT3-WT cells, but different from the ITD mutant. Finally, we found that Fut8KO could induce dimer-formation in FLT3 without ligand-stimulation. Taken together, the present study clearly defines the regulatory function of core fucosylation in FLT3, which could provide a valuable direction for development of drugs could be effective in the treatment of AML.

KEYWORDS

acute myeloid leukemia, cellular signaling, core fucosylation, FLT3, Fut8

Abbreviations: AAL, aleuria aurantia lectin; AML, acute myeloid leukemia; DMSO, dimethyl sulfoxide; EGF, epidermal growth factor; ER, endoplasmic reticulum; FBS, fetal bovine serum; FLT3, Fms-like tyrosine kinase 3; Fut8, α1,6-fucosyltransferase; GAPDH, glyceraldehyde-3-phosphate dehydrogenase; IL-3, interleukin-3; ITD, internal tandem duplication; KO, knockout; PBS, phosphate-buffered saline; PhosL, pholiota squarrosa lectin; PNGase F, peptide-N-glycosidase F; TKD, tyrosine kinase domain; WGA, wheat germ agglutinin; WT, wild type.

1 | INTRODUCTION

Acute myeloid leukemia (AML) is a heterogeneous aggressive disease that accounts for approximately 12% of all hematologic malignancies.[1] AML is characterized by the expansion of an abnormal stem cell clone and accumulation of immature blasts in the bone marrow.[2] Over the past decade, accumulating evidence has suggested that leukemogenesis is a process in which multiple events involving independent genetic alterations in proto-oncogene or suppressor genes, together with epigenetic or environmental factors, contribute to the development of a full malignant phenotype.[3-7]

Fms-like tyrosine kinase 3 (FLT3) is a proto-oncogene expressed in both normal hematopoietic cells and AML cells. FLT3 plays a pivotal role in hematopoiesis through regulating the hematopoietic cell proliferation, survival, and differentiation.[8-12] Internal tandem duplication (ITD) of the juxtamembrane domain of FLT3 is the most frequent kinase mutation in human AML (affecting 20%-30% of adult AML), and is significantly associated with leukocytosis and a poor prognosis.[11,13,14] The predominant point mutation within the tyrosine kinase domain (TKD) is D835Y mutation, which is found in 5%-10% of AML patients.[15,16] FLT3-ITD and FLT3-TKD are known to induce ligand-independent cell proliferation in cytokine-dependent Ba/F3 and 32D cells via the display of different signaling properties.[17-20] The most significant difference in these signaling properties is STAT5, which FLT3-ITD strongly and constitutively activates.[17,19] FLT3-ITD mutations lead to an endoplasmic reticulum (ER)-retained intracellular localization, and a change in the maturation of surface glycosylation and autophosphorylation of the receptor results in efficient activation of STAT5.[21,22] Mass spectrometry analysis exhibited nine potential N-glycosylation sites in the extracellular domain of FLT3.[23] These facts strongly suggest that surface glycosylation changes in the FLT3 receptor may affect the function and downstream signaling of FLT3.

N-Glycosylation plays critical roles in folding, stability, and a vast degree of biological functions of glycoproteins.[24-26] These different effects on glycoproteins mainly result from the different *N*-linked glycan structures determined by various glycosyltransferases. Among these, α1,6-fucosyltransferase (Fut8) is the only enzyme that catalyzes the transfer of a fucose from GDP-fucose to the innermost GlcNAc residue via α1,6-linkage to form α1,6-fucosylation in mammals.[27] The resulting core fucosylated *N*-glycans are widely distributed in a variety of glycoproteins.[28] Accumulating data suggests that Fut8 and its products may play important roles in various physiological and pathological processes, such as tumor formation,[29,30] inflammation and immune response,[31-33] as well as in central nervous system diseases.[34-36] Core fucosylation is known to be crucial for the ligand-binding affinity of transforming growth factor (TGF)-β1 receptor,[37] epidermal growth factor (EGF) receptor,[38] and integrin α3β1[39] for their downstream signaling. Conversely, a deficiency in core fucose leads to a marked enhancement of complex formation such as activin receptor[40] and α-amino-3-hydroxy-5-methyl-4-isoxazolepropionate receptor (AMPAR),[35] which constitutively activated intracellular signaling. Depletion of the core fucosylation of IgG1 is reported to be the most critical role in the enhancement of antibody-dependent cellular cytotoxicity.[41,42] Recently, the blocking of core fucosylation in programmed cell death protein 1 (PD-1) was shown to reduce the cell-surface expression of PD-1 and enhance T cell activation, which led to more efficient tumor eradication.[43] Those studies clearly suggest that core fucosylation plays important roles in cell-signal transduction.

In the present study, to clarify the impact of core fucosylation on FLT3, we employed a CRISPR/Cas9 system to knockout (KO) Fut8 gene in the Ba/F3 cell line, an interleukin-3 (IL-3) dependent hematopoietic progenitor cell.[44] We found that a deficiency of Fut8 increased the FLT3 dimeric formation and intracellular signaling, which led to IL-3 independent cell growth of the FLT3- wild type (WT) cells, but greatly chemosensitized the cells to PKC412, a tyrosine kinase inhibitor. These novel findings suggest that core fucosylation plays a pivotal role in both normal and malignant FLT3 signaling.

2 | MATERIALS AND METHODS

2.1 | Antibodies and reagents

Experiments were performed with the following antibodies: p-STAT5 (#4322S), ERK1/2 (#9102), p-ERK1/2 (#4370), AKT (#9272), p-AKT (#4060), and FLT3 (#3462S), all of which were acquired from Cell Signaling Technology (Danvers, MA, USA); Total STAT5 (#13-3600) was from Thermo Fisher, and monoclonal antibody against α-tubulin was acquired from Sigma (St. Louis, MO, USA). Rabbit polyclonal antibody against glyceraldehyde-3-phosphate dehydrogenase (GAPDH) (#sc-25778) and Mouse monoclonal antibodies against FLT3 (#sc-19635), p-Tyr (sc-7020), and p-Tyr agarose (sc-508 AC), all were from Santa Cruz (Santa Cruz, CA, USA). Biotinylated aleuria aurantia lectin (AAL) and wheat germ agglutinin (WGA) were obtained from the Seikagaku Corp (Tokyo, Japan). Biotinylated pholiota squarrosa lectin (PhosL), which specifically recognizes core fucosylated N-glycans, was a generous gift from Dr Yuka Kobayashi (J-oil Mills, Tokyo, Japan). TO-PRO-3 (#T3605) was obtained from Molecular Probes, Inc (Thermo Fisher, Waltham, MA, USA); The peroxidase-conjugated goat antibodies against mouse and rabbit IgG were from Cell Signaling Technology; Goat anti-mouse/rabbit IgG Alexa Fluor 568, goat anti-rabbit/mouse IgG Alexa Fluor 488, streptavidin-conjugate Alexa Fluor 647, and 488 were purchased from

Invitrogen (Carlsbad, CA, USA). Recombinant murine IL-3 was obtained from PeproTech (London, United Kingdom). Neomycin (G418) was purchased from Nacalai Tesque (Kyto, Japan). BS^3 linker (A39266, 2 mg × 10) was obtained from Thermo scientific; PKC412 (#M1323) and dimethyl sulfoxide (DMSO) were (#276855) from Sigma; and 2-fluoro-L-fucose (2FF) was from Synchem, Inc, IL, USA.

2.2 | Cell line and cell culture

Parental Ba/F3 cells (CTR) were maintained in RPMI with 10% heat-inactivated fetal bovine serum (FBS), 1 ng/mL recombinant murine IL-3, and 50 μmol/L of 2-mercaptoethanol. The stably transduced Ba/F3-FLT3-WT cell lines were maintained in RPMI containing 10% FBS, 1 ng/mL recombinant murine IL-3, 400 μg/mL G418, and 50 μmol/L 2-mercaptoethanol.[45] Ba/F3-FLT3-ITD and Ba/F3-FLT3-TKD cells were grown with 400 μg/mL G418 in RPMI containing 10% heat-inactivated FBS and 50 μmol/L 2-mercaptoethanol.[45]

The 293T (Human embryonic kidney cells) cell line was obtained from the RIKEN cell bank (Tsukuba, Japan). The 293T cells were grown in Dulbecco modified Eagle medium containing 10% FBS. Cells were cultured at 37°C in a humidified 5% CO_2 atmosphere.

2.3 | Expression plasmids and transfection

To confirm the glycosylation status of FLT3 proteins, we transfected them with expression pcDNA3.1 vectors containing human FLT3-WT,[46] FLT3-ITD,[47] or FLT3-TKD[45] in 293T cells using PEI MAX (molecular weight, 40 kDa; Polysciences Inc, PA) and followed the dictates of the US patent document (US20110020927A1) with minor modifications. Briefly, 12 hours prior to transfection, 5×10^6 cells were seeded on a 10 cm dish. Each expression vector (12 μg dissolved in 1mL of dilution buffer (20 mM CH3COONa, pH = 4.0, 150 mM NaCl) and PEI MAX (36 μg dissolved in 36 μL of 0.2 M HCl and then diluted with the dilution buffer to 1 mL) were mixed and incubated at RT for 20 min, and then 2 mL of the mixture was gently transferred to the cell cultured dish for transfection. After incubation for 6 hours, the conditioned medium was replaced with a normal culture medium for further incubation for 48 hours.[48] At 48 hours post transfection, the cell lysates were treated with or without peptide-N-glycosidase F (PNGase F) (New England BioLabs, Ipswich, MA, USA) according to the manufacturer's instructions. Then, the digested cell lysates were analyzed by Western blot. For immunoprecipitation, cell lysates (1 mg) were immunoprecipitated with anti-FLT3 antibody (1.25 μg) and 5 μL of Ab-Capcher Mag beads (P-050-1, Protenova). The immunoprecipitates were analyzed by Western blot.

2.4 | Plasmid constructions and establishment of Fut8KO cell

The pSpCas9 (BB)-2A-GFP plasmid was purchased from Addgene (PX458: Addgene #48138), which was deposited by Dr Feng Zhang.[49] The target vector of mouse Fut8 gene was constructed as previously described.[50] The plasmid was transfected into cells according to the manufacturer's instructions (Amaxa Cell Line Nucleofector kit V). After 2 days of transfection, GFP-positive cells were sorted using a FACSAria II (BD Bioscience). Following 3 weeks of culture, Fut8KO cells were sorted by PhosL lectin, and confirmed by FACS analysis and lectin blotting as described above. Fut8 expression was rescued by electroporating the Fut8KO cells with the pcDNA3.1 vector containing Fut8 gene as previously described.[40]

To establish a stable rescue cell line, the CSIV-TRE-RfA-CMV-KT-Fut8-lentivirus production and infection were performed as described previously.[51] In brief, the CSIV-TRE-RfA-CMV-KT-Fut8 vectors were co-transfected with pCAG-HIVgp and pCMV-VSV-G-RSV-Rev into 293T cells through calcium phosphate transfection method. After transfection for 48 hours, the lentivirus supernatants were collected. The Fut8KO FLT3-WT Ba/F3 cells were infected with the CSIV-TRE-RfA-CMV-KT-Fut8-lentivirus. The infected cells were first selected by the Kusabira Orange marker and then were sorted two times with PhosL lectin using FACS Aria II. The stable cell lines were used in subsequent studies.

2.5 | Flow cytometry analysis of cells

Flow cytometric analysis was performed as described before.[50] Briefly, cells that indicated a semi-confluency were collected from the 10 cm culture dishes and centrifuged at 90 *g*, for 10 minutes. Subsequently, collected cells were washed with chilled phosphate-buffered saline (PBS) and stained with biotinylated PhosL (1:1000) for 1 hour on ice, followed by incubation with streptavidin-conjugate Alexa Fluor 647 for 1 hour. During incubation, the cells were mixed gently every 10 minutes by flicking. After incubation, cells were washed three times with ice-cold PBS and then analyzed using a FACS Calibur flow cytometer (BD Biosciences, San Jose, CA, USA).

2.6 | RT-PCR for detection of mRNA expression levels

Total RNAs of Ba/F3 cell lines were extracted by Trizol reagent (Invitrogen), and then reverse-transcribed using a Prime Script RT Reagent kit with gDNA Eraser (Takara, Japan) according to the manufacturer's instructions. The

specific primers used for the PCR amplification were shown in Table 1. The GAPDH mRNA was served as a control. The obtained reaction products were then subjected to 1.2% agarose gels containing ethidium bromide for electrophoresis.

2.7 | Western blotting and lectin blotting

Western blot analysis was performed as described previously.[50] To prepare the cell lysate, cells were washed with chilled PBS three times and then lysed with cold lysis buffer (20 mM Tris-HCl (pH = 7.4), 150 mM NaCl, 1% TritonX-100) containing proteases and phosphatase inhibitor cocktail (Nacalai Tesque). After being subjected to a rotor shaker for 40 minutes at 4°C, cell lysates were cleared by centrifugation at 15 000 rpm, for 15 minutes at 4°C, and the supernatant was transferred to new marked tubes. The protein concentration was determined using a Pierce BCA protein assay kit (Thermo Fisher Scientific, Munich, Germany). Equal amounts of protein lysate were resolved by reducing SDS-PAGE. After electrophoresis, separated proteins were transferred to PVDF membranes (Millipore, Billerica, MA, USA) and incubated with indicated primary and secondary antibodies or with biotinylated lectins as indicated, and immunoreactive bands were detected using either an Immobilon Western Chemiluminescent HRP Substrate (Millipore) or a Vectastain ABC kit (Vector Laboratories, Burlingame, CA, USA), according to the manufacturer's instructions.

2.8 | Cell proliferation assay

After washing three times with prewarmed PBS, Ba/F3 parent cells then resuspended with the RPMI 1640 medium containing 10% FBS, 1 ng/mL recombinant murine IL-3, and 50 μmol/L of 2-mercaptoethanol. Ba/F3-FLT3-WT cells then resuspended with the RPMI 1640 medium containing 10% FBS, 1 ng/mL recombinant murine IL-3, 400 μg/mL G418, and 50 μmol/L of 2-mercaptoethanol. Ba/F3-FLT3-ITD and Ba/F3-FLT3-TKD cells were maintained with RPMI 1640 medium containing 10% FBS, 400 μg/mL G418, and 50 μmol/L of 2-mercaptoethanol. At daily intervals, following staining with trypan blue, the viable cell number was calculated by counting the unstained cells with a hemacytometer. Experiments were performed in biological triplicates.

2.9 | Confocal microscopy analysis

Cells were processed for immunofluorescence microscopy as previously described.[52] Briefly, cells were washed and suspended in cold PBS containing WGA lectin for 30 minutes at 4°C to stain the cell membrane. For intracellular staining, cells were fixed with 4% paraformaldehyde for 20 minutes at room temperature (RT), and washed twice with wash buffer (0.3% BSA in PBS). Cells were plated on poly-L-lysine coated slides for 20 minutes at RT. To block nonspecific staining, 400 μL of blocking buffer (10% normal donkey serum, 0.3% TritonX-100) was added with incubation for 45 minutes at RT. Cells were then stained with FLT3 antibody in dilution buffer (PBS, 1% bovine serum albumin, 1% normal donkey serum, 0.3% TritonX-100, and 0.01% sodium azide) overnight at 4°C followed by washing with wash buffer and incubation in secondary antibody and with TO-PRO-3. Slides were rinsed with PBS and mounted using coverslips, and fluorescence was detected via sequential excitation using an Olympus FV1000 laser-scanning confocal microscope with an UPlanSApo × 60/1.35 oil objective and high-sensitivity gallium arsenide phosphide detector units operated by F10-ASW version 4.02 software.

2.10 | MTT assay

To evaluate the cytotoxic effects of PKC412, an MTT (#341-01823, Dojindo) assay was performed. The WT Ba/F3 cells expressing FLT3 were pretreated with or without 2FF (100 μM) for 3 days. After 3 days, the WT Ba/F3 cells were plated in quintuplicate at 2×10^4 cells per well in 96-well plates under normal media containing 2FF and PKC412 at indicated concentrations for another 48 hours. Then, a 10 μL of MTT solution (5 mg/mL in PBS) was added to each well and let stand for 4 hours at 37°C. The plate was then centrifuged at 2,000 rpm, for 10 minutes. Subsequently, the supernatant was removed and 100 μL of DMSO was added to each well at 37°C, which was let stand for 10 minutes. Finally, absorption at 570 nm was measured using a microplate reader (Infinite M1000, TECAN, Japan).

TABLE 1 Primer sequences and annealing temperatures (Tm) for RT-PCR

Gene names	Sense primer (5′-3′)	Antisense primer (5′-3′)	Tm (°C)
FLT3	CCCAGTCAATCAGCTTTGGT	CCTGGCTGGTGCTTATGATT	55
Fut8	AGATCTGACAGAGCTGGTCCAG	TCTGTGCGTCTGACATGGACTC	56
GAPDH	ACCCAGAAGACTGTGGATGG	CACATTGGGGGTAGGAACAC	56

2.11 | Chemical cross-linking of FLT3

To assay the dimerization of FLT3, a cross-linking experiment was performed as previously described.[53] Briefly, 12 hours prior to transfections 1×10^6 cells were seeded on a 6 cm dish, then, transfected with the FLT3-WT expression vector (1 μg) in 293T or Fut8KO 293T cells[40] using PEI MAX as described above. The 293T cells were serum-starved for 8 hours before incubation with or without human FLT3 ligand (FL) at 100 ng/mL for 30 minutes in 4°C. Cross-linking was performed by an incubation with 1 mM BS3 for 15 minutes at 4°C. The reaction was stopped by adding glycine-HCl (pH = 7.5) to a final concentration at 150 mM and incubating for 5 minutes. After wash three times with chilled PBS, these cells were harvested with RIPA buffer (Tris-HCl (pH = 7.5), 150 mM NaCl, 1% TritonX-100, 0.1% SDS). The cell lysates were subjected to 7.5% SDS-PAGE, and analyzed by Western blot with anti-FLT3 antibody.

2.12 | Statistical analysis

Results are reported as the means ± SEM. Statistical analyses were performed using an unpaired Student's *t* test with Welch's correction (one-tailed) using GraphPad Prism 5.0 software (GraphPad Software Inc). $P < .05$ was regarded as statistically significant.

3 | RESULTS

3.1 | Comparing of the glycosylation status of WT with that of FLT3 mutants

Glycosylation of proteins often results in a heterogeneous pattern on Western blots. It is known that there are two forms of human FLT3. One is a mature form at around 150 kDa, which is thought to be completely glycosylated at the N-linked glycosylation sites of the extracellular domain of the Golgi apparatus to form complex types of N-glycans, and is then expressed on the cell surface. The other is an immature form around 130 kDa, which is incompletely glycosylated to form a high mannose type of N-glycans, and is mainly localized in the ER.[22] To confirm the differences in the glycosylation status of FLT3 WT and mutants, we transfected 293T cells with expression plasmids encoded with FLT3-WT,[46] FLT3-ITD,[47] or FLT3-TKD,[45] and extracted cell lysates after 48 hours for Western blotting. The bands of FLT3-WT that migrated on SDS-PAGE were totally different from the other two mutants (Figure 1A), which could be neutralized by the removal of N-glycans via treatment with PNGase F. All bands of FLT3 were shifted to around 120 kDa upon PNGase F treatment. On the contrary, we also were curious about the effects of FLT3 on glycosylation. The expression levels of core fucosylation confirmed by AAL lectin, which preferentially recognizes core fucosylated N-glycans,[40,50] were enhanced by expression of FLT3 either WT or mutants (Figure 1B), whereas the reactive abilities with WGA lectin, which recognizes GlcNAc-containing total glycans were similar among those cells (Figure 1C). To know whether or FLT3 was modified by core fucosylation, we performed an immunoprecipitation with anti-FLT3 antibody in Ba/F3 cells. Unfortunately, the experiment for detection of FLT3 protein expression was failed in the Ba/F3 cell. So, we used the 293T cell instead of Ba/F3 cell to improve protein expression levels, and found FLT3 was core fucosylation confirmed by AAL lectin blot as shown in Figure 1D, which was also confirmed in endogenous FLT3 expressed in THP-1 cells, a human acute monocytic leukemia cell line (data not shown). To explore whether the increased core fucosylation was due to a promotion of Fut8 expression by FLT3, semi-quantitative RT-PCR was performed and found that FLT3 did not express in CTR cell (Figure 1E). Overexpression of either WT- or mutant-FLT3 greatly induced Fut8 mRNA expression (Figure 1F). On the contrary, the increased levels of core fucosylation in those FLT3 expressing cells were inhibited by PKC412 (Figure 1G), a FLT3 kinase inhibitor, suggesting the FLT3-mediated signaling may induce Fut8 expression. That result suggested that core fucosylation is specifically increased by the expression of either WT or mutant FLT3.

3.2 | Establishment of FLT3-expressed Fut8KO Ba/F3 cells

To understand the mechanisms of induction for core fucosylation by FLT3, we established Fut8KO cell lines using a murine Ba/F3 cell line, an IL-3-dependent cell line that exhibits IL-3 independency in the presence of oncogenic signals such as FLT3-ITD and -TKD.[17] The pSpCas9 (BB)-2A-GFP vector containing target sequences were transduced into those Ba/F3 cell lines as indicated by electroporation, and stable cell lines were established by positive and negative sorting with GFP and PhosL lectin as described in the "Methods and Materials" section. Finally, we successfully confirmed stable Fut8KO cell lines by flow cytometric analysis using biotinylated PhosL lectin (Figure 2A) and lectin blotting with AAL (Figure 2B), which specifically recognizes core fucosylated N-glycans.[50,54]

3.3 | IL-3 independent proliferation in Fut8KO- FLT3-WT Ba/F3 cells

Fms-like tyrosine kinase 3 plays a crucial role in normal hematopoietic processes such as proliferation, differentiation,

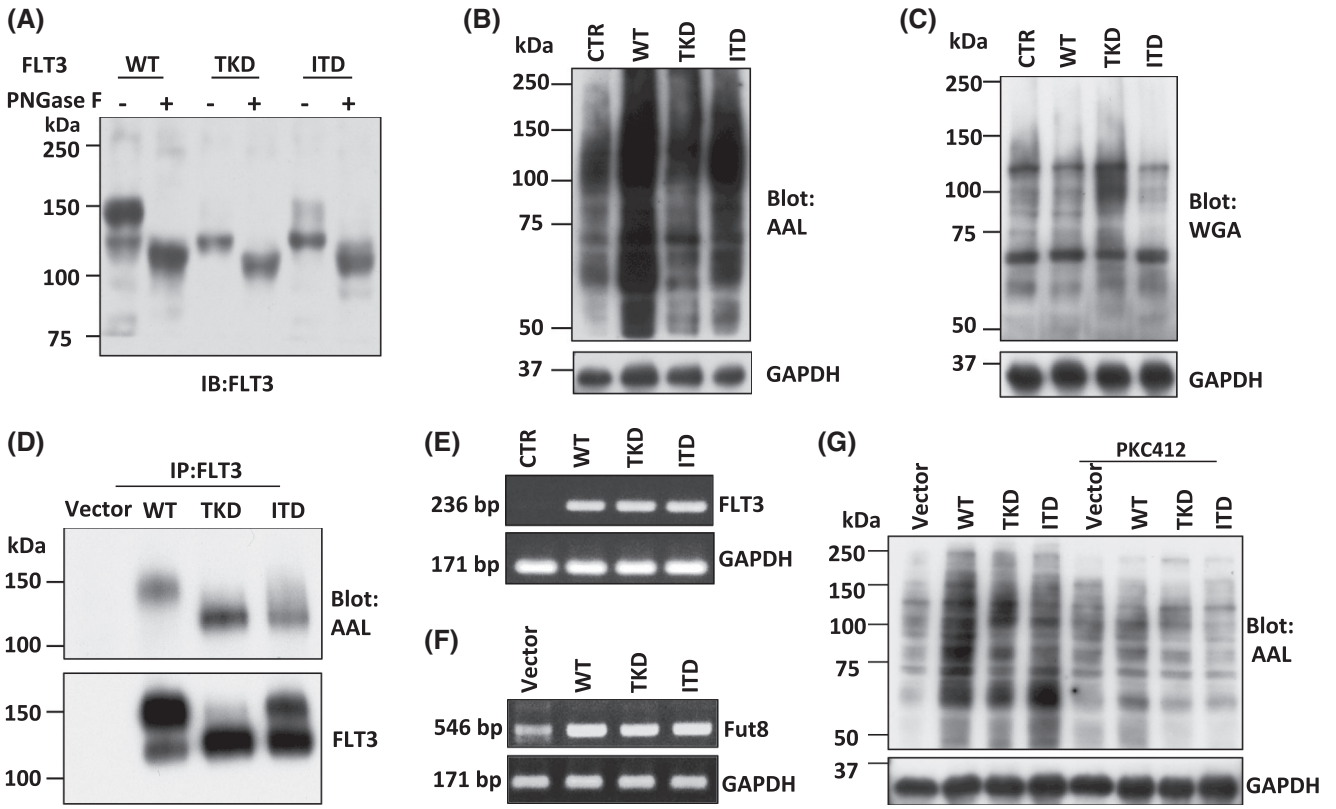

FIGURE 1 Glycosylation patterns of FLT3 proteins and the effects on fucosylation expression. A, The 293T cells were cultured at 70% confluency, and then transfected with plasmids containing human FLT3-WT, FLT3-ITD, or FLT3-TKD. At 48 hours post transfection, the cell lysates were treated with or without PNGase F, and analyzed by Western blot with anti-FLT3 antibody. The effects of FLT3 WT or mutants on core fucosylation in Ba/F3 cells were examined by AAL lectin blot (B) or WGA lectin blot (C). The same amounts of cell lysates were separated on 7.5% SDS-PAGE, and the membranes were probed with AAL (top panel), and then re-probed with anti-GAPDH antibody (bottom panel), which was used as a loading control. D, The same amounts of cell lysates from those indicated transfected 293T cells were immunoprecipitated with anti-FLT3 antibody, and then the immunoprecipitates were probed with AAL lectin (upper panel) and re-probed with anti-FLT3 antibody (lower panel) as a loading control. E, RT-PCR using total RNA extracted from different Ba/F3 cells were carried out to examine the mRNA levels of FLT3. GAPDH was used as control. F, RT-PCR was carried out to examine the mRNA levels of Fut8 in different Ba/F3 cells as indicated. GAPDH was used as control. G, The same amounts of cell lysates from the different Ba/F3 cells treated with or without PKC412 (1 nM) for 48 hours, were separated on 7.5% SDS-PAGE, and the membranes were probed with AAL (top panel), and then re-probed with anti-GAPDH antibody (bottom panel), which was used as a loading control

and survival.[8,12] To test whether Fut8KO regulates cell proliferation, we compared the viable cell number in different Ba/F3 cell lines. Fut8KO slightly increased cell proliferation in the presence of IL-3 in the CTR (Figure 3A). Quite interestingly, Fut8KO induced cell proliferation in FLT3-WT cells even in the absence of IL-3 (Figure 3B), whereas the Fut8KO CTR have no IL-3-independent proliferative activity (Figure 3A). What is more, the restoration with Fut8 gene in the Fut8KO WT cells (Rescue cell) resulted in an IL3-dependent cell growth (Figure 3B). The cell proliferation of the rescue cells was completely blocked in the absence of IL-3. These results suggest that FLT3 expression is necessary for Fut8KO-induced IL-3-independent cell proliferation. In addition, ablation of Fut8 partially blocked ITD (Figure 3C) and TKD (Figure 3D) cell proliferation. These results suggest that the lack of core fucosylation dramatically activate FLT3-WT. To clarify FLT3 receptor activation mechanisms related to core fucosylation depletion, we mainly focused on the FLT3-WT in subsequent studies.

3.4 | Effects of Fut8KO on cellular signaling in the FLT3-WT Ba/F3 cells

Next, we performed Western blotting to analyze the activation status of STAT5, AKT, and ERK signaling, which are important pathways for FLT3 WT and mutant downstream signaling.[17,19,55] Consistently, FLT3-WT could not induce phosphorylation of STAT5 in the absence of IL-3. However, Fut8KO greatly induced phosphorylation of STAT5 even without IL-3 (Figure 4A). The activation of AKT and ERK was also observed in the Fut8KO cells (Figure 4A).

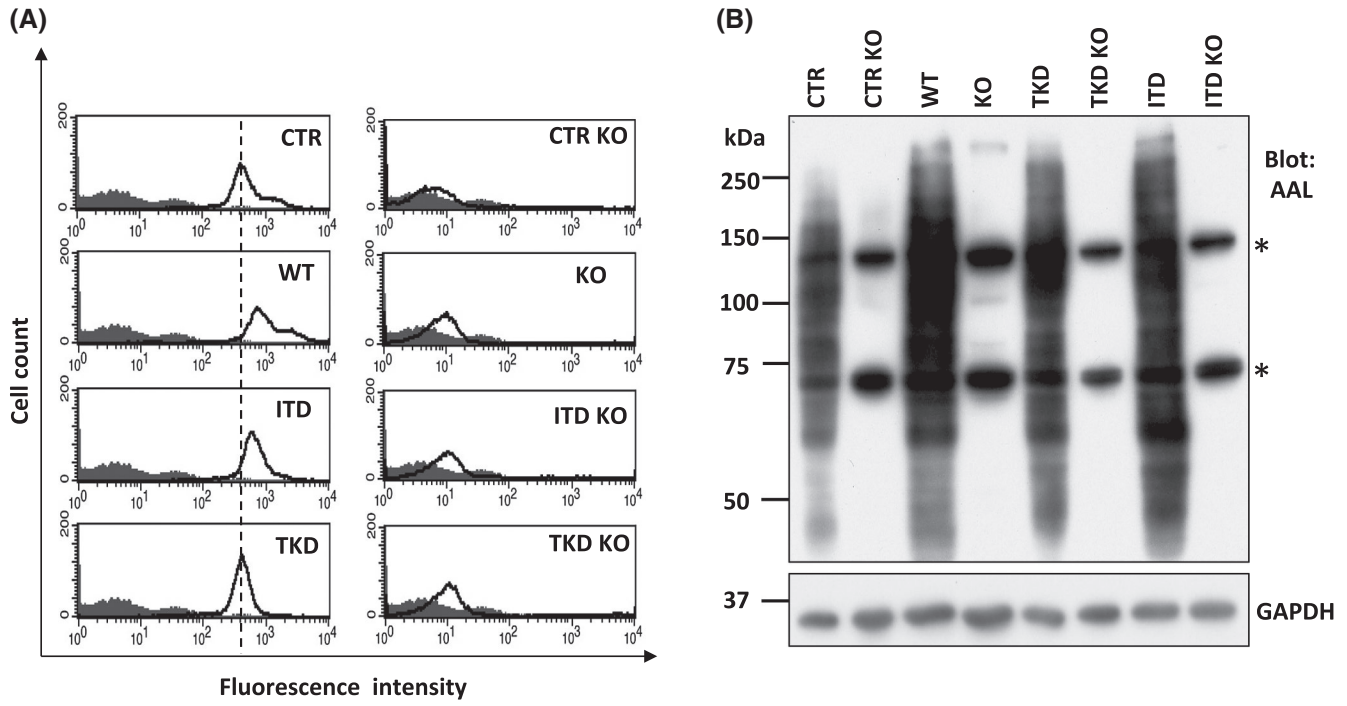

FIGURE 2 Established Fut8 deficient Ba/F3 cells. A, The parent (CTR), FLT3 WT and mutants of Ba/F3 cells, and Fut8KO cells were collected and incubated with (bold line) or without (gray shadow) the PhosL lectin, which preferentially recognizes core fucosylated N-glycans, followed by incubation with Biotinylated Alexa Fluor 647 streptavidin and flow cytometric analysis. The vertical dashed lines indicate the peak reacted with PhosL lectin expression in CTR cells. B, Equal amounts of cell lysates from CTR and stably expressed FLT3-WT or mutants were analyzed by immunoblot with AAL lectin; GAPDH served as a loading control. Asterisks represent nonspecific bands

Importantly, these inductions were blocked by reexpression of Fut8 in the KO cells (Figure 4A). The core fucosylation was confirmed by AAL lectin blotting (Figure 4B).

3.5 | Deficiency of core fucosylation did not affect FLT3 intracellular localization

Changes in FLT3 localization are known to influence downstream signaling. Mutations of FLT3 receptor result in localization in the ER, which affects surface glycoprotein maturation and activates STAT5, while ligand-activated WT FLT3 is mainly localized on the cell surface and activates MAP kinase.[21,56,57] Therefore, we next performed immunostaining with FLT3 antibody to examine the effects of core fucosylation on FLT3 intracellular localization. The FLT3-WT proteins were mainly localized on the cell surface, and co-localized with WGA staining (Figure 5, upper panel). In Fut8KO cells, the FLT3-WT proteins were also localized on the cell surface (Figure 5, middle panel). The localization pattern was quite different that of FLT3-ITD, in which FLT3-ITD proteins were mainly localized in the intracellular domain (Figure 5, lower panel), presumably in the ER, as previously described.[21,58] These results suggest that the underlying molecular mechanism for the induction of FLT3-WT by Fut8KO may be different from activation in the FLT3-ITD mutation.

3.6 | Deficiency of core fucosylation increased cellular tyrosine phosphorylation levels and dimerization of FLT3

As we revealed that Fut8KO resulted in the activation of FLT3-WT downstream signaling, we next examined the tyrosine phosphorylation levels of FLT3. The intracellular domain of FLT3 has 10 potential tyrosine phosphorylation sites.[59,60] The cell lysates and immunoprecipitates with p-Tyr agarose (PY20) from indicated cells were examined. As a result, ablation of core fucosylation potently increased total tyrosine phosphorylation levels (Figure 6A). There is evidence that the dimerization of FLT3-WT is an initial and essential event in ligand-induced signal transduction.[61] Therefore, we compared FLT3 dimerization in 293T and Fut8KO 293T cells with or without FL. As shown in Figure 6B, the dimer formation of FLT3 in WT or Fut8KO 293T cells could be induced by FL. Interestingly, the dimerization was observed in the Fut8KO 293T cells even without FL, but not in the WT 293T cells. In addition, the upper band of FLT3 (around 150 kDa, so called mature form) rather than lower band (around 130 kDa, so called immature form) participated in the dimer formation. Collectively, these data suggest that the deficiency of core fucosylation promotes the dimerization of FLT3 and results in the aberrant activation of FLT3-WT-mediated signaling such as p-STAT5, p-ERK, and p-AKT,

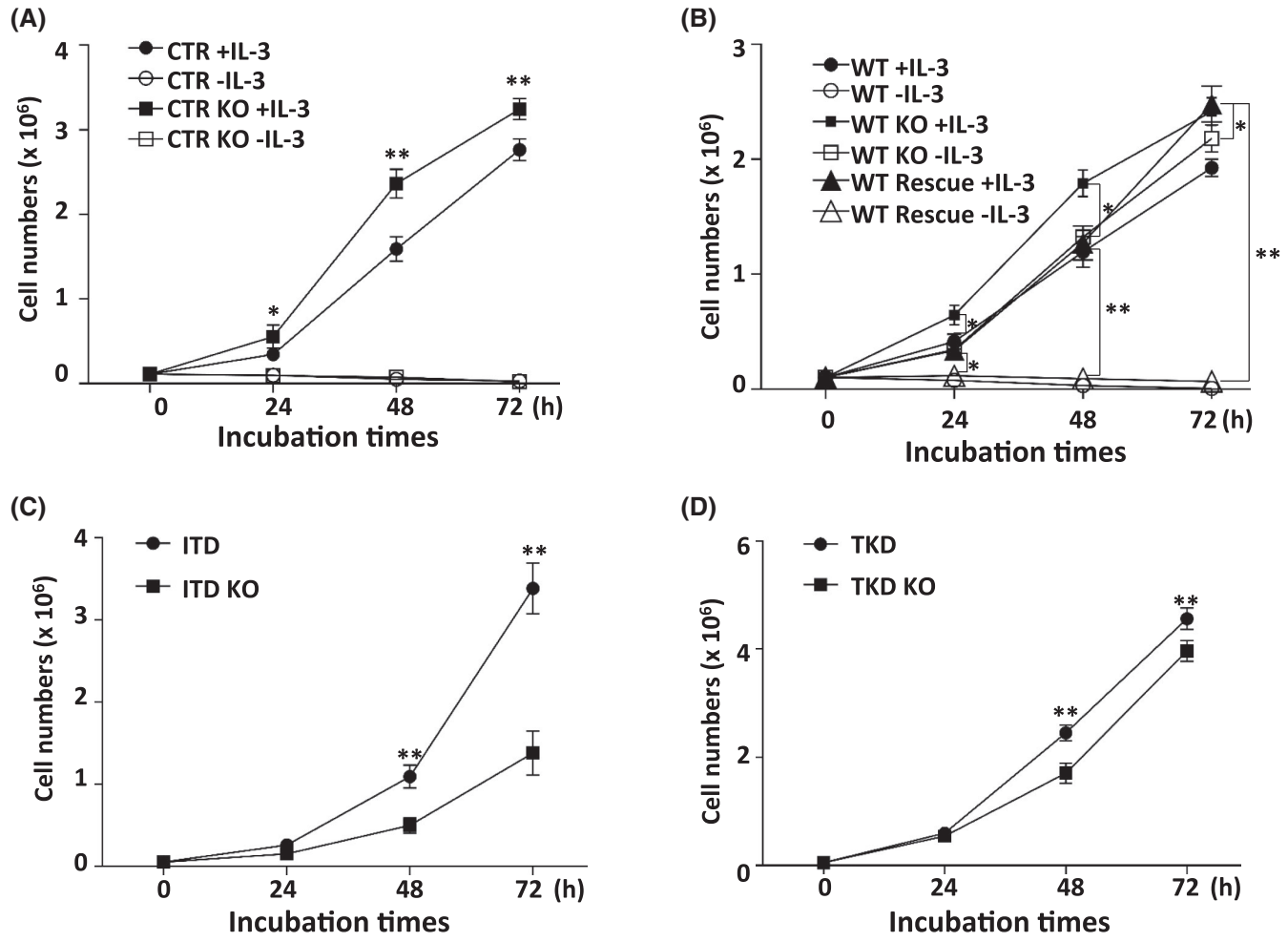

FIGURE 3 Influences of core fucosylation on Ba/F3 cell proliferation. A, The parent Ba/F3 cells (CTR) and CTR Fut8KO cells were cultured under normal culture media with or without IL-3 at 1 ng/mL final concentration, and the cell numbers of living cells were measured by trypan blue exclusion assay at indicated times. CTR KO with IL-3 versus CTR KO without IL-3. B, The parent cells expressing FLT3-WT (WT) or Fut8KO cells expressing FLT3-WT (WT KO), and the WT KO cells restored with Fut8 gene (WT Rescue) were cultured. Cell numbers were counted as described above. WT KO and WT Rescue with IL-3 versus WT KO and WT Rescue without IL-3, respectively. The parent or Fut8KO cells expressing FLT3-ITD (C) or FLT3-TKD (D) were also cultured under normal culture media without IL-3 for 24, 48, and 72 hours. The numbers of living cells were measured by trypan blue exclusion assay. Data represent the average of three independent experiments. All values are Means ± SEM (n = 3). *$P < .05$. **$P < .01$

which induces an IL-3-independent cell proliferation pathway in the Ba/F3 cell system.

3.7 | PKC412 efficiently inhibited cell proliferation of Fut8KO cells in a relatively lower dose

Since Fut8KO greatly induced tyrosine phosphorylation as described above, we examined the effects of PKC412, a tyrosine kinase inhibitor, on cell proliferation. In fact, it was reported that the inhibitory effects of PKC412 on cell proliferation could be observed with usage at 500 nM, but even at 100 nM in Ba/F3 cells expressed FLT3.[62] However, it was interesting, that PKC412 significantly inhibited cell proliferation even at 1 nM, which did not affect cell proliferation of the WT cells (Figure 7A). A fluorinated analog of fucose, 2FF, functions as a metabolic fucosylation inhibitor, which is taken up by cells and converted to GDP-2FF through endogenous salvage pathways.[63,64] Therefore, 2FF could be considered a specific inhibitor for fucosylation. In fact, a treatment with 2FF at 100 μM could suppressed core fucosylation in HepG2 cells.[30] We also confirmed the inhibitory effect on Ba/F3 cells. Similar to the Fut8KO cells, the sensitivities for the inhibitory effects of PKC412 on cell proliferation were also increased in the cells pretreated with 2FF (Figure 7B). These results suggested that a deficiency of core fucosylation induces a novel signal pathway, but not like the IL-3-dependent signal pathway, which is more sensitive to treatment with a tyrosine kinase inhibitor.

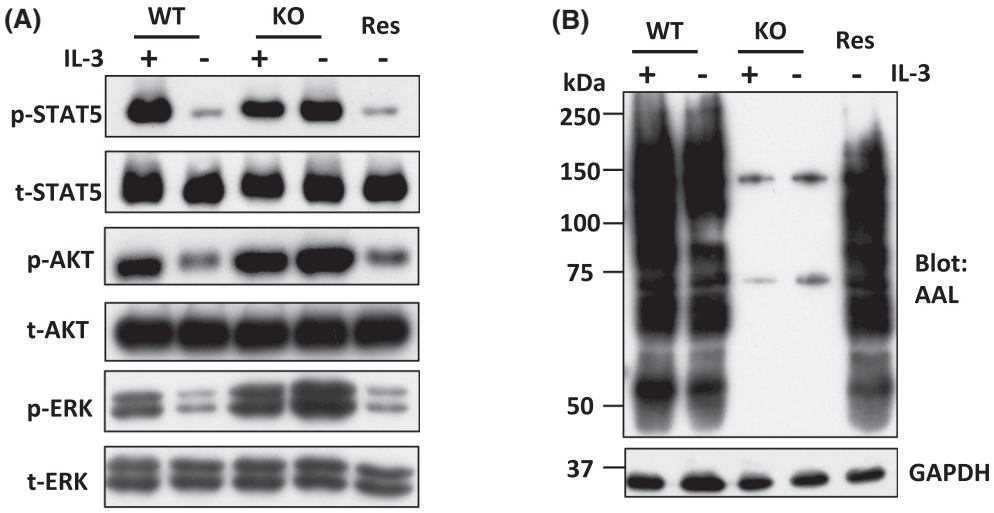

FIGURE 4 Effects of core fucosylation on intracellular signaling. The wild type (WT), Fut8KO (KO), or restoration of Fut8 in the KO cells (Res) of Ba/F3 cells expressing FLT3 were cultured under normal culture media with (+) or without IL-3 (−) for 24 hours. A, The same amounts of cell lysates were separated on 7.5% SDS-PAGE, and Western blotting with the indicated antibodies including both total and phospho-STAT5, ERK, and AKT. B, The expression levels of core fucosylation in these cells were blotted with AAL (top panel) and re-probed with anti-GAPDH (low panel). GAPDH served as a loading control

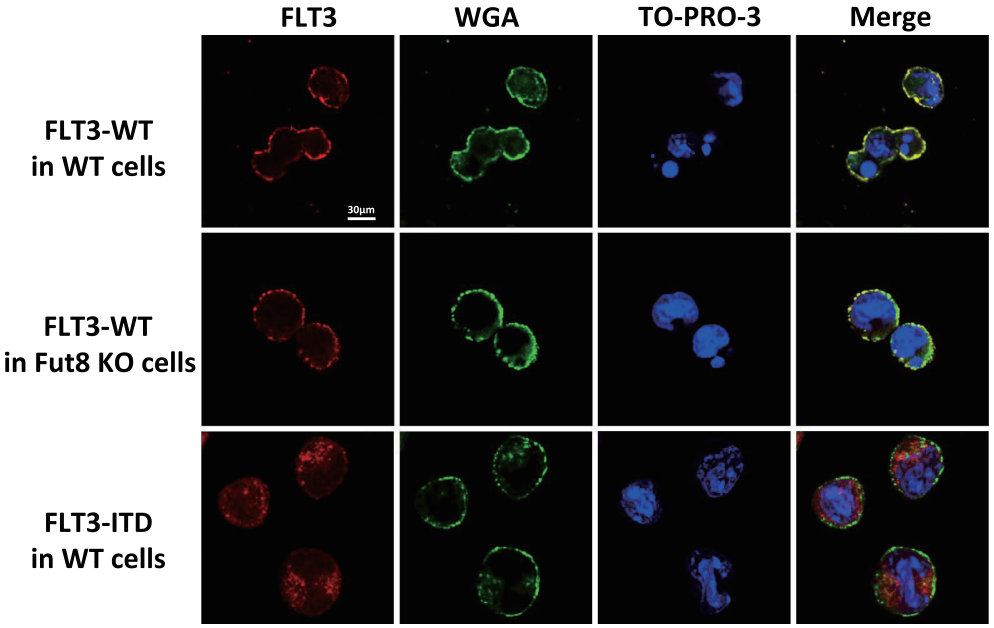

FIGURE 5 Effects of core fucosylation on FLT3 intracellular localization. The indicated cells were stained for plasma membrane using WGA lectin (Green), fixation and then adhered to slides coated with poly-L-lysine for further staining with FLT3 (Red) and TO-PRO-3 (Blue). Slides were visualized by immunofluorescence microscopy using an Olympus FV1000 laser-scanning confocal microscope as described in Methods and Materials. Bar shows 30 μm

4 | DISCUSSION

Fms-like tyrosine kinase 3 signaling is important for normal and oncogenic hematopoiesis, but the downstream effect from the modification of FLT3 surface glycoprotein remains to be elucidated. In the current study, we used the CRISPR/Cas9 system to establish Fut8KO Ba/F3 cell lines, and found that a deficiency of Fut8 resulted in cell proliferation in an IL-3 independent manner in FLT3-expressing cells, but not in FLT3-negative cells, which suggests that this cell proliferation is dependent on FLT3 expression (Figure 8). Of course, we could not exclude influences of Fut8KO from other receptors including IL-3 receptor. We revealed a novel effect for a deficiency of core fucosylation for FLT3 homodimerization and activation of several downstream signaling pathways in the absence of

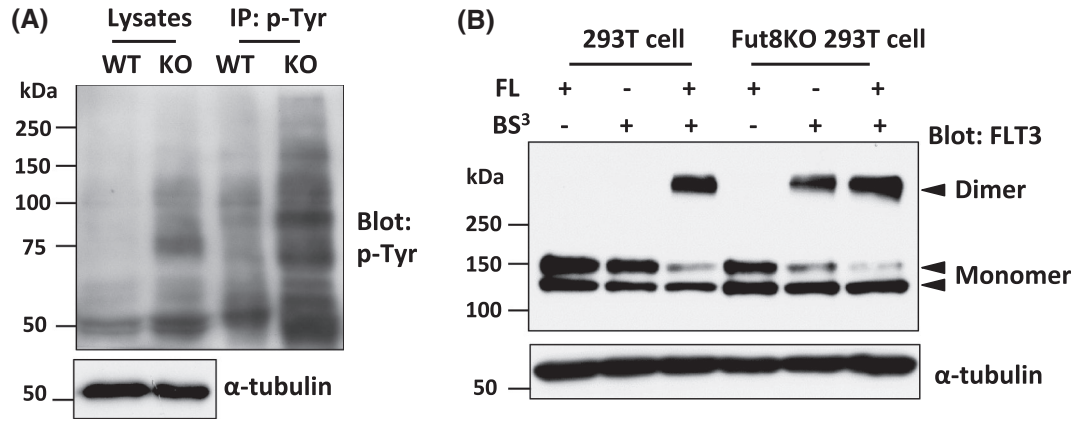

FIGURE 6 Deficiency of core fucosylation increased cellular tyrosine phosphorylation levels and dimerization of FLT3. The wild type (WT) and Fut8KO (KO) of Ba/F3 cells expressing FLT3 were cultured under normal culture media with or without IL-3 for 48 hours, respectively. A, The same amounts of cell lysates and immunoprecipitates with p-Tyr agarose (PY20) were separated on 7.5% SDS-PAGE, and the membranes were blotted with anti-p-Tyr (PY99) and re-probed with anti-α-tubulin, as a loading control. B, The FLT3-WT plasmid was transfected into 293T or Fut8KO 293T cells. After 48 hours, cells were treated for chemical cross-linking as described under "MATERIALS AND METHODS." Cell lysates were separated on 7.5% SDS-PAGE, and blotted with anti-FLT3 antibody to detect FLT3 monomer and dimer. α-Tubulin was used as a loading control

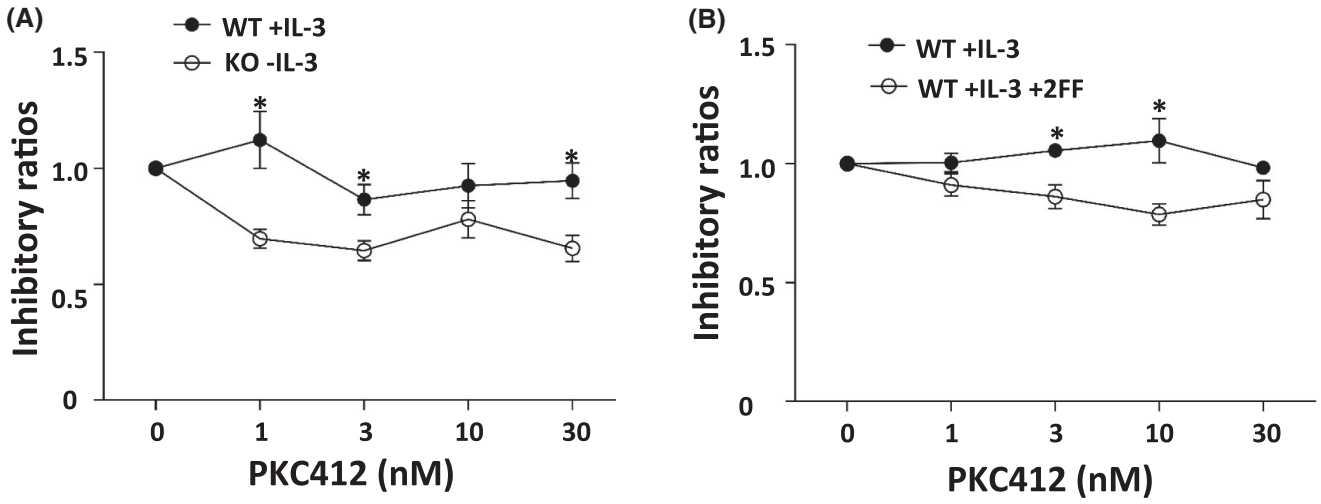

FIGURE 7 Loss of core fucosylation chemosensitized the cells to PKC412, a tyrosine kinase inhibitor. A, The wild type (WT) and the Fut8KO (KO) of Ba/F3 cells expressing FLT3-WT were cultured in the presence of PKC412 at indicated concentrations, and then cell numbers were examined after 48 hours. The WT and KO cells were cultured with or without IL-3, respectively. The inhibitory ratio was normalized to that of each group without the inhibitor as 1. Data are Means ± SEM (n = 3). *$P < .05$. B, The WT Ba/F3 cells expressing FLT3 were pretreated with or without 2FF (100 μM) for 3 days, and then cultured under normal media containing 2FF and PKC412 at indicated concentrations for another 48 hours. The cell numbers were measured using MTT assay. The inhibitory ratio was normalized to that of each group without the inhibitor as 1. Data are Means ± SEM (n = 3). *$P < .05$

a ligand. Furthermore, blockage of core fucosylation by Fut8KO or 2FF, a fucosylation inhibitor, greatly increased sensitivities for the suppression of cell proliferation by using PKC412, a tyrosine kinase inhibitor. Therefore, the manipulation of the core fucosylation could provide valuable direction for the development of drugs that could be effective in treating AML.

As mentioned above, core fucosylation is an important regulator for receptor-mediated signaling. Our group recently reported that Fut8 deficiency increases sensitivities to inflammatory stimulators such as IFN-γ or IL-6 in glial cell lines,[50] and sensitivities for postsynaptic depolarization by enhancing the heteromerization of AMPARs,[35] suggesting that without core fucosylation these receptors might exist in an active state. In contrast, core fucosylation represses several receptor functions as well. Deletion of core fucosylation down-regulated the EGF-induced phosphorylation of EGF receptor[38] and TGF-β1 receptor-mediated Smad activation.[37]

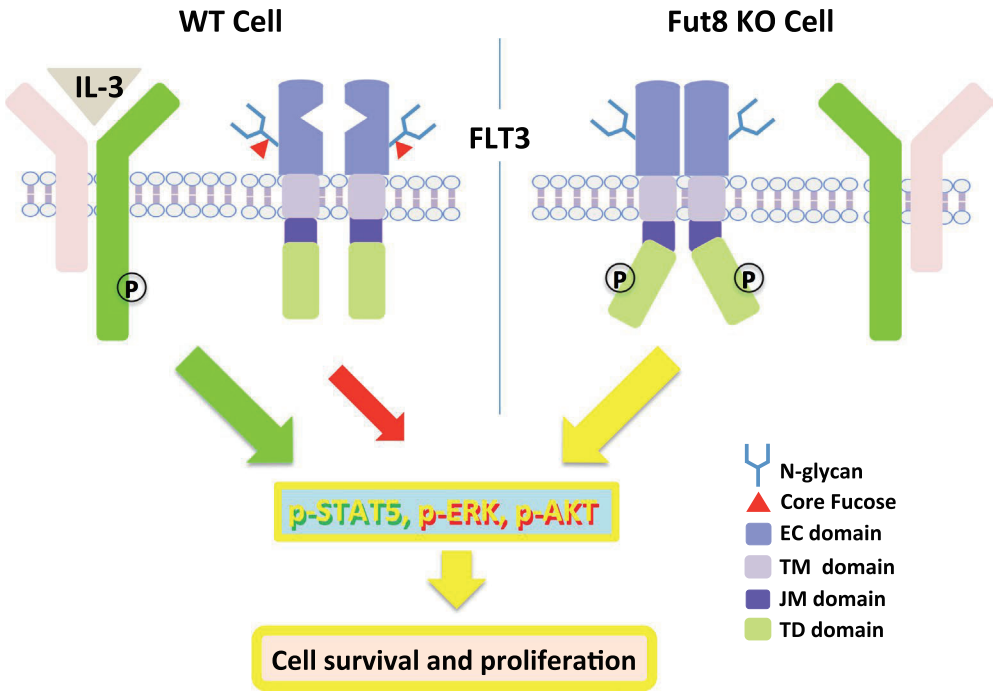

FIGURE 8 A working model for the role of core fucosylation in regulating FLT3 activity in Ba/F3 cells. As described previously, FLT3 is a member of the class III receptor tyrosine kinase family, which exists in the extracellular (EC) domain that contains 9 potential N-glycosylation sites, a transmembrane (TM), a juxtamembrane (JM), and tyrosine kinase (TK) domains.[23] Ba/F3 cells are an IL-3-dependent cell line, and in the presence of IL-3, STAT5 is potently activated[78] (shown in green arrow and green letters). The FLT3-WT signal mainly activates the ERK and AKT pathway in the absence of FLT3 ligand[79] (red arrow and red letters). In the present study, the deficiency of core fucosylation induced an IL-3-independent cell proliferation pathway in the Ba/F3 cell system, in which the expression of FLT3 is essential. A lack of core fucosylation triggers ligand-independent FLT3 dimerization on the cell surface, resulting in aberrant activation of FLT3-mediated signaling such as p-STAT5, p-ERK, and p-AKT (yellow arrow), which are different from the observations in the FLT3-ITD and -TKD mutants. Those two mutants are mainly expressed in the ER, and participate in activation of the STAT5 signaling pathway, rather than the ERK and AKT signaling pathways.[21] Thus, the underlying molecular mechanism for the induction of FLT3-WT by Fut8KO could be different from the activation in the FLT3-mutants, which could provide valuable direction for the development of drugs that could be effective in the treatment of AML

Sialylation and fucosylation of EGF receptor suppress its function and activation in lung cancer cells.[65] These data suggest that core fucosylation either positively or negatively affects receptor functions. In the present study, we also found that the effect of core fucosylation differs between WT and FLT3 mutant receptors. Considering the FLT3-TKD or -ITD mutant could activate downstream signaling pathways through different mechanisms such as conformation change, intracellular localization and/or modification status, which might be quite different from WT FLT3. Therefore, we could speculate that the disruption of Fut8 affects other glycoproteins, which interfere with those FLT3 signaling to down-regulate cell proliferation. Further clarifying the mechanisms of how fucosylation inhibition activates/suppresses FLT3 receptors may be helpful in developing novel targeted therapies for hematological malignancies.

Several important residues in FLT3 activation have been reported which includes tyrosine residues 589 and 591 for ligand-dependent activation of FLT3-WT Ba/F3 cells.[66] Tyrosine 589 and 591 are also reported to play important roles in STAT5 activation and transformation by FLT3-ITD.[67] Masson et al[59] reported that tyrosines 768, 955, and 969 of FLT3, as phosphorylation sites, and mediators of growth factor receptor binding protein (Grb2) interactions lead to the association of Grb2-associated binder 2 (Gab2), which contributes to proliferation and survival. They revealed that these residues are important for the activation of STAT5 and AKT.[59] STAT5 is mainly activated by FLT3-ITD signaling via aberrant localization in the ER of FLT3-ITD, but barely activated by FLT3-WT signaling.[21] We observed that the depletion of core fucosylation did not change the transmembrane localization of FLT3-WT. However, FLT3-WT activates not only ERK and AKT, but STAT5 in the Fut8KO cells (Figure 8). We postulate that the activation of STAT5 via the depletion of core fucosylation happens not by an intracellular localization change in FLT3, but by phosphorylation, or some modifications of the important residues of FLT3. The activation mechanisms of FLT3 receptor via the depletion of core fucosylation should be clarified in the future.

FLT3 is reported to undergo glycosylation in the ER,[22] and several glycosylation inhibitors were examined for their effect on the functions of FLT3. One of these compounds is fluvastatin, already approved by the FDA and clinically applied inhibitor of mevalonate synthesis, which apart from blocking cholesterol synthesis, also inhibits N-glycosylation by depleting the cells of dolichol phosphate, thus leading to a loss of surface expression and the induction of cell death in Ba/F3 cell.[52] The other compound is 2-deoxy-D-glucose which not only depletes cells of ATP but also impairs N-glycosylation.[68] A possible reason for the selective inhibition of FLT3-ITD-positive cells by compounds affecting glycosylation may be a further shift of FLT3-ITD toward intracellular localization, thereby abrogating signaling from the cell surface and in turn cell transformation. Tunicamycin is a bacterial antibiotic, which specifically inhibits the transfer of activated sugars to dolichol phosphate, an essential step in N-glycosylation of proteins in the ER.[69,70] These effects are partly mediated by arresting FLT3-ITD in an under-glycosylated state and thereby attenuating FLT3-ITD-driven AKT and ERK signaling.[71] Because FLT3 plays a very important role in the pathogenesis of AML, various FLT3 inhibitors have been developed.[72] However, their duration of clinical response is short because of the rapid development of resistance.[73]We found that depletion of fucosylation by Fut8KO in combination with PKC412 efficiently decreases the factor-independent growth of FLT3-WT cells. Inhibition of N-glycosylation may be a possible approach for cancer therapy. Theoretically, however, inhibition of core fucosylation inhibitors is less harmful and should have fewer side effects. To date, several fucosylation inhibitors have been developed,[63,64,74] and there are many good examples of combination therapy with FLT3 inhibitors for AML.[75-77] Therefore, the modulation of FLT3 glycosylation may provide a hint for development of a new therapy for different types of FLT3-mediated hematological malignancy.

ACKNOWLEDGMENTS

This work was supported in part by a Grant-in-Aid for Scientific Research (19H03184 to JG, 17K09019 to ST and 17K08284 to TF) from the Japan Society for the Promotion of Science, by a grant from National Natural Science Foundation of China (No. 31670807), and by a Grant-in-Aid for Scientific Research on Innovative Areas (18H04868 to JG) from the Ministry of Education, Culture, Sports, Science, and Technology of Japan.

CONFLICT OF INTEREST

The authors declare no conflicts of interest and no competing financial interests.

AUTHOR CONTRIBUTIONS

C. Duan, Y. Wang, T. Fukuda, S. Takahashi, and J. Gu designed the research; C. Duan performed all experiments; C. Duan and T. Isaji performed flow cytometric analysis; T. Isaji, F. Qi, J. Yang, and T. Fukuda assisted with experiments; T. Isaji, Y. Wang, T. Fukuda, S. Takahashi, and J. Gu analyzed and interpreted the data; C. Duan, S. Takahashi, and J. Gu wrote and revised the manuscript; and all authors approved the final version of the manuscript.

REFERENCES

1. Siegel RL, Miller KD, Jemal A. Cancer statistics, 2016. *CA Cancer J Clin*. 2016;66:7-30.
2. Arber DA, Orazi A, Hasserjian R, et al. The 2016 revision to the World Health Organization classification of myeloid neoplasms and acute leukemia. *Blood*. 2016;127:2391-2405.
3. Cancer Genome Atlas Research Network, Ley TJ, Miller C, et al. Genomic and epigenomic landscapes of adult de novo acute myeloid leukemia. *N Engl J Med*. 2013;368:2059-2074.
4. McKerrell T, Park N, Moreno T, et al. Leukemia-associated somatic mutations drive distinct patterns of age-related clonal hemopoiesis. *Cell Rep*. 2015;10:1239-1245.
5. Papaemmanuil E, Gerstung M, Bullinger L, et al. Genomic classification and prognosis in acute myeloid leukemia. *N Engl J Med*. 2016;374:2209-2221.
6. Jaiswal S, Fontanillas P, Flannick J, et al. Age-related clonal hematopoiesis associated with adverse outcomes. *N Engl J Med*. 2014;371:2488-2498.
7. Xie M, Lu C, Wang J, et al. Age-related mutations associated with clonal hematopoietic expansion and malignancies. *Nat Med*. 2014;20:1472-1478.
8. Gilliland DG, Griffin JD. The roles of FLT3 in hematopoiesis and leukemia. *Blood*. 2002;100:1532-1542.
9. Mrozek K, Marcucci G, Paschka P, Whitman SP, Bloomfield CD. Clinical relevance of mutations and gene-expression changes in adult acute myeloid leukemia with normal cytogenetics: are we ready for a prognostically prioritized molecular classification? *Blood*. 2007;109:431-448.
10. Steffen B, Muller-Tidow C, Schwable J, Berdel WE, Serve H. The molecular pathogenesis of acute myeloid leukemia. *Crit Rev Oncol Hematol*. 2005;56:195-221.
11. Levis M, Small D. FLT3: ITDoes matter in leukemia. *Leukemia*. 2003;17:1738-1752.
12. Kazi JU, Ronnstrand L. FMS-like tyrosine kinase 3/FLT3: from basic science to clinical implications. *Physiol Rev*. 2019;99:1433-1466.
13. Nakao M, Yokota S, Iwai T, et al. Internal tandem duplication of the flt3 gene found in acute myeloid leukemia. *Leukemia*. 1996;10:1911-1918.
14. Schnittger S, Schoch C, Dugas M, et al. Analysis of FLT3 length mutations in 1003 patients with acute myeloid leukemia: correlation to cytogenetics, FAB subtype, and prognosis in the AMLCG study and usefulness as a marker for the detection of minimal residual disease. *Blood*. 2002;100:59-66.
15. Yamamoto Y, Kiyoi H, Nakano Y, et al. Activating mutation of D835 within the activation loop of FLT3 in human hematologic malignancies. *Blood*. 2001;97:2434-2439.
16. Bacher U, Haferlach C, Kern W, Haferlach T, Schnittger S. Prognostic relevance of FLT3-TKD mutations in AML: the combination matters–an analysis of 3082 patients. *Blood*. 2008;111:2527-2537.
17. Hayakawa F, Towatari M, Kiyoi H, et al. Tandem-duplicated Flt3 constitutively activates STAT5 and MAP kinase and introduces

autonomous cell growth in IL-3-dependent cell lines. *Oncogene*. 2000;19:624-631.
18. Brandts CH, Sargin B, Rode M, et al. Constitutive activation of Akt by Flt3 internal tandem duplications is necessary for increased survival, proliferation, and myeloid transformation. *Cancer Res*. 2005;65:9643-9650.
19. Choudhary C, Schwable J, Brandts C, et al. AML-associated Flt3 kinase domain mutations show signal transduction differences compared with Flt3 ITD mutations. *Blood*. 2005;106:265-273.
20. Leischner H, Albers C, Grundler R, et al. SRC is a signaling mediator in FLT3-ITD- but not in FLT3-TKD-positive AML. *Blood*. 2012;119:4026-4033.
21. Choudhary C, Olsen JV, Brandts C, et al. Mislocalized activation of oncogenic RTKs switches downstream signaling outcomes. *Mol Cell*. 2009;36:326-339.
22. Schmidt-Arras DE, Bohmer A, Markova B, Choudhary C, Serve H, Bohmer FD. Tyrosine phosphorylation regulates maturation of receptor tyrosine kinases. *Mol Cell Biol*. 2005;25:3690-3703.
23. Verstraete K, Vandriessche G, Januar M, et al. Structural insights into the extracellular assembly of the hematopoietic Flt3 signaling complex. *Blood*. 2011;118:60-68.
24. Helenius A, Aebi M. Intracellular functions of N-linked glycans. *Science*. 2001;291:2364-2369.
25. Ohtsubo K, Marth JD. Glycosylation in cellular mechanisms of health and disease. *Cell*. 2006;126:855-867.
26. Pinho SS, Reis CA. Glycosylation in cancer: mechanisms and clinical implications. *Nat Rev Cancer*. 2015;15:540-555.
27. Wilson JR, Williams D, Schachter H. The control of glycoprotein synthesis: N-acetylglucosamine linkage to a mannose residue as a signal for the attachment of L-fucose to the asparagine-linked N-acetylglucosamine residue of glycopeptide from alpha1-acid glycoprotein. *Biochem Biophys Res Commun*. 1976;72:909-916.
28. Schneider M, Al-Shareffi E, Haltiwanger RS. Biological functions of fucose in mammals. *Glycobiology*. 2017;27:601-618.
29. Wang Y, Fukuda T, Isaji T, et al. Loss of alpha1,6-fucosyltransferase inhibits chemical-induced hepatocellular carcinoma and tumorigenesis by down-regulating several cell signaling pathways. *FASEB J*. 2015;29:3217-3227.
30. Zhou Y, Fukuda T, Hang Q, et al. Inhibition of fucosylation by 2-fluorofucose suppresses human liver cancer HepG2 cell proliferation and migration as well as tumor formation. *Sci Rep*. 2017;7:11563.
31. Fujii H, Shinzaki S, Iijima H, et al. Core fucosylation on T cells, required for activation of T-cell receptor signaling and induction of colitis in mice, is increased in patients with inflammatory bowel disease. *Gastroenterology*. 2016;150:1620-1632.
32. Li W, Yu R, Ma B, et al. Core fucosylation of IgG B cell receptor is required for antigen recognition and antibody production. *J Immunol*. 2015;194:2596-2606.
33. Liang W, Mao S, Sun S, et al. Core fucosylation of the T cell receptor is required for T cell activation. *Front Immunol*. 2018;9:78.
34. Fukuda T, Hashimoto H, Okayasu N, et al. Alpha 1,6-fucosyltransferase-deficient mice exhibit multiple behavioral abnormalities associated with a schizophrenia-like phenotype: importance of the balance between the dopamine and serotonin systems. *J Biol Chem*. 2011;286:18434-18443.
35. Gu W, Fukuda T, Isaji T, et al. Loss of alpha1,6-fucosyltransferase decreases hippocampal long term potentiation: implications for core fucosylation in the regulation of AMPA receptor heteromerization and cellular signaling. *J Biol Chem*. 2015;290:17566-17575.
36. Ng BG, Xu G, Chandy N, et al. Biallelic mutations in FUT8 cause a congenital disorder of glycosylation with defective fucosylation. *Am J Hum Genet*. 2018;102:188-195.
37. Wang X, Inoue S, Gu J, et al. Dysregulation of TGF-beta1 receptor activation leads to abnormal lung development and emphysema-like phenotype in core fucose-deficient mice. *Proc Natl Acad Sci USA*. 2005;102:15791-15796.
38. Wang X, Gu J, Ihara H, Miyoshi E, Honke K, Taniguchi N. Core fucosylation regulates epidermal growth factor receptor-mediated intracellular signaling. *J Biol Chem*. 2006;281:2572-2577.
39. Zhao Y, Itoh S, Wang X, et al. Deletion of core fucosylation on alpha3beta1 integrin down-regulates its functions. *J Biol Chem*. 2006;281:38343-38350.
40. Gu W, Fukuda T, Isaji T, Hashimoto H, Wang Y, Gu J. alpha1,6-Fucosylation regulates neurite formation via the activin/phospho-Smad2 pathway in PC12 cells: the implicated dual effects of Fut8 for TGF-beta/activin-mediated signaling. *FASEB J*. 2013;27:3947-3958.
41. Shields RL, Lai J, Keck R, et al. Lack of fucose on human IgG1 N-linked oligosaccharide improves binding to human Fcgamma RIII and antibody-dependent cellular toxicity. *J Biol Chem*. 2002;277:26733-26740.
42. Shinkawa T, Nakamura K, Yamane N, et al. The absence of fucose but not the presence of galactose or bisecting N-acetylglucosamine of human IgG1 complex-type oligosaccharides shows the critical role of enhancing antibody-dependent cellular cytotoxicity. *J Biol Chem*. 2003;278:3466-3473.
43. Okada M, Chikuma S, Kondo T, et al. Blockage of core fucosylation reduces cell-surface expression of PD-1 and promotes anti-tumor immune responses of T cells. *Cell Rep*. 2017;20:1017-1028.
44. Daley GQ, Baltimore D. Transformation of an interleukin 3-dependent hematopoietic cell line by the chronic myelogenous leukemia-specific P210bcr/abl protein. *Proc Natl Acad Sci USA*. 1988;85:9312-9316.
45. Takahashi S, Shirahama K. Internal tandem duplication and tyrosine kinase domain mutations in FLT3 alter the response to daunorubicin in Ba/F3 cells. *Biomed Rep*. 2016;4:83-86.
46. Takahashi S, Harigae H, Ishii KK, et al. Over-expression of Flt3 induces NF-kappaB pathway and increases the expression of IL-6. *Leuk Res*. 2005;29:893-899.
47. Takahashi S, McConnell MJ, Harigae H, et al. The Flt3 internal tandem duplication mutant inhibits the function of transcriptional repressors by blocking interactions with SMRT. *Blood*. 2004;103:4650-4658.
48. Xu Z, Isaji T, Fukuda T, Wang Y, Gu J. O-GlcNAcylation regulates integrin-mediated cell adhesion and migration via formation of focal adhesion complexes. *J Biol Chem*. 2019;294:3117-3124.
49. Cong L, Ran FA, Cox D, et al. Multiplex genome engineering using CRISPR/Cas systems. *Science*. 2013;339:819-823.
50. Lu X, Zhang D, Shoji H, et al. Deficiency of alpha1,6-fucosyltransferase promotes neuroinflammation by increasing the sensitivity of glial cells to inflammatory mediators. *Biochim Biophys Acta Gen Subj*. 2019;1863:598-608.
51. Hang Q, Isaji T, Hou S, Im S, Fukuda T, Gu J. Integrin alpha5 suppresses the phosphorylation of epidermal growth factor receptor and its cellular signaling of cell proliferation via N-glycosylation. *J Biol Chem*. 2015;290:29345-29360.
52. Williams AB, Li L, Nguyen B, Brown P, Levis M, Small D. Fluvastatin inhibits FLT3 glycosylation in human and murine cells and prolongs survival of mice with FLT3/ITD leukemia. *Blood*. 2012;120:3069-3079.

53. Kiyoi H, Ohno R, Ueda R, Saito H, Naoe T. Mechanism of constitutive activation of FLT3 with internal tandem duplication in the juxtamembrane domain. *Oncogene*. 2002;21:2555-2563.
54. Kobayashi Y, Tateno H, Dohra H, et al. A novel core fucose-specific lectin from the mushroom *Pholiota squarrosa*. *J Biol Chem*. 2012;287:33973-33982.
55. Tse KF, Mukherjee G, Small D. Constitutive activation of FLT3 stimulates multiple intracellular signal transducers and results in transformation. *Leukemia*. 2000;14:1766-1776.
56. Schmidt-Arras D, Bohmer SA, Koch S, et al. Anchoring of FLT3 in the endoplasmic reticulum alters signaling quality. *Blood*. 2009;113:3568-3576.
57. Koch S, Jacobi A, Ryser M, Ehninger G, Thiede C. Abnormal localization and accumulation of FLT3-ITD, a mutant receptor tyrosine kinase involved in leukemogenesis. *Cells Tissues Organs*. 2008;188:225-235.
58. Reiter K, Polzer H, Krupka C, et al. Tyrosine kinase inhibition increases the cell surface localization of FLT3-ITD and enhances FLT3-directed immunotherapy of acute myeloid leukemia. *Leukemia*. 2018;32:313-322.
59. Masson K, Liu T, Khan R, Sun J, Ronnstrand L. A role of Gab2 association in Flt3 ITD mediated Stat5 phosphorylation and cell survival. *Br J Haematol*. 2009;146:193-202.
60. Razumovskaya E, Masson K, Khan R, Bengtsson S, Ronnstrand L. Oncogenic Flt3 receptors display different specificity and kinetics of autophosphorylation. *Exp Hematol*. 2009;37:979-989.
61. Grafone T, Palmisano M, Nicci C, Storti S. An overview on the role of FLT3-tyrosine kinase receptor in acute myeloid leukemia: biology and treatment. *Oncol Rev*. 2012;6:e8.
62. Weisberg E, Boulton C, Kelly LM, et al. Inhibition of mutant FLT3 receptors in leukemia cells by the small molecule tyrosine kinase inhibitor PKC412. *Cancer Cell*. 2002;1:433-443.
63. Rillahan CD, Antonopoulos A, Lefort CT, et al. Global metabolic inhibitors of sialyl- and fucosyltransferases remodel the glycome. *Nat Chem Biol*. 2012;8:661-668.
64. Okeley NM, Alley SC, Anderson ME, et al. Development of orally active inhibitors of protein and cellular fucosylation. *Proc Natl Acad Sci USA*. 2013;110:5404-5409.
65. Liu YC, Yen HY, Chen CY, et al. Sialylation and fucosylation of epidermal growth factor receptor suppress its dimerization and activation in lung cancer cells. *Proc Natl Acad Sci USA*. 2011;108:11332-11337.
66. Vempati S, Reindl C, Wolf U, et al. Transformation by oncogenic mutants and ligand-dependent activation of FLT3 wild-type requires the tyrosine residues 589 and 591. *Clin Cancer Res*. 2008;14:4437-4445.
67. Rocnik JL, Okabe R, Yu JC, et al. Roles of tyrosine 589 and 591 in STAT5 activation and transformation mediated by FLT3-ITD. *Blood*. 2006;108:1339-1345.
68. Larrue C, Saland E, Vergez F, et al. Antileukemic activity of 2-deoxy-d-glucose through inhibition of N-linked glycosylation in acute myeloid leukemia with FLT3-ITD or c-KIT mutations. *Mol Cancer Ther*. 2015;14:2364-2373.
69. Keenan RW, Hamill RL, Occolowitz JL, Elbein AD. Biological activities of isolated tunicamycin and streptovirudin fractions. *Biochemistry*. 1981;20:2968-2973.
70. Heifetz A, Keenan RW, Elbein AD. Mechanism of action of tunicamycin on the UDP-GlcNAc:dolichyl-phosphate Glc-NAc-1-phosphate transferase. *Biochemistry*. 1979;18:2186-2192.
71. Tsitsipatis D, Jayavelu AK, Muller JP, et al. Synergistic killing of FLT3ITD-positive AML cells by combined inhibition of tyrosine-kinase activity and N-glycosylation. *Oncotarget*. 2017;8:26613-26624.
72. Daver N, Schlenk RF, Russell NH, Levis MJ. Targeting FLT3 mutations in AML: review of current knowledge and evidence. *Leukemia*. 2019;33:299-312.
73. Wu M, Li C, Zhu X. FLT3 inhibitors in acute myeloid leukemia. *J Hematol Oncol*. 2018;11:133.
74. Kizuka Y, Nakano M, Yamaguchi Y, et al. An alkynyl-fucose halts hepatoma cell migration and invasion by inhibiting GDP-fucose-synthesizing enzyme FX, TSTA3. *Cell Chem Biol*. 2017;24(12):1467–1478.e5.
75. Takahashi S, Harigae H, Yokoyama H, et al. Synergistic effect of arsenic trioxide and flt3 inhibition on cells with flt3 internal tandem duplication. *Int J Hematol*. 2006;84:256-261.
76. Takahashi S. Combination therapy with arsenic trioxide for hematological malignancies. *Anticancer Agents Med Chem*. 2010;10:504-510.
77. Nagai K, Hou L, Li L, et al. Combination of ATO with FLT3 TKIs eliminates FLT3/ITD+ leukemia cells through reduced expression of FLT3. *Oncotarget*. 2018;9:32885-32899.
78. Callus BA, Mathey-Prevot B. Interleukin-3-induced activation of the JAK/STAT pathway is prolonged by proteasome inhibitors. *Blood*. 1998;91:3182-3192.
79. Takahashi S. Downstream molecular pathways of FLT3 in the pathogenesis of acute myeloid leukemia: biology and therapeutic implications. *J Hematol Oncol*. 2011;4:13.

How to cite this article: Duan C, Fukuda T, Isaji T, et al. Deficiency of core fucosylation activates cellular signaling dependent on FLT3 expression in a Ba/F3 cell system. *The FASEB Journal*. 2020;00:1–14. https://doi.org/10.1096/fj.201902313RR

＜分子認識部門＞
教授　細野 雅祐
講師　菅原 栄紀
講師　立田 岳生

レクチンの抗腫瘍メカニズムの解明とがん薬物治療への応用

１）HeLa 細胞における SAL 取り込み機構の解明

当研究室では，ナマズ卵レクチン（SAL）は，HeLa 細胞膜上に発現しているグロボトリアオシルセラミド(Gb3)の糖鎖に結合することによりスニチニブ(SU)の細胞内への取り込み増加及び細胞外への排出抑制を引き起こし，SU の作用を増強することを報告している．しかし，Gb3 に結合した SAL 自身は細胞膜に留まるのか，あるいは細胞内へ移行するかについては明らかにしていなかった．本年度は蛍光標識 SAL（HL-SAL）を作製し，HeLa 細胞への取り込み及び細胞内における挙動について検討した．HL-SAL（50 μg/mL）24 時間処理で，HeLa 細胞膜への結合および細胞内への移行が観察された．細胞内の蛍光は，膜に結合した HL-SAL をハプテン糖により除去してもこの蛍光は残存していた．SAL が細胞内に取り込まれる時間を検討したところ，処理後 0.5 時間以内で膜結合し，約 1 時間後から濃度依存的に取り込まれ始め，3 時間後には核近傍への集積が認められた．また，細胞内に取り込まれる SAL が処理濃度に依存するか否かを調べたところ，3.125 μg/mL では SAL の取り込みは見られなかったものの，それより高い濃度では濃度依存的に取り込まれることも分かった．この取り込みは，CRIPR/Cas9 システムにより Gb3 合成酵素遺伝子を欠損させた Gb3 陰性 HeLa（⊿Gb3-HeLa）において減少することが示されたことから，SAL の取り込みは，Gb3 を介するものであることが示された．Gb3 は脂質ラフト（GEM）に存在する糖脂質であることから，SAL の取り込みは脂質ラフト介在型エンドサイトーシスによるのではないかと考え，この機構の阻害剤であるメチル-β-シクロデキストリン（MβCD）を用いて検討したところ，細胞内に取り込まれる SAL の量が減少する様子が認められた．これらの結果から，SAL は HeLa 細胞膜に存在する Gb3 に結合し，脂質ラフトを介したエンドサイトーシスにより HeLa 内に取り込まれている可能性が示された．しかし，MβCD では SAL の取り込みが完全に阻害されなかったことから，エンドサイトーシス以外の取り込み機構も関与していることが考えられ，別の取り込み機構を含めて今後詳細に検討する必要がある．

２）小麦胚芽レクチン処理 HeLa 細胞内に見られる液胞様構造物について

これまでに SAL とスニチニブ（SU）の併用処理により HeLa 細胞の生存率を有意に低下させることを報告している．さらに，このメカニズに関しては，１）

SAL 処理により細胞内に取り込まれる SU が増加する，2）SAL 処理により内部が中性のリソソーム様液胞（lysosome like vesicle, LLV）が形成され，この構造物に SU がトラップされることにより薬剤の排泄が抑制されるという 2 つの機構により引き起こされると考えている．以前より小麦胚芽レクチン（WGA）は，細胞に対して細胞死を引き起こすことが知られている．この細胞死は，近年の研究で細胞死の一種であるパラプトーシスによることが示され，SAL 処理の場合と類似した液胞様構造物が形成されるのが特徴である．しかし，この液胞の特徴および形成機構に関する詳細は報告されていない．本年度は，この点に着目して検討した．WGA は，HeLa 細胞に対して細胞死を誘導することから，液胞形成実験には生存率がほぼ変化しない 6.25 あるいは 12.5 μg/mL の濃度を利用した．WGA（6.25 μg/mL）処理では，SAL で見られる LLV と形態的に同様の構造物が細胞内に認められた．この構造物は，他の植物レクチン（PNA および ConA）処理では見られず，GlcNAc 処理により有意に形成が阻害された．液胞内部の pH を neutral red を用いて調べたところ，LLV と同様に中性であることが分かった．また，液胞の形成は M□CD 処理により一部抑制されたことから，脂質ラフト介在性に起こる可能性が示唆されたが, この点についてはまだ不明な点が多い. 我々は，SAL 処理により誘導される LLV は，Brefeldin A（BFA）による阻害実験の結果から，ゴルジ体から出芽したリソソームに由来するのではないかと考えている．WGA により形成される液胞についても BFA を用いて検討したが，細胞死を誘導しない濃度の BFA と WGA をそれぞれ用いて併用処理しても細胞死が起こるため，この点に関してもさらなる検討が必要である．一方，HeLa 細胞では，WGA 処理によりオートファジーマーカーである LC3 の発現量が増加することから，この液胞はオートファゴソーム由来である可能性が示唆された．これらのことから，WGA は，GlcNAc 依存的に脂質ラフトに局在する糖タンパク質あるいは糖脂質を介して LLV と特徴が類似した液胞の形成を誘導し, この細胞内変化が細胞生存率の低下に関与しているものと考えられるが，一方で SAL は HeLa 細胞に対して細胞死を誘導しないことから，この相違点について現在さらに検討を行っている．

3）ウシガエル卵由来シアル酸結合性レクチン（cSBL）は，レクチン活性とリボヌクレアーゼ活性を併せ持つ多機能タンパク質である．cSBL は，細胞内 RNA の分解を基盤とした，新規抗がん剤候補として期待されているが，その抗腫瘍作用機序は不明な点も多く, 特に cSBL により発現変化する遺伝子についての報告はほとんどない．cSBL を含む抗腫瘍性リボヌクレアーゼの遺伝子発現調節研究の課題として，リボヌクレアーゼ自体が RNA を分解するため，実験系の確立が困難という点がある．これまでに，いくつかの抗腫瘍性リボヌクレアーゼを用いたマイクロアレイ解析が行われているが，RNA 分解がほとんど起こらない低濃

度，すなわち，抗腫瘍作用がほとんど進行していない条件下においての報告のみである．

本研究室では，cSBL 耐性がん細胞を，cSBL の長期間処理により樹立している．本年度は，cSBL 処理により発現変化する遺伝子を，RNA 分解の影響が無い条件下で検出することを目的に研究を行った．cSBL 非存在下でもその耐性を維持することが確認された，複数株ある cSBL 耐性細胞の耐性度を，コロニー形成法により評価し，より高い耐性を示した細胞（cSR-A1 および cSR-B1 細胞）の RNA サンプルを調整した．遺伝子マイクロアレイは，60K Agilent 60-mer oligomicroarray を用いて行った．その後得られた情報を元に，DAVID ソフトウェアを用い，Gene Ontology (GO) 解析およびパスウェイ解析を行った．

cSBL 耐性細胞において発現が変化する遺伝子を同定した結果，上昇または低下する遺伝子として，それぞれ 440，487，計 927 遺伝子が同定された．GO 解析およびパスウェイ解析の結果から，細胞増殖に関連する遺伝子や細胞膜上のタンパク質をコードする遺伝子の他，特に糖や脂質の代謝に関わる遺伝子に多くの発現変動があることが明らかになった．マイクロアレイ解析で得られた遺伝子の中から，発現低下が最も大きかった 5 つの遺伝子（THY1，AKR1B15，AKR1B10，SLC47A2，CBR1; Table 1）に着目し，リアルタイム PCR 法によりその結果を再確認した結果，いずれの遺伝子も cSBL 耐性細胞においてその発現が大きく(-22 ～-480 倍) 減少することが示され，マイクロアレイ解析の結果と同様な傾向が得られた．また，各遺伝子の分子機能を調べた結果，酸化還元酵素活性など代謝に関わる機能を有しているものが多く見られた（Table 1). このことから，cSBL で長期間処理されたがん細胞では，代謝に関与する遺伝子の発現が恒常的に影響を受けている可能性が考えられる．今後の課題として，今回同定された遺伝子の過剰発現やノックアウト実験を通して，cSBL の抗腫瘍作用に直接関与する遺伝子の同定があげられる．これらの情報を元に，cSBL の抗腫瘍作用機序の解明の他，cSBL の効果自体を高める方策や，有効な併用薬の探索など，cSBL を利用した新規のがん治療法の開発が期待できると考えている．

Gene Symbol	Description	Molecular functions
THY1	Thy-1 cell surface antigen	GPI anchor binding GTPase activator activity integrin binding etc.
AKR1B15	Aldo-keto reductase family 1, member B15	estradiol 17-beta-dehydrogenase activity oxidoreductase activity, acting on the CH-OH group of donors, NAD or NADP as acceptor
AKR1B10	Aldo-keto reductase family 1, member B10	aldo-keto reductase (NADP) activity geranylgeranyl reductase activity indanol dehydrogenase activity
SLC47A2	Solute carrier family 47 (multidrug and toxin extrusion), member 2	drug:proton antiporter activity drug transmembrane transporter activity
CBR1	Carbonyl reductase 1	15-hydroxyprostaglandin dehydrogenase (NADP+) activity carbonyl reductase (NADPH) activity oxidoreductase activity, acting on

Table 1 Known molecular function of THY1, AKR1B15, AKR1B10, SLC47A2 and CBR1

＜発表論文＞

A GM1b/asialo-GM1 oligosaccharide-binding R-type lectin from purplish bifurcate mussels Mytilisepta virgata and its effect on MAP kinases.
Fujii Y, Gerdol M, Kawsar S.M.A, Hasan I, Spazzali F, Yoshida T, Ogawa Y, Rajia S, Kamata K, Koide Y, Sugawara S, Hosono M, Tame J.R.H, Fujita H, Pallavicini A and Ozeki Y., *FEBS J*., doi:10.1111/febs.15154, 2019

＜学会発表＞

・ナマズ卵レクチンは脂質ラフト依存性エンドサイトーシスにより細胞内に取り込まれる
菅原栄紀，本田捷太，立田岳生，細野 雅祐
第 38 回日本糖質学会年会，名古屋，2019 年 8 月，要旨集 p.222

・**Bullfrog sialic acid-binding lectin reduces the expression of EGF receptors in cancer cells**
Tatsuta T., Sato S., Sugawara S., Hosono M.
25th International Symposium on Glycoconjugates, ミラノ，2019 年 8 月，要旨集 p.324

・**Catfish (Silurus asotus) lectin enhances the cytotoxic effects of sunitinib on renal**

cell carcinoma

Ito J., Sugawara S., Hosono M., Sato M.

25th International Symposium on Glycoconjugates，ミラノ，2019 年 8 月，要旨集 p.327

・**Glycosphingolipid-binding lectin modifies tumor cell membrane transport**

Hosono M.

1st Japan-Europe Workshop on Glycosphingolipids and Membrane Homeostasis，ストラスブール，2019 年 9 月，要旨集 p.10

・**ナマズ卵レクチンはヒト子宮頸がん由来 HeLa におけるスニチニブの取り込みおよび排出に影響をおよぼす**

菅原栄紀，本田捷太，立田岳生，伊藤淳 [a]，佐藤　信 [a]，細野 雅祐

（東北医薬大・医学部・泌尿器科学講座 [a]）

第 13 回東北糖鎖研究会，新潟，2019 年 9 月，要旨集 p.49

・**cSBL 耐性細胞における遺伝子発現変化**

立田岳生，菅原 栄紀，細野 雅祐

第 92 回日本生化学会大会，横浜，2019 年 9 月，演題番号 1P-013

・**小麦胚芽レクチン処理 HeLa 細胞内に見られる液胞様構造物について**

須藤実咲，菅原栄紀，本田捷太，立田岳生，細野 雅祐

第 58 回日本薬学会東北支部大会，仙台，2019 年 10 月，要旨集 p.95

・**シアル酸結合性レクチン (cSBL) は乳がん細胞に ER，PgR および HER family タンパクの減少を伴う細胞死を誘導する**

佐藤 祥子，立田 岳生，佐藤 稔之，菅原 栄紀，鈴木 常義，細野 雅祐

第 40 回日本臨床薬理学会学術総会，新宿，2019 年 12 月，演題番号 1P-71

The FEBS Journal

FEBS PRESS science publishing by scientists

A GM1b/asialo-GM1 oligosaccharide-binding R-type lectin from purplish bifurcate mussels *Mytilisepta virgata* and its effect on MAP kinases

Yuki Fujii[1], Marco Gerdol[2], Sarkar M. A. Kawsar[3,4], Imtiaj Hasan[4,5], Francesca Spazzali[2], Tatsusada Yoshida[1], Yukiko Ogawa[1], Sultana Rajia[4,6], Kenichi Kamata[7], Yasuhiro Koide[4], Shigeki Sugawara[8], Masahiro Hosono[8], Jeremy R. H. Tame[7], Hideaki Fujita[1], Alberto Pallavicini[2,9] and Yasuhiro Ozeki[4]

1 Graduate School of Pharmaceutical Sciences, Nagasaki International University, Sasebo, Japan
2 Department of Life Sciences, University of Trieste, Italy
3 Department of Chemistry, Faculty of Science, University of Chittagong, Bangladesh
4 School of Sciences, Yokohama City University, Japan
5 Department of Biochemistry and Molecular Biology, Faculty of Science, University of Rajshahi, Bangladesh
6 Department of Pharmacy, Varendra University, Rajshahi, Bangladesh
7 Graduate School of Medical Life Science, Yokohama City University, Japan
8 Institute of Molecular Biomembrane and Glycobiology, Tohoku Medical and Pharmaceutical University, Sendai, Japan
9 Department of Biology and Evolution of Marine Organisms, Stazione Zoologica Anton Dohrn Napoli, Italy

Keywords
bivalves; ganglioside; *Mytilisepta virgata*; purplish bifurcate mussels; R-type lectin

Correspondence
Y. Fujii, Graduate School of Pharmaceutical Sciences, Nagasaki International University, 2825-7 Huis Ten Bosch, Sasebo, Nagasaki 859-3298, Japan
Tel: +81 956 20 5642
E-mail: yfujii@niu.ac.jp
Y. Ozeki, School of Sciences, Yokohama City University, 22-2 Seto, Kanazawa-ku, Yokohama 236-0027, Japan
Tel: +81 45 787 2221
E-mail: ozeki@yokohama-cu.ac.jp

(Received 12 March 2019, revised 16 September 2019, accepted 22 November 2019)

doi:10.1111/febs.15154

A 15-kDa lectin, termed SeviL, was isolated from *Mytilisepta virgata* (purplish bifurcate mussel). SeviL forms a noncovalent dimer that binds strongly to ganglio-series GM1b oligosaccharide (Neu5Acα2-3Galβ1-3GalNAcβ1-4Galβ1-4Glc) and its precursor, asialo-GM1 (Galβ1-3GalNAcβ1-4Galβ1-4Glc). SeviL also interacts weakly with the glycan moiety of SSEA-4 hexaose (Neu5Acα2-3Galβ1-3GalNAcβ1-3Galα1-4Galβ1-4Glc). A partial protein sequence of the lectin was determined by mass spectrometry, and the complete sequence was identified from transcriptomic analysis. SeviL, consisting of 129 amino acids, was classified as an R(icin B)-type lectin, based on the presence of the QxW motif characteristic of this fold. SeviL mRNA is highly expressed in gills and, in particular, mantle rim tissues. Orthologue sequences were identified in other species of the family Mytilidae, including *Mytilus galloprovincialis*, from which lectin MytiLec-1 was isolated and characterized in our previous studies. Thus, mytilid species contain lectins belonging to at least two distinct families (R-type lectins and mytilectins) that have a common β-trefoil fold structure but differing glycan-binding specificities. SeviL displayed notable cytotoxic (apoptotic) effects against various cultured cell lines (human breast, ovarian, and colonic cancer; dog kidney) that possess asialo-GM1 oligosaccharide at the cell surface. This cytotoxic effect was inhibited by the presence of anti-asialo-GM1 oligosaccharide antibodies. With HeLa ovarian cancer cells, SeviL showed dose- and time-dependent activation of kinase MKK3/6, p38 MAPK, and caspase-3/9. The transduction pathways activated by SeviL via the glycosphingolipid oligosaccharide were triggered apoptosis.

Abbreviations
Gb3, globotriaosylceramide; GM1, monosialotetrahexosylganglioside; MAPK, mitogen-activated protein kinase; MKK, MAPK kinase; MytiLec-1, *Mytilus galloprovincialis* α-Gal-binding lectin; SeviL, *Mytilisepta virgata* R-type lectin; SSEA-4, stage-specific embryonal antigen 4.

287 () 2612–2630

Database
Nucleotide sequence data have been deposited in the GenBank database under accession numbers MK434191, MK434192, MK434193, MK434194, MK434195, MK434196, MK434197, MK434198, MK434199, MK434200, and MK434201.

Introduction

Many marine invertebrates possess lectins (glycan-binding proteins) with various glycan-binding properties [1–3]. In the differentiation of phylogeny, lectin-mediated interactions between glycans and proteins were adapted into various kinds of key pathways involved in a variety of fundamental biological processes, including embryonic development, immune responses, and cell growth regulation [4–6]. During this functional diversification, marine invertebrates developed an unusually large number of lectins, many having convergent structures that facilitate binding to specific glycan structures exposed on the surface of target cells. This combination of functional divergence and structural convergence has resulted in many unique sequences and unusual glycan-binding specificities among lectins isolated from marine invertebrates [7–11].

We described in 2012 a novel lectin (termed 'MytiLec-1'), isolated from the Mediterranean mussel *Mytilus galloprovincialis* (family Mytilidae), that had a unique primary structure [12]. MytiLec-1 has a β-trefoil fold [13], a 3-D structure typically found in R-type lectins, including ricin B-chain [14]. However, MytiLec-1 bound specifically to the α-galactoside globotriose (Galα1-4Galβ1-4Glc) [12,13], whereas many other R-type lectins bind to β-galactosides such as N-acetyllactosamine. MytiLec-1 induced apoptosis in Gb3-expressing human Burkitt's lymphoma cells. Following the identification of similar lectins in various other mussel species [15–17], we referred collectively to such lectins as members of the 'mytilectin family' [18]. The taxonomic distribution of mytilectins known to date is limited to the protostome clade *Lophotrochozoa* and discontinuous; members of this family have been identified only in the subclass *Pteriomorphia* (phylum Mollusca) and the order *Lingulida* (phylum Brachiopoda) [19].

Progress in 'omics' studies of mussels and other bivalve mollusks during the past decade has greatly enhanced our understanding of their genetics and molecular biology, leading to major advances in basic and applied scientific research. Mussels are a traditional seafood consumed heavily in Europe and increasingly in other parts of the world and are widely used as 'sentinel' organisms for biomonitoring [20]. Molecular studies have revealed the essential role of lectins as pattern recognition receptors (PRRs) for microbe-associated molecular patterns (MAMPs) in the innate immune systems of mussels [21,22]. A more complete understanding of these lectins will therefore provide a useful basis for improved mussel breeding practices and prevention of infections. Physiological processes and the immune system in mussels are strongly correlated with exposure to biotic and abiotic stress factors [23,24]. Numerous mussel immune system molecules including lectins were recently shown to be functionally modulated by pathogen exposure and ocean acidification [25,26], so that bivalve lectins are suggested to be important molecules which respond to the marine environment. The large and highly diverse lectin repertoire of mytilids [27,28], which probably includes several components yet to be identified, will facilitate effective new approaches for monitoring health status of mussel species, associated organisms, and their marine environments.

Since no R-type lectin had been biochemically purified from the family Mytilidae, mytilectins were considered for some time to be the only β-trefoil lectins present in mytilids, and it was speculated that their natural function related to the innate immune response [12,15–17]. However, the isolation of a novel lectin from the purplish bifurcate mussel (*Mytilisepta virgata*) in this study suggests the possibility of greater diversification among lectins in this family. Furthermore, the transcriptome of this species revealed a lack of mRNAs encoding mytilectins and instead revealed the expression of multiple distinct mRNAs encoding proteins characterized by the presence of a ricin B-chain domain, typical of R-type lectins [29]. SeviL found from *M. virgata* shows characteristics of sugar chain binding and cell toxicity unlike any lectin reported to date. SeviL activated intracellular signaling pathways that resulted in cell death of mammalian carcinoma cells expressing asialo-GM1, whereas MytiLec-1 binds to Gb3 glycan. This is the first report that two different β-trefoil lectin families (each with its own glycan-binding specificity) coexist in the same animal species.

Results

Purification of lectin (SeviL) from *M. virgata*

Supernatant 'Sup 1'(see Materials and methods 'Lectin purification') from homogenized *M. virgata* tissues displayed hemagglutination activity despite the absence of MytiLec-1 from this species. Repeated homogenization of precipitates yielded supernatants with successively reduced activity (data not shown). The precipitates were homogenized again with 50 mM lactose to obtain supernatants. The hemagglutinating activity was recovered by dialyzing the supernatant 'Sup 2' (see Materials and methods 'Lectin purification'). Sup 1 and 2 were applied to a lactosyl-agarose column, and the new lectin could be eluted with TBS containing 50 mM lactose (Fig. 1A). The lectin was characterized as a single polypeptide with molecular mass 15 kDa by SDS/PAGE under both reducing and nonreducing conditions (Fig. 1A) and was termed 'SeviL'. Purification from 400 g fresh tissue yielded 6.5 mg SeviL (Table 1). Hemagglutination activity of SeviL was required to the addition of calcium chloride (Fig. S1A), indicating that the activity was dependent on divalent cations such as Ca^{2+}. Analytical ultracentrifugation revealed that SeviL was a tightly but noncovalently bound dimer (Fig. 1B).

Sugar-binding specificity of SeviL

Sugar-binding specificity of SeviL is summarized in Table 2. Hemagglutination activity was weakly inhibited by addition of monosaccharides such as D-Gal (25 mM), D-GalNAc (25 mM), and D-Fuc (25 mM) and of disaccharides such as melibiose (25 mM) and lactose (25 mM). These findings suggest that the chirality of the C3 and C4 carbons in galactose is essential for protein–glycan interaction. Hemagglutination activity was inhibited by administration of bovine submaxillary mucin (0.125 $mg{\cdot}mL^{-1}$), but not porcine stomach mucin or fetuin, even at concentrations > 1 $mg{\cdot}mL^{-1}$ (Table 2). These findings suggested that SeviL does not bind to porcine stomach mucin or fetuin, possibly because these glycoproteins have clusters of GlcNAc or sialyllactosamine at the reducing end [30].

Deduced primary structure of SeviL

The cDNA sequence of SeviL was identified using a combination of *de novo* peptide sequencing and our earlier transcriptomics results [29]. The peptide sequence obtained from trypsin digestion of SeviL (*m/z* 685.81 $(MH_2)^{2+}$) was LDYN(M/T/S/C) GDLVANK (Fig. S1B), which we compared with the mRNA sequences of five *M. virgata* tissues determined previously. A single sequence match was found with one protein product including the sequence ^{104}LDYNGGDLVANK^{115} (Fig. 2A). The complete 129 amino acid residue sequence was classified as an R-type lectin by the Pfam protein database (http://pfam.xfam.org/) but is unrelated to MytiLec-1. At least two distinct lectin types (R-type lectins and mytilectins) having the β-trefoil fold structure are evidently present in the family Mytilidae.

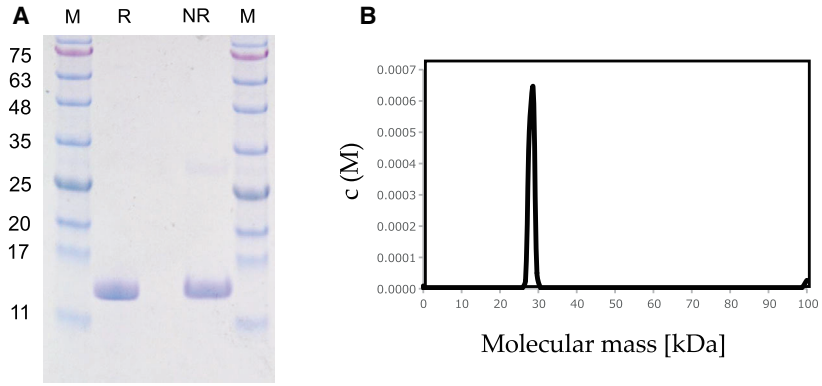

Fig. 1. Purification of *Mytilisepta virgata* lectin, SeviL. (A) SDS/PAGE pattern under reducing (R) and nonreducing (NR) conditions. Numbers on the left indicate molecular masses (kDa) of marker proteins (M). (B) The molecular weight of the native protein (30 kDa) obtained from distribution of sedimentation coefficient by sedimentation velocity AUC. It indicates the presence of dimers in solution, with negligible amounts of monomer. Concentration c(M) was measured in absorption units (A_{280}).

Table 1. Purification of SeviL from *Mytilisepta virgata*.

Fraction	Titer (HU)	Volume (mL)	Total activity[a]	Protein conc. (mg·ml^{-1})	Protein amount (mg)	Specific activity[b]	Purification ratio (fold)[c]	Recovery of activity (%)[d]
Crude extract obtained by TBS	128	500	64 000	6.5	3525	0.04	1	100
Purified lectin	512	10	5120	0.27	2.7	190	4750	8
Crude extract obtained by lactose in TBS	512	100	51 200	2.1	2100	0.24	1	100
Purified lectin	4096	10	40 960	0.38	3.8	1024	4491	80

[a] Total activity is shown by Titer × volume; [b] Specific activity was shown by titer per mg of protein; [c] Purification ratio was shown by comparing the value of specific activity on the crude extract vs. purified lectin; [d] Recovery of activity was revealed by comparing the value of total activity on the crude extract vs. purified lectin.

Table 2. Saccharide and glycoprotein specificity of SeviL[a].

Saccharides	Minimum inhibitory concentration (mM)
D-GalNAc	25
D-GlcNAc	N.I.[b]
D-Gal	25
D-Glc	> 50
D-Man	> 50
D-Fuc	25
Lactose	25
Melibiose	25
Sucrose	N.I.[b]

Glycoproteins	Minimum inhibitory concentration (mg·mL^{-1})
Bovine submaxillary mucin	0.125
Fetuin	N.I.[c]
Porcine stomach mucin	N.I.[c]

[a] Titer of SeviL was previously diluted to 16; [b] Inhibition was not occurred even at 200 mM; [c] Fetuin and bovine submaxillary mucin did not inhibit even at 2 mg·mL^{-1}.

Tandem-repeat structure of SeviL

SeviL has a triple tandem-repeat structure with three subdomains, each consisting of ~ 40 amino acids, with 13–21% sequence similarity, consistent with a β-trefoil fold (Fig. 2B). A QxW motif is conserved in each subdomain of R-type lectins, and SeviL shows a similar pattern at residues 40–42 (QxW), 79–81 (TxW), and 121–123 (ExW). The SeviL sequence included only one Cys (C) residue, which does not form a disulfide bond (Fig. 1A).

A second sequence, highly homologous to SeviL and named SeviL-2, was identified in the *M. virgata* transcriptome. The two sequences only differ at 10 out of 129 amino acid residues (Fig. S1C). Due to the high heterozygosity of mussels, SeviL and SeviL-2 may either represent allelic variants of the same locus or the product of distinct orthologue genes, but the absence of a reference genome for this species hampered an in-depth investigation. All the experiments carried out and reported in this paper refer to SeviL-1, as the analysis of RNA-sequencing data [29] revealed that this variant was expressed > 4-fold higher than SeviL-2 in all tissues.

Comparison of SeviL orthologues among mytilid species

One or more SeviL orthologues are found in several other members of the family Mytilidae, including *M. galloprovincialis*, *M. edulis*, *M. californianus*, and *M. trossulus*, *P. purpuratus* and *L. lithophaga*, with a level of interspecies sequence conservation ranging from 25% to 99%, depending on the species considered (Fig. S2A). Like the aforementioned case of *M. virgata*, some species (i.e., *P. purpuratus*, *M. galloprovincialis,* and *L. lithophaga*) display two sequence variants, which were characterized more in detail in the Mediterranean mussel genome [32], revealing a two exons/one intron gene organization, with the ORF entirely contained within exon 2 (Fig. S2B). The three Trp residues of SeviL (residues 43, 81, 123; Fig. 3) are notably conserved in all of Mytilidae SeviL-like proteins.

The distribution of SeviL-like R-type lectins and mytilectins in the different mytilid subfamilies is variable and partially overlapping (Fig. 4). Transcriptome analysis suggests that R-type lectins (SeviL orthologues) are present in the subfamilies Brachidontinae (*Mytilisepta*, *Perumytilus*) and Lithophaginae (*Lithophaga*). On the other hand, both R-type lectins and mytilectins were found in the transcriptomes of Mytilinae (*Mytilus*, *Perna*), and neither of the two lectin families were detected in the genomes of Modiolinae, *Bathymodiolinae* (deep-sea mussels), or Arcuatulinae. While no SeviL-like R-type lectins could be found in the genomes of non-mytilid bivalves, mytilectin genes are present in Pectinidae (scallops). Overall, these observations reveal a

A

```
1                                                                   gaa aca gcc   9
10   gcc aca cat gtg cac aaa tct agc tgc gtg ggt cgt aca aag cat ata aaa aga gct gta  69
70   caa gac tgg tat gca gaa cca cta gaa gac att aca gaa gtc cag ttt aaa gac tta aaa 129
130  ATG AGT TCT GTT ACG ATT GGG AAA TGT TAT ATA CAG AAC AGA GAA AAT GGA GGG AGA GCC 189
1     M   S   S   V   T   I   G   K   C   Y   I   Q   N   R   E   N   G   G   R   A  20
190  TTT TAT AAT TTG GGG CGT AAA GAC CTC GGA ATA TTT ACT GGA AAA ATG TAT GAT GAC CAA 249
21    F   Y   N   L   G   R   K   D   L   G   I   F   T   G   K   M   Y   D   D   Q  40
250  ATA TGG AGC TTC CAG AAA TCT GAT ACA CCA GGT TAT TAC ACC ATC GGA AGA GAG TCC AAG 309
41    I   W   S   F   Q   K   S   D   T   P   G   Y   Y   T   I   G   R   E   S   K  60
310  TTT TTA CAG TAC AAT GGG GAG CAA GTT ATA ATG TCT GAC ATC GAA CAA GAT ACT ACT TTA 369
61    F   L   Q   Y   N   G   E   Q   V   I   M   S   D   I   E   Q   D   T   T   L  80
370  TGG TCA CTA GAA GAA GTA CCG GAA GAC AAA GGA TTC TAC CGT CTA CTG AAC AAA GTA CAC 429
81    W   S   L   E   E   V   P   E   D   K   G   F   Y   R   L   L   N   K   V   H 100
430  AAG GCT TAT CTG GAT TAT AAC GGC GGG GAT CTT GTA GCA AAT AAG CAT CAA ACA GAA AGC 489
101   K   A   Y   L   D   Y   N   G   G   D   L   V   A   N   K   H   Q   T   E   S 120
490  GAA AAA TGG ATC TTG TTT AAA GCA TAC TAA taa ctg aag gat gac atg act att atc gaa 549
121   E   K   W   I   L   F   K   A   Y   *                                       129
550  ctt aaa tat cgg tct ata tag gac ggc ttt cat tat tca ctt tat tat taa taa att caa 609
610  gct tat ata ttt tct gaa gaa tag ttt aac tgt gct tat tat aaa aaa ttc tat gta aaa 669
670  att aaa  t                                                                    676
```

B

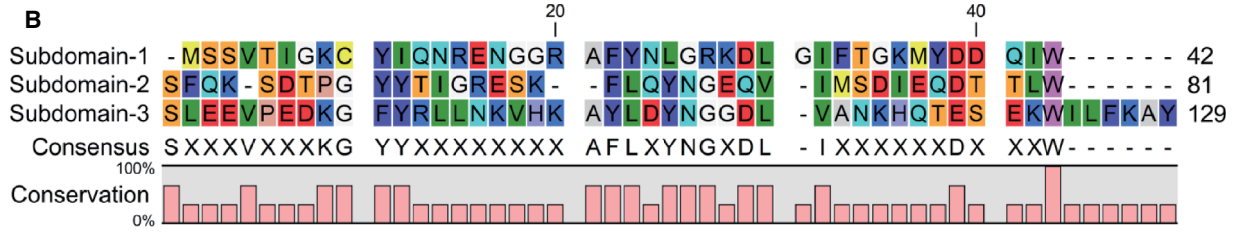

Fig. 2. cDNA sequence and deduced amino acid sequence of SeviL. (A) The asterisk indicates the stop codon. The peptide fragment obtained from mass spectrometric analysis is underlined. (B) Amino acid sequence alignment of the internal tandem-repeat subdomains of SeviL. The consensus at bottom summarizes the residues shared by the three domains. The sequence alignment within the polypeptide is analyzed by using MUSCLE program [31].

markedly discontinuous distribution of SeviL-like lectins and mytilectins in the bivalve tree of life, which suggests that their loss or retention may be dependent on unknown environmental or ecological factors.

Expression of SeviL mRNA in *M. virgata* tissues

RNA-seq mapping graphs based on various tissues collected from a pool of adult mussels (Fig. 5A) show high expression of SeviL (TPM > 10) in gills and mantle rim. SeviL expression levels were much lower in the digestive gland and posterior adductor muscle and barely detectable in foot (TPM < 1). The high expression of SeviL in mantle rim was confirmed by qRT/PCR on individual mussels (Fig. 5B). The specificity of expression of SeviL in tissues (gills and mantle) that are constantly exposed to the external environment suggests the possibility that this lectin is involved in recognition of glycans found on parasitic or symbiotic microorganisms.

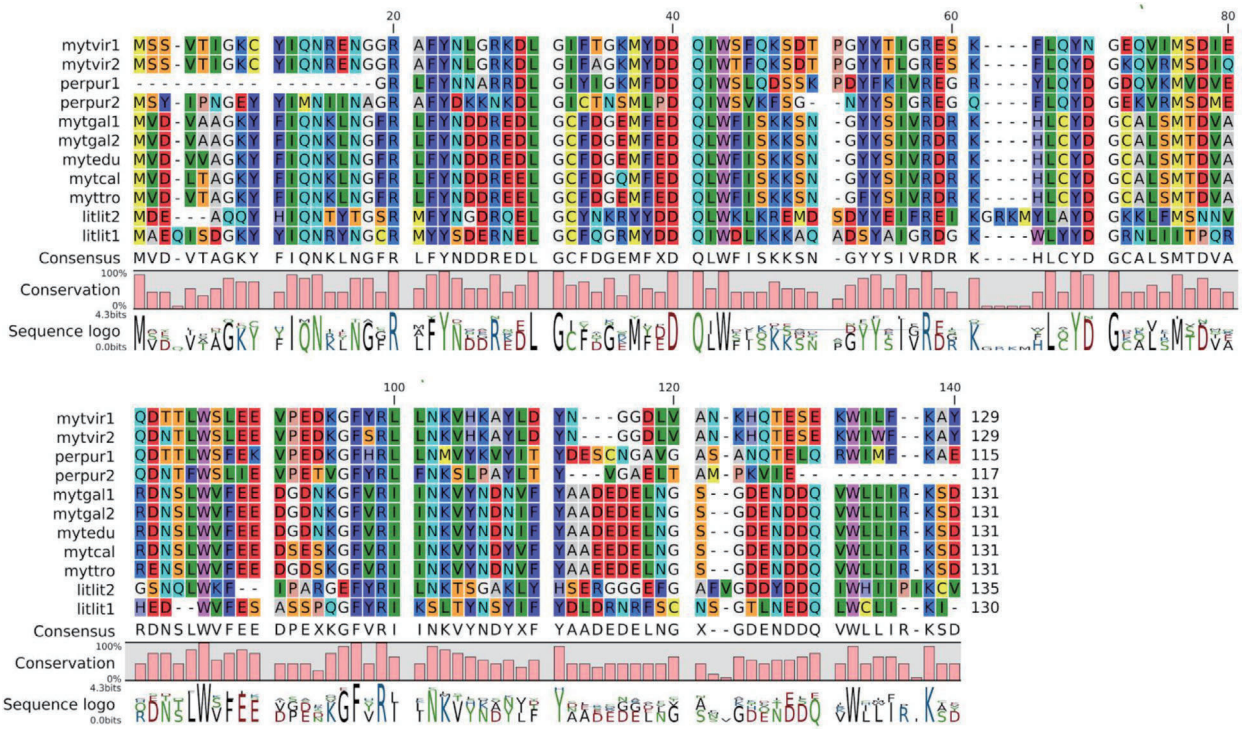

Fig. 3. Multiple sequence alignment of SeviL orthologues in various mytilid species, detected in publicly available genomic or transcriptomic resources. mytvir1 (GenBank accession number MK434191) and mytvir2 (MK434192): *Mytilisepta virgata*; mytgal1 (MK434193) and mtgel2 (MK434194): *Mytilus galloprovincialis*; litlit1 (MK434195) and litlit2 (MK434196): *Lithophaga lithophaga*; mytedu (MK434197): *Mytilus edulis*; mytcal (MK434198): *Mytilus californianus*; myttro (MK434199): *Mytilus trossulus*; perpur1 (MK434200) and perpur2 (MK434201): *Perumytilus purpuratus*. Names with numbers (*e.g.*, mytvir1, mytvir2) indicate lectin variants from the same organism. Note that the sequence perpur1 and perpur2 display incomplete N-terminal and C-terminal regions, respectively. The sequence alignment within the polypeptide is analyzed by using MUSCLE program [31].

Glycan-binding profile of SeviL

The glycan-binding profile of SeviL was determined by array analysis using 52 representative glycans, as illustrated and numbered in Fig. S3A and Table S1. SeviL bound significantly to the GM1b oligosaccharide (Neu5Acα2-3Galβ1-3GalNAcβ1-4Galβ1-4Glc; **36**) and its precursor asialo-GM1 oligosaccharide (Galβ1-3GalNAcβ1-4Galβ1-4Glc; **41**) (Fig. 6B and Fig. S3B). The lectin also interacted weakly with the glycan moiety of asialo-GM2 (GalNAcβ1-4Galβ1-4Glc; **43**) oligosaccharide (which contains a GM1b or asialo-GM1 oligosaccharide component) and the globo-series SSEA-4 hexaose (Neu5Acα2-3Galβ1-3GalNAcβ1-3Galα1-4Galβ1-4Glc; **51**) (Fig. 6B). The total amount of SeviL bound with these three glycans was concentration-dependent (Fig. 6B and Fig. S3B).

On the other hand, SeviL showed no notable binding to Thomsen–Friedenreich (TF-) antigen (Galβ1-3GalNAc; **9**) nor GM1a (Galβ1-3GalNAcβ1-4[Neu5Acα2-3]Galβ1-4Glc; **35**). SeviL displayed no significant interaction with N-glycans (Fig. 6A: **1**–**7**), O-glycans (Fig. 6A: **8** and **9**), and glycosaminoglycans (Fig. 6A: **10**–**14**), which are derived from glycoproteins.

Asialo-GM1 oligosaccharide-dependent apoptosis

Possible triggering of ganglioside-dependent signals by SeviL was examined. Anti-asialo-GM1 pAb was applied to HeLa, MCF7, BT474, Caco2, and MDCK cells (see Materials and methods 'Mussels, cell lines, and reagents') and caused surface staining of each cell line except BT474 (Fig. 7A). Next, cells (10^5 mL^{-1}) were incubated with various concentrations of SeviL for 48 h, and cell viability and proportions of living cells were determined by WST-8 assay. Increasing the SeviL concentration from 25 to 100 μg·mL^{-1} resulted in apoptosis (cell death) for HeLa, MCF7, Caco2, and MDCK (Fig. 7B), but not for BT474. Cotreatment with anti-asialo-GM1 pAb blocked the cytotoxic effect of SeviL (Fig. 7B, 'SeviL + pAb'). These findings

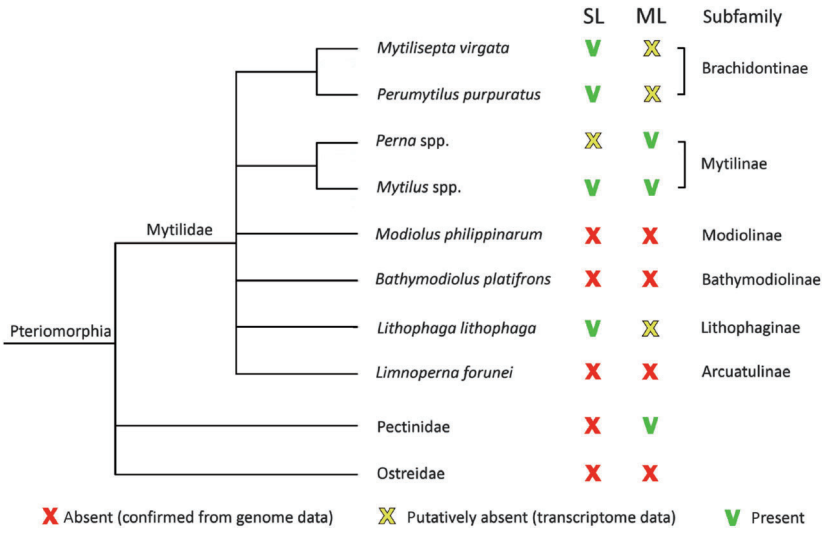

Fig. 4. Comparative distribution of SeviL/R-type (SL) lectin and mytilectin (ML) family members in bivalves. The presence of ML and SL was confirmed by genomic and/or transcriptomic data in the family Mytilidae, using Pectinidae, and Ostreidae as outgroups in the subclass Pteriomorphia. The cladogram was drawn based on the classification of bivalve species based on WoRMS data [33]ription levels of SeviL in various *M. virgata* tissues, calculated *in silico* from RNA-seq data in a pool of individuals and expressed as trascripts per milion (TPM) (panel A), or determined in single individuals with qRT/PCR (panel B) (see Materials and methods). Each bar represents the mean plus standard deviation of three technical replicates.

indicate that SeviL induced apoptosis mediated by ganglioside at the cell surface.

Activation in HeLa cells of MAPK pathway and caspases

In HeLa cells, SeviL activated the MAPK pathway of extracellular signal-regulated kinase $(ERK)_{1/2}$ signaling cascade in dose-dependent manner, as shown by Western blotting (Fig. 8, P-$ERK_{1/2}$ vs. $ERK_{1/2}$). SeviL treatment also phosphorylated p38 mitogen-activated protein kinase (Fig. 8, P-p38 vs. p38) and activated caspase-3/9 (Fig. 9, procaspase-3 and 9 vs. activated caspase 3 and 9). These findings suggest that SeviL regulates cell physiological processes through similar MAPK pathways, including MEK/ERK and p38, and activate caspase-3 via mitochondrial cycles.

Localization of SeviL in *M. virgata* tissues

SeviL signals detected by the antiserum indicated its specific presence in the outer part of the mantle rim and gills (Fig. 10A,C), but not in the foot (Fig. 10E). This localization pattern reflected the transcriptional levels of SeviL-encoding mRNA coding in mussel tissues (Fig. 5A). The signals detected by the anti-GM1 pAb showed the same pattern of distribution as the expression of SeviL (Fig. 10B,D). These findings suggest that the main sites of expression of SeviL in *M. virgata* match with the location of detection of the antigens detected by the asialo-GM1 pAb. Since SeviL was obtained by the elution with the sugar-containing buffer from the mantle and gills of the mussels during the purification, it seems reasonable for the lectin to be found in these tissues with binding its ligands (Table 1).

Discussion

Over the past decade, glycobiological studies of nontraditional model organisms (such as bivalve mollusks) have revealed an unexpected diversity of lectins in various taxonomic groups. In this study, we have demonstrated the presence of an R-type lectin (SeviL) in *Mytilisepta virgata*, a member of the family Mytilidae. This lectin family is characterized by a β-trefoil fold structure and occurs across a wide range of animals, from microorganisms to humans. R-type lectins have been reported previously from the invertebrate phyla Porifera [34], Annelida [35], and Echinodermata [36]. SeviL was assigned to the R-type lectin family on the basis of sequence similarities to the prototypical ricin B-chain domain, but it displays features not found in other members of this family. First identified in a plant, R-type lectins are found in a wide variety of organisms from bacteria to mammals, and numerous structures from this group have been analyzed in detail. Although

287 2612–2630 © 2019 The Authors. The *FEBS Journal* published by John Wiley & Sons Ltd on behalf of Federation of European Biochemical Societies

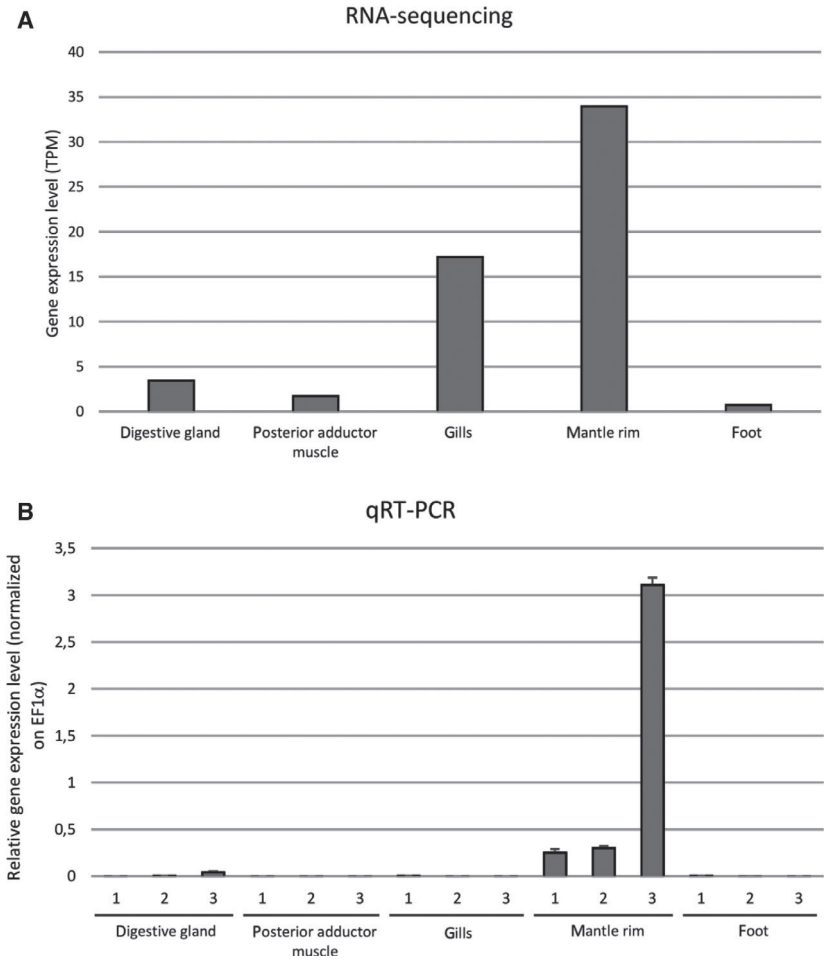

Fig. 5. Transcription levels of SeviL in various M. virgata tissues, calculated in silico from RNA-seq data in a pool of individuals and expressed as trascripts per milion (TPM) (panel A), or determined in single individuals with qRT/PCR (panel B) (see Materials and methods). Each bar represents the mean plus standard deviation of three technical replicates.

a QxW motif is conserved in each of the three subdomains, no overall consensus sequence is found like that of C-type lectins or galectins. The primary structure of SeviL shares less than 20% similarity with other invertebrate R-type lectins (Fig. S2C), but there is much greater similarity (40–90%) among mytilid proteins (Fig. S2A). Both acidic and basic amino acids are found throughout the sequence of SeviL, in contrast to MytiLec-1, which has acidic amino acids only on the C-terminal side of each subdomain [12]. Surprisingly, SeviL also possesses 6 hydrophobic amino acids at the C terminus, as found with MytiLec-1 [12]. In the case of MytiLec-1, these residues were essential for dimerization [13], but structural analysis will be needed to determine whether the same is true of SeviL.

Several similar sequences in other Mytilidae species besides *M. virgata* (Fig. 3) define a cluster of orthologues that we have named 'SeviL-like R-type lectins'. Curiously, the taxonomic spread of these lectins only partially overlaps that of mytilectins [18]. While no mytilectin was detected in the transcriptome of *M. virgata*, some mussel species (such as *Mytilus galloprovincialis*) possess both types of lectin, and others (such as *Modiolus philippinarum*) have neither (Fig. 4).

The transcription of *M. virgata* SeviL-like lectin and *M. galloprovincialis* MytiLec-1 was similarly confined to mantle and gills in both species (Fig. 5), suggesting that these lectins have similar roles in mussel physiology. However, while only the R-type lectin family is expressed in *M. virgata*, both members of the R-type family and the mytilectin family are encoded by the genome of *M. galloprovincialis*. It is presently unknown whether these two lectin families display an overlapping pattern of expression and are coregulated in this species. Determining how the expression of mussel lectins is modulated in response to external stimuli may bring new insights into the molecular ecology of these proteins, and helping to understand the role of lectin-glycan interactions in the notable capacity of bivalve mollusks to adapt to new environments.

SeviL was purified by using a lactose-conjugated affinity column, and its ability to hemagglutinate was

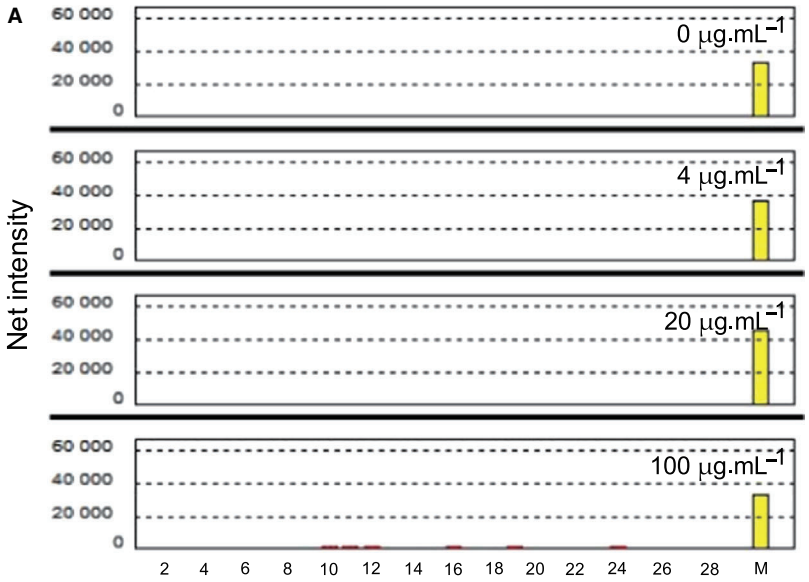

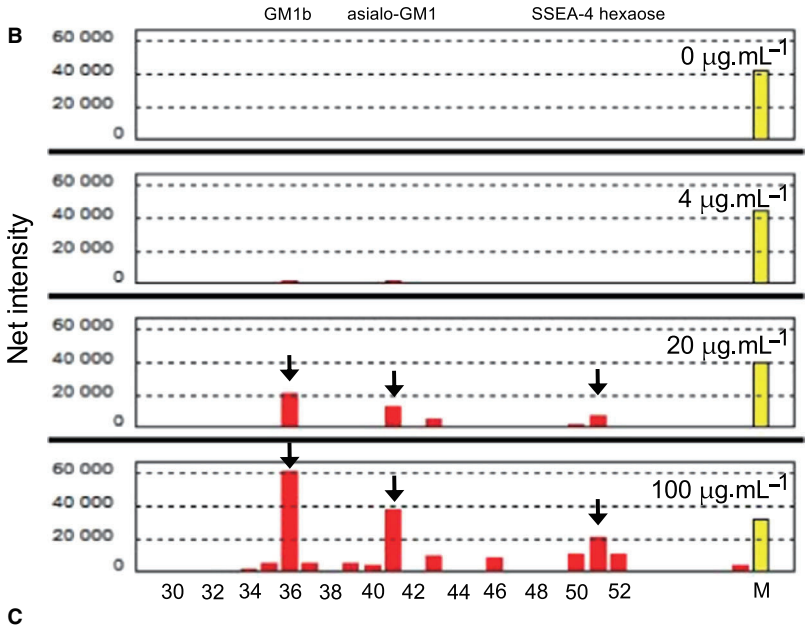

C

Glycans	Structures	Binding
GM1b (36)	Neu5Acα2-3Galβ1-3GalNAcβ1-4Galβ1-4Glc	**Strong**
asialo-GM1 (41)	Galβ1-3GalNAcβ1-4Galβ1-4Glc	**Middle**
SSEA-4 hexa (51)	Neu5Acα2-3Galβ1-3GalNAcβ1-3Galα1-4Galβ1-4Glc	**Weak**
GM1a (35)	Galβ1-3GalNAcβ1-4Galβ1-4Glc (3 Neu5Acα2)	None
TF (9)	Galβ1-3GalNAc	
SSEA-4 tetra (50)	Neu5Acα2-3Galβ1-3GalNAcβ1-3Gal	

Fig. 6. Glycan-binding profile of SeviL. HyLite555-labeled SeviL (0–100 μg·mL^{-1}: right upper) was subjected to glycan array analysis combining glycan-conjugated chips in which 52 glycan structures were immobilized and a surface plasmon resonance scanning detector (numbering as in Fig. S3A and Table S1). The evanescent-field fluorescence occurring by the binding between HyLite555-SeviL and the glycans (Fig. S3B) is represented as net intensities (*y*-axis of these graphs). (A) The chip includes N-glycans, O-glycans, glycosaminoglycans, Lewis type oligosaccharides, derivatives of lactose and N-acetyllactosamine and ABH-type oligosaccharides (No. 1-28 in Table S1). (B) The chip includes ganglio-series oligosaccharides and globo-series oligosaccharides (No. 29-52 in Table S1). Arrows indicate positions (glycans number 36, 41 and 51) of glycans of GM1b, asialo-GM1, and SSEA-4 hexsaose, respectively. M. Internal standard marker for fluorescence. C. The structural motif of the glycans recognized by SeviL. The colored part highlights the structure shared by GM1b, asialo-GM1 and SSEA-4 hexa(ose), whose glycans are bound by SeviL (see panel B). GM1a, TF, and SSEA-4 tetra(ose) are glycans that are not bound by the lectin.

287 2612–2630 © 2019 The Authors. The *FEBS Journal* published by John Wiley & Sons Ltd on behalf of Federation of European Biochemical Societies

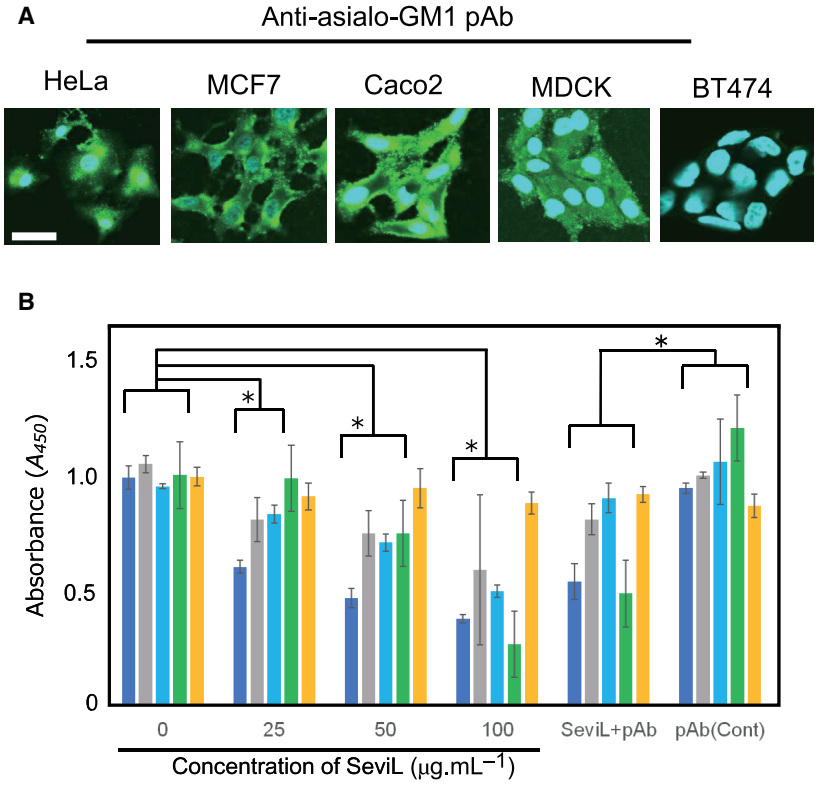

Fig. 7. Detection of asialo-GM1 expression on cell membranes by immunostaining. (A) Paraformaldehyde-fixed cells were stained with anti-asialo-GM1 oligosaccharide pAb and AF488-tagged goat anti-rabbit Ab (green). Nuclei were counterstained with DAPI (blue). Magnification: ×40. Scale bar: 10 mm. (B) Cytotoxic effects of SeviL on human ovarian cancer (HeLa), breast cancer (MCF7, BT474), colonic cancer (Caco2), and dog kidney (MDCK) cells. Cells were treated with SeviL at various concentrations (0–100 μg·mL^{-1}) for 24 h, and cell viability (expressed as A_{450}; see M & M/ 'Cell viability and cytotoxicity assays') was determined by WST-8 assay. SeviL + pAb: treatment with 50 μg·mL^{-1} SeviL plus anti-asialo-GM1 oligosaccharide polyclonal antibody (pAb). pAb (Cont): anti-asialo-GM1 oligosaccharide pAb without SeviL, as control. Data shown are mean ± SE (n = 3). P values (*P < 0.05) were obtained with Dunnett's test.

inhibited in the presence of lactose and melibiose. However, such inhibition required a high concentration, 20 mM or more of the sugars, roughly 100 times the ligand concentration used in the glycan array analysis. This observation suggests that the binding by these disaccharides does not occur under physiological conditions.

SeviL, in same with an R-type lectin from sea cucumber [36], requires divalent cations such as Ca^{2+} for its hemagglutination activity (Fig. S1A), whereas MytiLec-1 shows no dependence on metal ions [12]. In contrast to members of the mytilectin family, including MytiLec-1 and CGL, which bind to α-Gal in Gb3 [13,37], SeviL strongly binds to ganglio-series GM1b oligosaccharide (Neu5Acα2-3Galβ1-3GalNAcβ1-4Galβ1-4Glc) and asialo-GM1 (Galβ1-3GalNAcβ1-4Galβ1-4Glc). SSEA-4 hexaose (Neu5Acα2-3Galβ1-3GalNAcβ1-3Galα1-4Galβ1-4Glc) and asialo-GM2 (GalNAcβ1-4Galβ1-4Glc), which weakly interacted with SeviL, comprises a part of the structure of GM1b (Fig. 6B and Fig. S3B). On the other hand, SeviL did not bind to TF antigens (Galβ1-3GalNAc), GM1a (Galβ1-3GalNAcβ1-4[Neu5Acα2-3]Galβ1-4Glc). These results suggest that Galβ1-3GalNAcβ1-4Galβ1-4Glc is the core structure recognized by SeviL and that the presence of Neu5Ac at the nonreducing terminus is a desirable feature for sugar binding (Fig. 6C). Furthermore, the hydroxyl group at the C-3 position of the 3rd Gal from the nonreducing terminus is required to be free (Fig. 6C). SeviL displayed a different carbohydrate-binding specificity with GM1b and asialo-GM1 compared with the cholera toxin, which bound to GM1a and fucosyl-GM1 [38]. After all, this study found that this R-type lectin of the mussels was glycosphingolipid glycan-binding specific such as ganglioside and globoside, not but glycoprotein glycans (Fig. 6A).

The binding of SeviL to two ganglio-series (GM1b and its precursor asialo-GM1) and one globo-series (SSEA-4 hexaose) oligosaccharides is very interesting, since each glycan is expressed specifically by the target antigen for Guillain–Barré syndrome (GM1b) [39], natural killer cells and basophils (asialo-GM1) [40], and glioblastoma multiforme (SSEA-4) [41] in vertebrates, respectively. SeviL has potential clinical applications, similar to those of other invertebrate R-type lectins that recognize specific glycans such as TF antigen (Galβ1-3GalNAc) and LacdiNAc (GalNAcβ1-4GlcNAc) [42,43].

Exposure to SeviL led to increased metabolism and induction of apoptosis in mammalian cells bearing asialo-GM1 oligosaccharide (Fig. 7), indicating the

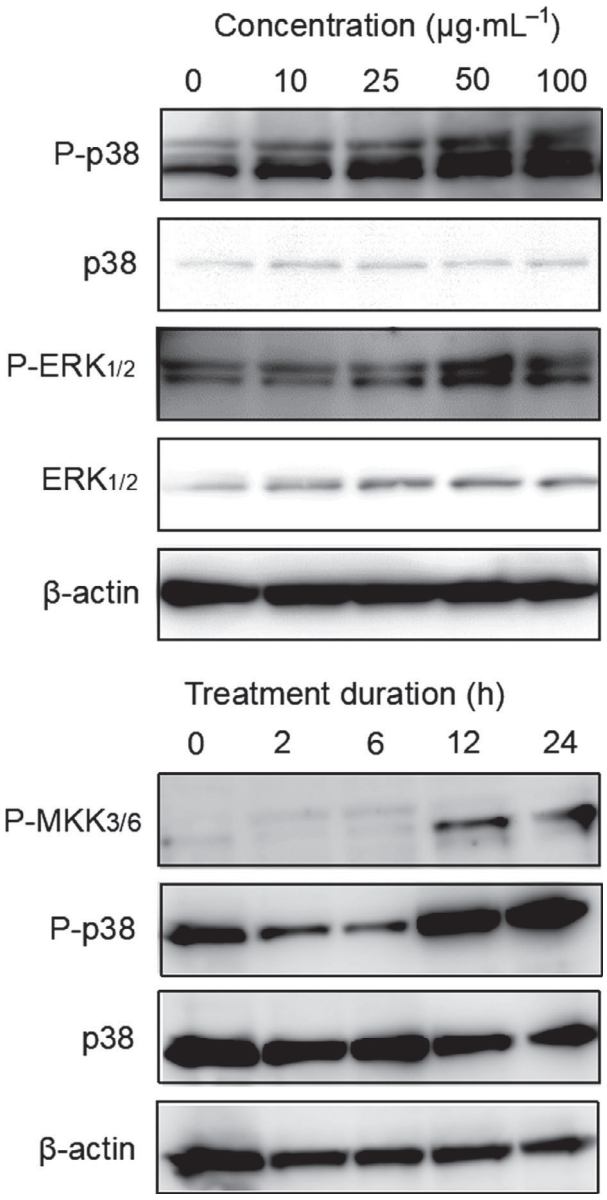

Fig. 8. Phosphorylation of MAPKs by SeviL in HeLa cells. Cells (5×10^5) were treated with SeviL at various concentration (0–100 μg·mL^{-1}) or durations (0–24 h). Phosphorylation of kinases was evaluated by Western blotting of cell lysates. P-p38, P-ERK$_{1/2}$, and P-MKK3/6: phosphorylated forms of p38, ERK$_{1/2}$ and MKK3/6 kinase, respectively. MKK3/6 is the upstream kinase of ERK$_{1/2}$.

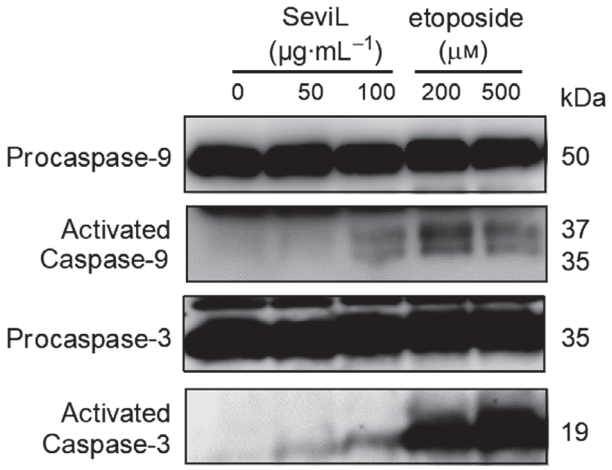

Fig. 9. Induction of caspase-3/9 cleavage by SeviL. HeLa cells were treated for 48 h with SeviL (50, 100 μg·mL^{-1}), anticancer reagent etoposide (200, 500 μM) or lysates were prepared, and caspase-3/9 activation was detected by Western blotting. Each experiment was performed in triplicate.

ability of the protein to regulate cell proliferation. SeviL is a dimer like MytiLec-1 (Fig. 1B), whose self-association is essential for cytotoxicity. The use of an anti-asialo-GM1 polyclonal antibody (pAb), which blocked the access to the target of SeviL, completely abrogated the effect of the lectin (Fig. 7B). The cell regulatory mechanisms triggered by the interaction between SeviL and GM1b oligosaccharides will also be clarified by using a specific anti-GM1b antibody in future. SeviL activated various metabolic pathways (including MKK3/6, ERK$_{1/2}$, p38, and caspase-3/9). Both MytiLec-1 and SeviL therefore can potentially regulate the growth of human cancer cells by binding their respective ligands and activating similar metabolic pathways (Figs 8 and 9). The mytilectin family is known to play roles not only in the regulation of cell death [44] and also cell proliferation [45], through the activation of kinases. SeviL and the other R-type lectins isolated from Mytilidae may similarly have multiple activities, and it is possible that their expression may be regulated by signals external to the organism.

β-Trefoil lectins of mussels have been proposed to be involved in defense against pathogenic microorganisms typically encountered by bivalves due to their filter-feeding habits [16,18,46]. By using immunohistochemistry techniques, the expression of SeviL was detected in tissues which are in direct contact with the internal and external environment (Fig. 10). The comparison between the transcriptional levels of SeviL-like lectin and mytilectin in mussels grown in different environments may clarify the specific role of these lectins in immune defense against invading microorganisms. The spatial overlap between the signals detected with the anti-asialo GM1 polyclonal antibody and the anti-SeviL antibody (Fig. 10) suggests the presence of similar or identical antigens with asialo-GM1 in the mussel tissues. The autoantibody which recognizes GM1b raised in patients affected by the Guillain–Barré syndrome arises from infection with Campylobacter, because

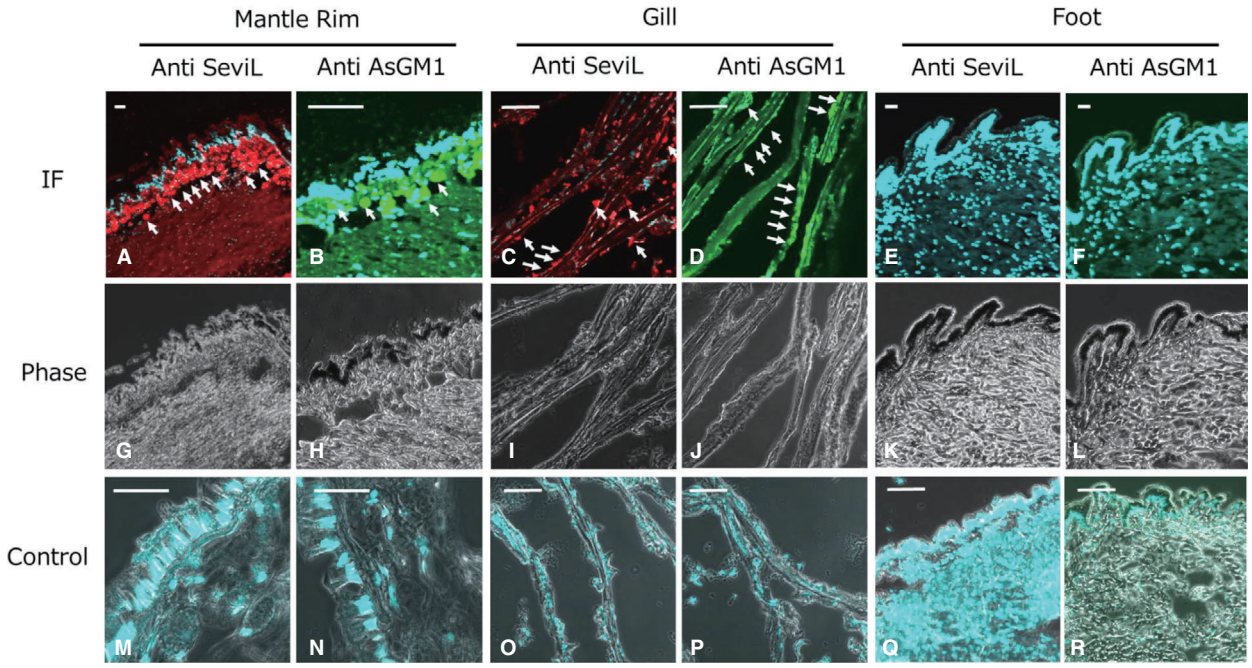

Fig. 10. Localization of SeviL and substances which reacted with anti-asialo-GM1 polyclonal antibody in *M. virgata* tissues. Tissue sections derived from mantle rim, gill, and foot were applied by anti-SeviL (column anti-SeviL: A, C, E, G, I and K) and anti-asialo-GM1 (column Anti AsGM1: B, D, F, H, J, and I) polyclonal antibodies followed by Alexa 568 (red: for the detection Anti-SeviL) or Alexa488 (green: for the detection of As asialo-GM1) conjugated secondary anti-rabbit IgG antibody. All sections were stained also with DAPI to detect nuclei (blule: A–F and M-R). IF: immunofluoresence (A–F), phase: phase contrast (G–L) and control: applying nonimmune primary antibody (for SeviL: M, O, and Q) and without primary antibody (for asialo-GM1 antibody reactant: N, P and R), respectively. Scale bars: 20 μm each.

specific lipopolysaccharides of the bacteria possess structures similar to gangliosides [39]. This evidence may support the hypothesis that the glycans recognized by SeviL may be present both in invading microorganisms and in the tissues of species pertaining to the family Mytilidae. It has been recently reported that the lectin subunit of the cholera toxin, which is known to bind GM1a, also binds to lipooligosaccharides and is capable of inhibiting the growth of genus *Campylobacter* [47]. The glycan structures of most invertebrates and microorganisms remain to be thoroughly investigated [48,49], and the application of structural glycobiology approaches to these phyla will provide a significant improvement in the knowledge on this subject.

Besides the immune response of bivalves in response to infection by pathogenic microorganisms, the study of the infection and defense mechanisms enacted by these marine bivalves against neoplasia has also met a considerable interest in recent years. The group of Goff showed that horizontal transmission of cancer cells in bivalves resulted from activation of the retrotransposon gene 'Steamer' [50]. Such neoplastic cells may be propagated from one individual and transmitted to others through sea water [51]. In recent, the group of Metzger elucidated how the cancer cells of mussels were transferred across the Atlantic and Pacific Oceans and between the Northern and Southern hemispheres [52]. By knowing this situation, we will have more interest in how the cancer cells transfer into the mussels in the Asian area. In order to better elucidate the physiological role of SeviL-like lectins, one of our next goals will be to investigate whether their administration to tumor cells derived from bivalves may have a significant effect on cell growth regulation.

SeviL and MytiLec-1 bind to β- and α-galactosides, respectively, but it is not yet certain whether the natural ligand of these proteins is found within the organism itself or in the surrounding environment. The physiological roles of these proteins will remain unclear, however, until their target glycans are identified. Certain mollusks have characteristic glycosphingolipids with Gal or GalNAc at their glycan termini [53,54]. Such glycans are potential ligands for mytilectins, and similar ligands may exist for SeviL as well. Although the protein appears from its sequence to be a β-trefoil, it shows limited conservation to other such proteins at the sugar-binding sites (Fig. S4). Characteristics of the molecular

structure of the protein may help understand the function of lectins by revealing the modes of endogenous and exogenous ligand binding. Although the history of lectins in the mollusks is so long, the studies on the functional characterization of the β-trefoil fold lectin in the bivalves have just begun.

Materials and methods

Mussels, cell lines, and reagents

Mussels (*M. virgata*) were collected from the seashore at Saikai City, Nagasaki prefecture, Japan, under the permission of the Saikai-Oosaki fisheries union. The shells were removed, and bodies were stored whole at −80 °C. Human cell lines HeLa (cervical cancer), MCF7 and BT474 (breast cancer), and Caco2 (colonic cancer) were from American Type Culture Collection (ATCC). Dog kidney cell line MDCK was kindly provided by T. Fujiwara. Lactose, melibiose, sucrose, D-Gal, D-Glc, D-Man, D-Fuc, D-GalNAc, D-GlcNAc, standard protein markers for SDS/PAGE, porcine stomach mucin, fetuin, and penicillin–streptomycin for cell culture were from FUJIFILM Wako Pure Chemical Corp. (Osaka, Japan). Bovine submaxillary mucin was from MP Biomedical (Illkirch-Graffenstaden, France). Lactosyl-agarose gel was from EY Laboratories (San Mateo, CA, USA). RPMI 1640 medium and fetal bovine serum (FBS) were from Thermo Fisher Scientific (Waltham, MA, USA). Cell Counting Kit-8 including 2-(2-methoxy-4-nitrophenyl)-3-(4-nitrophenyl)-5-(2,4-disulfophenyl)-2H-tetrazolium) monosodium salt (WST-8), HiLyte Fluor 555 labeling kit-NH_2, and Biotin Labeling kit-NH_2 were from Dojindo Laboratories (Kumamoto, Japan). HRP-conjugated β-actin monoclonal antibody (mAb) was from FUJIFILM. Anti-asialo-GM1 polyclonal antibody (pAb) (rabbit immunoglobulin) was from Cedarlane (Ontario, Canada). Anti-p38, antiphosphorylated p38 (pT180/pY182), anti-Erk1, and antiphosphorylated $ERK_{1/2}$ (pT202/pY204) monoclonal antibodies (mAbs) were from Becton Dickinson (Franklin Lakes, NJ, USA). Antiphosphorylated MKK3/6 (MKK3(S189)6(S207) 22A8) and anticaspase-9 mAbs were from Medical and Biological Laboratories (Nagoya, Japan). Anticaspase-3 mAb was from Cell Signaling Technology (Danvers, MA, USA). HRP-conjugated anti-mouse or anti-rabbit IgG as secondary antibody was from Chemicon International (Temecula, CA, USA). Alexa Fluor® 568-labeled goat anti-rabbit IgG and Alexa Fluor® 488-labeled goat anti-rabbit IgG were from Abcam (Cambridge, UK). Can Get Signal® Immunoreaction Enhancer Solution 1 and 2 were from Toyobo Co. (Osaka, Japan). Tissue-tek compound was from Sakura Finetek Co (Tokyo, Japan). Low fluorescence and silicon-coated glass slides were from Matsunami Glass Industry (Kishiwada, Osaka, Japan).

Lectin purification

Mussel mantles and gills were homogenized with 10 volumes (w/v) 150 mM NaCl containing 10 mM Tris/HCl, pH 7.5 (TBS) with 10 mM $CaCl_2$. Supernatant (Sup 1) was collected by centrifugation at 27 500 ***g*** for 1 h at 4 °C as described in our previous study [12], with some modification. Precipitate was homogenized with 10 volumes (w/v) TBS containing 50 mM lactose, and supernatant (Sup 2) was collected as above. Sup 2 was dialyzed extensively against TBS. Both Sup 1 and Sup 2 were applied to lactosyl-agarose column (5.0 mL), and the column was washed with TBS until absorbance at 280 nm (A_{280}) of effluent reached baseline level. Lectin was eluted with TBS containing 50 mM lactose.

Hemagglutination assay and sugar-binding specificity assay

Hemagglutination assay was performed in 96-well V-shaped plates as described previously [55]. Twenty microliters of twofold dilution of purified lectin in TBS was mixed with 20 μL of a 1% suspension (with TBS; v/v) of trypsinized, glutaraldehyde-fixed rabbit erythrocytes, TBS, or TBS with 0.2% Triton X-100. Plates were incubated for 1 h at room temp, and formation of a sheet (agglutination-positive) or dot (agglutination-negative) was observed and scored as lectin titer. For sugar-binding specificity assay, 20 μL of sugar solution (200 mM) was serially diluted with TBS and mixed with 20 μL of lectin solution (adjusted to titer 16), trypsinized/glutaraldehyde-fixed rabbit erythrocytes, or TBS containing 1% Triton X-100. Plates were incubated for 1 h at room temp, and minimal inhibitory sugar concentration was determined.

Protein quantification and molecular mass determination

Protein was quantified using a protein assay kit (Thermo Fisher/ Pierce) based on the principle of bicinchoninic acid for colorimetric detection [56,57], using ovalbumin as standard. SDS/PAGE [58] was performed in 15% (w/v) acrylamide gel under reducing or nonreducing conditions, and gels were stained by Coomassie Brilliant Blue R-250.

Analytical ultracentrifugation

Sample concentration was estimated as 1.0 $mg{\cdot}mL^{-1}$ from A280 measurement. Sedimentation velocity experiments were performed using an Optima XL-I analytical ultracentrifuge (Beckman Coulter, Brea, CA, USA) with An-50 Ti rotor. Analytical cells (with standard Epon two-channel centerpiece and sapphire windows) were loaded with 400 μL sample and 420 μL reference solution (50 mM potassium phosphate, pH 7.4, 0.1 M NaCl). Prior to each

run, the rotor was kept stationary at 293 K in vacuum chamber for 1 h for temperature equilibration. A280 scans were performed at 10-min intervals during sedimentation at 201 600 ***g*** and analyzed using the continuous distribution (c(s)) analysis module in SEDFIT [59]. Frictional ratio (f/f_0) was allowed to float during fitting. c(s) distribution was converted to molar mass distribution c(M). Partial specific volume of protein, solvent density, and solvent viscosity were calculated from standard tables using the program SEDNTERP [60].

Determination of primary structure of SeviL by mass spectrometry

The partial peptide sequence of SeviL was derived by Proteomics International (Nedlands, WA, Australia). 200 μg lectin was dialyzed extensively against distilled water to remove salt, lyophilized, and digested by trypsin, and peptides were extracted by standard techniques [61]. Peptides were analyzed by electrospray ionization mass spectrometry using Prominence nano HPLC system (Shimadzu, Kyoto, Japan) coupled to 5600 triple time-of-flight (TOF) mass spectrometer (AB Sciex, Framingham, MA, USA). Tryptic peptides were loaded onto Zorbax 300SB-C18 column, 3.5 mm (Agilent, Santa Clara, CA, USA) and separated on a linear gradient of water/ acetonitrile/ 0.1% formic acid (v/v). MS/MS spectra were analyzed using PEAKS Studio software platform v. 4.5 SP2 (Bioinformatics Solutions, Waterloo, ON, Canada) with manual interpretation.

Transcriptomic analysis of full-length cDNA

cDNA sequence of SeviL obtained as above was used to screen *de novo*-assembled transcriptome data of *M. virgata* obtained from four tissues (i.e., gills, mantle rim, posterior adductor muscle, and digestive gland) from a pool of mussels collected at the seashore of Saikai city [29].

The assembled contig corresponding to the putative mRNA lectin sequence was identified by tBLASTn (e-value threshold was set at 0.05). The partial peptides sequences obtained as described in the previous section were used as queries for BLAST searches against the transcriptome. Correct assembly of the consensus transcript was confirmed by back-mapping RNA-seq reads to the sequence and by assessment of uniform and homogenous mapping along the entire coding sequence. The expression level of SeviL in various tissues was calculated *in silico* as TPM (transcripts per million) using CLC Genomics Workbench v.10 RNA-seq mapping tool (Qiagen, Hilden, Germany), setting length fraction parameter to 0.75, similarity fraction parameter to 0.98, and match/mismatch/deletion penalties to 3/3/3. RNA-seq datasets from the tissues mentioned above were used for this analysis [29].

To further confirm the tissue specificity of SeviL, qRT/PCR analyses were carried out on three individual mussels, as described in [29]. In this case, the sequence-specific primers designed for SeviL are (5′ -> 3′): AATTTGGGGCG TAAAGACCT (forward primer) and GGACTCTCTTCC GAGGGTG (reverse), aiming at the amplification of a 111-bp target sequence.

Sequence data availability

The cDNA sequence of SeviL, SeviL-2, and the orthologue sequences identified in publicly available transcriptomes of other mytilid species have been deposited in the GenBank repository, under the accession numbers MK434191–MK434201. The sequence alignments among each orthologue in the different species or the subdomains in the polypeptide are analyzed by using the MUSCLE program (http://www.drive5.com/muscle) [31].

Glycan array analysis

Glycan array analysis was performed by Sumitomo Bakelite Co. (Tokyo, Japan). SeviL was fluorescence-labeled ($\lambda_{ex/em}$ 555/570 nm) using HiLyte Fluor 555 labeling kit-NH_2 as per the manufacturer's instructions. A wide range of 52 glycans including N-glycans, O-glycans, Lewis glycans, lactosamine, blood-type glycans, gangliosides, and globosides were immobilized on wells. Fluorescence-labeled SeviL at concentrations ranging from 0 to 100 $\mu g \cdot mL^{-1}$ were incubated overnight at 4 °C with shielding from light. SeviL-binding glycans were detected by using Bio-REX Scan 300, an evanescent fluorescence scanner (Rexxam Co. Ltd., Osaka, Japan). Wavelength of laser light was used for Cy3, and the exposure time was 300 ms [62].

Cell viability and cytotoxicity assays

Cells were maintained in RPMI 1640 supplemented with heat-inactivated FBS 10% (v/v), penicillin (100 $IU \cdot mL^{-1}$), and streptomycin (100 $\mu g \cdot mL^{-1}$) at 37 °C. Cytotoxic effects and cell growth following treatment with SeviL at concentrations ranging from 0 to 100 $\mu g \cdot mL^{-1}$ were determined using Cell Counting Kit-8 containing WST-8 [12]. Cells (2×10^4, in 90 μL solution) were seeded into 96-well flat-bottom plates and treated with 10 μL lectin for 24 h at 37 °C. To evaluate glycan-inhibitory effects, anti-asialo-GM1 oligosaccharide pAb (50 $\mu g \cdot mL^{-1}$) was co-incubated with cells in addition to lectin for 24 h and then applied to the assay system. For assay of effect on cell growth, each well was added with 10 μL WST-8 solution and incubated 4 h at 37 °C. Cell survival rate was determined by measuring A_{450} (reference: A_{600}) with a microplate reader (model iMark; Bio-Rad, Tokyo, Japan).

Detection of activated signal transduction molecules and their phosphorylated forms

HeLa cells (5×10^5) were cultured with SeviL (0–100 $\mu g \cdot mL^{-1}$) for 24 h and then lysed in 200 μL RIPA buffer. Lysate was separated by SDS/PAGE and electrotransferred onto PVDF membrane as described previously [63]. Primary mAbs used were directed to p38 (1:3000; mouse), phospho-p38 (1:3000; mouse), ERK_1 (1:3000; mouse), phospho-$ERK_{1/2}$ (1:3000; mouse), phospho-MKK3/6 (1:3000; mouse), caspase-3 (1:5000; rabbit), and caspase-9 (1:5000; mouse). These antibodies were applied in Can Get Signal solution 1. Membrane was incubated for 24 h at 4 °C. HRP-conjugated secondary antibody was diluted 1:5000 in Can Get Signal solution 2 [64].

Immunocytochemical analysis of asialo-GM1 oligosaccharide expression

Cells (1×10^6) were fixed with 4% paraformaldehyde in PBS for 15 min at room temperature, washed 3× with PBS, blocked with 1% BSA in PBS for 30 min at room temperature. They were washed 3× with PBS, incubated with or without 100 μL anti-asialo-GM1 oligosaccharide pAb (dilution 1:200 with PBS) at 4 °C for 30 min, washed 3× with PBS, treated with 100 μL Alexa Fluor® 488-tagged goat anti-rabbit IgG (dilution 1:200 in PBS) at 4 °C for 30 min. Cells were placed onto low fluorescence glass slides, mounted with 50% glycerol solution, and examined by confocal microscopy. Confocal images were obtained using FV10i FLUOVIEW (Olympus, Tokyo, Japan).

Immunohistochemistry of SeviL expressions on the mussel tissues

Mussel organs (gill, mantle rim, and foot) were cut into around 1-cm-square pieces, embedded in the Tissue-tek compound and frozen in isopentane, cooled in by liquid nitrogen. The frozen tissue block was sliced on 6-μm-thick with Leitz cryostat (Leica Instruments, Nussloch, Germany), placed on silicon-coated glass slides. Sections were sequentially fixed in PBS containing 4% paraformaldehyde for 15 min at room temperature, incubated in blocking solution containing 0.05% saponin and 1% BSA in PBS for 30 min, incubated with or without anti-SeviL or anti-asialo-GM1 oligosaccharide pAb (dilution 1:100 with blocking solution) at room temperature for 1 h. After washing the tissues with PBS, they were treated with Alexa Fluor® 568-labeled goat anti-rabbit IgG or Alexa Fluor® 488-labeled goat anti-rabbit IgG (dilution 1:100 in blocking solution) at room temperature for 1 h, washed with PBS, mounted with 50% glycerol solution, and observed by confocal microscopy FV10i FLUOVIEW. Nuclei were stained by DAPI (364/454 nm) [64].

Statistical analysis

Experiments were performed in triplicate, and results presented as mean ± standard error (SE). Data were subjected to one-way analysis of variance (ANOVA) followed by Dunnett's test, using SPSS STATISTICS software package, v. 10 (www.ibm.com/products/spss-statistics). Differences with $P < 0.05$ were considered significant.

Acknowledgements

This study was supported by the Research Promotion Fund of Nagasaki International University and Yokohama City University. This work was also supported by JSPS Grant-in-Aid for Scientific Research-KAKENHI under Grant No. JP19K06239 (YO and YF) and JP18K07458 (YOg and YF). MG and AP were supported by funding from the European Union's Horizon 2020 research and innovation program under grant agreement No. 678589. JRHT thanks OpenEye Scientific Software for financial support. YO thanked Research and Developmental Support 2018–2019 for Life Sciences from the City of Yokohama (Life Innovation Platform, LIP. Yokohama, Project No 1842110002). YF and YO were supported by funding from Sugiyama Chemical and Industrial Laboratory 2019. The authors are grateful to Mr. Yasunori Imura for directing us to an excellent *M. virgata* sampling area and to Dr. S. Anderson for English editing of the manuscript.

Conflict of interest

The authors declare no conflict of interest.

Author contributions

YF, MG, JRHT, and YO designed the study; YF, MG, FS, KK, IH, SR, SMAK HF, and YO performed the experiments; JRHT, YOg, MH, and AP contributed new reagents/analytic tools; YF, MG, KK, SS, YK, TY, YOg, and YO analyzed data; YF, YO, MG, and JRHT wrote the paper.

References

1 Ogawa T, Watanabe M, Naganuma T & Muramoto K (2011) Diversified carbohydrate-binding lectins from marine resources. *J Amino Acids* **2011**, 1–20.
2 Cheung RC, Wong JH, Pan W, Chan YS, Yin C, Dan X & Ng TB (2015) Marine lectins and their medicinal applications. *Appl Microbiol Biotechnol* **99**, 3755–3773.

3 Chernikov OV, Molchanova VI, Chikalovets IV, Kondrashina AS, Li W & Lukyanov PA (2013) Lectins of marine hydrobionts. *Biochemistry (Mosc)* **78**, 760–770.
4 Rao A, Seto J, Berg JK, Kreft SG, Scheffner M & Cölfen H (2013) Roles of larval sea urchin spicule SM50 domains in organic matrix self-assembly and calcium carbonate mineralization. *J Struct Biol* **183**, 205–215.
5 Motohashi S, Jimbo M, Naito T, Suzuki T, Sakai R & Kamiya H (2017) Isolation, amino acid sequences, and plausible functions of the galacturonic acid-binding egg lectin of the sea hare *Aplysia kurodai*. *Mar Drugs* **15**, 161.
6 Gorbushin AM (2019) Derivatives of the lectin complement pathway in Lophotrochozoa. *Dev Comp Immunol* **94**, 35–58.
7 Maehashi E, Sato C, Ohta K, Harada Y, Matsuda T, Hirohashi N, Lennarz WJ & Kitajima K (2003) Identification of the sea urchin 350-kDa sperm-binding protein as a new sialic acid-binding lectin that belongs to the heat shock protein 110 family: implication of its binding to gangliosides in sperm lipid rafts in fertilization. *J Biol Chem* **278**, 42050–42057.
8 Carneiro RF, Teixeira CS, de Melo AA, de Almeida AS, Cavada BS, de Sousa OV, da Rocha BA, Nagano CS & Sampaio AH (2015) L-Rhamnose-binding lectin from eggs of the *Echinometra lucunter*: Amino acid sequence and molecular modeling. *Int J Biol Macromol* **78**, 180–188.
9 Unno H, Matsuyama K, Tsuji Y, Goda S, Hiemori K, Tateno H, Hirabayashi J & Hatakeyama T (2017) Identification, characterization, and X-ray crystallographic analysis of a novel type of mannose-specific lectin CGL1 from the pacific oyster *Crassostrea gigas*. *Sci Rep* **6**, 29.
10 Kita A, Jimbo M, Sakai R, Morimoto Y, Takeuchi R, Tanaka H, Takahashi T & Miki K (2017) Crystal structure of octocoral lectin SLL-2 complexed with Forssman antigen tetrasaccharide. *Glycobiology* **27**, 696–700.
11 Carneiro RF, Torres RC, Chaves RP, de Vasconcelos MA, de Sousa BL, Goveia AC, Arruda FV, Matos MN, Matthews-Cascon H, Freire VN *et al.* (2017) Purification, biochemical characterization, and amino acid sequence of a novel type of lectin from *Aplysia dactylomela* eggs with antibacterial/antibiofilm potential. *Mar Biotechnol (NY)* **19**, 49–64.
12 Fujii Y, Dohmae N, Takio K, Kawsar SM, Matsumoto R, Hasan I, Koide Y, Kanaly RA, Yasumitsu H, Ogawa Y *et al.* (2012) A lectin from the mussel *Mytilus galloprovincialis* has a highly novel primary structure and induces glycan-mediated cytotoxicity of globotriaosylceramide-expressing lymphoma cells. *J Biol Chem* **287**, 44772–44783.
13 Terada D, Kawai F, Noguchi H, Unzai S, Hasan I, Fujii Y, Park SY, Ozeki Y & Tame JR (2016) Crystal structure of MytiLec-1, a galactose-binding lectin from the mussel *Mytilus galloprovincialis* with cytotoxicity against certain cancer cell types. *Sci Rep* **6**, 28344.
14 Montfort W, Villafranca JE, Monzingo AF, Ernst SR, Katzin B, Rutenber E, Xuong NH, Hamlin R & Robertus JD (1987) The three-dimensional structure of ricin at 2.8 Å. *J Biol Chem* **262**, 5398–5403.
15 Kovalchuk SN, Chikalovets IV, Chernikov OV, Molchanova VI, Li W, Rasskazov VA & Lukyanov PA (2013) cDNA cloning and structural characterization of a lectin from the mussel *Crenomytilus grayanus* with a unique amino acid sequence and antibacterial activity. *Fish Shellfish Immunol* **35**, 1320–1324.
16 Chikalovets IV, Kovalchuk SN, Litovchenko AP, Molchanova VI, Pivkin MV & Chernikov OV (2016) A new Gal/GalNAc-specific lectin from the mussel *Mytilus trossulus*: Structure, tissue specificity, antimicrobial and antifungal activity. *Fish Shellfish Immunol* **50**, 27–33.
17 García-Maldonado E, Cano-Sánchez P & Hernández-Santoyo A (2017) Molecular and functional characterization of a glycosylated galactose-binding lectin from *Mytilus californianus*. *Fish Shellfish Immunol* **66**, 564–574.
18 Hasan I, Gerdol M, Fujii Y, Rajia S, Koide Y, Yamamoto D, Kawsar SM & Ozeki Y (2016) cDNA and gene structure of MytiLec-1, a bacteriostatic R-type lectin from the Mediterranean mussel (*Mytilus galloprovincialis*). *Mar Drugs* **14**, 92.
19 Gerdol M, Luo YJ, Satoh N & Pallavicini A (2018) Genetic and molecular basis of the immune system in the brachiopod *Lingula anatina*. *Dev Comp Immunol* **82**, 7–30.
20 Melwani AR, Gregorio D, Jin Y, Stephenson M, Ichikawa G, Siegel E, Crane D, Lauenstein G & Davis JA (2014) Mussel watch update: long-term trends in selected contaminants from coastal California, 1977–2010. *Mar Pollut Bull* **81**, 291–302.
21 Gerdol M & Venier P (2015) An updated molecular basis for mussel immunity. *Fish Shellfish Immunol* **46**, 17–38.
22 Venier P, Varotto L, Rosani U, Millino C, Celegato B, Bernante F, Lanfranchi G, Novoa B, Roch P, Figueras A & *et al.* (2011) Insights into the innate immunity of the Mediterranean mussel *Mytilus galloprovincialis*. *BMC Genom* **12**, 69.
23 Gerdol M, Manfrin C, De Moro G, Figueras A, Novoa B, Venier P & Pallavicini A (2011) The C1q domain containing proteins of the Mediterranean mussel *Mytilus galloprovincialis*: a widespread and diverse family of immune-related molecules. *Dev Comp Immunol* **35**, 635–643.

24 Di Leo A, Annicchiarico C, Cardellicchio N, Giandomenico S, Conversano M, Castellano G, Basile F, Martinelli W, Scortichini G & Spada L (2014) Monitoring of PCDD/Fs and dioxin-like PCBs and seasonal variations in mussels from the Mar Grande and the Mar Piccolo of Taranto (Ionian Sea, Southern Italy). *Environ Sci Pollut Res Int* **21**, 13196–13207.
25 Wu F, Lu W, Shang Y, Kong H, Li L, Sui Y, Hu M & Wang Y (2016) Combined effects of seawater acidification and high temperature on hemocyte parameters in the thick shell mussel *Mytilus coruscus*. *Fish Shellfish Immunol* **56**, 554–562.
26 Castillo N, Saavedra LM, Vargas CA, Gallardo-Escárate C & Détrée C (2017) Ocean acidification and pathogen exposure modulate the immune response of the edible mussel *Mytilus chilensis*. *Fish Shellfish Immunol* **70**, 149–155.
27 Pales Espinosa E, Perrigault M & Allam B (2010) Identification and molecular characterization of a mucosal lectin (MeML) from the blue mussel *Mytilus edulis* and its potential role in particle capture. *Comp Biochem Physiol A Mol Integr Physiol* **156**, 495–501.
28 Romero A, Dios S, Poisa-Beiro L, Costa MM, Posada D, Figueras A & Novoa B (2011) Individual sequence variability and functional activities of fibrinogen-related proteins (FREPs) in the Mediterranean mussel (*Mytilus galloprovincialis*) suggest ancient and complex immune recognition models in invertebrates. *Dev Comp Immunol* **35**, 334–344.
29 Gerdol M, Fujii Y, Hasan I, Koike T, Shimojo S, Spazzali F, Yamamoto K, Ozeki Y, Pallavicini A & Fujita H (2017) The purplish bifurcate mussel *Mytilisepta virgata* gene expression atlas reveals a remarkable tissue functional specialization. *BMC Genom* **18**, 590.
30 Ishii-Karakasa I, Iwase H & Hotta K (1997) Structural determination of the O-linked sialyl oligosaccharides liberated from fetuin with endo-alpha-N-acetylgalactosaminidase-S by HPLC analysis and 600-MHz 1H-NMR spectroscopy. *Eur J Biochem* **247**, 709–715.
31 Edgar RC (2004) MUSCLE: multiple sequence alignment with high accuracy and high throughput. *Nucleic Acids Res* **32**, 1792–1797.
32 Murgarella M, Puiu D, Novoa B, Figueras A, Posada D & Canchaya C (2016) A first insight into the genome of the filter-feeder mussel *Mytilus galloprovincialis*. *PLoS ONE* **11**, e0151561.
33 WoRMS Editorial Board (2019) World register of marine species. http://www.marinespecies.org VLIZ (The Flanders Marine Institute) accessed 22nd Oct 2019.
34 Buck F, Luth C, Strupat K & Bretting H (1992) Comparative investigations on the amino-acid sequences of different isolectins from the sponge *Axinella polypoides* (Schmidt). *Biochim Biophys Acta* **1159**, 1–8.
35 Hirabayashi J, Dutta SK & Kasai K (1998) Novel galactose-binding proteins in Annelida. Characterization of 29-kDa tandem repeat-type lectins from the earthworm *Lumbricus terrestris*. *J Biol Chem* **273**, 14450–14460.
36 Uchida T, Yamasaki T, Eto S, Sugawara H, Kurisu G, Nakagawa A, Kusunoki M & Hatakeyama T (2004) Crystal structure of the hemolytic lectin CEL-III isolated from the marine invertebrate *Cucumaria echinata*: implications of domain structure for its membrane pore-formation mechanism. *J Biol Chem* **279**, 37133–37141.
37 Liao JH, Chien CT, Wu HY, Huang KF, Wang I, Ho MR, Tu IF, Lee IM, Li W, Shih YL *et al.* (2016) A multivalent marine lectin from *Crenomytilus grayanus* possesses anti-cancer activity through recognizing globotriose Gb3. *J Am Chem Soc* **138**, 4787–4795.
38 Worstell NC, Krishnan P, Weatherston JD & Wu HJ (2016) Binding cooperativity matters: A GM1-like ganglioside-cholera toxin B subunit binding study using a nanocube-based lipid bilayer array. *PLoS ONE* **11**, e0153265.
39 Koga M, Gilbert M, Li J & Yuki N (2015) Complex of GM1- and GD1a-like lipo-oligosaccharide mimics GM1b, inducing anti-GM1b antibodies. *PLoS ONE* **10**, e0124004.
40 Nishikado H, Mukai K, Kawano Y, Minegishi Y & Karasuyama H (2011) NK cell-depleting anti-asialo GM1 antibody exhibits a lethal off-target effect on basophils in vivo. *J Immunol* **186**, 5766–5771.
41 Lou YW, Wang PY, Yeh SC, Chuang PK, Li ST, Wu CY, Khoo KH, Hsiao M, Hsu TL & Wong CH (2014) Stage-specific embryonic antigen-4 as a potential therapeutic target in glioblastoma multiforme and other cancers. *Proc Natl Acad Sci USA* **111**, 2482–2487.
42 Bovi M, Cenci L, Perduca M, Capaldi S, Carrizo ME, Civiero L, Chiarelli LR, Galliano M & Monaco HL (2013) BEL β-trefoil: a novel lectin with antineoplastic properties in king bolete (*Boletus edulis*) mushrooms. *Glycobiology* **23**, 578–592.
43 Pohleven J, Renko M, Magister Š, Smith DF, Künzler M, Štrukelj B, Turk D, Kos J & Sabotič J (2012) Bivalent carbohydrate binding is required for biological activity of *Clitocybe nebularis* lectin (CNL), the N, N'-diacetyllactosediamine (GalNAcβ1-4GlcNAc, LacdiNAc)-specific lectin from basidiomycete *C. nebularis*. *J Biol Chem* **287**, 10602–10612.
44 Hasan I, Sugawara S, Fujii Y, Koide Y, Terada D, Iimura N, Fujiwara T, Takahashi KG, Kojima N, Rajia S *et al.* (2015) MytiLec, a mussel R-type lectin,

interacts with surface glycan Gb3 on Burkitt's lymphoma cells to trigger apoptosis through multiple pathways. *Mar Drugs* **13**, 7377–7389.
45 Chernikov OV, Wong WT, Li LH, Chikalovets IV, Molchanova VI, Wu SH, Liao JH & Hua KF (2017) A GalNAc/Gal-specific lectin from the sea mussel *Crenomytilus grayanus* modulates immune response in macrophages and in mice. *Sci Rep* **7**, 6315.
46 Chikalovets IV, Chernikov OV, Pivkin MV, Molchanova VI, Litovchenko AP, Li W & Lukyanov PA (2015) A lectin with antifungal activity from the mussel *Crenomytilus grayanus*. *Fish Shellfish Immunol* **42**, 503–507.
47 Patry RT, Stahl M, Perez-Munoz ME, Nothaft H, Wenzel CQ, Sacher JC, Coros C, Walter J, Vallance BA & Szymanski CM (2019) Bacterial AB_5 toxins inhibit the growth of gut bacteria by targeting ganglioside-like glycoconjugates. *Nat Commun* **10**, 1390.
48 Zhu F, Li D & Chen K (2019) Structures and functions of invertebrate glycosylation. *Open Biol* **9**, 180232.
49 Itonori S & Sugita M (2005) Diversity of oligosaccharide structures of glycosphingolipids in invertebrates. *Trends Glycosci Glycotechnol* **17**, 15–25.
50 Arriagada G, Metzger MJ, Muttray AF, Sherry J, Reinisch C, Street C, Lipkin WI & Goff SP (2014) Activation of transcription and retrotransposition of a novel retroelement, Steamer, in neoplastic hemocytes of the mollusk *Mya arenaria*. *Proc Natl Acad Sci USA* **111**, 14175–14180.
51 Metzger MJ, Villalba A, Carballal MJ, Iglesias D, Sherry J, Reinisch C, Muttray AF, Baldwin SA & Goff SP (2016) Widespread transmission of independent cancer lineages within multiple bivalve species. *Nature* **534**, 705–709.
52 Yonemitsu MA, Giersch RM, Polo-Prieto M, Hammel M, Simon A, Cremonte F, Avilés FT, Merino-Véliz N, Burioli EA, Muttray AF *et al.* (2019) A single clonal lineage of transmissible cancer identified in two marine mussel species in South America and Europe. *elife* **8**, e47788.
53 Sugita M, Nakae H, Yamamura T, Takamiya Y, Itasaka O & Hori T (1985) The occurrence of glycosphingolipids containing mannose in the sea-water bivalve, *Meretrix lusoria* (Hamaguri). *J Biochem* **98**, 27–34.
54 Araki S, Yamada S, Abe S, Waki H, Kon K, Itonori S, Sugita M & Ando S (2001) Characterization of a novel triphosphonooctaosylceramide from the eggs of the sea hare, *Aplysia kurodai*. *J Biochem* **129**, 93–100.
55 Gourdine JP, Cioci G, Miguet L, Unverzagt C, Silva DV, Varrot A, Gautier C, Smith-Ravin EJ & Imberty A (2008) High affinity interaction between a bivalve C-type lectin and a biantennary complex-type *N*-glycan revealed by crystallography and microcalorimetry. *J Biol Chem* **283**, 30112–30120.
56 Smith PK, Krohn RI, Hermanson GT, Mallia AK, Gartner FH, Provenzano MD, Fujimoto EK, Goeke NM, Olson BJ & Klenk DC (1985) Measurement of protein using bicinchoninic acid. *Anal Biochem* **150**, 76–85.
57 Wiechelman KJ, Braun RD & Fitzpatrick JD (1988) Investigation of the bicinchoninic acid protein assay: identification of the groups responsible for color formation. *Anal Biochem* **75**, 231–237.
58 Laemmli UK (1970) Cleavage of structural proteins during the assembly of the head of bacteriophage T4. *Nature* **227**, 680–685.
59 Schuck P, Perugini MA, Gonzales NR, Howlett GJ & Schubert D (2002) Size-distribution analysis of proteins by analytical ultracentrifugation: strategies and application to model systems. *Biophys J* **82**, 1096–1111.
60 Laue T, Shah B, Ridgeway TM & Pelletier SL (1992) Computer-aided interpretation of analytical sedimentation data for proteins. In Analytical Ultracentrifugation in Biochemistry and Polymer Science (Harding SE, Rowe AJ & Horton JC, eds), pp. 90–125. Royal Society of Chemistry, Cambridge, UK.
61 Usami Y, Fujimura Y, Suzuki M, Ozeki Y, Nishio K, Fukui H & Titani K (1993) Primary structure of two-chain botrocetin, a von Willebrand factor modulator purified from the venom of *Bothrops jararaca*. *Proc Natl Acad Sci USA* **90**, 928–932.
62 Tateno H, Mori A, Uchiyama N, Yabe R, Iwaki J, Shikanai T, Angata T, Narimatsu H & Hirabayashi J (2008) Glycoconjugate microarray based on an evanescent-field fluorescence-assisted detection principle for investigation of glycan-binding proteins. *Glycobiology* **18**, 789–798.
63 Goldman A, Ursitti JA, Mozdzanowski J & Speicher DW (2015) Electroblotting from polyacrylamide gels. *Curr Protoc Protein Sci* **82**, 1–16.
64 Fujii Y, Fujiwara T, Koide Y, Hasan I, Sugawara S, Rajia S, Kawsar SM, Yamamoto D, Araki D, Kanaly RA *et al.* (2017) Internalization of a novel, huge lectin from *Ibacus novemdentatus* (slipper lobster) induces apoptosis of mammalian cancer cells. *Glycoconj J* **34**, 85–94.

Supporting information

Additional supporting information may be found online in the Supporting Information section at the end of the article.

Fig. S1. Calcium-dependent hemagglutination and *de novo* sequence of SeviL.

Fig. S2. Pairwise sequence comparison of SeviL, and schematic organization of *M. galloprovincialis* locus encoding of SeviL-like lectin.
Fig. S3. Glycan-array analysis.
Fig. S4. A homology model of SeviL.
Table S1. List of 52 oligosaccharides used for the glycan-array analysis.

＜薬品物理化学部門＞
教授　山口 芳樹
講師　真鍋 法義
助手　大野 詩歩

糖鎖構造解析のための技術基盤の構築

タンパク質・脂質に結合している糖鎖は，様々な生理的機能を発現していると考えられており，これまで多くの研究者が様々なアプローチにより，その機能的側面を明らかにしてきている．糖鎖の機能の多くは，糖結合タンパク質であるレクチン受容体との分子間相互作用を介して発揮されている．例えば，細胞間の特異的な相互作用や病原菌・ウイルスの感染においても糖鎖-レクチン相互作用が関与している．我々は構造生物学の立場に基づき，糖鎖の機能を明らかにするためには，糖鎖の立体構造上の特徴を理解し，レクチン・抗体などによる糖鎖の認識の構造的基礎を理解することが必要であると考えて研究を進めている．2019 年より分子生体膜研究所の一員となり，今後は糖鎖構造生物学のプロフェッショナルとして専門性を一層深めるとともに，既成概念に囚われずに新しい分野に挑戦する．本年度はこれまでの研究成果のまとめを行うとともに，糖鎖構造解析の技術基盤の構築および計算化学・インフォマティクスの基礎構築を目指した．

I.　抗体の糖鎖改変と抗体-薬物複合体の作製

免疫グロブリンは，糖鎖の機能が最も研究された糖タンパク質の一つといっても過言ではない．近年，バイオ医薬品・抗体-薬物複合体としての抗体の利用が増加しており，糖鎖の構造とその機能制御にますます注目が集まっている．抗体に結合している糖鎖がその機能に及ぼす影響について，最近の報告をまとめ，特に立体構造の観点から議論して総説とした(1)．また，抗体の糖鎖改変技術や分析技術が進展したことも抗体の糖鎖の構造機能相関の研究を後押ししており，抗体糖鎖改変の応用も可能になっている．現在様々なエンド-β-*N*-アセチルグルコサミニダーゼ変異体が糖鎖のリモデリングのために開発されている．一方で，糖鎖活性中間体とリジン側鎖アミノ基の間での酵素非依存的な副反応が存在することも報告されている．本共同研究では，副反応の詳細な解析を行い，副反応の抑制とグリコシル化反応の効率最大化を目指した．わずかに酸性の条件下で段階的に糖鎖活性中間体を反応液中に添加することにより副反応を抑制できることを見出した．また最適化された条件を用いて，抗体-薬物複合体（ADC）の合成に応用した．その結果，抗体-薬物比が 4 に制御された均一な ADC の作成に成功した(2)．実際ハーセプチンを基にして作成した ADC は，HER2 高発現細胞に対して顕著な細胞毒性を示した．また，本共同研究で得られた ADC に関する知見を中心に総説と

してまとめ報告した(3,4).

II. C 型レクチン受容体の構造と機能に関する研究

レクチンは糖鎖を特異的に認識する分子として幅広く機能している．レクチンは単糖に対しての親和性は低く mM 程度の解離定数であるが，多くのレクチンはオリゴマー化により，複数の結合部位を提示することにより見かけの親和性を向上させている．レクチンの親和性向上のストラテジーは巧妙であり，個々のレクチンに特徴がある．レクチンによる糖鎖認識様式を解明することは，糖鎖のもつ生理機能の解明につながり，ひいてはレクチンをターゲットとした創薬に貢献する．その点を踏まえつつ，レクチンの糖鎖認識の物理化学的な側面を総説にまとめた(5).

我々はこれまで主に C 型レクチン受容体を中心に構造生物学研究を行ってきた．特に C 型レクチン受容体の共通のフォールドから糖鎖結合の多様性はどのように生み出されるかという問題を設定して構造解析を行ってきた．構造解析を通じて得た知見および他グループの報告も引用しながら，C 型レクチン受容体の糖鎖認識についての現状の理解を総説としてまとめた(6).

C 型レクチン受容体は糖鎖結合に Ca^{2+}イオンが必須であるが，共通のフォールドを持つにも拘わらず，Ca^{2+}イオンを要求しないレクチンも存在する．C 型レクチン様受容体と呼ばれ，Dectin-1 もそのファミリーの一員である．Dectin-1 は β グルカンの受容体として自然免疫システムとしての役割を果たしている．国際共同研究により，Dectin-1 は β グルカンとは異なる種類のリガンドとも結合し得ることを示した(7).

III. NMR 法による糖鎖の構造解析技術の構築

NMR 法は，糖鎖の化学構造決定，特にアノマーの決定・糖結合部位の同定において威力を発揮する．これは他の方法では同定が著しく困難であり、NMR 法による迅速かつ確実な解析が重要かつユニークな位置を占める．本年度は，糖脂質糖鎖やグリケーション産物の構造解析結果を以下報告することができた.

リポ多糖（LPS）は，Toll 様受容体（TLR）4-MD-2 複合体を介して宿主の自然免疫系を刺激するグラム陰性細菌細胞表面の成分である．ロドバクター属の LPS はエンドトキシン活性を持たず，逆にアンアゴニストとして機能することが示されている．本研究では IL-8 の産生を促し，逆に IL-6 の産生を抑制する働きをもつ *Rhodobacter azotoformans* のリポオリゴ糖（LOS）画分に注目して構造解析を行った． 詳細な NMR および質量分析の共同研究の結果，通常見出されるヘプトースを含まず，グルクロン酸を含む短い糖鎖からなる新規 LOS の構造を決定した(8).

Campylobacter jejuni のリポオリゴ糖は，哺乳類ガングリオシド GM1 との構

造類似性からギランバレー症候群を引き起こすことが提唱されている．本論文では，*Campylobacter jejuni* のリポオリゴ糖鎖のコア部分の化学合成に成功した．各種多次元 NMR 法を実施し，オリゴ糖鎖中のグリコシド結合の決定を行い，共同研究として本論文に貢献した．特に構造決定の際に唯一存在する OH 基プロトンを同定して帰属の拠点とすることを工夫した(9).

フルクトースはタンパク質のリジン側鎖と非酵素的に反応して AGE 産物となる．今回開発された抗体と反応性を有する AGE に対して NMR 解析を行った結果，リジンの側鎖 ε 位 NH がグルコースの 2 位と反応したグルコースリジンであることを明らかにし，共同研究として本論文に貢献した(10).

NMR 法は，糖鎖の化学構造決定のみならず，立体構造・運動性・相互作用に関する原子レベルの情報をもたらす．糖鎖の新機能を開拓するためには非天然型糖鎖の合成も選択肢の一つである．本共同研究ではシアル酸のセレノグリコシドを対象とした．合成によりセレン含有糖鎖は，^{77}Se-NMR により解析可能となる．実際，本セレノ糖鎖をタンパク質との相互作用解析に応用したところ，シアル酸結合タンパク質の種類によって結合プロファイルが異なることを ^{77}Se-NMR により明らかにした(11)．現在は，糖鎖・糖ペプチドの NMR 信号の帰属を進めており，今後は結合分子との相互作用解析を行う予定である．

IV.　計算化学・データベースの基盤構築

糖鎖の立体構造･ダイナミクスの解析には NMR 法などの実験的手法に加えて，分子動力学計算などの計算化学的手法が必要になる．我々は以前に，糖鎖の準安定構造をレクチンに結合されることにより実験的に捉えることを行ってきた．本共同研究では，分岐型糖鎖の分子動力学計算を行い，糖鎖構造の違いがダイナミクスに与える影響を調べた．糖鎖構造の違いにより，2 本鎖糖鎖の各分枝のダイナミクスが異なること，またその結果，糖転移酵素の基質へのなりやすさに影響することを提示することができた(12)．現在は非典型糖であるリビトールの構造特性について，計算と実験の両面から詳しく調査している．

またデータベースから，糖鎖立体構造・相互作用の法則性を見出すことを進めている(13)．現在は抗糖鎖抗体の立体構造データを集積するための方法を検討しており，データの分類を進めている段階である．合わせて抗体の超可変領域を含む Fv 領域のモデリング手法の検討を行っている。

V.　その他

糖鎖構造の制御メカニズムや糖鎖の関わる遺伝性疾患の原因を明らかにするためには、糖鎖構造を調べるとともに、糖転移酵素など糖鎖生合成に関わる一連の蛋白質の立体構造情報が必須である。加えてアミノ酸置換がその活性や立体構造に及ぼす影響を予測・調査することも重要になる。現在、共同研究により糖鎖関

連遺伝子の変異がそのタンパク質の活性や安定性に及ぼす影響を系統的に調べるための方法を検討中である。本年度は、糖鎖の構造解析技術とその周辺で関連する技術について将来の展望とともにまとめて報告をした(14-17).

＜発表論文＞

1. Yamaguchi, Y., and Barb, A. W. (2020) A synopsis of recent developments defining how N-glycosylation impacts immunoglobulin G structure and function. Glycobiology, 30, 214-225
2. Manabe, S., Yamaguchi, Y., Matsumoto, K., Fuchigami, H., Kawase, T., Hirose, K., Mitani, A., Sumiyoshi, W., Kinoshita, T., Abe, J., Yasunaga, M., Matsumura, Y., and Ito, Y. (2019) Characterization of antibody products obtained through enzymatic and nonenzymatic glycosylation reactions with a glycan oxazoline and preparation of a homogeneous antibody-drug conjugate via Fc N-glycan. Bioconjug. Chem. 30, 1343-1355
3. 眞鍋史乃，山口芳樹. (2019) ADC 開発におけるリンカー設計の意義. がん分子標的治療 17, 11-15
4. 眞鍋史乃，山口芳樹. (2019) 糖鎖改変による抗体―薬物複合体合成. 月刊ファインケミカル 48, 51-59
5. 山口芳樹. (2019) レクチンの糖鎖認識とは. 医学のあゆみ 269, 750-755
6. Nagae, M., and Yamaguchi, Y. (2019) Structural aspects of carbohydrate recognition mechanisms of C-type lectins. Curr. Top. Microbiol. Immunol., 1-30
7. Manabe, Y., Marchetti, R., Takakura, Y., Nagasaki, M., Nihei, W., Takebe, T., Tanaka, K., Kabayama, K., Chiodo, F., Hanashima, S., Kamada, Y., Miyoshi, E., Dulal, H. P., Yamaguchi, Y., Adachi, Y., Ohno, N., Tanaka, H., Silipo, A., Fukase, K., and Molinaro, A. (2019) The core fucose on an IgG antibody is an endogenous ligand of Dectin-1. Angew. Chem. Int. Ed. 58, 18697-18702
8. Kanie, Y., Yamaguchi, Y., Hayashi, A., Uzawa, J., Hatakeyama, M., Hidaka, Y., Toda, N., Nakamura, S., and Kanie, O. (2019) Structural analysis of a novel lipooligosaccharide (LOS) from Rhodobacter azotoformans. Carbohydr. Res. 473, 104-114
9. Yoshida, F., Yoshinaka, H., Tanaka, H., Hanashima, S., Yamaguchi, Y., Ishihara, M., Saburomaru, M., Kato, Y., Saito, R., Ando, H., Kiso, M., Imamura, A., and Ishida, H. (2019) Synthesis of the core oligosaccharides of lipooligosaccharides from Campylobacter jejuni: A putative cause of Guillain-Barre syndrome. Chem. Eur. J. 25, 796-805
10. Ohno, R., Ichimaru, K., Tanaka, S., Sugawa, H., Katsuta, N., Sakake, S., Tominaga, Y., Ban, I., Shirakawa, J., Yamaguchi, Y., Ito, E., Taniguchi, N., and Nagai, R. (2019) Glucoselysine is derived from fructose and accumulates in the eye lens of diabetic rats. J. Biol. Chem. 294, 17326-17338
11. Suzuki, T., Hayashi, C., Komura, N., Tamai, R., Uzawa, J., Ogawa, J., Tanaka, H. N.,

Imamura, A., Ishida, H., Kiso, M., Yamaguchi, Y., and Ando, H. (2019) Synthesis and glycan-protein interaction studies of Se-sialosides by 77Se NMR. Org. Lett. 21, 6393-6396

12. Nakano, M., Mishra, S. K., Tokoro, Y., Sato, K., Nakajima, K., Yamaguchi, Y., Taniguchi, N., and Kizuka, Y. (2019) Bisecting GlcNAc is a general suppressor of terminal modification of N-glycan. Mol. Cell. Proteomics 18, 2044-2057
13. Yamaguchi, Y. (2019) A struggle of the last eleven years after getting JSCR award. Trends Glycosci. Glycotechnol. 31, SE50-SE52, SJ50-SJ52
14. Yamaguchi, Y. (2019) Ion mobility-mass spectrometry (IM-MS). Glycoscience: Basic Science to Application, pp.6-7
15. Yamaguchi, Y. (2019) Conformational analysis of glycans. Glycoscience: Basic Science to Application, pp.40-41
16. Yamaguchi, Y. (2019) Computational science (supercomputer) and AI (artificial intelligence). Glycoscience: Basic Science to Application, pp.42-43
17. Yamaguchi, Y. (2019) Core technologies for elucidating the role of glycans in disease. Glycoscience: Basic Science to Application, pp.265-266

＜学会発表＞

・**Asp-Asp モチーフにおける非酵素反応**

大野 詩歩

第 7 回物理・分析系若手研究者セミナー，仙台，2019 年 2 月

・**リン酸二水素イオンを触媒とする Asp-Ser 配列からのスクシンイミド生成**

大野 詩歩，真鍋 法義，高橋 央宜

日本薬学会第 139 年会，千葉，2019 年 3 月，演題番号 p.143

・**白内障の病態形成に関与するクリスタリン中 Asp 残基異性化の乳酸による触媒機構～計算化学的・生化学的検討～**

真鍋 法義，佐々木 雅人，田中 大，大野 賢一，大野 詩歩，桐越 亮太，加藤 創，藤村 務，柴田 信之，高橋 央宜

日本薬学会第 139 年会，千葉，2019 年 3 月，要旨集 p.161

・**Solution NMR and docking simulation analysis of interaction between tau aggregates and low-molecular-weight compounds**

Yoshiki Yamaguchi

International Academic Forum on Neuroinflammation and Psychopharmacology, Nantong, China, May 2019, 演題番号 3

・**錠剤観察における走査電子顕微鏡用の広領域断面作製法**

應本 玉恵[a]，淺野 奈津子[a]，朝比奈 俊輔[a]，真鍋 法義

（日本電子株式会社[a]）

日本薬剤学会第 34 年会，富山，2019 年 5 月，要旨集 p.42

・**錠剤成分の分布分析に用いる断面試料の作製とその分析法**

真鍋 法義，應本 玉恵[a]，淺野 奈津子[a]，長谷部 祐治[a]，朝比奈 俊輔[a]
（日本電子株式会社[a]）
日本薬剤学会第 34 年会，富山，2019 年 5 月，要旨集 p.65

・**糖鎖の構造解析とその機能の解明**
山口 芳樹
日本臓器製薬（株）特別講演会，兵庫，2019 年 7 月，演題番号 2

・**水溶液中における糖脂質の脱ミセル化と NMR 法による性状解析**
山口 芳樹
第 38 回日本糖質学会年会，名古屋，2019 年 8 月，演題番号 WS-04

・**糖鎖構造の多様性とその生物学的意義の探求**
山口 芳樹
第 13 回東北糖鎖研究会，新潟，2019 年 9 月，演題番号 S-1

・**グルコシルセラミド分解酵素による新規脳内ステロール代謝物・ステロール配糖体の代謝制御**
秋山 央子[a]，井手 三津子[b]，中西 悦郎[c]，上村 紀仁[c]，山口 芳樹，Peter Greimel[d]，上口 裕之[a]，高橋 良輔[c]，平林 義雄[b]
(理化学研究所 脳神経科学研究センター 神経細胞動態研究チーム[a]，.理化学研究所 佐甲細胞情報研究室[b]，京都大学大学院 医学研究科 臨床神経学[c]，理化学研究所 脳神経科学研究センター 細胞機能探索技術研究チーム[d])
第 92 回日本生化学大会，新潟，2019 年 9 月，演題番号 1P-011 (1T10a-06)

・**Solution NMR and docking simulation analysis of interaction between tau aggregates and small chemicals**
Yoshiki Yamaguchi
Asian Pacific Prion Symposium2019 (APPS2019), Wako, October 2019, 演題番号 O-3

・**糖鎖プローブを活用した構造解析**
山口 芳樹
Pioneering Project: Chemical Probe（生命現象探索分子）第二回合同合宿セミナー，比企，2019 年 10 月，演題番号 OP-3

・**計算化学によるリビトールのコンフォメーション空間の解析**
大野 詩歩，真鍋 法義，山口 芳樹
第 58 回日本薬学会東北支部大会，仙台，2019 年 10 月，演題番号 PE-08

・**糖鎖の高次構造と相互作用原理の解明に向けて**
山口 芳樹
第 17 回糖鎖科学コンソーシアムシンポジウム，京都，2019 年 10 月，要旨集 p.14

・**完全重水素化シクロデキストリンの化学酵素合成と糖脂質の NMR 解析**

山口 芳樹[a], 眞鍋 史乃[a], Peter Greimel[a], 伊藤 幸成[a]
（理化学研究所[a]）
第 58 回 NMR 討論会・SEST2019 合同シンポジウム，川崎，2019 年 11 月，演題番号 P41

・**残余双極子カップリング測定における配向力、温度安定性、有機溶媒耐性を兼ね備えた新規配向剤**
内田 紀之[a], 山口 芳樹, 海老名 保男[b], 佐々木 高義[b], 石田 康博[a]
（理化学研究所[a], 物質・材料研究機構[b]）
第 58 回 NMR 討論会・SEST2019 合同シンポジウム，川崎，2019 年 11 月，演題番号 L3-3

・**NMR structural analysis of glycolipid in aqueous solution**
Yoshiki Yamaguchi[a], Shino Manabe[a], Peter Greimel[a], Yukishige Ito[a]
（RIKEN[a]）
11th ACGG Conference, Busan, Korea, November 2019, 演題番号 SS 8-3

・**糖鎖構造解析の基礎とその実際**
山口 芳樹
第 410 回 CBI 学会講演会，田町，2019 年 11 月，演題番号 2

・**An NMR approach to investigate glycolipid structure**
Yoshiki Yamaguchi
TMPU-AS Joint Glycoscience Symposium, Taiwan

Glycobiology, 2020, vol. 30, no. 4, 214–225
doi: 10.1093/glycob/cwz068
Advance Access Publication Date: 10 September 2019
Review

Review

A synopsis of recent developments defining how N-glycosylation impacts immunoglobulin G structure and function

Yoshiki Yamaguchi[2] **and Adam W Barb**[3,1]

[2]Tohoku Medical and Pharmaceutical University, Sendai, Japan, 981-8558 and [3]Department of Biochemistry and Molecular Biology and Complex Carbohydrate Research Center, University of Georgia, Athens, Georgia, 30602

[1]To whom correspondence should be addressed: Tel: 706-542-1773; Fax: 706-542-1718; e-mail: abarb@uga.edu

Received 22 April 2019; Revised 26 July 2019; Editorial Decision 21 August 2019; Accepted 21 August 2019

Abstract

Therapeutic monoclonal antibodies (mAbs) are the fastest growing group of drugs with 11 new antibodies or antibody-drug conjugates approved by the Food and Drug Administration in 2018. Many mAbs require effector function for efficacy, including antibody-dependent cell-mediated cytotoxicity triggered following contact of an immunoglobulin G (IgG)-coated particle with activating crystallizable fragment (Fc) γ receptors (FcγRs) expressed by leukocytes. Interactions between IgG1 and the FcγRs require post-translational modification of the Fc with an asparagine-linked carbohydrate (N-glycan). Though the structure of IgG1 Fc and the role of Fc N-glycan composition on disease were known for decades, the underlying mechanism of how the N-glycan affected FcγR binding was not defined until recently. This review will describe the current understanding of how N-glycosylation impacts the structure and function of the IgG1 Fc and describe new techniques that are poised to provide the next critical breakthroughs.

Key words: antibody, Fc gamma receptor, immunoglobulin G, N-glycosylation

Introduction

Monoclonal antibodies (mAbs) are powerful drugs for cancers, autoimmune disorders and infection in addition to many other diseases. Positive drug attributes including high specificity and tolerance promote the development of mAbs for a wide variety of targets. Antibodies are complex molecules with multiple polypeptide chains and post-translational modifications; human immunoglobulin G1 (IgG1) is a 150 kDa heterotetramer with two conserved Asn-linked carbohydrate chains (N-glycans) and 16 disulfide bonds (Figure 1) (Liu and May 2012). Furthermore, proper 3D structure is critical for mAb function and an important quality attribute concerning commercial mAb production (Berkowitz et al. 2012). Thus, the development, evaluation, validation and quality control of mAbs as drugs differs substantially from small molecule therapeutics that previously represented the pharmaceutical industry's primary products.

Complex molecules have a long history in human health that begins with undefined mixtures used as vaccines and arriving at a seminal moment in 1922 with the administration of a bovine pancreatic extract to successfully treat a young male diabetic (Bliss 2007). Each basic discovery, from defining insulin as a protein to sequencing the polypeptide chains to identifying residues that promote stability, has led to the improvement of human health through enhancing insulin formulations, production and from protein engineering (Brange et al. 1991). The development of modern insulin variants informs the future development of IgG analogs as therapeutics. MAbs are predominantly built on an IgG scaffold though atomic-level details governing critical interactions with the immune system remain undefined. Based on the recent development of mAbs and protein therapeutics in general, it is clear that basic descriptions of IgG structure/function relationships will drive development of the next generation of drugs.

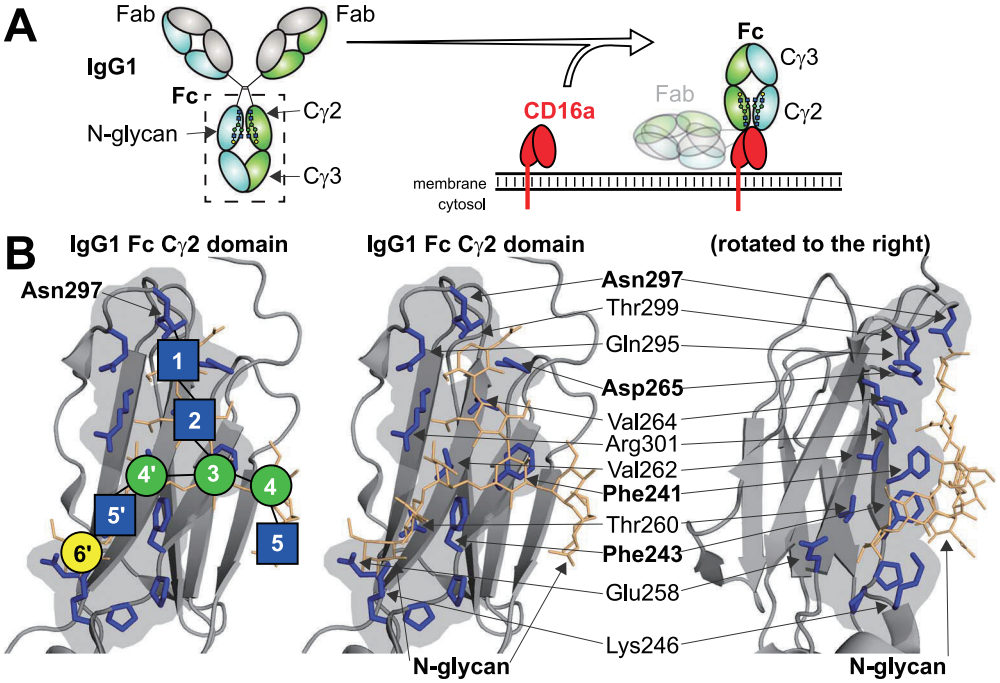

Figure 1. The IgG1 Fc N-glycan is essential for binding to the Fc γ receptors. (**A**) IgG1 Fc is a heterotetramer consisting of two Fabs and a single Fc that binds receptors. (**B**) The Fc N-glycan forms an interface with Cγ2 residues through noncovalent intramolecular interactions. The volume of interacting residues is shown with a *gray* background, and individual N-glycan and protein residues are highlighted. Blue squares represent N-acetylglucosamine residues; green circles, mannose; and yellow circles, galactose.

Two heavy polypeptide chains and two light chains form an IgG heterotetramer (Figure 1). IgG binds to a target through specifically optimized loops contained in the antigen binding fragments (Fabs). The C-terminal halves of the heavy chains form the crystallizable fragment (Fc) that binds various surface-borne and soluble receptors. IgG Fc contains an N-glycan at Asn297 that is required for proper interactions with Fc γ receptors (FcγRs) and the therapeutic efficacy of mAbs that elicit antibody-dependent cell-mediated cytotoxicity (Nose and Wigzell 1983; Guilleréy et al. 2016). Humans express as many as five activating FcγRs including the high-affinity FcγRI (CD64) and the low-affinity activating receptors FcγRIIa, FcγRIIc (expressed by ~20% of individuals (Ernst et al. 2002; Breunis et al. 2008)), FcγRIIIa and FcγRIIIb (CD32a, CD32c, CD16a and CD16b, respectively). Humans also express a single inhibitory receptor FcγRIIb (CD32b). IgG also binds the C1q component of complement to elicit complement-dependent cytotoxicity. Though C1q binding requires oligomerized IgG and binds to a different Fc surface than the FcγRs (Ugurlar et al. 2018), there are reports that N-glycan composition affects efficacy (Peschke et al. 2017). The neonatal Fc receptor and TRIM21 also bind IgG Fc and binding may be influenced by N-glycan composition (James et al. 2007; Jennewein et al. 2019). A few groups provided data that indicated DC-SIGN and CD23 bind sialylated IgG (reviewed in Pincetic et al. 2014), though recent results cast these conclusions into doubt (Temming et al. 2019).

N-glycan composition impacts mAb recognition, and the composition of serum IgG shows strong correlations to disease. The predominant structure found on serum IgG1 is a complex-type, core fucosylated, biantennary N-glycan (Figure 2). Modifications at the non-reducing termini can add one or two galactose residues that each may be modified with one N-acetylneuraminic acid residue. A correlation between the degree of galactose modification on IgG1 and rheumatoid arthritis provided the first indication that Fc N-glycosylation may impact antibody structure and function (Parekh et al. 1985). More recently, strong connections between the addition of a core fucose residue to autoimmune disorders among many IgG studies in serum and in vitro demonstrated that IgG N-glycan composition is a crucial factor in human health and disease (Figure 2, residue "0") (Shields et al. 2002; Lauc et al. 2013; Chung et al. 2014; Kapur et al. 2014; Mahan et al. 2016; Sonneveld et al. 2017; Clerc et al. 2018; Doherty et al. 2018).

Surprisingly, the first atomic-resolution structure showed no direct contact between the Fc N-glycans and the FcγR (Sondermann et al. 2000). Later x-ray crystallography studies revealed small differences in IgG Fc quaternary structure, and solution nuclear magnetic resonance (NMR) spectroscopy showed subtle changes in Fc structure and FcγR binding that correlated with N-glycan composition (Krapp 2003; Yamaguchi et al. 2006). These results did not reveal how N-glycan composition impacted receptor affinity, a fact complicated by the observation that the Fc N-glycans appeared immobilized through contacts with the polypeptide (Huber et al. 1976). However, this interpretation was challenged by NMR data showing that polypeptide contacts only partially restricted motion of the N-glycan under more physiological conditions and led to the hypothesis that the N-glycan modulated receptor binding through an indirect mechanism (Barb and Prestegard 2011).

Here we will review the most recent developments toward understanding how N-glycan composition impacts IgG1 Fc structure and receptor binding. An article that thoroughly covers this entire history would prove too expansive for this format. The understanding of IgG Fc structure and function has changed dramatically in recent years, and recent studies will form the focus of this review.

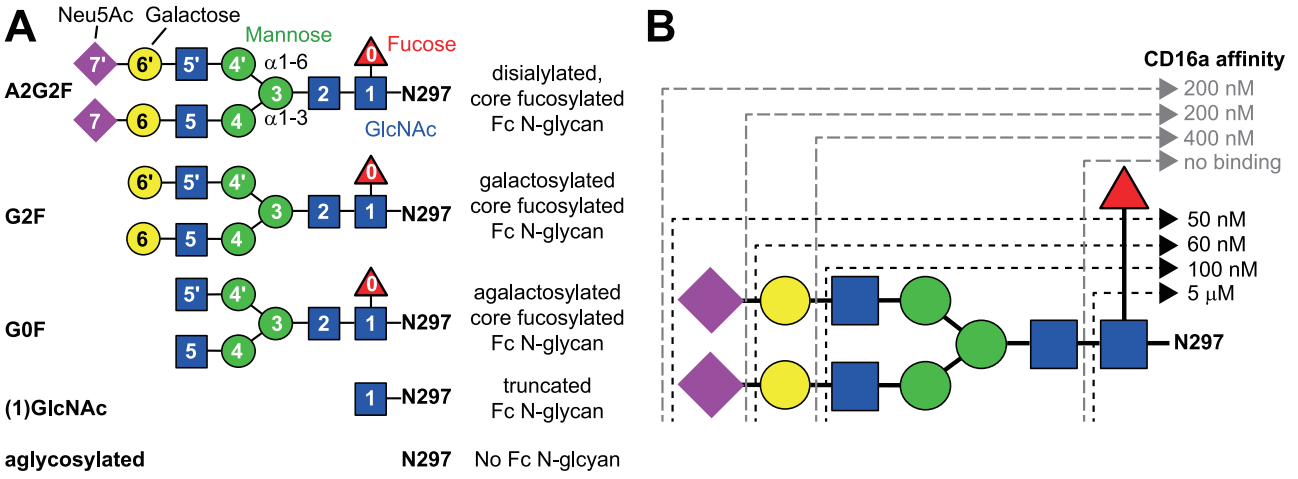

Figure 2. The different Fc N-glycan compositions provide Fc with variable affinity for CD16a. (**A**) N-glycan compositions as discussed in the text; note the abbreviated identifier to the left of the cartoon figures. (**B**) IgG1 Fc with each different N-glycan binds with different affinity to CD16a. These K_D values were adapted directly from (Subedi and Barb 2016) but are consistent with other reports (Yamaguchi et al. 2006; Thomann et al. 2015; Dekkers et al. 2017). GlcNAc, N-acetylglucosamine; Neu5Ac, N-acetylneuraminic acid.

The structure and function of IgG1 Fc is mediated by interactions between the Fc polypeptide and N-glycan residues

IgG1 Fc N-glycan composition impacts FcγR binding. Systematic investigations into the role of Fc N-glycan composition on FcγR binding emerged in the past few years. Though it was known that FcγR binding was sensitive to glycosylation, these recent efforts probed interactions for the entire set of human FcγRs with high sensitivity and a large number of Fc glycoforms. One common feature of these studies is the unique sensitivity of CD16 affinity to Fc N-glycan composition (Thomann et al. 2015; Subedi and Barb 2016; Dekkers et al. 2017). Though CD32 likewise requires Fc N-glycosylation for binding, CD16a and CD16b show a much greater sensitivity to IgG1 Fc N-glycan composition with longer N-glycans promoting tighter interactions (Figure 2B).

The most dramatic affinity differences are due to the addition of a fucose residue to the N-linked GlcNAc residue that reduces affinity for CD16a in vitro (Shields et al. 2002; Shinkawa et al. 2003). Two studies recapitulated the negative impact of core fucosylation on CD16 affinity with a large number of Fc glycoforms, though one study using isolated Fc showed a smaller 4 to 8-fold reduction of binding (Subedi and Barb 2016) compared to another using full length antibodies with a 40-fold reduction (Dekkers et al. 2017). These differences may reflect additional sensitivity of the full-length antibody to Fc N-glycan fucosylation. These studies also showed a moderate benefit of galactosylation (~2-fold) and no consistent measurable impact resulting from sialylation. One study reported only a minimal effect of bisecting N-acetylglucosamine (linked β1–4 to the (3) mannose residue) (Dekkers et al. 2017).

Human IgG1 Fc displaying only a single N-acetylglucosamine residue attached to N297 is produced in situ by the digestion of IgG1 containing an afucosylated N-glycan by EndoS ((1)GlcNAc-Fc; Figure 2B) (Collin and Olsen 2001). Surprisingly, this Fc glycoform binds to CD16a, though with reduced affinity compared to Fc with a larger N-glycan (Subedi and Barb 2015; Okbazghi et al. 2016). Furthermore, human IgG trimmed to the single GlcNAc residue is capable of clearing B cells in a mouse xenograft model (Kao, et al. 2015). These results may be explained by the identification of the first N-glycan residue as contributing a greater degree of stability than any other residue in the glycan (Hanson et al. 2009). The structural relationship of this unique glycoform and the IgG1 Fc structure will be discussed below.

Interactions at the Fc N-glycan/polypeptide interface stabilize N-glycan motion. Following the definition of how Fc N-glycan composition affects receptor binding and the identification of N-glycan motion, multiple studies investigated N-glycan motion further to probe the relationship between N-glycan composition, motion and receptor binding affinity. An all-atom solvated molecular dynamics study demonstrated that the galactose residue attached to the (α1–6mannose) branch of a complex-type N-glycan on Fc exhibited motion (Frank et al. 2014). These simulations were initialized with the starting coordinates observed by x-ray crystallography and showed the detachment of this glycan branch from the protein surface, further supporting the earlier observation by NMR and revealing how the glycan might deform to accommodate conformational exchange (Barb and Prestegard 2011).

Studies on the motion of the Fc N-glycan with multiple glycoforms in solution show that composition impacts glycan interactions. Measurements of the galactose residues before and after sialylation using NMR spectroscopy showed that the modification slightly stabilized the (α1–6mannose) branch (Barb et al. 2012). A later study investigated the motion of the branch N-acetylglucosamine residues during N-glycan maturation starting with a hybrid $Mannose_5$ + N-acetylglucosamine form and ending with a core-fucosylated, complex type N-glycan with N-acetylglucosamine termini (Barb 2015). These results indicated that each remodeling step increased the contact between polypeptide and N-glycan residues during the remodeling of an oligomannose precursor to a final disialylated complex-type N-glycan and are consistent with previous observations in vitro and in vivo (Butler et al. 2003; Bowden et al. 2012). This result suggests that the αmannose residues on the (α1–6mannose) branch of the oligomannose N-glycan likely form unfavorable contacts with the polypeptide and each subsequent glycosyltransferase reaction exploited different contact surfaces.

Hydrogen-deuterium exchange mass spectrometry (HDX) experiments supported the conclusion that extending the Fc N-glycan increases intramolecular interactions, revealing a reduction in

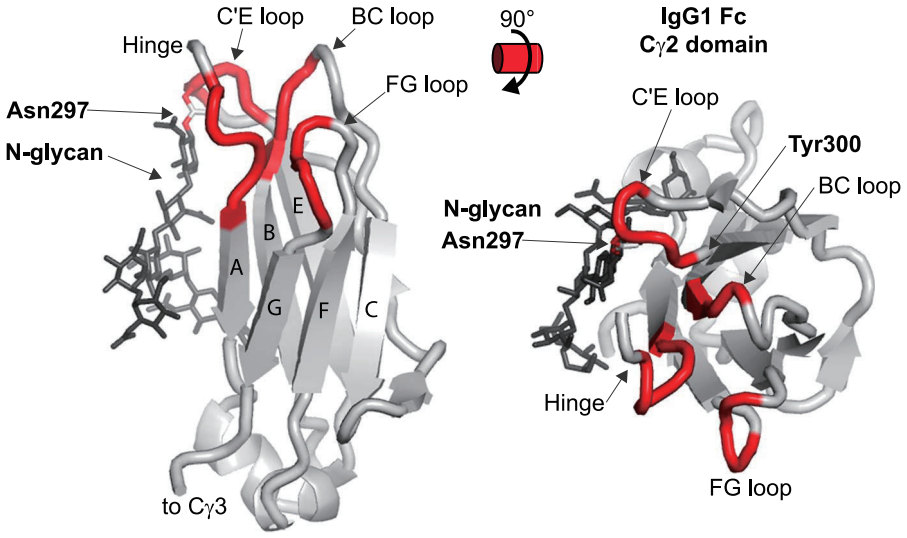

Figure 3. IgG1 Fc Cγ2 domain structure. Residues that are within 5 Å of CD16a are highlighted in red. These contacts are draw for residues that form contacts in either the Fc a or b chain. Strands are labeled with letters.

deuterium uptake in the P245-T256 peptide following galactosylation (Kiyoshi et al. 2018). The galactose residue directly interacts with residues on this peptide, potentially reducing deuterium uptake by occluding solvent. The authors indicate these data represent changes in the Cγ2/Cγ3 domain orientation. A comparable HDX-MS study followed a greater number of N-glycan compositions, including aglycosylated, (1) GlcNAc, $Mannose_5$ and a mixture of $Mannose_8$-$Mannose_{12}$ and identified less polypeptide flexibility in Fcs with longer N-glycans (More et al. 2018). Interestingly, the authors identified decreased flexibility in two key regions, the N297-containing C'E loop and the region surrounding N315 and that these two surfaces mediate aggregation. Consistent with the CD16a binding data presented above, this study also reported a substantial reduction in deuterium uptake for the (1)GlcNAc-Fc when compared to the aglycosylated Fc.

Thus far, these data indicate a relationship between N-glycan length and Fc affinity for CD16a. Furthermore, a longer N-glycan appears to stabilize glycan motion and Fc structure. An experiment to mutate phenylalanine residues at the intramolecular interface directly probed this relationship. Prior studies showed that mutating residues at the interface increased N-glycan processing during expression, potentially indicating increased motion of the N-glycans on mutated Fcs and greater exposure to glycan modifying enzymes in the Golgi (Lund et al. 1996; Yu, Baruah, et al. 2013). The observation of Kelly and coworkers that aromatic residues form the strongest interactions with carbohydrate residues through dispersive interactions led to the choice to mutate the Phe241 and Phe243 residues (Chen, Enck, et al. 2013). Mutated Fcs exhibited greater N-glycan processing, with the proteins containing two Phe to Ser mutations showing the greatest processing (Subedi, Hanson, et al. 2014). NMR analyses of mutant Fcs, enzymatically remodeled to have nearly homogeneous G2F glycans, indicated N-glycans on mutant Fcs experienced increased mobility resulting from reduced intramolecular contacts.

Interactions at the Fc N-glycan/polypeptide interface stabilize Fc polypeptide motion and receptor binding. The IgG1 Fc Phe mutants showed greater N-glycan motion with double mutants revealing greater motion than single mutants and single mutants characterized by greater motion than wild-type Fc. An additional experiment demonstrated that these double Phe mutants, enzymatically remodeled to display G2F N-glycans, also bound CD16a with less affinity that the single Phe mutants that bound with less affinity than the wild-type Fc (Subedi, Hanson, et al. 2014). Thus, weaker intramolecular interactions between N-glycan and polypeptide residues led to greater N-glycan motion and weaker receptor binding. A 2D NMR fingerprint of the wild-type and mutant Fcs using [^{15}N]-Tyr labeling indicated that Fc structure was largely preserved in the mutants though one Tyr residue at position 300, near the site of N-glycan attachment to Asn297, showed perturbation of the local structure. A follow-up study indicated that the chemical environment surrounding Tyr300 is uniquely sensitive to the N-glycan composition and that the presence of an IgG1 Fc N-glycan largely impacts structure of the C′ strand and C'E loop, minimally affecting on other areas of the protein (shown in Figure 3) (Subedi and Barb 2015). Furthermore, the N-glycan stabilized C'E loop motions on a μs-ms timescale.

Extensive molecular dynamics simulations show comparable results with oligomannose-type N-glycans (Lee and Im 2017). These glycans exchange with the Fc surface and form fewer intramolecular contacts than complex type N-glycans particularly at the non-reducing termini. Notably, the presence of a glycan stabilized the C'E loop, leading to stronger receptor interactions.

Thus, the Fc N-glycan dampens motion of the C′ strand and C'E loop. This dampening is enhanced by extending the N-glycan to utilize a greater number of intramolecular interactions. Though CD16a does not directly contact the bulk of the Fc N-glycan, and certainly not the non-reducing termini, CD16a does contact the C'E loop (Sondermann, P., Huber, R., et al. 2000). These results are consistent with the HDX-MS results discussed previously indicating the presence of greater polypeptide structural heterogeneity in Fcs with less stabilizing N-glycan contacts (Kiyoshi et al. 2018; More et al. 2018). One exception to the statement that extending the N-glycan enhances contacts and CD16a binding affinity is modification of the core N-acetylglucosamine residue with fucose. This topic will be specifically addressed in the "IgG sialylation and fucosylation affects IgG Fc structure and function" section below.

Controversy: Does the N-glycan contribute to Fc quaternary structure? Evidence to support the stabilization of the IgG1 Fc C′ strand and C'E loop through intramolecular contacts mediated by the N-glycan appears well established. However, recent evidence both supports and contradicts the hypothesis that the N-glycan affects Fc quaternary structure. Recent studies in this area have focused on comparing glycosylated Fc with Fc that contains either a shortened (1) GlcNAc N-glycan or completely lacks modification.

It has been assumed that deglycosylation alters Fc conformation, thereby reducing affinity for proteins that elicit effector functions. This assumption has been examined by x-ray crystallographic analysis of deglycosylated Fc. The crystal structures of aglycosylated human IgG1 Fc (produced in *Escherichia coli*) (Borrok et al. 2012) and enzymatically deglycosylated murine IgG1-Fc (PNGase F treatment) (Feige et al. 2009) showed a closed conformation of the two Cγ2 domains, as judged from Pro239-Pro239 Cα distances ranging from 18.9Å to 19.6 Å. Hence, an idea was proposed that the closed conformation prevents interaction with FcγRs and the N-glycan at Asn297 stabilizes the open conformation of Fc. Another model of Fc with the N-glycan truncated to a single GlcNAc residue following digestion with EndoS revealed a similarly collapsed conformation (Baruah et al. 2012); however, this glycoform binds CD16a with moderate affinity (Subedi and Barb 2015), indicating that the quaternary structures observed by crystallography fail to clearly separate Fc forms capable of binding receptor from inert forms.

In contrast to these observations, a crystal structure of fully deglycosylated human IgG1 Fc (produced in *E. coli*) was revealed with an open conformation with the Pro239-Pro239 Cα distance of 27.6 Å (PDB ID: 3DNK). A later study reported a crystal structure of enzymatically deglycosylated human IgG4-Fc (PNGase F treatment) that also adopted an open conformation with the Pro239-Pro239 Cα distance of 29.1 Å (Davies, Jefferis, et al. 2014). The results are inconsistent with the earlier crystallographic results. Taken together, it is likely that deglycosylated Fc adopts a set of conformations (including open and closed) and the observed structures in the crystal may be highly dependent on the crystal packing environment. Therefore, the crystal structures of deglycosylated Fc might not reflect the predominant conformation sampled in solution. Thus, other biophysical techniques are required to characterize conformation in the solution state.

One approach is small-angle x-ray scattering (SAXS), a method to analyze the conformation of macromolecules in solution. Several groups reported SAXS analysis of glycosylated and aglycosylated Fc. The radius of gyration (R_g) was obtained from the SAXS analysis, which is defined as the root mean square distance of all atoms from the common center of mass. Borrok et al. (2012) reported that the glycosylated human IgG1 Fc displayed a R_g of 27.4 Å, compared to 28.3 Å for aglycosylated Fc (*E. coli* expression). They suggest that in solution the absence of a glycan promotes a more open conformation. Yageta et al. (2019) performed a similar SAXS analysis of glycosylated and aglycosylated Fc (*E. coli* expression) that is consistent with the former result with R_g values of 26.4 Å and 28.9 Å, respectively. Owing to the availability of many Fc crystal structures, these authors analyzed the theoretical SAXS profiles based on individual crystal structures. The data indicated that both glycosylated and aglycosylated Fc adopt a "semi-closed" Cγ2 domain orientation. The conclusion is rather different from that of Borrok et al., but they reasonably assumed that the scattering from the N-glycan itself reduces the R_g of glycosylated Fc compared with the aglycosylated Fc, without any changes in the Cγ2 domain orientation. Comparable MD simulations identified smaller distances between the Cγ2 domains for Fc with truncated N-glycans (Lee and Im 2017). It is also possible that disorder of protein loops *or* quaternary structure changes contributed to changes in Fc tumbling.

Relative orientation of the Cγ2 and Cγ3 domains were also analyzed by stable isotope-assisted solution NMR spectroscopy (Subedi and Barb 2015). Residual dipolar couplings (RDCs) can be used to define the relative orientation of each observable amide N-H bond vector for ^{15}N-labeled samples. RDCs from selectively ^{15}N-labeled Fc samples (^{15}N-Tyr and ^{15}N-Lys labeled) were measured for both glycosylated and aglycosylated (T299A) human IgG1 Fc. RDCs reveal little difference between the predominant quaternary structures of glycosylated and aglycosylated Fc in solution.

SAXS and NMR analysis were usually analyzed assuming a single averaged conformation without consideration for a distribution of multiple sampled conformations. Recent analysis using single molecule Förster Resonance Energy transfer (FRET) is advantageous, since this technique provides a histogram of the conformations present in solution allowing conformational populations to be detected (Kelliher et al. 2014; Piraino et al. 2015). To introduce a probe into Fc, Ser258 of human IgG-Fc was mutated into Cys and the acceptor and donor fluorescent dyes were introduced to give antibody-dye conjugates with homo- and hetero-combinations of acceptor and donor dyes. A comparison of the FRET efficiency histograms obtained for glycosylated and deglycosylated human IgG indicates that the Fc region becomes more flexible and can assume a wider variety of structures upon deglycosylation with PNGase F or EndoS. This observation further supports the idea that x-ray crystallographic data of deglycosylated Fc captures one out of many Fc conformations in solution.

Then why does removing the Fc N-glycan reduce the affinity with effector molecules? Aglycosylated Fc likely samples a set of multiple conformations while glycosylated Fc experiences a relatively limited range of mobility. The more flexible nature of aglycosylated Fc may be unfavorable for the interaction with effector molecules such as the FcγRs. From a local viewpoint, the orientation of C'E loop, which harbors the Fc N-glycosylation site at Asn297, is thought to be critical for the binding to FcγRs. Solution NMR spectroscopy can provide information on macromolecular motion by measuring the relaxation parameters. By comparing the relaxation rates of glycosylated (WT) and aglycosylated (T299A) human IgG1 Fc, it was found that the C'E loop is relatively more flexible in aglycosylated Fc upon comparison to glycosylated Fc (Subedi and Barb 2015). This is consistent with the x-ray crystallographic data, in which human aglycosylated Fc structure displays high crystallographic temperature factors (B-factors) for the C'E loop, relative to the core of the protein (Borrok et al. 2012). These observations suggest that the conformation of the C'E loop is stabilized by the presence of the N-glycan and the loop conformation is essential for forming the FcγR interface.

Fc engineering targeting the C'E loop and glycan remodeling. The ultimate goal of a structural definition is to generate sufficient data to design Fcs with altered properties. A number of studies support the role of the C'E loop and N-glycan in receptor binding and Fc stability. A study by Isoda et al. (2015) tested the effect of each amino acid type substituted at position 296. This residue is a Tyr in human IgG1 Fc and located immediately adjacent to the glycosylated Asn297 residue. Tyr300 may form contacts with the core fucose residue (Matsumiya et al. 2007). With the exception of a Trp substitution, all residues reduced affinity for CD16a and CD16b. A crystal structure of the Fc Tyr296Trp variant indicated a presence of greater contacts that slightly increase affinity for CD16a.

The directed replacement of both the Gln295 and Tyr296 residues increased Fc thermal stability and decreased N-glycan processing (Chen et al. 2016). Based on an idealized structure, the Fc Gln295Phe Tyr296Ala variant revealed reduced N-glycan processing evident from the appearance of high levels of minimally-processed hybrid-type N-glycans rarely observed on IgG1 Fc. The enhanced thermal stability resulted from stabilization of the Cγ2; however, this mutation decreased binding to CD32a, CD16a and CD16b. It is evident that decreased FcγR affinity in a mAb would severely limit efficacy if FcγR-mediated effector function is desired because the high concentration of serum IgG ($\sim$10 mg/mL = 67 μM) is far above the dissociation constant for IgG1 (50–400 nM).

A mutation to the Cγ3 domain that disrupted Fc dimer formation also increased N-glycan processing (Rose et al. 2013). The Fc Tyr403Glu variant of IgG1 and IgG4 showed increased N-glycan processing similar to the Phe243 variant, indicating that Fc dimer formation contributes to restricted processing of the Fc N-glycan. These results are important for efforts to alter Fc properties by modifying N-glycan processing during protein expression.

IgG sialylation and fucosylation affects IgG Fc structure and function

Structural consequences of core fucosylation. Antibody-dependent cellular cytotoxicity is a key effector function, relying on the binding of antigen-antibody complexes to FcγRs. Most natural antibodies are highly fucosylated. It was discovered that antibodies lacking core fucosylation show a large increase in affinity for CD16a leading to an enhanced ADCC activity. This discovery stimulated the development of therapeutic antibodies with desired activity by specifically increasing or decreasing fucosylation. Many therapeutic antibodies are, however, modified with core fucose, which may indicate that FcγR-mediated activity is not desired for therapeutic purpose. One possible mechanism explaining affinity enhancement by defucosylation was revealed from x-ray crystallographic analysis, using afucosylated Fc and glycosylated CD16a. Ferrara et al. (2011) reported a crystal structure of afucosylated human IgG1 Fc in complex with a glycosylated CD16a. Afucosylated Fc was prepared by introducing the GnTIII gene into the host cell to produce bisected and afucosylated N-glycans. For the preparation of the human CD16a, three out of five N-linked glycosylation sites (38, 74 and 169) were removed by changing the Asn residues (38, 74 and 169) to Gln. Asn162 and Asn45 were kept because they are essential for the affinity toward IgG1 and for expression, respectively. Further, the CD16a was expressed in the presence of kifunensine, producing the oligomannose-type N-glycans. In the crystal structure of the afucosylated Fc-glycosylated CD16a complex, unique intermolecular carbohydrate–carbohydrate interactions appeared, connecting N-glycans of the receptor the afucosylated Fc N-glycan. In order to understand the regulatory mechanism of IgG core fucosylation, fucosylated Fc was used for comparison. In contrast to the complex with afucosylated Fc, carbohydrate–carbohydrate contact area was significantly decreased in the complex structure of fucosylated Fc with glycosylated CD16a. Core fucose linked to the Fc is oriented toward the second N-acetylglucosamine residue of the Asn162-glycan and as a result the Asn162-glycan must move and hence carbohydrate–carbohydrate contact is not properly formed.

Independently, Mizushima et al. (2011) reported the crystal structure of afucosylated IgG1-Fc in complex with glycosylated CD16a. In this case, CD16a possesses a complex-type biantennary complex glycan at Asn45 and Asn162 and the other remaining N-glycosylation sites were similarly mutated to abolish N-glycosylation. Although the CD16a glycan composition differs between the two reports (high mannose vs complex), carbohydrate–carbohydrate interactions were observed. Ten sugar residues were observed with the oligomannose-type Asn162-glycan (Ferrara et al. 2011) and eight residues were detected in the complex with the complex-type Asn162-glycan (Mizushima et al. 2011).

Recently, Falconer et al. (2018) reported the crystal structure of afucoylated IgG1 Fc in complex with CD16a with $Mannose_5$ N-glycans, which was different from the previous reports. Among the CD16a glycoforms ($Mannose_5$, $Mannose_9$ and complex-type), the $Mannose_5$ form showed the highest affinity toward afucosylated Fc. In fact, CD16a isolated from NK cells contains a substantial amount of oligomannose and hybrid-type glycans (Patel et al. 2018). In the crystal structure of the complex, in contrast with earlier reports, electron density was detected only from single N-acetylglucosamine residue attached to Asn162 of CD16a. It is unclear why the intermolecular N-glycan contacts were not observed. It is possible that intermolecular N-glycan contacts in the previous cases formed as a result of the crystal contacts. To better understand this point, the analysis of N-glycan dynamics is required.

MD simulations were performed to examine the effect of Fc afucosylation on the dynamics of the CD16a Asn162-glycan (Sakae et al. 2017). The root mean square fluctuation of Asn162-complex-type glycan was significantly higher (5.5 Å) in the fucosylated Fc system than in the afucosylated Fc system (3.7 Å). This can be interpreted as a significant disruption of proper carbohydrate-carbohydrate interactions upon Fc fucosylation. MD simulations were also performed with CD16a displaying a $Mannose_5$ glycoform with either fucosylated or afucosylated Fc (Falconer et al. 2018). The addition of an Fc core fucose residue decreased the volume sampled by the Asn162-linked glycan from 10,800 Å^3 to 9,100 Å^3. Falconer et al. interpreted these results to indicate that the Fc core fucose restricts the conformational space of Asn162, introducing a fucose-dependent energetic penalty upon binding to Fc. This idea is opposed to the previously proposed mechanism that direct intermolecular glycan-glycan contacts stabilized the complex (Ferrara et al. 2011; Mizushima et al. 2011). The mechanism of affinity enhancement upon defucosylation is still controversial, but we must pay attention to the interpretation of crystal structures which rather reflect a snapshot from many possible conformations and are often affected by unwanted crystal contacts.

Structural consequences of sialylation. Another topic regarding the structure and function of the Fc N-glycan is sialylation. In general, sialic acid can be incorporated in α2–3 or α2–6 linkages to a Gal residue. Looking at the Fc part of natural IgG, sialylated glycans are only a small population and are connected only through α2–6 linkages. α2–3 Neu5Ac onto the α1–6 branch of the Fc glycan is predicted to have a big impact on the native glycan-polypeptide interface. In vivo studies have shown that intravenous immunoglobulin G (IVIG) enriched in (α2–6) sialylation of the Fc glycan increased anti-inflammatory activity by up to 10-fold when compared to nonenriched IgG (Anthony, Nimmerjahn, et al. 2008; Anthony et al. 2011). When IVIG was treated with a sialidase to remove the modification, the anti-inflammatory activity was abrogated (Kaneko et al. 2006). Furthermore, ADCC activity is enhanced by (α2–6) sialylation in the absence of core fucosylation in in vitro and in vivo assays (Li et al. 2017).

How sialylation regulates the Fc activity is still unclear, but several mechanisms were discussed and proposed. One proposed mechanism

is that sialylated IgG-Fc is recognized by a specific receptor. In vivo experiments showed that the anti-inflammatory effect of Fc required expression of the murine C-type lectin receptor SIGN-R1 (Anthony, Wermeling, et al. 2008). A human orthologue for SIGN-R1 is the C-type lectin DC-SIGN, and it is also proposed to bind to sialylated Fc (Anthony, Wermeling, et al. 2008). Later, Sondermann et al. (2013) showed that α2,6-sialylated IgG binds to the IgE receptor CD23 in a cell-based ELISA assay. The model was based on a hypothesis that sialylation of IgG Fc leads to a conformational change, which triggers receptor binding. It should be noted that conflicting results have been reported (Yu, Vasiljevic, et al. 2013; Temming et al. 2019), thus further analysis will be required for the identification of *bona fide* receptor(s). Other candidate receptors are implicated, including DCIR (Massoud et al. 2014) and Siglecs (von Gunten and Simon 2008; Seite et al. 2010).

Attention has been paid to examine the effect of sialylation on the conformational property of Fc. Several crystal structures of sialylated Fc have been reported from several groups (Crispin et al. 2013; Ahmed et al. 2014; Chen et al. 2017). Overall, the conformations of sialylated Fc are within the range of Fc structures without sialylation. In a representative crystal structure of sialylated Fc, electron density of Neu5Ac residue is observed only on the (α1–6Mannose) branch and Neu5Ac interacted through water-mediated hydrogen bonds with residues found at the interface formed between the Cγ2 and Cγ3 domains (Chen et al. 2017). The observed interaction between Neu5Ac and residues at the Cγ2-Cγ3 interface may modulate the orientation of the Cγ2-Cγ3 domain and affect the binding affinity toward FcγRs and the neonatal Fc receptor (Chen et al. 2017). Based on the observation that certain N-glycan compositions caused increased variation in Fc crystal structures, Bjorkman and coworkers suggested that sialylation increases conformational flexibility of the Cγ2 domain which is associated with anti-inflammatory activity of the Fc (Ahmed et al. 2014). However, this hypothesis does not explain how the conformational flexibility of Fc affects receptor binding. Thus, the mechanism behind the anti-inflammatory activity of sialylated IgG is still an open question.

Studies on other IgGs

There are four human IgG antibody subclasses: IgG1, IgG2, IgG3 and IgG4, which are homologous to over 90% at the amino acid level (Vidarsson et al. 2014). The global structures of the four human IgG subclasses are thus similar. However, the subclasses have sequence variations especially in the hinge region and N-terminal Cγ2 domain (Vidarsson et al. 2014). This variation is likely linked to differing affinities for the specific FcγRs and different abilities to activate complement (Bruhns et al. 2009; Vidarsson et al. 2014). So far, most studies have been conducted for human IgG1 subclasses and a large set of human IgG1 crystal structures have been reported. In contrast, the structural information on other subclasses is rather limited.

Human IgG4 is the least abundant of the four classes of IgG in serum, but displays unique biological properties. One is heavy chain exchange, also known as Fab-arm exchange, to form a bispecific but monovalent antibody (Aalberse and Schuurman 2002; Davies et al. 2013). IgG4 binds Fcγ receptors with lower affinity than IgG3 with the exception of FcγRI (Bruhns et al. 2009) and does not activate complement (van der Zee et al. 1986); these properties make IgG4 suitable for therapeutics when effector functions are undesired (Davies and Sutton 2015). For this reason, the IgG4 subclass is collecting a lot of attention as a preferred subclass for immunotherapy, exemplified by the anti-PD1 therapeutic antibodies (pembrolizumab/Keytruda® and nivolumab/Opdivo®).

Davies, Rispens, et al. (2014) reported the high-resolution crystal structure of human IgG4 Fc, prepared from papain digestion of serum IgG4 and using recombinant Fc. The overall topology of human IgG4 Fc is very similar to human IgG1 Fc fragments. The Asn297 glycans were facing each other in the cavity formed between two Cγ2 domains. Shortly thereafter, the crystal structure of full-length human IgG4 antibody S228P (pembrolizumab) was reported at 2.3 Å resolution (Scapin et al. 2015). Looking at the Fc region, the orientation of one Cγ2 domain is different from the previously reported IgG4 Fc structure. In the structure of the full-length antibody, the orientation of one Cγ2 domain (chain B) displayed a rotation of 120° relative to the position observed in the isolated Fc, maintaining the immunoglobulin fold. Consequently, the Asn297 glycan on chain B is more solvent-exposed than chain A. This nature is verified by measuring the deglycosylation rate of IgG4 and a reference IgG1. The rate of IgG4 deglycosylation by PNGase F is faster than for IgG1, suggesting that IgG4 N-glycan is more solvent-exposed than in IgG1. However, one cannot rule out the possibility that this unusual Cγ2 conformation represents only one of many possible conformations.

IgG3 is the third most abundant human IgG subclass. It contains a long hinge region which is thought to provide additional flexibility toward antigen binding (Vidarsson, G., Dekkers, G., et al. 2014). A high-resolution (1.8 Å) crystal structure utilized human IgG3 Fc expressed with a modified yeast strain that added homogeneous $Mannose_5$ N-glycans (Shah et al. 2017). Out of the five sugar residues, the first three sugar residues corresponding to Mannose(β1–4)N-acetylglucosamine(β1–4)N-acetylglucosamine revealed electron density. The terminal mannose residues were not observed. The protein-carbohydrate interactions for the three visible sugar residues were identical to those previously reported for human IgG1 Fc structures (Deisenhofer 1981, Nagae and Yamaguchi 2012).

Human IgG2 is known to form structural isomers that originate from alternative disulfide bond formation of between the cysteines in the hinge region (Wypych et al. 2008). It is suggested that the activity of each human IgG2 isomer will be different (Dillon et al. 2008), and hence this point needs to be analyzed in detail. So far two IgG2 Fc crystal structures were reported, one is isolated after papain digestion and the other is from a recombinant construct (Teplyakov et al. 2013). The human IgG2 Fc structures are very similar to human IgG1 Fc structures. It is likely that sequence differences in the lower high region between IgG1 and IgG2 account for differences in FcγR binding affinity.

Structural studies on non-human IgG are limited. Recently, a comprehensive study was performed for all IgG subclasses, IgG1, IgG2, IgG3 and IgG4-Fc of an Old-World monkey, Rhesus macaque (*Macaca mulatta*, Mm) (Tolbert et al. 2019). Crystal structures of the Fc from MmIgG1–4 were solved with resolutions from 2.8 Å to 3.5 Å. The overall topologies of the MmIgG1–4 Fc resemble that of human IgG1 Fc. Solution NMR spectroscopy was employed to analyze the dynamics of the Fc-glycan at Asn297, with the aid of metabolic ^{13}C-labeling (Tolbert et al. 2019). N-glycan dynamics were evaluated from the linewidth of anomeric ^{1}H signals from Asn297-linked N-acetylglucosamine residues. The linewidth is in the following order: human IgG1-Fc (125 Hz) > Mm IgG1-Fc (102 Hz) > Mm IgG2-Fc (83 Hz) > Mm IgG4-Fc (75 Hz) > Mm IgG3 (66 Hz). This indicates that among Mm IgGs, the Fc N-glycan dynamics is the most restricted in Mm IgG1. This data is supported by the observation that the N-glycan of Mm IgG1-Fc is more stabilized through

glycan-polypeptide interaction than Mm IgG2–4. Interestingly, Mm IgG1 experienced the most glycan processing as compared to other Mm IgGs, suggesting that the Mm IgG1 N-glycan is more accessible to glycosyltransferases (galactosyltransferase, sialyltransferase etc.) and this may be correlated with the slowest dynamics of Mm IgG1 Fc glycan.

Mice express different IgG subclasses that vary by strain and include IgG1, IgG2a, IgG2b, IgG2c and IgG3. Subclass nomenclature has arisen independently for each species and there is no general relationship between the subclasses from different species. A recent study indicates that mouse FcγRIV is the homolog of human FcγRIIIa (Dekkers et al. 2018). However, much less is known about mouse IgG2 or mouse FcγRIV. Crystal structures of mouse IgG2c Fc have been reported recently (Falconer and Barb 2018) and compared with that of mouse IgG2b Fc. These two Fcs showed a high degree of similarity with differences in loop residues including Tyr296. Solution NMR analysis of the Asn297-linked N-acetylglucosamine residue shows differences between mouse IgG2b, mouse IgG2c and human IgG1, in terms of anomeric ^{1}H chemical shift, and that correlates to receptor binding affinity. Even in highly conserved molecules, structural and functional differences are present which should be further investigated to fully establish structure/function relationships across important model species.

Noteworthy technical achievements

Recent technical advances have provided a wealth of new tools to probe Fc structure and motion. Progress is focused in two primary areas. Developments in IgG1 Fc expression, purification and glycoengineering are substantial; this topic is directly related to pharmaceutical development and too broad to appropriately cover here (see Loos and Steinkellner 2012; Subedi et al. 2015; Mimura et al. 2018). The second major group of advances results from improvements to analytical techniques or new analyses of IgG. These reports have not themselves elucidated new aspects of the IgG Fc structure/function relationship; however, these techniques warrant a separate section highlighting significant progress in the past few years that may be a foundation for future advances.

Solution NMR studies designed to probe protein motion require assignment of the backbone nuclei. This allows the extraction of atomic-level detail regarding protein structure and motion. Kato and coworkers reported a major advance with the backbone resonance assignment of the glycosylated IgG1 Fc fragment (Yagi et al. 2015). Ordinarily, Fc would be a challenging NMR target due to the size of the molecule alone (~52 kDa). However, the challenges are magnified because appropriately glycosylated IgG1 Fc cannot be expressed in prokaryotic hosts and mammalian hosts are often used instead. This requirement introduces two additional limitations. First, proteins expressed in mammalian hosts, like the CHO cells used in this study, cannot be deuterated because high deuterium content of the medium is toxic to the host. Second, labeling expressed protein with stable ^{13}C and ^{15}N isotopes is much more expensive in a mammalian host compared to a prokaryotic host. The authors reported the nearly complete assignment of IgG1 Fc (99% of HN, N and Cα). This assignment provided a crucial starting point for at least two studies described above (Subedi et al. 2014; Subedi and Barb 2015).

IgG1 Fc binds multiple protein ligands through many different interfaces (Hanson and Barb 2015). The Fc-binding portion of one ligand, protein A, was developed to simultaneously bind IgG1 Fc and lanthanide ions with high affinity (Barb and Subedi 2016). Paramagnetic lanthanide ions provide a means to study distance and orientation up to 50 Å from the ion using solution NMR spectroscopy, but some ions also provide luminescence for microscopy and fluorescence-type solution measurements, unpaired electrons for EPR, and electron dense nuclei for electron and x-ray diffraction (Su and Otting 2010; Koehler and Meiler 2011). This specific construct revealed minimal motion of the paramagnetic ion relative to IgG1 Fc, expanding the utility of the tag for probing glycan and protein motion and conformation (Barb and Subedi 2016).

An additional advance included the development of a suite of NMR experiments to probe commercial antibodies and other therapeutic proteins. One challenge facing the pharmaceutical industry is appropriately validating the composition and structure of each product batch. Unlike small molecule drugs, three-dimensional conformation is an essential property of therapeutic proteins and is challenging to probe with traditional techniques used by the manufacturers. A simple mass analysis is insufficient. Developing techniques with suitable sensitivity, resolution and throughput represents a major challenge. Marino and coworkers developed multiple methods that provide sufficient resolution and are capable of characterizing pharmaceutical products using natural abundance of ^{13}C and ^{15}N. One method utilizes the unique property of methyl groups that provide superior detection sensitivity and resolution (Arbogast et al. 2015). Their developments reduced experimental time to 30 min and were sensitive enough to show resolvable differences in antibodies with different N-glycan composition. The next experiments correlated backbone amide protons to the nitrogen nuclei, an approach that is inherently less sensitive than detecting methyl correlations but provides a fingerprint of the protein that is likely more influenced by subtle conformational changes including changes in hydrogen bonding (Arbogast et al. 2016). These experiments required more instrument time of ~17 h for a single analysis, but provided a greater magnitude of changes, detecting large differences in peak positions following deglycosylation and applying a rigorous statistical analysis to the spectra (Arbogast et al. 2017). Thus, NMR is capable of detecting large conformational differences and small structural differences resulting from processing (Brinson et al. 2019). A related study by a group at Pfizer identified spectral features from ^{1}H-^{13}C methyl groups that correlated with aggregation (Majumder et al. 2018). Aggregation is another significant problem in pharmaceutical production, and is specific to individual mAb clones. This report indicates that surprisingly melting temperature did not correlate with aggregation behavior in a pilot study using three mAbs, but spectral features measured by NMR did. This result may represent a significant advance toward characterizing therapeutic proteins, though future studies with a larger number of proteins will determine if spectral features are reliable probes of aggregation behavior.

Though the common application of mass spectrometry provides mass information and generally does not probe molecular shape, advances in ion mobility mass spectrometry are providing new insight into protein structure and function. Tian and Ruotolo (2018) reported the unfolding of different antibody glycoforms in the gas phase. Though they observed greater sensitivity using the isolated Fc fragment, this team differentiated antibodies that differed only in glycoform.

Future considerations

Fundamental properties of IgG emerged in the past few years that define how Fc composition impacts structure and receptor binding.

This may appear surprising due to the importance and intense scrutiny focused on this molecule since the description of IgG in 1939 and high-resolution models of the Fab and Fc in 1973 and 1976, respectively (Tiselius and Kabat 1939; Poljak et al. 1973; Huber et al. 1976). Recent advances were largely driven by developments in physical techniques and Fc preparation methods, allowing researchers to break free from the bounds imposed by the crystal lattice. It is then worthwhile to consider which remaining undefined aspects may lead to better therapies once defined. Here we identify three primary areas for future research.

1. Future studies of unglycosylated antibodies may provide insight into which conformations are disfavored by intramolecular N-glycan interactions. A quantitative analysis of conformation states sampled by the FcγR-binding loops of aglycosylated Fc that defines the populations of each state will guide Fc engineering to limit the exposure of residues that promote aggregation and potentially enhance FcγR binding affinity. Similarly, it is likely that the Fc N-glycan completely dissociates from the protein surface and becomes accessible to glycan modifying enzymes. The structure of this state, and the definition of the conformational rearrangements that promote sampling this state, will impact Fc engineering to modify N-glycan composition during expression.

2. IgG1 is now a well-defined molecule, though some questions still remain. Much less is known about IgG2,3,4, IgD, IgM and IgE. Each of these share an N-glycan at a position homologous to N297 of IgG1 Fc and display an aromatic residue similar to F243 (Subedi, G.P., Hanson, Q.M., et al. 2014). IgE likewise shares a comparable receptor binding mode though the role of N-glycosylation in receptor interactions is less well defined thatn IgG (Shade et al. 2019). It is currently not known how N-glycosylation impacts structure and function for these less-studied antibodies. Furthermore, little is known about antibodies from other species which may provide complementary evolutionarily-selected solutions to stability and receptor binding. Unique among the five human antibody classes, IgA is much different, lacking homologous glycosylation, the key aromatic residue, and IgA displays a different receptor binding mode (Herr et al. 2003).

3. Differences between the behavior of IgG1 and isolated Fc and how Fc modulates interactions between two antibodies may provide insight into improving Fc designs. The 10-fold greater impact of IgG1 Fc fucosylation when compared to isolated Fc in measurements of CD16a binding indicates that the presence of Fab domains may impact Fc activity. Detailed studies to define these interactions will lead to a more complete definition of antibody function. Hints to the presence of intra- and inter-antibody interactions exist, including the observation that IgG1 forms hexamers on surfaces (Saphire et al. 2001; Ugurlar et al. 2018). N-glycans are poised to modulate these interactions as well, though sensitive techniques must be developed to investigate these phenomena further.

It is likely studies of antibody structure and function will continue for decades into the future. The results of these studies stand to improve existing therapies and create engineered mAb backbones for a wide range of future clinical applications, if investigators are sufficiently bold and inventive to identify key features and residues that may be altered for improved drug properties.

Funding

This work was supported by the National Institutes of Health (grant number R01 GM115489) to A.W.B. and by Japan Society for the Promotion of Science Kakenhi (grant numbers JP16H04758 and JP19H03362) to Y.Y.

References

Aalberse R, Schuurman J. 2002. IgG4 breaking the rules. *Immunology*. 105:9–19.

Ahmed AA, Giddens J, Pincetic A, Lomino JV, Ravetch JV, Wang LX, Bjorkman PJ. 2014. Structural characterization of anti-inflammatory immunoglobulin G Fc proteins. *J Mol Biol*. 426:3166–3179.

Anthony RM, Kobayashi T, Wermeling F, Ravetch JV. 2011. Intravenous gammaglobulin suppresses inflammation through a novel T(H)2 pathway. *Nature*. 475:110–113.

Anthony RM, Nimmerjahn F, Ashline DJ, Reinhold VN, Paulson JC, Ravetch JV. 2008. Recapitulation of IVIG anti-inflammatory activity with a recombinant IgG Fc. *Science*. 320:373–376.

Anthony RM, Wermeling F, Karlsson MC, Ravetch JV. 2008. Identification of a receptor required for the anti-inflammatory activity of IVIG. *Proc Natl Acad Sci U S A*. 105:19571–19578.

Arbogast LW, Brinson RG, Formolo T, Hoopes JT, Marino JP. 2016. 2D (1)H(N), (15) N correlated NMR methods at natural abundance for obtaining structural maps and statistical comparability of monoclonal antibodies. *Pharm Res*. 33:462–475.

Arbogast LW, Brinson RG, Marino JP. 2015. Mapping monoclonal antibody structure by 2D 13C NMR at natural abundance. *Anal Chem*. 87:3556–3561.

Arbogast LW, Delaglio F, Schiel JE, Marino JP. 2017. Multivariate analysis of two-dimensional (1) H, (13) C methyl NMR spectra of monoclonal antibody therapeutics to facilitate assessment of higher order structure. *Anal Chem*. 89:11839–11845.

Barb AW. 2015. Intramolecular N-glycan/polypeptide interactions observed at multiple N-glycan remodeling steps through [(13)C,(15)N]-N-acetylglucosamine labeling of immunoglobulin G1. *Biochemistry*. 54:313–322.

Barb AW, Meng L, Gao Z, Johnson RW, Moremen KW, Prestegard JH. 2012. NMR characterization of immunoglobulin G Fc glycan motion on enzymatic sialylation. *Biochemistry*. 51:4618–4626.

Barb AW, Prestegard JH. 2011. NMR analysis demonstrates immunoglobulin G N-glycans are accessible and dynamic. *Nat Chem Biol*. 7:147–153.

Barb AW, Subedi GP. 2016. An encodable lanthanide binding tag with reduced size and flexibility for measuring residual dipolar couplings and pseudocontact shifts in large proteins. *J Biomol NMR*. 64:75–85.

Baruah K, Bowden TA, Krishna BA, Dwek RA, Crispin M, Scanlan CN. 2012. Selective deactivation of serum IgG: A general strategy for the enhancement of monoclonal antibody receptor interactions. *J Mol Biol*. 420:1–7.

Berkowitz SA, Engen JR, Mazzeo JR, Jones GB. 2012. Analytical tools for characterizing biopharmaceuticals and the implications for biosimilars. *Nat Rev Drug Discov*. 11:527–540.

Bliss M. 2007. *The Discovery of Insulin*. 25th anniversary ed. Chicago: University of Chicago Press.

Borrok MJ, Jung ST, Kang TH, Monzingo AF, Georgiou G. 2012. Revisiting the role of glycosylation in the structure of human IgG Fc. *ACS Chem Biol*. 7:1596–1602.

Bowden TA, Baruah K, Coles CH, Harvey DJ, Yu X, Song BD, Stuart DI, Aricescu AR, Scanlan CN, Jones EY *et al.* 2012. Chemical and structural analysis of an antibody folding intermediate trapped during glycan biosynthesis. *J Am Chem Soc*. 134:17554–17563.

Brange J, Dodson G, Xiao B. 1991. Designing insulin for diabetes therapy by protein engineering. *Current Opinion in Structural Biology*. 1:934–940.

Breunis WB, van Mirre E, Bruin M, Geissler J, de Boer M, Peters M, Roos D, de Haas M, Koene HR, Kuijpers TW. 2008. Copy number variation of the activating FCGR2C gene predisposes to idiopathic thrombocytopenic purpura. *Blood*. 111:1029–1038.

Brinson RG, Marino JP, Delaglio F, Arbogast LW, Evans RM, Kearsley A, Gingras G, Ghasriani H, Aubin Y, Pierens GK *et al.* 2019. Enabling adoption of 2D-NMR for the higher order structure assessment of monoclonal antibody therapeutics. *MAbs*. 11:94–105.

Bruhns P, Iannascoli B, England P, Mancardi DA, Fernandez N, Jorieux S, Daeron M. 2009. Specificity and affinity of human Fcgamma receptors and their polymorphic variants for human IgG subclasses. *Blood*. 113:3716–3725.

Butler M, Quelhas D, Critchley AJ, Carchon H, Hebestreit HF, Hibbert RG, Vilarinho L, Teles E, Matthijs G, Schollen E *et al.* 2003. Detailed glycan analysis of serum glycoproteins of patients with congenital disorders of glycosylation indicates the specific defective glycan processing step and provides an insight into pathogenesis. *Glycobiology*. 13: 601–622.

Chen CL, Hsu JC, Lin CW, Wang CH, Tsai MH, Wu CY, Wong CH, Ma C. 2017. Crystal structure of a homogeneous IgG-fc glycoform with the N-glycan designed to maximize the antibody dependent cellular cytotoxicity. *ACS Chem Biol*. 12:1335–1345.

Chen W, Enck S, Price JL, Powers DL, Powers ET, Wong CH, Dyson HJ, Kelly JW. 2013. Structural and energetic basis of carbohydrate-aromatic packing interactions in proteins. *J Am Chem Soc*. 135: 9877–9884.

Chen W, Kong L, Connelly S, Dendle JM, Liu Y, Wilson IA, Powers ET, Kelly JW. 2016. Stabilizing the CH2 domain of an antibody by engineering in an enhanced aromatic sequon. *ACS Chem Biol*. 11: 1852–1861.

Chung AW, Crispin M, Pritchard L, Robinson H, Gorny MK, Yu X, Bailey-Kellogg C, Ackerman ME, Scanlan C, Zolla-Pazner S *et al.* 2014. Identification of antibody glycosylation structures that predict monoclonal antibody Fc-effector function. *AIDS*. 28: 2523–2530.

Clerc F, Novokmet M, Dotz V, Reiding KR, de Haan N, Kammeijer GSM, Dalebout H, Bladergroen MR, Vukovic F, Rapp E *et al.* 2018. Plasma N-glycan signatures are associated with features of inflammatory bowel diseases. *Gastroenterology*. 155:829–843.

Collin M, Olsen A. 2001. EndoS, a novel secreted protein from streptococcus pyogenes with endoglycosidase activity on human IgG. *EMBO J*. 20:3046–3055.

Crispin M, Yu X, Bowden TA. 2013. Crystal structure of sialylated IgG fc: Implications for the mechanism of intravenous immunoglobulin therapy. *Proc Natl Acad Sci U S A*. 110:E3544–E3546.

Davies AM, Jefferis R, Sutton BJ. 2014. Crystal structure of deglycosylated human IgG4-fc. *Mol Immunol*. 62:46–53.

Davies AM, Rispens T, den Bleker TH, McDonnell JM, Gould HJ, Aalberse RC, Sutton BJ. 2013. Crystal structure of the human IgG4 C(H)3 dimer reveals the role of Arg409 in the mechanism of fab-arm exchange. *Mol Immunol*. 54:1–7.

Davies AM, Rispens T, Ooijevaar-de Heer P, Gould HJ, Jefferis R, Aalberse RC, Sutton BJ. 2014. Structural determinants of unique properties of human IgG4-fc. *J Mol Biol*. 426:630–644.

Davies AM, Sutton BJ. 2015. Human IgG4: A structural perspective. *Immunol Rev*. 268:139–159.

Deisenhofer J. 1981. Crystallographic refinement and atomic models of a human Fc fragment and its complex with fragment B of protein A from Staphylococcus aureus at 2.9- and 2.8-A resolution. *Biochemistry*. 20:2361–2370.

Dekkers G, Bentlage AEH, Plomp R, Visser R, Koeleman CAM, Beentjes A, Mok JY, van Esch WJE, Wuhrer M, Rispens T *et al.* 2018. Conserved FcgammaR- glycan discriminates between fucosylated and afucosylated IgG in humans and mice. *Mol Immunol*. 94:54–60.

Dekkers G, Treffers L, Plomp R, Bentlage AEH, de Boer M, Koeleman CAM, Lissenberg-Thunnissen SN, Visser R, Brouwer M, Mok JY *et al.* 2017. Decoding the human immunoglobulin G-glycan repertoire reveals a spectrum of Fc-receptor- and complement-mediated-effector activities. *Front Immunol*. 8:877.

Dillon TM, Ricci MS, Vezina C, Flynn GC, Liu YD, Rehder DS, Plant M, Henkle B, Li Y, Deechongkit S *et al.* 2008. Structural and functional characterization of disulfide isoforms of the human IgG2 subclass. *J Biol Chem*. 283:16206–16215.

Doherty M, Theodoratou E, Walsh I, Adamczyk B, Stockmann H, Agakov F, Timofeeva M, Trbojevic-Akmacic I, Vuckovic F, Duffy F *et al.* 2018. Plasma N-glycans in colorectal cancer risk. *Sci Rep*. 8:8655.

Ernst LK, Metes D, Herberman RB, Morel PA. 2002. Allelic polymorphisms in the FcgammaRIIC gene can influence its function on normal human natural killer cells. *J Mol Med (Berl)*. 80:248–257.

Falconer DJ, Barb AW. 2018. Mouse IgG2c fc loop residues promote greater receptor-binding affinity than mouse IgG2b or human IgG1. *PLoS One*. 13: e0192123.

Falconer DJ, Subedi GP, Marcella AM, Barb AW. 2018. Antibody fucosylation lowers the FcgammaRIIIa/CD16a affinity by limiting the conformations sampled by the N162-glycan. *ACS Chem Biol*. 13:2179–2189.

Feige MJ, Nath S, Catharino SR, Weinfurtner D, Steinbacher S, Buchner J. 2009. Structure of the murine unglycosylated IgG1 Fc fragment. *J Mol Biol*. 391:599–608.

Ferrara C, Grau S, Jager C, Sondermann P, Brunker P, Waldhauer I, Hennig M, Ruf A, Rufer AC, Stihle M *et al.* 2011. Unique carbohydrate-carbohydrate interactions are required for high affinity binding between FcgammaRIII and antibodies lacking core fucose. *Proc Natl Acad Sci U S A*. 108:12669–12674.

Frank M, Walker RC, Lanzilotta WN, Prestegard JH, Barb AW. 2014. Immunoglobulin G1 fc domain motions: Implications for Fc engineering. *J Mol Biol*. 426:1799–1811.

Guillerey C, Huntington ND, Smyth MJ. 2016. Targeting natural killer cells in cancer immunotherapy. *Nat Immunol*. 17:1025–1036.

Hanson QM, Barb AW. 2015. A perspective on the structure and receptor binding properties of immunoglobulin G Fc. *Biochemistry*. 54:2931–2942.

Hanson SR, Culyba EK, Hsu TL, Wong CH, Kelly JW, Powers ET. 2009. The core trisaccharide of an N-linked glycoprotein intrinsically accelerates folding and enhances stability. *Proc Natl Acad Sci U S A*. 106:3131–3136.

Herr AB, Ballister ER, Bjorkman PJ. 2003. Insights into IgA-mediated immune responses from the crystal structures of human FcalphaRI and its complex with IgA1-Fc. *Nature*. 423:614–620.

Huber R, Deisenhofer J, Colman PM, Matsushima M, Palm W. 1976. Crystallographic structure studies of an IgG molecule and an Fc fragment. *Nature*. 264:415–420.

Isoda Y, Yagi H, Satoh T, Shibata-Koyama M, Masuda K, Satoh M, Kato K, Iida S. 2015. Importance of the side chain at position 296 of antibody fc in interactions with FcgammaRIIIa and other Fcgamma receptors. *PLoS One*. 10:e0140120.

James LC, Keeble AH, Khan Z, Rhodes DA, Trowsdale J. 2007. Structural basis for PRYSPRY-mediated tripartite motif (TRIM) protein function. *Proc Natl Acad Sci U S A*. 104:6200–6205.

Jennewein MF, Goldfarb I, Dolatshahi S, Cosgrove C, Noelette FJ, Krykbaeva M, Das J, Sarkar A, Gorman MJ, Fischinger S *et al.* 2019. Fc glycan-mediated regulation of placental antibody transfer. *Cell*. 178 202–215.

Kaneko Y, Nimmerjahn F, Ravetch JV. 2006. Anti-inflammatory activity of immunoglobulin G resulting from Fc sialylation. *Science*. 313:670–673.

Kao D, Danzer H, Collin M, Gross A, Eichler J, Stambuk J, Lauc G, Lux A, Nimmerjahn F. 2015. A monosaccharide residue is sufficient to maintain mouse and human IgG subclass activity and directs IgG effector functions to cellular Fc receptors. *Cell Rep*. 13:2376–2385.

Kapur R, Kustiawan I, Vestrheim A, Koeleman CA, Visser R, Einarsdottir HK, Porcelijn L, Jackson D, Kumpel B, Deelder AM *et al.* 2014. A prominent lack of IgG1-Fc fucosylation of platelet alloantibodies in pregnancy. *Blood*. 123:471–480.

Kelliher MT, Jacks RD, Piraino MS, Southern CA. 2014. The effect of sugar removal on the structure of the Fc region of an IgG antibody as observed with single molecule Forster resonance energy transfer. *Mol Immunol*. 60:103–108.

Kiyoshi M, Caaveiro JMM, Tada M, Tamura H, Tanaka T, Terao Y, Morante K, Harazono A, Hashii N, Shibata H *et al.* 2018. Assessing the heterogeneity of the Fc-glycan of a therapeutic antibody using an engineered FcgammaReceptor IIIa-immobilized column. *Sci Rep*. 8:3955.

Koehler J, Meiler J. 2011. Expanding the utility of NMR restraints with paramagnetic compounds: Background and practical aspects. *Prog Nucl Magn Reson Spectrosc*. 59:360–389.

Krapp S, Mimura Y, Jefferis R, Huber R, Sondermann P. 2003. Structural analysis of human IgG-fc glycoforms reveals a correlation between glycosylation and structural integrity. *J Mol Biol*. 325:979–989.

Lauc G, Huffman JE, Pucic M, Zgaga L, Adamczyk B, Muzinic A, Novokmet M, Polasek O, Gornik O, Kristic J *et al*. 2013. Loci associated with N-glycosylation of human immunoglobulin G show pleiotropy with autoimmune diseases and haematological cancers. *PLoS Genet*. 9:e1003225.

Lee HS, Im W. 2017. Effects of N-glycan composition on structure and dynamics of IgG1 Fc and their implications for antibody engineering. *Sci Rep*. 7:12659.

Li T, DiLillo DJ, Bournazos S, Giddens JP, Ravetch JV, Wang LX. 2017. Modulating IgG effector function by Fc glycan engineering. *Proc Natl Acad Sci U S A*. 114:3485–3490.

Liu H, May K. 2012. Disulfide bond structures of IgG molecules: Structural variations, chemical modifications and possible impacts to stability and biological function. *MAbs*. 4:17–23.

Loos A, Steinkellner H. 2012. IgG-Fc glycoengineering in non-mammalian expression hosts. *Arch Biochem Biophys*. 526:167–173.

Lund J, Takahashi N, Pound JD, Goodall M, Jefferis R. 1996. Multiple interactions of IgG with its core oligosaccharide can modulate recognition by complement and human Fc gamma receptor I and influence the synthesis of its oligosaccharide chains. *J Immunol*. 157:4963–4969.

Mahan AE, Jennewein MF, Suscovich T, Dionne K, Tedesco J, Chung AW, Streeck H, Pau M, Schuitemaker H, Francis D *et al*. 2016. Antigen-specific antibody glycosylation is regulated via vaccination. *PLoS Pathog*. 12:e1005456.

Majumder S, Jones MT, Kimmel M, Alphonse IA. 2018. Probing conformational diversity of Fc domains in aggregation-prone monoclonal antibodies. *Pharm Res*. 35:220.

Massoud AH, Yona M, Xue D, Chouiali F, Alturaihi H, Ablona A, Mourad W, Piccirillo CA, Mazer BD. 2014. Dendritic cell immunoreceptor: A novel receptor for intravenous immunoglobulin mediates induction of regulatory T cells. *J Allergy Clin Immunol*. 133:853–863.

Matsumiya S, Yamaguchi Y, Saito J, Nagano M, Sasakawa H, Otaki S, Satoh M, Shitara K, Kato K. 2007. Structural comparison of fucosylated and nonfucosylated Fc fragments of human immunoglobulin G1. *J Mol Biol*. 368:767–779.

Mimura Y, Katoh T, Saldova R, O'Flaherty R, Izumi T, Mimura-Kimura Y, Utsunomiya T, Mizukami Y, Yamamoto K, Matsumoto T *et al*. 2018. Glycosylation engineering of therapeutic IgG antibodies: Challenges for the safety, functionality and efficacy. *Protein Cell*. 9: 47–62.

Mizushima T, Yagi H, Takemoto E, Shibata-Koyama M, Isoda Y, Iida S, Masuda K, Satoh M, Kato K. 2011. Structural basis for improved efficacy of therapeutic antibodies on defucosylation of their fc glycans. *Genes Cells*. 16:1071–1080.

More AS, Toth RT, Okbazghi SZ, Middaugh CR, Joshi SB, Tolbert TJ, Volkin DB, Weis DD. 2018. Impact of glycosylation on the local backbone flexibility of well-defined IgG1-Fc glycoforms using hydrogen exchange-mass spectrometry. *J Pharm Sci*. 107:2315–2324.

Nagae M, Yamaguchi Y. 2012. Function and 3D structure of the N-glycans on glycoproteins. *Int J Mol Sci*. 13:8398–8429.

Nose M, Wigzell H. 1983. Biological significance of carbohydrate chains on monoclonal antibodies. *Proc Natl Acad Sci U S A*. 80:6632–6636.

Okbazghi SZ, More AS, White DR, Duan S, Shah IS, Joshi SB, Middaugh CR, Volkin DB, Tolbert TJ. 2016. Production, characterization, and biological evaluation of well-defined IgG1 Fc glycoforms as a model system for biosimilarity analysis. *J Pharm Sci*. 105:559–574.

Parekh RB, Dwek RA, Sutton BJ, Fernandes DL, Leung A, Stanworth D, Rademacher TW, Mizuochi T, Taniguchi T, Matsuta K *et al*. 1985. Association of rheumatoid arthritis and primary osteoarthritis with changes in the glycosylation pattern of total serum IgG. *Nature*. 316: 452–457.

Patel KR, Roberts JT, Subedi GP, Barb AW. 2018. Restricted processing of CD16a/Fc gamma receptor IIIa N-glycans from primary human NK cells impacts structure and function. *J Biol Chem*. 293:3477–3489.

Peschke B, Keller CW, Weber P, Quast I, Lunemann JD. 2017. Fc-Galactosylation of human immunoglobulin gamma Isotypes improves C1q binding and enhances complement-dependent cytotoxicity. *Front Immunol*. 8:646.

Pincetic A, Bournazos S, DiLillo DJ, Maamary J, Wang TT, Dahan R, Fiebiger BM, Ravetch JV. 2014. Type I and type II Fc receptors regulate innate and adaptive immunity. *Nat Immunol*. 15:707–716.

Piraino MS, Kelliher MT, Aburas J, Southern CA. 2015. Single molecule Forster resonance energy transfer studies of the effect of EndoS deglycosylation on the structure of IgG. *Immunol Lett*. 167:29–33.

Poljak RJ, Amzel LM, Avey HP, Chen BL, Phizackerley RP, Saul F. 1973. Three-dimensional structure of the Fab' fragment of a human immunoglobulin at 2,8-A resolution. *Proc Natl Acad Sci U S A*. 70:3305–3310.

Rose RJ, van Berkel PH, van den Bremer ET, Labrijn AF, Vink T, Schuurman J, Heck AJ, Parren PW. 2013. Mutation of Y407 in the CH3 domain dramatically alters glycosylation and structure of human IgG. *MAbs*. 5:219–228.

Sakae Y, Satoh T, Yagi H, Yanaka S, Yamaguchi T, Isoda Y, Iida S, Okamoto Y, Kato K. 2017. Conformational effects of N-glycan core fucosylation of immunoglobulin G fc region on its interaction with Fcgamma receptor IIIa. *Sci Rep*. 7:13780.

Saphire EO, Parren PW, Pantophlet R, Zwick MB, Morris GM, Rudd PM, Dwek RA, Stanfield RL, Burton DR, Wilson IA. 2001. Crystal structure of a neutralizing human IGG against HIV-1: A template for vaccine design. *Science*. 293:1155–1159.

Scapin G, Yang X, Prosise WW, McCoy M, Reichert P, Johnston JM, Kashi RS, Strickland C. 2015. Structure of full-length human anti-PD1 therapeutic IgG4 antibody pembrolizumab. *Nat Struct Mol Biol*. 22: 953–958.

Seite JF, Cornec D, Renaudineau Y, Youinou P, Mageed RA, Hillion S. 2010. IVIg modulates BCR signaling through CD22 and promotes apoptosis in mature human B lymphocytes. *Blood*. 116:1698–1704.

Shade KT, Conroy ME, Anthony RM. 2019. IgE glycosylation in health and disease. *Curr Top Microbiol Immunol*. .

Shah IS, Lovell S, Mehzabeen N, Battaile KP, Tolbert TJ. 2017. Structural characterization of the Man5 glycoform of human IgG3 fc. *Mol Immunol*. 92:28–37.

Shields RL, Lai J, Keck R, O'Connell LY, Hong K, Meng YG, Weikert SH, Presta LG. 2002. Lack of fucose on human IgG1 N-linked oligosaccharide improves binding to human Fcgamma RIII and antibody-dependent cellular toxicity. *J Biol Chem*. 277:26733–26740.

Shinkawa T, Nakamura K, Yamane N, Shoji-Hosaka E, Kanda Y, Sakurada M, Uchida K, Anazawa H, Satoh M, Yamasaki M *et al*. 2003. The absence of fucose but not the presence of galactose or bisecting N-acetylglucosamine of human IgG1 complex-type oligosaccharides shows the critical role of enhancing antibody-dependent cellular cytotoxicity. *J Biol Chem*. 278:3466–3473.

Sondermann P, Huber R, Oosthuizen V, Jacob U. 2000. The 3.2-A crystal structure of the human IgG1 Fc fragment-Fc gammaRIII complex. *Nature*. 406:267–273.

Sondermann P, Pincetic A, Maamary J, Lammens K, Ravetch JV. 2013. General mechanism for modulating immunoglobulin effector function. *Proc Natl Acad Sci U S A*. 110:9868–9872.

Sonneveld ME, de Haas M, Koeleman C, de Haan N, Zeerleder SS, Ligthart PC, Wuhrer M, van der Schoot CE, Vidarsson G. 2017. Patients with IgG1-anti-red blood cell autoantibodies show aberrant Fc-glycosylation. *Sci Rep*. 7:8187.

Su XC, Otting G. 2010. Paramagnetic labelling of proteins and oligonucleotides for NMR. *J Biomol NMR*. 46:101–112.

Subedi GP, Barb AW. 2015. The structural role of antibody N-glycosylation in receptor interactions. *Structure*. 23:1573–1583.

Subedi GP, Barb AW. 2016. The immunoglobulin G1 N-glycan composition affects binding to each low affinity Fc gamma receptor. *MAbs*. 8:1512–1524.

Subedi GP, Hanson QM, Barb AW. 2014. Restricted motion of the conserved immunoglobulin G1 N-glycan is essential for efficient FcgammaRIIIa binding. *Structure*. 22:1478–1488.

Subedi GP, Johnson RW, Moniz HA, Moremen KW, Barb A. 2015. High yield expression of recombinant human proteins with the transient transfection of HEK293 cells in suspension. *J Vis Exp*. 106:e53568.

Temming AR, Dekkers G, van de FS, Plomp HR, Bentlage AEH, Szittner Z, Derksen NIL, Wuhrer M, Rispens T, Vidarsson G. 2019. Human DC-SIGN and CD23 do not interact with human IgG. *Sci Rep*. 9:9995.

Teplyakov A, Zhao Y, Malia TJ, Obmolova G, Gilliland GL. 2013. IgG2 Fc structure and the dynamic features of the IgG CH2-CH3 interface. *Mol Immunol*. 56:131–139.

Thomann M, Schlothauer T, Dashivets T, Malik S, Avenal C, Bulau P, Ruger P, Reusch D. 2015. In vitro glycoengineering of IgG1 and its effect on Fc receptor binding and ADCC activity. *PLoS One*. 10: e0134949.

Tian Y, Ruotolo B. 2018. Collision induced unfolding detects subtle differences in intact antibody glycoforms and associated fragments. *Int J Mass Spectrom*. 425:1–9.

Tiselius A, Kabat EA. 1939. An electrophoretic study of immune sera and purified antibody preparations. *J Exp Med*. 69:119–131.

Tolbert WD, Subedi GP, Gohain N, Lewis GK, Patel KR, Barb AW, Pazgier M. 2019. From rhesus macaque to human: Structural evolutionary pathways for immunoglobulin G subclasses. *MAbs*. 11:709–724.

Ugurlar D, Howes SC, de Kreuk BJ, Koning RI, de Jong RN, Beurskens FJ, Schuurman J, Koster AJ, Sharp TH, Parren P *et al.* 2018. Structures of C1-IgG1 provide insights into how danger pattern recognition activates complement. *Science*. 359:794–797.

van der Zee JS, van Swieten P, Aalberse RC. 1986. Inhibition of complement activation by IgG4 antibodies. *Clin Exp Immunol*. 64:415–422.

Vidarsson G, Dekkers G, Rispens T. 2014. IgG subclasses and allotypes: From structure to effector functions. *Front Immunol*. 5: 520.

von Gunten S, Simon HU. 2008. Natural anti-Siglec autoantibodies mediate potential immunoregulatory mechanisms: Implications for the clinical use of intravenous immunoglobulins (IVIg). *Autoimmun Rev*. 7:453–456.

Wypych J, Li M, Guo A, Zhang Z, Martinez T, Allen MJ, Fodor S, Kelner DN, Flynn GC, Liu YD *et al.* 2008. Human IgG2 antibodies display disulfide-mediated structural isoforms. *J Biol Chem*. 283: 16194–16205.

Yageta S, Imamura H, Shibuya R, Honda S. 2019. CH2 domain orientation of human immunoglobulin G in solution: Structural comparison of glycosylated and aglycosylated Fc regions using small-angle X-ray scattering. *MAbs*. 11:453–462.

Yagi H, Zhang Y, Yagi-Utsumi M, Yamaguchi T, Iida S, Yamaguchi Y, Kato K. 2015. Backbone (1) H, (13) C, and (15) N resonance assignments of the Fc fragment of human immunoglobulin G glycoprotein. *Biomol NMR Assign*. 9:257–260.

Yamaguchi Y, Nishimura M, Nagano M, Yagi H, Sasakawa H, Uchida K, Shitara K, Kato K. 2006. Glycoform-dependent conformational alteration of the Fc region of human immunoglobulin G1 as revealed by NMR spectroscopy. *Biochim Biophys Acta*. 1760:693–700.

Yu X, Baruah K, Harvey DJ, Vasiljevic S, Alonzi DS, Song BD, Higgins MK, Bowden TA, Scanlan CN, Crispin M. 2013. Engineering hydrophobic protein-carbohydrate interactions to fine-tune monoclonal antibodies. *J Am Chem Soc*. 135:9723–9732.

Yu X, Vasiljevic S, Mitchell DA, Crispin M, Scanlan CN. 2013. Dissecting the molecular mechanism of IVIg therapy: The interaction between serum IgG and DC-SIGN is independent of antibody glycoform or fc domain. *J Mol Biol*. 425:1253–1258.

Structural Aspects of Carbohydrate Recognition Mechanisms of C-Type Lectins

Masamichi Nagae and Yoshiki Yamaguchi

Contents

Abstract Carbohydrate recognition is an essential function occurring in all living organisms. Lectins are carbohydrate-binding proteins and are classified into several families. In mammals, Ca^{2+}-dependent C-type lectins, such as β-galactoside-binding galectin and sialic acid-binding siglec, play crucial roles in the immune response and homeostasis. C-type lectins are abundant and diverse in animals. Their immunological activities include lymphocyte homing, pathogen recognition, and clearance of apoptotic bodies. C-type lectin domains are composed of 110–130 amino acid residues with highly conserved structural folds. Remarkably, individual lectins can accept a wide variety of sugar ligands and can distinguish subtle

M. Nagae (✉)
Department of Pharmaceutical Sciences, The University of Tokyo, Hongo 7-3-1, Bunkyo-Ku, Tokyo 113-0033, Japan
e-mail: mnagae@mol.f.u-tokyo.ac.jp

Y. Yamaguchi (✉)
Faculty of Pharmaceutical Sciences, Tohoku Medical and Pharmaceutical University, Miyagi 981-8558, Japan
e-mail: yyoshiki@tohoku-mpu.ac.jp

Current Topics in Microbiology and Immunology
https://doi.org/10.1007/82_2019_181

structural differences in closely related ligands. In addition, several C-type lectin-like proteins specifically bind to carbohydrate ligands in Ca^{2+}-independent ways. The accumulated 3D structural evidence clarifies the unexpected structural versatility of C-type lectins underlying the variety of ligand binding modes. In this issue, we focus on the structural aspects of carbohydrate recognition mechanisms of C-type lectins and C-type lectin-like proteins.

1 Introduction

Carbohydrates, most often linked to proteins or lipids, cover the surface of all living cells and are fundamental determinants of health and disease. Carbohydrate-binding proteins or lectins interact with glycans in specific ways, eliciting many important cellular responses including those involved in immune cell homeostasis. The Ca^{2+}-dependent or C-type lectins are the largest and most diverse lectin family found in animals (Zelensky and Gready 2005; Drickamer and Taylor 2015). Well-studied members include galectin and siglec in mammals. C-type lectins share highly homologous structural modules in their carbohydrate recognition domains. These domains are ubiquitously found both in soluble and membrane proteins. More than 100 human proteins contain at least one C-type lectin domain. The C-type lectin family is subdivided into 16 groups (Groups 1–16) based on phylogenetic relationships and domain architecture (Cummings and McEver 2015) (Fig. 1a). Most of these groups have a single C-type lectin domain. Exceptions with 8–10 C-type lectin domains in their polypeptides (e.g. macrophage mannose receptor and DEC-205) are found in Group 6. Also, many proteins have C-type lectin domains that lack the conserved Ca^{2+} binding site, designated as "C-type lectin-like domains," and thus do not always bind carbohydrate ligands (e.g., Group 5 in Fig. 1a). This has allowed for distinction between sugar-binding C-type lectins and the broader family of C-type lectin-like domains (Zelensky and Gready 2005).

C-type lectins accept a wide variety of carbohydrate and non-carbohydrate ligands such as lipids and proteins via their lectin or lectin-like domains. Some C-type lectins play specific roles in glycoconjugate recognition, with the aglycon moiety of the ligand often contributing to the interaction. From an immunological point of view, various C-type lectins work as pattern recognition receptors (PRRs) which recognize highly conserved specific molecular signatures called pathogen-associated molecular patterns (PAMPs) and damage-associated molecular patterns (DAMPs) that are crucial for discrimination of self from non-self (Varki 2017; Sancho and Reis e Sousa 2013). In order to understand the physiological roles of C-type lectins in detail, 3D structural information is essential. We describe our current knowledge of the carbohydrate recognition mechanism of C-type lectins at monosaccharide, oligosaccharide, and polysaccharide levels.

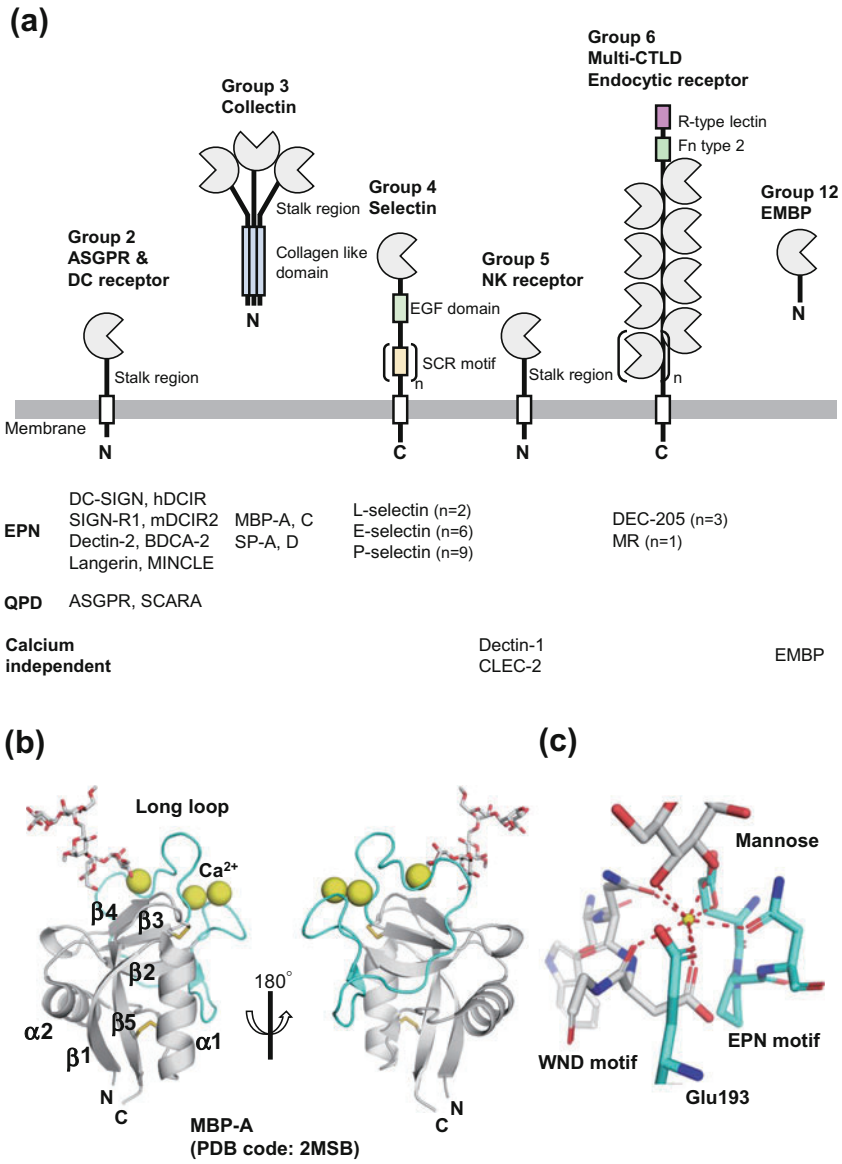

Fig. 1 **a** Domain architecture of representative C-type lectin-containing proteins described in this issue. This figure is prepared from the review (Zelensky and Gready 2005) with modifications. C-type lectins are classified into three sugar-binding motifs (EPN, QPD, and calcium independent). Fn type 2: Fibronectin type 2, SCR: Short consensus repeat, EGF: Epidermal Growth Factor, ASGPR: Asialoglycoprotein receptor, SRACLA: scavenger receptor C-type lectin. **b** Overall structure of C-type lectin domain (Rat mannose binding protein A (MBP-A), *PDB code* 2MSB). Polypeptide, carbohydrate and calcium ions are shown in ribbon, stick, and sphere models, respectively. The long loop region is colored in cyan. Disulfide bonds are shown in yellow stick model. **c** Close-up view of the primary binding site of MBP-A. The coordination and hydrogen bonds are depicted with red dotted lines

2 C-Type Lectin Fold

Since the pioneering work on the mannose-binding protein was reported (Weis et al. 1992), hundreds of atomic structures have been elucidated for C-type lectins. As of July 2019, over 250 atomic structures of C-type lectins were deposited in the Protein Data Bank. Overall fold and disulfide bond pattern are highly conserved among C-type lectins and C-type lectin-like domains. The C-type lectin domain is typically composed of 110–130 amino acid residues and the overall fold is formed by two α-helices and six or seven β-strands forming two antiparallel β-sheets (Fig. 1b). A long loop is found around the "top face" and inserted between two β-strands (β2 and β3 in typical cases). This loop is characteristic of C-type lectins, playing crucial roles in calcium coordination and sugar recognition (colored in cyan in Fig. 1b). C-type lectin domains accept one to four calcium ions (Zelensky and Gready 2005). The sugar-binding calcium ion is located at the top face of the C-type lectin domain. In the sugar-binding site, the calcium ion makes coordination bonds with both the lectin domain and bound monosaccharide (Fig. 1c). The other calcium ions mainly stabilize the 3D structure and occasionally form a secondary sugar-binding site.

3 Sugar Binding Motifs: EPN and QPD

A calcium ion forms multiple coordination bonds with amino acid residues that are well conserved among C-type lectins. The residues that define the sugar binding are called motifs. The asparagine and aspartate from the WND (Trp-Asn-Asp) motif and one carbonyl side chain (Glu side chain in Fig. 1c) form coordination bonds with Ca^{2+} in all C-type lectins. In addition, the EPN (Glu-Pro-Asn) or QPD (Gln-Pro-Asp) motif contributes to calcium coordination and forms the sugar-binding site. These motifs have two carbonyl groups separated by a proline residue. Two adjacent hydroxyl groups from a monosaccharide make coordination bonds with the calcium ion and hydrogen bonds with the EPN or QPD motif (Zelensky and Gready 2005). C-type lectin-like domains lack these conserved motifs and do not bind a calcium ion.

EPN and QPD motifs define the monosaccharide specificity of C-type lectins. Hence, C-type lectins can be classified into three groups: (i) EPN motif-containing C-type lectins, (ii) QPD motif-containing C-type lectins, and (iii) C-type lectin-like domains without these two motifs. EPN motif-containing C-type lectins usually accept D-mannose, D-glucose, L-fucose, and *N*-acetyl-D-glucosamine (GlcNAc) through equatorial 3-OH and 4-OH groups (left panel in Fig. 2a). In contrast, QPD motif-containing C-type lectins bind *N*-acetyl-D-galactosamine (GalNAc) and D-galactose through equatorial 3-OH and axial 4-OH groups (right panel in Fig. 2a). In both cases, bound monosaccharide is stabilized through hydrogen bonds with the carboxyl ($–COO^-$) and amide (–CONH) groups from these motifs. Importantly,

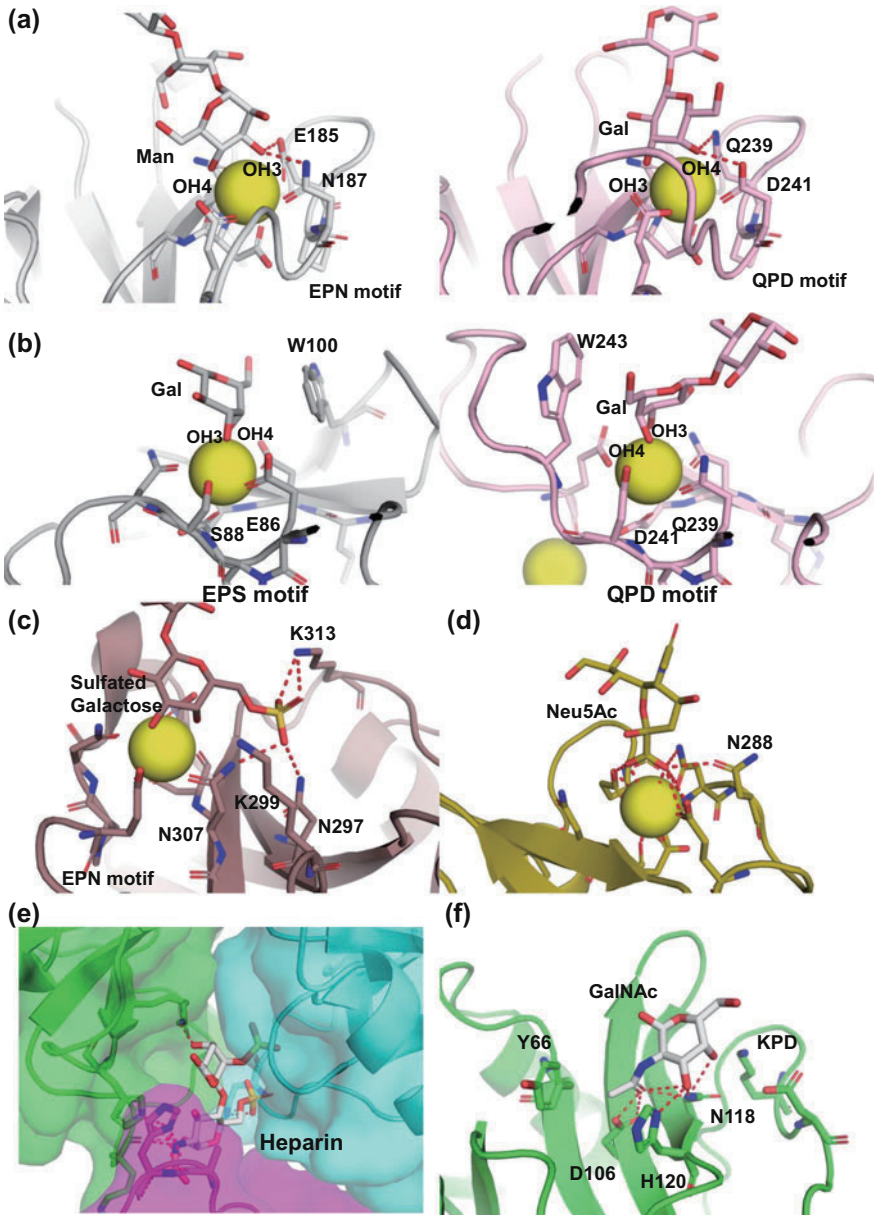

hydrogen donors and acceptors are switched in the two cases. In this way, the hydrogen bond network defines the position and orientation of the bound monosaccharide. In fact, replacing the EPN motif with QPD in mannose binding protein A (MBP-A) changes the binding ability to favor galactose. This result proves the role of these motifs in monosaccharide specificity (Drickamer 1992). In a

◂**Fig. 2** **a** Monosaccharide recognition by EPN (MBP-A, *PDB code* 2MSB, left panel) and QPD motifs (ASGPR, *PDB code* 5JPV, right panel). The amino acid residues which contribute to calcium ion coordination and sugar binding are shown in stick models. The positions of EPN and QPD motifs are indicated. **b** Galactose recognition by TC14 (*PDB code* 1TLG, left panel) and ASGPR (*PDB code* 5JPV, right panel). The tryptophan residues (W100 in TC14 and W243 in ASGPR) are shown in stick model and make stacking interactions with galactose rings. **c** Sulfated galactose recognition by langerin (*PDB code* 3P5I). The amino acid residues interacting with the sulfate group are highlighted. **d** Sialic acid recognition by murine SIGN-R1 (*PDB code* 4CAJ). Coordination and hydrogen bonds are depicted with red dotted lines. An additional hydrogen bond with asparagine (N288) is also shown. **e** Heparin disaccharide recognition by EMBP (*PDB code* 2BRS). One disaccharide unit (colored in white) is surrounded by three EMBP molecules (shown in semitransparent surface models, and colored in green, cyan, and magenta). Direct intermolecular hydrogen bonds are shown in red dotted lines. **f** Calcium-independent GalNAc recognition by SPL-2 (*PDB code* 6A7S). Direct intermolecular hydrogen bonds are shown in red dotted lines. Y66 contacts the GalNAc residue

ligand-free form, two water molecules occupy the positions which will be taken over by 3-OH and 4-OH groups of the binding sugar residue, forming an eight-coordinated calcium ion (Ng et al. 1996; Feinberg et al. 2000). The orientation of the sugar ring at the primary binding site is affected by the surrounding amino acid residues. Occasionally, the bound sugar occurs as a mixture of the two orientations in a single crystal structure (Ng et al. 2002).

3.1 Other Monosaccharide Binding Modes

Monosaccharide specificities of C-type lectins are generally defined by these two motifs, but there are several known exceptions. A tunicate lectin TC14 from *Polyandrocarpa misakiensis* has an EPS motif and a sea cucumber lectin CEL-IV from *Cuvumaria echinate* has the EPN motif. Contrary to the motif rule, they bind galactose at the primary binding site (Poget et al. 1999; Hatakeyama et al. 2011). In each structure, a tryptophan side chain stacks with the apolar face of the galactose ring (left panel in Fig. 2b). In the case of galactose recognition by the QPD motif, the sugar is typically stabilized with the tryptophan side chain, which is located on the opposite side (right panel in Fig. 2b). Consequently, the orientation of the galactose ring observed in TC14 and CEL-IV is inverted compared with the typical galactose-QPD motif interaction.

A second example is the mammalian C-type lectin receptor langerin which is expressed on Langerhans cells and mediates carbohydrate-dependent uptake of pathogens. Langerin has an EPN motif but, atypically, it accepts glycans with terminal 6-sulfated galactose. A crystal structure of langerin complexed with $6SO_4$-Galβ1-4GlcNAc shows that the galactose residue coordinates a calcium ion and the sulfate group forms salt bridges with two lysine residues located close to the primary binding site. This electrostatic interaction appears to compensate for the

nonoptimal binding of galactose with the EPN motif (Fig. 2c) (Feinberg et al. 2011).

Another exception is the interaction between SIGN-R1 and sialic acid (Neu5Ac) (Silva-Martin et al. 2014). SIGN-R1, also known as CD209a, is a murine C-type lectin receptor with an EPN motif and is expressed in myeloid cells. A crystal structure of SIGN-R1 in complex with Neu5Ac shows that the carboxylic group, not the hydroxyl groups, of the sialic acid makes coordination bonds with the calcium ion of SIGN-R1 and hydrogen bonds with adjacent amino acid residues (Fig. 2d). One asparagine residue (N288) contributes to sialic acid binding, independent of calcium coordination.

C-type lectin-like domains without an EPN or QPD motif are predicted to lack typical sugar-binding ability. Nevertheless, several do bind carbohydrate ligands. For instance, the eosinophil major basic protein (EMBP) is a constituent of the eosinophil secondary granule and has a C-type lectin-like domain. Surface plasmon resonance assay demonstrated that EMBP directly binds to heparin and heparan sulfate, but not to hyaluronic acid (Swaminathan et al. 2005). A crystal structure of human EMBP in complex with heparin disaccharide has been reported (Swaminathan et al. 2005). The authors introduced the disaccharide ligand by soaking into ligand-free crystals. Three EMBP molecules in the crystal lattice contact one heparin disaccharide unit. The major contact site is located close to the primary binding site of typical C-type lectins and the bound disaccharide unit is mainly stabilized by electrostatic interactions and hydrogen bonds (Fig. 2e).

One more example is the bivalve lectins SPL-1 and SPL-2, which show high affinities for GlcNAc or GalNAc containing glycans. Intriguingly, RPD and KPD motifs are found in SPL-1 and SPL-2, instead of EPN or QPD. Crystal structures of SPL-2 in complex with GalNAc demonstrated that the sugar binds near the putative primary binding site. However, the interaction mode is different from typical sugar binding via an EPN or QPD motif (Unno et al. 2019). 3-OH and 4-OH groups of GalNAc make hydrogen bonds with the putative primary binding site of the C-type lectin, and the acetamido group is sandwiched by tyrosine and histidine side chains via a stacking interaction (Fig. 2f).

A shrimp C-type lectin MjGCTL has a QAP (Gln-Ala-Pro) motif which was predicted to not to have calcium binding ability. However, a recent study shows that the lectin has sugar-dependent hemocyte encapsulation activity (Alenton et al. 2017). The carbohydrate recognition mechanism of this C-type lectin-like domain could be different. Structural analysis of carbohydrate recognition mechanisms with novel motifs will expand our understanding of this lectin family.

4 Oligosaccharide Recognition

C-type lectins have individual specificities despite the high sequence and structural similarities. For instance, langerin binds a diverse range of carbohydrates including high-mannose-type glycan, fucosylated blood group antigens, and glycans with

terminal 6-sulfated galactose. Meanwhile, a C-type lectin receptor DCAR specifically recognizes phosphatidylinositol mannoside (PIM), a mycobacteria glycolipid, promoting a Th1 response during infection (Toyonaga et al. 2016). A fundamental question is how highly conserved C-type lectins recognize various types of glycan ligands.

Monosaccharide binding preference is defined by an EPN or QPD motif, while the specificity toward oligo- and polysaccharides is determined by the secondary binding site which is located near the primary binding site. The amino acid residues coordinating calcium ions are highly conserved, while the amino acid residues located within ~15 Å from calcium ion are less so. In particular, the secondary binding site is often formed by amino acid residues on the top face, where three β-strands (β2–β4), the long loop region and a part of two α-helices are located. The specific residues in the secondary binding site usually contribute additional interactions, or conversely, work to discourage binding of certain ligands.

From a structural aspect, it is important to understand how each C-type lectin attains specificity for the target glycan. To get a broader picture, 3D structures of C-type lectin domains in complexes with oligosaccharide ligands were extracted from the PDB and these are summarized in Table 1. In this chapter, we describe the structural basis for the specific oligosaccharide recognition mechanism of C-type lectins.

Table 1 List of 3D structures of C-type lectins and C-type lectin-like domains complexed with glycan ligands. The glycan complex structures were extracted to include more than just the disaccharide units. Crystal structures of C-type lectins in ligand free forms and complexed with monosaccharide or non-carbohydrate ligands were omitted

Receptor	Source	Ligand	PDB ID	References
(i) EPN motif				
High-mannose-type N-glycan				
MBP-A	Rat	Man_5	2MSB	Weis et al. (1992)
MBP-A	Rat	Manα1-3Man	1KWY	Ng et al. (2002)
MBP-A (H189V)	Rat	Manα1-3Man	1KWZ	Ng et al. (2002)
MBP-A	Rat	$Man_6GlcNAc_2$	1KX1	Ng et al. (2002)
SP-D	Human	Manα1-2Man	3G83	Crouch et al. (2009)
SP-D (R343V)	Human	Manα1-2Man	3G84	Crouch et al. (2009)
DC-SIGN	Human	Man_4	1SL4	Guo et al. (2004)
DC-SIGN	Human	Man_6	2IT5	Feinberg et al. (2007)
DC-SIGN	Human	Man_2	2IT6	Feinberg et al. (2007)
DC-SIGN	Human	Pseudo-dimannose mimic	2XR5	Sutkeviciute et al. (2014)

(continued)

Table 1 (continued)

Receptor	Source	Ligand	PDB ID	References
DC-SIGN	Human	Pseudo-trimannose mimic	2XR6	Sutkeviciute et al. (2014)
Dectin-2	Human	Man_9	5VYB	Feinberg et al. (2017)
L-selectin	Human	$Man_5GlcNAc_2$	5VC1	Wedepohl et al. (2017)
L-selectin	Human	$Man_5GlcNAc_2$	3CFW	Mehta-D'souza et al. (2017)
Langerin	Human	Manα1-3Man (Man_5)	3P5D	Feinberg et al. (2011)
Langerin	Human	Manα1-2Man	3P5F	Feinberg et al. (2011)
Complex-type *N*-glycan				
DC-SIGN	Human	$GlcNAc_2Man_3$	1K9I	Feinberg et al. (2001)
DC-SIGNR	Human	$GlcNAc_2Man_3$	1K9 J	Feinberg et al. (2001)
hDCIR	Human	GlcNAcβ1-2Man	5B1X	Nagae et al. (2016)
mDCIR2	Mouse	Bisected glycan	3VYK	Nagae et al. (2013)
BDCA-2	Human	Galβ1-4GlcNAcβ1-2Man	4ZET	Jegouzo et al. (2015)
Codakine	Bivalve	Biantennary glycan	2VUZ	Gourdine et al. (2008)
SP-D	Porcine	Biantennary glycan	6BBE	van Eijk et al. (2018)
Fucose-containing glycan				
P-selectin	Human	PSGL-1	1G1S	Somers et al. (2000)
P-selectin	Human	Sialyl-$Lewis^X$ (soaked)	1G1R	Somers et al. (2000)
E-selectin	Human	Sialyl-$Lewis^X$ (soaked)	1G1T	Somers et al. (2000)
DC-SIGN	Human	Lacto-*N*-fucopentaose III	1SL5	Guo et al. (2004)
DC-SIGNR	Human	$Lewis^X$	1SL6	Guo et al. (2004)
MBP-A (K3)	Rat	3'-NeuAc-Le^X	2KMB	Ng and Weis (1997)
MBP-A (K3)	Rat	3'-sulfo-Le^X	3KMB	Ng and Weis (1997)
MBP-A (K3)	Rat	4'-sulfo-Le^X	4KMB	Ng and Weis (1997)
E-selectin	Human	Sialyl-$Lewis^X$	4CSY	Preston et al. (2016)
Langerin	Human	Galα1-3[Fucα1-2]Gal	3P5G	Feinberg et al. (2011)
Glucose-containing glycan				
SP-D	Human	Maltose	1PWB	Shrive et al. (2003)
Mincle	Cow	Trehalose (Glcα1-α1Glc)	4KZV	Feinberg et al. (2013)
Mincle	Cow	Trehalose monobutylate	4ZRV	Feinberg et al. (2016)

(continued)

Table 1 (continued)

Receptor	Source	Ligand	PDB ID	References
Mincle	Cow	Trehalose	4ZRW	Feinberg et al. (2016)
Mincle	Cow	KMJ1	5KTI	Feinberg et al. (2016)
Mincle	Cow	Brartemicin	5KTH	Feinberg et al. (2016)
Langerin	Human	Laminaritriose	3P5H	Feinberg et al. (2011)
Langerin	Human	Maltose (Glcα1-4Glc)	3P7H	Chatwell et al. (2008)
SIGN-R1	Mouse	Dextran sulfate	4C9F	Silva-Martin et al. (2014)
Others				
CEL-IV	Sea cucumber	Raffinose (Galα1-6Glcβ1-2Fru)	3ALU	(Hatakeyama et al. 2011)
CEL-IV	Sea cucumber	Melibiose (Galα1-6Glc)	3ALT	Hatakeyama et al. (2011)
Langerin	Human	$6SO_4$-Galβ1-4GlcNAc	3P5I	Feinberg et al. (2011)
Langerin	Human	GlcNAcβ1-3Galβ1-4Glc	4N33	Feinberg et al. (2013)
Langerin	Human (K313I)	GlcNAcβ1-3Galβ1-4Glc	4N35	Feinberg et al. (2013)
Langerin	Human (N288D/K313I)	GlcNAcβ1-3Galβ1-4GlcNAc	4N38	Feinberg et al. (2013)
(ii) QPD motif				
RSL	Rattlesnake	Lactose (Galβ1-4Glc)	1JZN	Walker et al. (2004)
SCARA4	Mouse	$Lewis^X$	2OX9	Feinberg et al. (2007)
ASGPR	Human	Lactose (Galβ1-4Glc)	5JPV	Sanhueza et al. (2017)
(iii) C-type lectin-like domains				
EMBP	Human	Heparin	2BRS	Swaminathan et al. (2005)
Dectin-1	Mouse	Glcβ1-3Glcβ1-3Glc	2CL8	Brown et al. (2007)
CLEC-2	Human	*O*-glycosylated podoplanin	3WSR	Nagae et al. (2014)

4.1 Oligosaccharide Recognition via EPN Motif

The structural basis for the specific oligosaccharide recognition of EPN motif-containing C-type lectins has been well studied. Here, we introduce the recognition mechanism of EPN motif-containing C-type lectins toward representative oligosaccharides such as high-mannose type, complex-type *N*-glycans,

sialyl-Lewis^X, and glucose-containing glycans. The primary binding sites of corresponding C-type lectins bind mannose, fucose, and glucose residues of these oligosaccharides, and the secondary binding sites define their specificities.

4.1.1 Oligosaccharide Recognition of EPN Motif-Containing C-Type Lectins Through Mannose

(I) Recognition of high-mannose-type *N*-glycan through mannose

High-mannose-type *N*-glycans are often found in viral and fungal glycoproteins as well as in nascent mammalian glycoproteins. A representative structure of mammalian high-mannose-type *N*-glycan is shown as $Man_9GlcNAc_2$ which contains mannose residues of α1-2, α1-3, and α1-6 linkages (Fig. 3a). The Manα1-2 Man unit is a common terminal structure on mannans of yeast and other fungi. Therefore, this disaccharide unit can be a target for several C-type lectins working as pattern recognition receptors in the immune system. Crystal structures of 16 EPN motif-containing C-type lectins have been reported in complexes with high-mannose-type glycans (Table 1). Of these, mannose-binding protein A (MBP-A) and pulmonary surfactant protein D (SP-D) are soluble proteins categorized as the collectin family (Group 3). DC-specific intercellular adhesion molecule-3-grabbing nonintegrin (DC-SIGN), langerin, and DC-associated C-type lectin-2 (Dectin-2) are type II membrane proteins which belong to the NK receptors family (group 5). L-Selectin is an adhesion receptor of the selectin family (Group 4) (Fig. 1a). The interaction modes of these lectins with high-mannose-type glycans are visualized in Fig. 3b. C-type lectins accept α1-2, 1-3 and 1-6 linkages of the mannose disaccharide unit at their primary binding sites with several variations. In this section, the atomic recognition modes of high-mannose-type glycan are discussed for each glycosidic linkage.

(I-1) Manα1-2Man unit recognition

There are two known binding modes for the α1-2 linkage: (a) mannose at the non-reducing end (non-reducing mannose) bound to the primary site (SP-D wild type and MBP-A in Fig. 3b), and (b) mannose at the reducing end (reducing mannose) bound to the primary site (Dectin-2, SP-D R343 V mutant, DC-SIGN and langerin in Fig. 3b). The surrounding amino acid residues determine the choice of the binding modes. In SP-D, Arg313 is located close to the primary site and the replacement of this arginine with valine dramatically changes the disaccharide binding mode (Crouch et al. 2009). The R343 V mutant accepts reducing mannose at the primary binding site and forms additional hydrogen bonds with the non-reducing mannose via the secondary binding site (Fig. 3b). Compared with mode (a), the orientation of mannose in mode (b) is flipped in the primary binding sites of Dectin-2, SP-D R343 V and DC-SIGN. Dectin-2 mainly recognizes inner mannose residues of Man_7 glycan (Man-A and C) and the disaccharide recognition mode seems similar to that of DC-SIGN. However, in DC-SIGN-Man_2 complex,

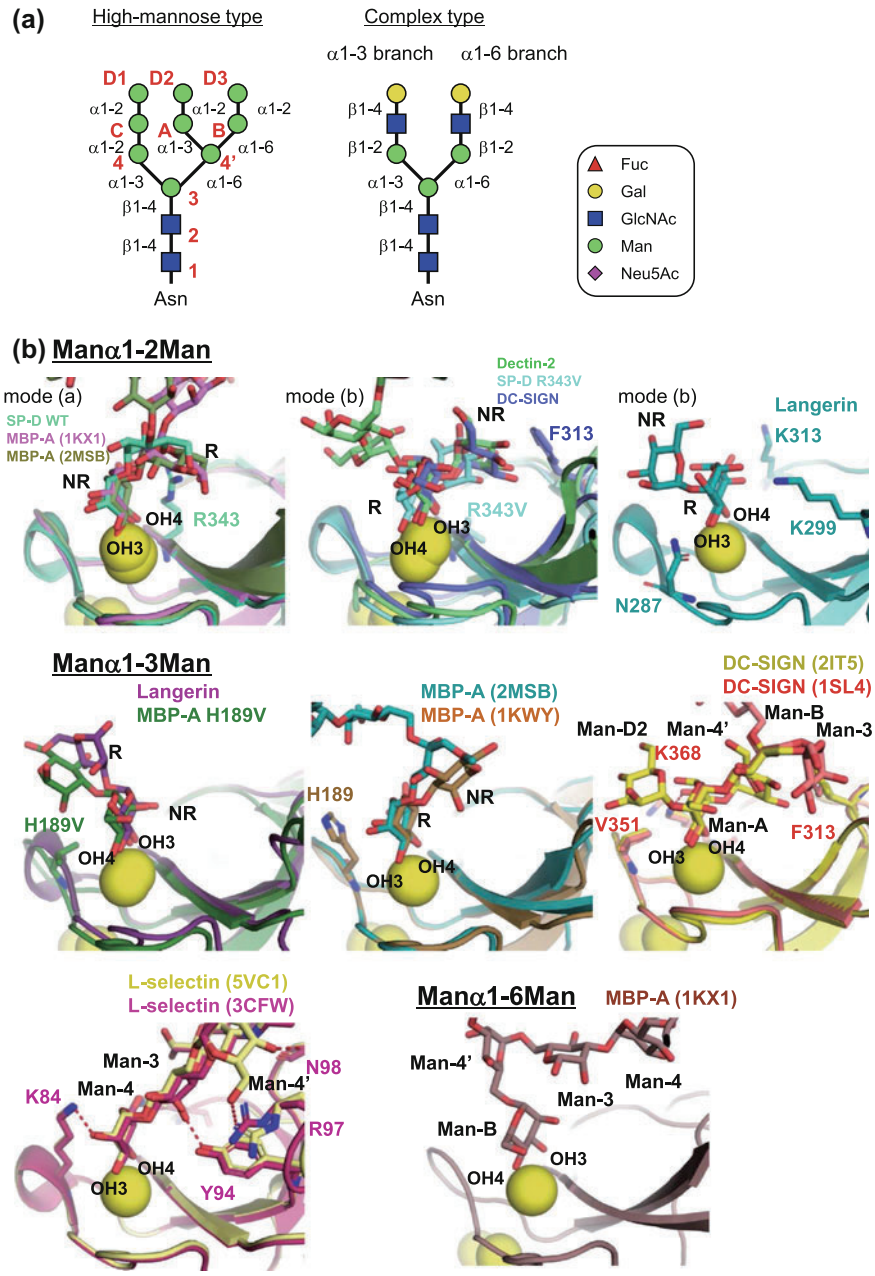
(a)
High-mannose type
Complex type
α1-3 branch
α1-6 branch
D1
D2
D3
α1-2
α1-2
α1-2
C
A
B
α1-2
α1-3
α1-6
4
4'
α1-3
α1-6
3
β1-4
2
β1-4
1
Asn
β1-4
β1-4
β1-2
β1-2
α1-3
α1-6
β1-4
β1-4
Asn
Fuc
Gal
GlcNAc
Man
Neu5Ac
(b) Manα1-2Man
mode (a)
SP-D WT
MBP-A (1KX1)
MBP-A (2MSB)
R
NR
OH4
R343
OH3
mode (b)
Dectin-2
SP-D R343V
DC-SIGN
NR
F313
R
R343V
OH3
OH4
mode (b)
NR
Langerin
K313
R
OH4
K299
OH3
N287
Manα1-3Man
Langerin
MBP-A H189V
R
NR
H189V
OH3
OH4
MBP-A (2MSB)
MBP-A (1KWY)
H189
NR
R
OH4
OH3
DC-SIGN (2IT5)
DC-SIGN (1SL4)
Man-B
Man-D2
Man-4'
Man-3
K368
V351
Man-A
F313
OH4
OH3
L-selectin (5VC1)
L-selectin (3CFW)
Man-3
N98
Man-4
Man-4'
K84
R97
OH4
OH3
Y94
Manα1-6Man
MBP-A (1KX1)
Man-4'
Man-4
Man-3
Man-B
OH3
OH4

◀**Fig. 3** **a** A typical high-mannose-type glycan ($Man_9GlcNAc_2$, left panel) and biantennary complex-type glycan (right panel) linked to asparagine. Monosaccharide symbols follow the SNFG (symbol nomenclature for glycans) system (Varki et al. 2015). The glycosidic linkages and residue numbers are labeled at each position. **b** Summary of the interaction between high-mannose-type glycan and C-type lectins. Structures are classified based on the glycosidic linkages (Manα1-2Man, Manα1-3Man and Manα1-6Man) of the mannose residues. The positions of reducing and non-reducing mannose residues are labeled as "R" and "NR," respectively. The residue names are also labeled. **c** Three cross-linked structures of C-type lectin-high-mannose glycan complexes. Two MBP-A glycan complexes (*PDB code* 2MSB, left and *PDB code* 1KX1, middle panels) and one Dectin-2 complex (*PDB code* 5VYB, right panel) are shown. The mannose residues at the primary binding sites are labeled. **d** Complex-type *N*-glycan recognition by BDCA-2 (*PDB code* 4ZET, left panel), hDCIR (*PDB code* 5B1X, middle panel), and mDCIR2 (*PDB code* 3VYK, right panel). **e** The branch-specific interaction with complex-type *N*-glycan. All four C-type lectins (mDCIR2 (*PDB code* 3VYK), DC-SIGN (*PDB code* 1K9I), Codakine (*PDB code* 2VUZ), and SP-D (*PDB code* 6BBE)) accept mannose residues (Man-4) of the α1-3 branch at the primary binding sites. It should be noted that the relative position of the α1-6 branch of the mDCIR2 complex is different from the other C-type lectins. C-type lectin domains are shown in surface models

2-OH and 3-OH groups of the non-reducing mannose residue are adjacent to phenylalanine (F313 in Fig. 3b), which prevents further extension toward the non-reducing side. A structure of langerin with a Manα1-2Man oligosaccharide has also been described (Fig. 3b right panel), showing that the bound reducing mannose residue is flipped 180° compared with the other complexes in mode (b). Since the reducing mannose residue is clamped between asparagine (N287) and lysine (K299), the 1-OH group cannot be used for extension to a larger glycan. Another conformation has also been reported in which the non-reducing mannose resides in the primary binding site, though the electron density of reducing mannose is missing. Langerin preferentially binds the reducing mannose of the disaccharide, but rather binds the non-reducing end of whole high-mannose glycan.

(I-2) Manα1-3Man unit recognition

C-type lectins can bind the terminal and inner Manα1-3Man unit of *N*-glycan (Fig. 3b). Langerin and MBP-A H189 V mutant recognize the non-reducing mannose residue of Manα1-3Man unit. Langerin Manα1-3Man disaccharide unit complex was obtained by using core Man_5 oligosaccharide (Manα1-3[Manα1-3[Manα1-6]Manα1-6]Man). In this complex, non-reducing mannose tightly interacts with the primary binding site, while the reducing ends are exposed to solvent (Fig. 3b). Wild-type MBP-A recognizes the reducing end of the Manα1-3Man disaccharide unit, and however, introduction of an H189 V mutation causes a change in the bound residue (non-reducing end) as well as a 180° flip of the bound ligand (Ng et al. 2002) (Fig. 3b). The position of this histidine in MBP-A is different from that of R343 in SP-D, indicating that the binding mode is determined by a marginal balance of the surrounding residues.

DC-SIGN recognizes inner α1-3 linked mannose residues. A DC-SIGN-Man_4 (Manα1-3[Manα1-6]Manα1-6Man) complex shows that all four mannose residues (corresponding to Man-A, Man-B, Man-4' and Man-3 in Fig. 3a) are uniquely

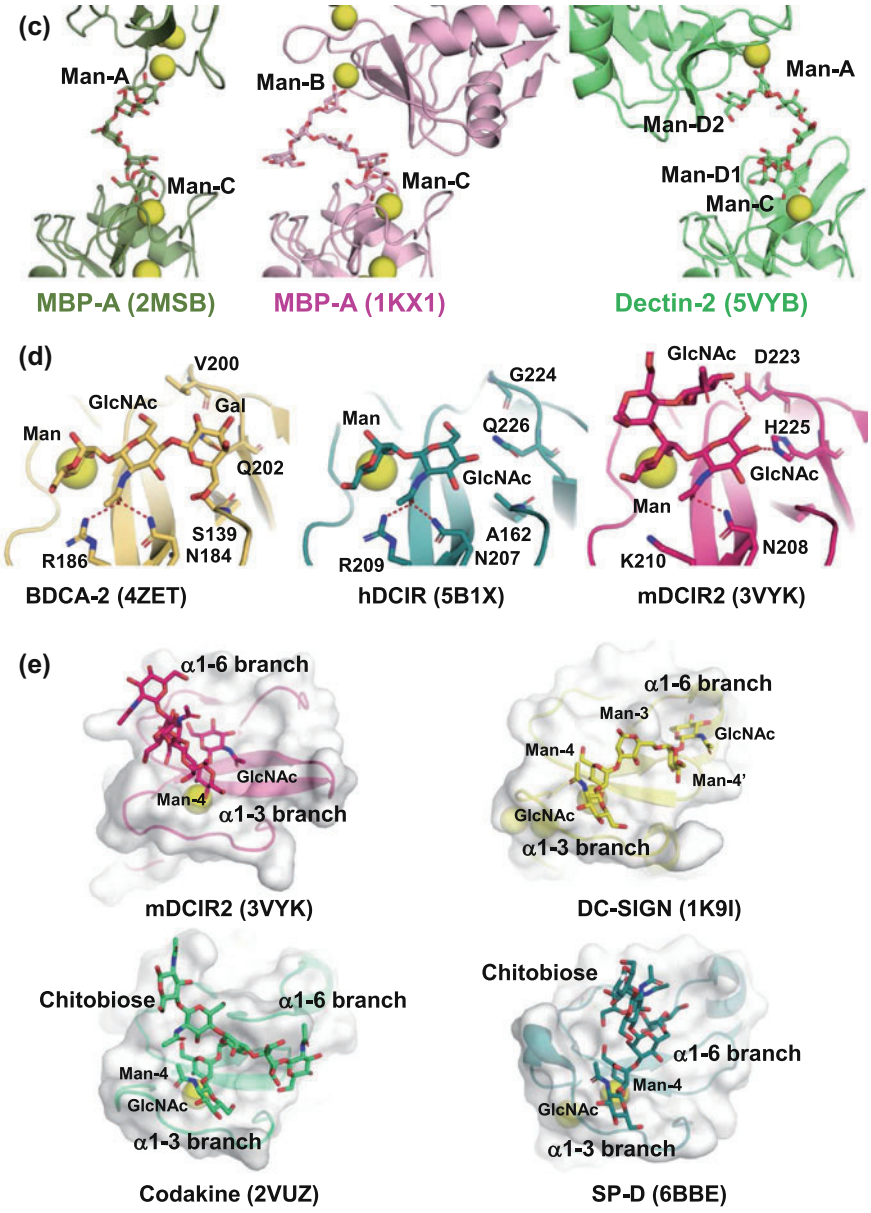

Fig. 3 (continued)

defined. In DC-SIGN-Man_6 (Manα1-2Manα1-3Man[Manα1-2Manα1-6]Man) complex, Manα1-2Manα1-3Man, which is a part of the D2 arm, interacts with DC-SIGN in a major conformation. In addition, only the terminal Manα1-2Man unit (Man-A and Man-D2 residues) binds in a minor conformation. The interaction mode of the major conformation is similar to that of the Man_4 complex and these two glycans are well superimposable (Fig. 3b). This observation indicates that DC-SIGN tightly associates with the inner tetrasaccharide unit (Manα1-2Manα1-3Manα1-6Man) of high-mannose-type glycan. The mannose residue (Man-A in Fig. 3b) coordinates with the calcium ion and both ends of the mannose residues are located at the secondary binding sites. The minor conformation of Man_6 complex is similar to the major conformation of Man_2 complex. Hence, DC-SIGN can recognize the inner α1-3 linked mannose residue as well as terminal α1-2 linked mannose of high mannose glycan. These multiple binding modes of DC-SIGN may enhance its apparent affinity towards glycoproteins carrying high-mannose glycan under physiological conditions.

L-selectin is a member of the selectin family and mediates cell adhesion and signaling in inflammation. A major physiological ligand of L-selectin is thought to be sialyl-$Lewis^X$ (sLe^X) as described in a later section. In addition to this ligand, L-selectin binds inner α1-3 linked mannose residues of high-mannose-type glycan. Interestingly, the binding mode is different from that of DC-SIGN. Crystal structures of *N*-glycosylated L-selectin were reported by two groups (Wedepohl et al. 2017; Mehta-D'souza et al. 2017). In these structures, L-selectin tightly binds to the *N*-glycan ($Man_5GlcNAc_2$) from the symmetry related L-selectin molecule via the sugar-binding site. The mannose at α1-3 branch (Man-4) resides in the primary binding site and the adjacent sugar residues, GlcNAc, β-mannose (Man-3) and α1-6 branched mannose (Man-4'), interact with L-selectin via the secondary binding site (Fig. 3b).

(I-3) Manα1-6Man recognition

To date there is only one example showing the binding mode of α1-6 linked mannose. The 3D structure is obtained from an MBP-A-Man_5 (Manα1-2Manα1-3[Manα1-3Manα1-6]Man) complex (PDB code: 2MSB). Remarkably, one high-mannose -type glycan bridges two MBP-A molecules (discussed in the next section). The Man-B residue at the non-reducing end of the Manα1-6Man unit binds to MBP-A. However, there is no apparent interaction between MBP-A and the mannose at the reducing side (Fig. 3b).

(I-4) Cross-linking by high-mannose-type glycan

High-mannose-type glycan can function as a multivalent ligand for C-type lectins. Three cross-linked structures have been reported so far (Fig. 3c). Two out of three are MBP-A-high-mannose-type glycan complexes, while the other structure is Dectin-2-high-mannose-type glycan complex. Crystal structure of an MBP-A-Man_5 (Manα1-2Manα1-3[Manα1-3Manα1-6]Man) complex (PDB code: 2MSB) shows that one high-mannose-type glycan is simultaneously recognized by two MBP-A molecules (Weis et al. 1992). One MBP-A molecule binds to the Manα1-2Man unit

of the α1-3 branch (especially the Man-C residue), and the other MBP-A molecule binds to the Manα1-3Man unit of the α1-6 branch (Man-A, left panel in Fig. 3c). In both molecules, non-reducing mannose residues occupy the primary binding sites. The other complex, MBP-A-$Man_6GlcNAc_2$ complex, shows that one high-mannose glycan bridges two MBP-A trimers (Ng et al. 2002). In this MBP-A complex, one MBP-A molecule interacts with the Manα1-2Man unit, and the other MBP-A molecule interacts with the Manα1-6Man units of the α1-6 branches (especially the Man-B residue, middle panel in Fig. 3c). Comparing the two MBP-A cross-linked structures, all four MBP-A molecules recognize Man-C residues at the non-reducing end.

The Dectin-2-high-mannose-type glycan complex differs from the MBP-A complexes in terms of glycan binding mode. A crystal structure of Dectin-2 in complex with Man_9 glycan shows that two Dectin-2 molecules sandwich one high-mannose-type glycan (Feinberg et al. 2017). One Dectin-2 recognizes the Manα1-2Man unit (Man-C and D1 residues) of the D1 arm, and the other Dectin-2 molecule interacts with the same disaccharide unit (Man-A and D2 residues) of the D2 arm (right panel in Fig. 3c). The interaction modes of the two Dectin-2 molecules are the same. The reducing end of the disaccharide resides in the primary binding site, while the non-reducing end is located at the secondary binding site. The recognition mode of inner mannose residues seems suitable for binding fungal mannans which have variable structures at their non-reducing ends.

(II) Complex-type *N*-glycan recognition via mannose

Complex-type *N*-glycan is synthesized from high-mannose-type glycan by a series of enzymatic processes (Fig. 3a). Several C-type lectin receptors encoded in the Dectin-2 cluster on the natural killer gene complex preferentially interact with complex-type *N*-glycans, such as blood DC antigen 2 (BDCA-2), human DC immunoreceptor (hDCIR), and murine DCIR2 (mDCIR2) (Fig. 1a). These C-type lectins share high amino acid sequence identities; however, their ligand preferences are slightly different.

BDCA-2 binds to galactose-terminated biantennary glycans, defining an epitope found on a limited number of bi- and triantennary glycans (Riboldi et al. 2011). Unusually, BDCA-2 with an EPN motif binds galactosylated glycan. A crystal structure shows why. BDCA-2 primarily recognizes a mannose residue of the trisaccharide unit (Galβ1-4GlcNAcβ1-2Man) with a serine residue (S139) and additional interactions define the specificity between BDCA-2 and Galβ1-4GlcNAc (Fig. 3d (Jegouzo et al. 2015)).

In contrast, human DCIR (hDCIR) binds to GlcNAc-terminated biantennary *N*-glycan. The binding mode of hDCIR toward the disaccharide unit (GlcNAcβ1-2Man) is similar to that of BDCA-2 [Fig. 3d, (Nagae et al. 2016)]. However, the serine residue (S139) interacting with galactose in BDCA-2 is not conserved in hDCIR (A162). This indicates that the specificity is defined by the additional interaction with the terminal glycan residue.

BDCA-2 and hDCIR can interact with both α1-3 and α1-6 arms of biantennary complex-type *N*-glycan. mDCIR2 has unique specificity toward GlcNAc-

terminated biantennary glycan with bisecting GlcNAc (Nagae et al. 2013). mDCIR2 shows arm preference, and the galactosylation of the α1-3 branch strongly inhibits binding. A crystal structure of a mDCIR2-bisected glycan complex demonstrated that mDCIR2 strictly recognizes the disaccharide unit (GlcNAcβ1-2Man) of the α1-3 arm as well as bisecting GlcNAc (Fig. 3d). The binding mode of GlcNAcβ1-2Man is similar to those of BDCA-2 and hDCIR. However, aspartate (D223) tightly interacts with the bisecting GlcNAc (Fig. 3d), which is not conserved in BDCA-2 or hDCIR. Due to the simultaneous interaction with both GlcNAcβ1-2Man and bisecting GlcNAc, mDCIR2 selects the α1-3 branch. Such simultaneous interaction is impossible using the α1-6 branch because it is located slightly too far from the bisecting GlcNAc.

As described in the previous paragraph, DC-SIGN (and DC-SIGNR) preferentially interact with high-mannose-type glycans and 3D structures of DC-SIGN have been reported bound to high-mannose glycan. Additionally, DC-SIGN and DC-SIGNR bound to complex-type glycans have been reported (Feinberg et al. 2001). The interaction modes of these receptors are different from those of BDCA-2, hDCIR, and mDCIR2. The mannose residue of the α1-3 branch (Man-4) coordinates a calcium ion, but the orientation is flipped compared with the mDCIR2-bisected glycan complex (Fig. 3e). The GlcNAc residue of the α1-3 branch is located away from the secondary binding site due to this flipping and the α1-6 branch is located on the surface of DC-SIGN. The mannose (Man-4') and GlcNAc residues of the α1-6 branch form hydrogen bonds with DC-SIGN.

The bivalve lectin, codakine, from *Codakia orbicularis* binds a biantennary complex-type glycan (Gourdine et al. 2008). The binding mode of codakine is similar to that of DC-SIGN rather than mDCIR2 (Fig. 3e). The α1-3 branched mannose (Man-4) makes coordination bonds with a calcium ion and the α1-6 branch interacts with codakine via its secondary binding site.

A crystal structure of glycosylated porcine SP-D demonstrates that the sugar-binding site of SP-D accepts complex-type *N*-glycan attached on symmetry-related SP-D (van Eijk et al. 2018). The interaction mode is similar to those of DC-SIGN and codakine. The α1-6 branch is strongly kinked, possibly due to crystal packing (Fig. 3e).

4.1.2 Oligosaccharide Recognition of EPN Motif-Containing C-Type Lectins Through Fucose

C-type lectins primarily recognize mannose residues of high-mannose and complex-type *N*-glycans. In contrast, several C-type lectins such as selectins recognize the OH3 and OH4 groups of the fucose residue in sialyl-Lewis^X (sLe^X, Neu5Acα2-3Galβ1-4[Fucα1-3]GlcNAcβ1-R). sLe^X is a terminal component of *N*- and *O*-glycans on hematopoietic and endothelial cells. L-selectin prefers sLe^X modified with sulfate on the GlcNAc residue. Selectins are expressed on vascular endothelium, platelets, or leukocytes and bind to cell surface glycoproteins harboring sLe^X glycans such as PSGL-1. Upon ligand binding, selectins show the

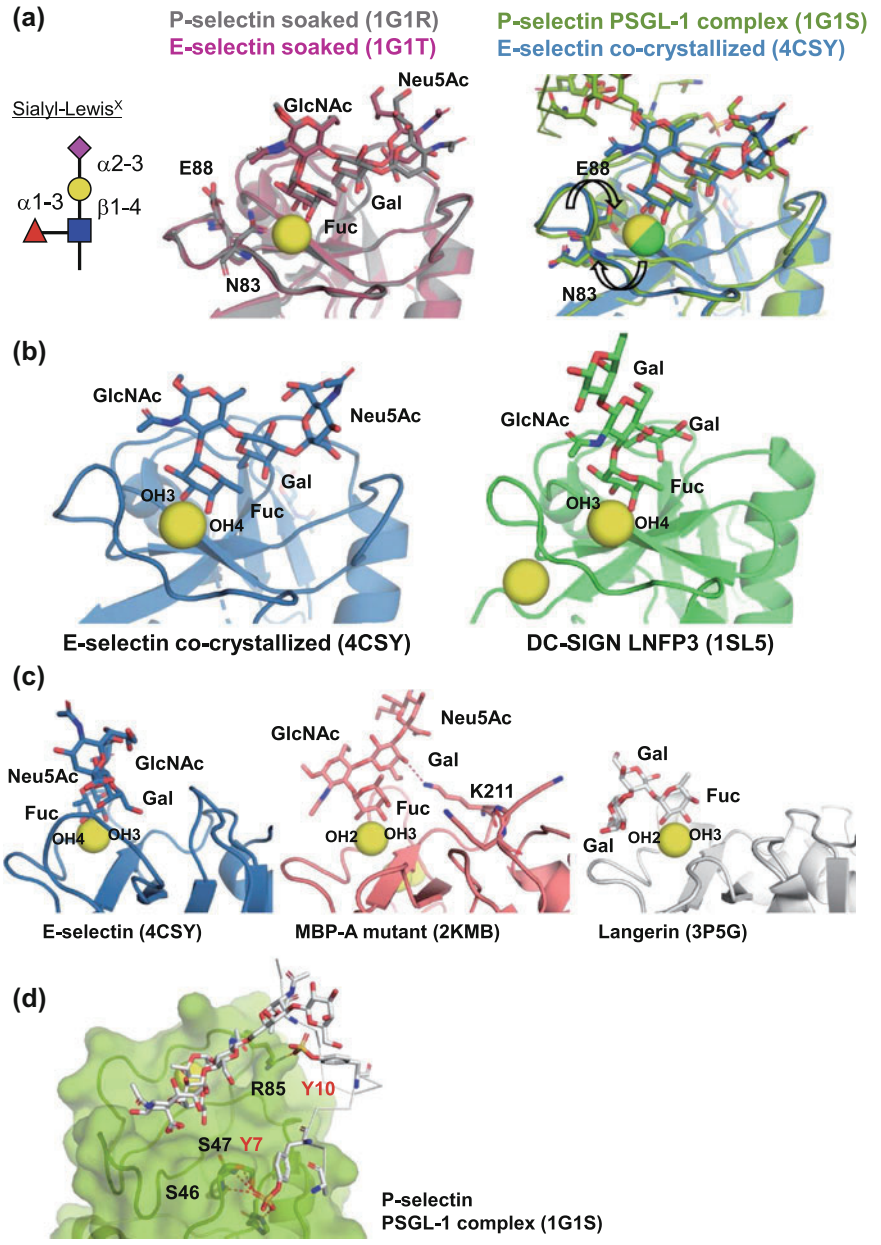

catch-bond behavior which is essential for initial tethering and rolling along the vascular endothelium and subsequent firm adhesion (Kansas 1996).

Crystal structures of E- and P-selectins complexed with sLe^X have been reported (Somers et al. 2000; Preston et al. 2016). These lectins recognize a fucose residue at

◀**Fig. 4** **a** Sialyl-Lewis^X recognition by P- and E-selectins. Bent conformations (low affinity state) of P-selectin (*PDB code* 1G1R) and E-selectin (*PDB code* 1G1T) are shown in left panel. Extend conformations (high affinity state) of P-selectin (*PDB code* 1G1S) and E-selectin (*PDB code* 4CSY) are shown in right panel. Two amino acid residues (N83 and E88) which take different positions in two conformations are shown in stick models. **b** Structural superposition of E-selectin-sialyl-Lewis^X complex (*PDB code* 4CSY, left panel) and DC-SIGN-LNFP3 complex (*PDB code* 1SL5, right panel). **c** Structural comparisons between E-selectin (*PDB code* 4CSY), MBP-A K3 mutant (*PDB code* 2KMB) and Langerin (*PDB code* 3P5G) in complexes with fucose-containing glycans. **d** Aglycon recognition observed in P-selectin-PSGL-1 complex (*PDB code* 1G1S). The interactions between P-selectin and sulfated tyrosine residues of PSGL-1 are highlighted and labeled. The P-selectin molecule is shown in surface model

the primary binding site and form additional interactions with adjacent residues (GlcNAc, Gal, and Neu5Ac). A structural comparison of four structures shows that the positions of fucose, GlcNAc, and Gal are well superimposable, while the position of the terminal Neu5Ac is variable (Fig. 4a). Interestingly, a 3D structural difference is observed between sLe^X co-crystallized and soaked complexes. In the soaked complexes, asparagine (N83) makes coordination bonds with the calcium ion (left panel in Fig. 4a). In contrast, glutamate (E88) makes coordination bonds with the calcium ion in co-crystallized complexes (right panel in Fig. 4a). This difference causes a positional shift of the flexible loop, leading to a global conformational change from bend (low affinity) to extend (high affinity) forms. The glutamate is therefore a key residue in stabilizing the high affinity conformation (Mehta-D'souza et al. 2017).

The structure of L-selectin in complex with high-mannose-type glycan is similar to the co-crystallized complex, rather than the sLe^X soaked complex, even though it assumes a bend conformation (Fig. 3b). The glutamate coordinates with the calcium ion and the flexible loop takes a similar position as in the co-crystallized complex.

Other C-type lectins, such as DC-SIGN, MBP-A mutant, and langerin, also bind to fucose-containing glycans. A crystal structure of DC-SIGN in complex with lacto-*N*-fucopentaose III (Galβ1-4[Fucα1-3]GlcNAcβ1-3Galβ1-4Glc) shows that the position of the fucose coincides well with those of selectins. However, the positions of GlcNAc and galactose are slightly different. This subtle difference may be derived from differences in the secondary binding site of DC-SIGN (Fig. 4b).

The introduction of a triple mutation (K211-K212-K213) in MBP-A (K3 mutant) enables it to accept a series of Lewis^X glycans as P- and E-selectins do (Ng and Weis 1997). However, the binding mode is quite different from those of selectins and DC-SIGN (middle panel in Fig. 4c). In this case, 2-OH (equatorial) and 3-OH (equatorial) groups of the fucose make coordination bonds with the calcium ion. One of three lysine residues (K211) makes a hydrogen bond with the galactose residue.

The fucose recognition mode of langerin is also different from those of selectins and DC-SIGN (Feinberg et al. 2011). In the structure of langerin-blood group B trisaccharide (Galα1-3[Fucα1-2]Gal) complex, 2-OH and 3-OH groups of the fucose residue also coordinate with the calcium ion (right panel in Fig. 4c).

The aglycon moiety of PSGL-1 contributes to the specific interaction with selectins. Of particular note, the physiological interaction between human P-selectin and PSGL-1 requires both sLe^X capped core 2 *O*-glycan and one or more sulfated tyrosine residues in the N-terminal region of PSGL-1. In the crystal structure (Somers et al. 2000), human P-selectin recognizes both the sLe^X attached to threonine and the sulfated tyrosine residues of human PSGL-1 (Fig. 4d). P-selectin also binds to the N-terminus of murine PSGL-1, although the sequence is different from human PSGL-1. Cell-based biochemical assays suggest that sulfation of tyrosine (Y13) and the *O*-glycan on T17 are necessary for murine PSGL-1 to bind optimally to P-selectin (Xia et al. 2003). The spacing of these residues in the sequence is considerably closer than the corresponding residues in the human PSGL-1 sequence (Y7, Y10 and T16). It is likely that murine PSGL-1 binds to P-selectin using a different conformation of the polypeptide.

4.1.3 Oligosaccharide Recognition of EPN Motif-Containing C-Type Lectins Through Glucose

A representative glucose specific C-type lectin is Macrophage inducible calcium-dependent lectin (Mincle), also known as CLEC4E. Mincle is expressed on macrophages and interacts with trehalose-6-6′-dimycolate (TDM), a glycolipid found on the surface of *Mycobacterium tuberculosis* (Matsunaga and Moody 2009; Ishikawa et al. 2009). TDM comprises a trehalose (Glcα1-α1Glc) headgroup and two complex branched and hydroxylated acyl chains. The acyl chains are attached to the 6-OH groups of each of the sugar residues. Crystal structures of bovine Mincle C-type lectin domains in complexes with a series of ligands allow visualization of the interaction modes with glycolipids. A Mincle–trehalose complex structure shows that both glucose residues interact tightly with Mincle. The 3-OH and 4-OH of one glucose coordinate with the calcium ion and the second glucose contacts a second binding site via hydrogen bonds (Feinberg et al. 2013) (Fig. 5a). The additional interaction of the aglycon moiety, such as the lipid part, should greatly improve the specificity. The Mincle–trehalose monobutyrate complex shows that the alkyl chain is located near the hydrophobic groove of Mincle (Feinberg et al. 2016). These hydrophobic residues likely form the extended binding site for the lipid moiety.

In addition to Mincle, langerin, SP-D, and SIGN-R1 can bind glucose residues at their primary binding sites. The structure of a langerin-laminaritoriose (Glcβ1-3Glcβ1-3Glc) complex contrasts markedly with the Mincle–trehalose complex structure. In the langerin complex, the 1-OH and 2-OH of the glucose at the reducing end resides in the primary binding site and the other glucose at the non-reducing end points away towards solvent (Feinberg et al. 2011) (Fig. 5b). The langerin–maltose (Glcα1-4Glc) complex reveals that the 3-OH and 4-OH of glucose at the reducing end also coordinate with the calcium ion, but the orientation is totally flipped compared with that in the Mincle–treharose complex (Chatwell et al. 2008). The glucose at the non-reducing end is also exposed to solvent (Fig. 5c).

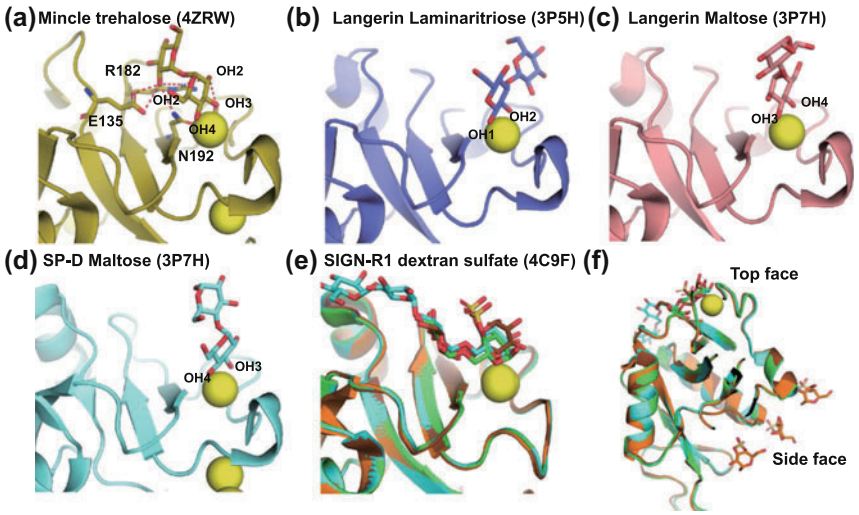

Fig. 5 Glucose recognition mechanism of EPN motif-containing C-type lectins: **a** Mincle-trehalose complex (*PDB code* 4ZRW). **b** Langerin-laminaritriose complex (*PDB code* 3P5H). **c** Langerin-maltose complex (*PDB code* 3P7H). **d** SP-D-maltose complex (*PDB code* 3P7H). **e** Dextran sulfate recognition of SIGN-R1 (*PDB code* 4C9F). Four complexes in the asymmetric unit are superimposed. **f** Two sugar-binding sites (top face and side face) of SIGN-R1 (*PDB code* 4C9F)

In contrast, the orientation of glucose in a SP-D-maltose complex is the same as in the Mincle complex (Fig. 5d). A crystal structure of SIGN-R1 in complex with oligo-dextran sulfate (α1-3 and α1-6 linked glucose polymer with sulfation) demonstrates a somewhat unusual binding mode (Silva-Martin et al. 2014). The glucose at the primary binding site is positioned differently compared with typical C-type lectins. Although the top face of the lectin accepts at least four glucose residues, only 4-OH of Glcα1-6Glc is located within the coordination bond in the primary binding site (Fig. 5e). In the case of sulfated glucose, ring oxygen (O5) seems to make a coordination bond with the calcium ion. It is noteworthy that "side" face of SIGN-R1 can accept the repetitive molecular patterns of the polysaccharide chain (Fig. 5f). This binding mode seems favorable for an interaction of a small globular domain with long polysaccharide chains.

4.2 *Oligosaccharide Recognition of QPD Motif-Containing C-Type Lectins*

QPD motif-containing C-type lectins have been less studied than those with EPN. Only three structures, Rattlesnake venom lectin (RSL) in complex with lactose (Walker et al. 2004), asialoglycoprotein receptor (ASGPR) lactose complex

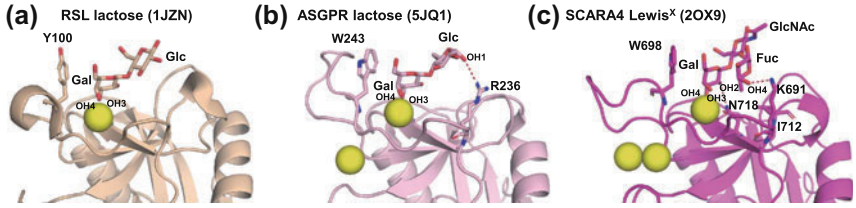

Fig. 6 Carbohydrate recognition of QPD motif-containing C-type lectins: **a** RSL-lactose complex (*PDB code* 1JZN). **b** ASGPR-lactose complex (*PDB code* 5JQ1) and **c** SCARA4-Lewis^X complex (*PDB code* 2OX9)

(Sanhueza et al. 2017) and scavenger receptor C-type lectin (SRACLA4) in complex with Lewis^X trisaccharide (Fucα1-3[Galβ1-4]GlcNAc) (Feinberg et al. 2007), are deposited in the PDB. In these structures, the 3-OH and 4-OH groups of galactose form coordination bonds with the calcium ion and the apolar face of the galactose is stabilized by a stacking interaction with hydrophobic amino acid residues (Fig. 6a–c). RSL recognizes only the galactose residue of lactose. In contrast, the βOH1 group of the glucose residue makes a hydrogen bond with arginine (R236) in an ASGPR-lactose complex (Fig. 6a and b). In the SRACLA4-Lewis^X complex, the fucose residue makes additional hydrophobic contact with isoleucine (I712) and hydrogen bonds with lysine (K691) (Fig. 6c). A structural comparison among the three complexes clarifies that the aromatic residues (Y100 in RSL, W243 in ASGPR, and W698 in SRACLA4) are located in equivalent positions and positively charged residues (R236 in ASGPR and K691 in SRACLA4) occupy similar positions in two of the complexes, evidently engaged in ligand recognition.

It is tempting to compare the recognition modes of Lewis^X by the EPN and QPD motifs. In EPN motif-containing C-type lectins, fucose coordinates a calcium ion in the primary binding site and galactose resides in the secondary binding site (Fig. 4a, b). In the case of the QPD motif, by contrast, galactose resides in the primary binding site and fucose is located in the secondary binding site. Interestingly, the conformation of the Lewis^X trisaccharide is similar in both complexes. This observation suggests that both lectins recognize a stable conformation of the glycan. Glycan array analysis revealed that SRCL preferentially binds to Lewis^a and Lewis^X, while DC-SIGN widely accepts various types of glycan such as Lewis^a, Lewis^b, Lewis^X, and Lewis^Y (Feinberg et al. 2007; Guo et al. 2004). This may originate from differences in the binding modes of galactose/fucose.

4.3 Oligosaccharide Recognition of C-Type Lectin-like Domains

C-type lectin-like domains do not bind calcium due to the lack of conserved calcium binding motifs. However, some C-type lectin-like domains directly bind to carbohydrates in calcium independent ways. The sugar-binding modes of C-type lectin-like domains are thus expected to be completely different from those of typical C-type lectin domains and can be expected to be diverse.

Dectin-1 is a C-type lectin-like receptor having a single extracellular C-type lectin-like domain, a short stalk region, a single transmembrane helix and a cytoplasmic ITAM. Dectin-1 is a β-glucan receptor and shows preference for the β1-3 linked glucose polymer (Palma et al. 2006). Since the C-type lectin-like domain of Dectin-1 lacks a QPD or EPN motif, it loses its calcium binding ability at the primary site. A crystal structure of Dectin-1 complexed with laminaritriose shows that two C-type lectin domains sandwich one laminaritriose via their lateral faces (Brown et al. 2007) (Fig. 7a). Laminaritiose assumes a planar conformation and is stabilized by several hydrogen bonds. It should be noted that mutational experiments suggested that the top face of the Dectin-1 C-type lectin-like domain contributes to β-glucan binding, which is located far from the binding site observed in the crystal structure (Dulal et al. 2018). Direct evidence, as for example solution NMR analysis, is strongly needed to solve this discrepancy.

Another example is C-type lectin like receptor 2 (CLEC-2), also known as CLEC1B. CLEC-2 is a type II transmembrane receptor with a short N-terminal cytoplasmic tail containing a single tyrosine-based activation motif (hemITAM), a transmembrane segment, an extracellular stalk region and a C-type lectin-like domain which has no calcium binding activity. Podoplanin is a transmembrane *O*-glycoprotein that binds to CLEC-2 in a glycosylation-dependent manner.

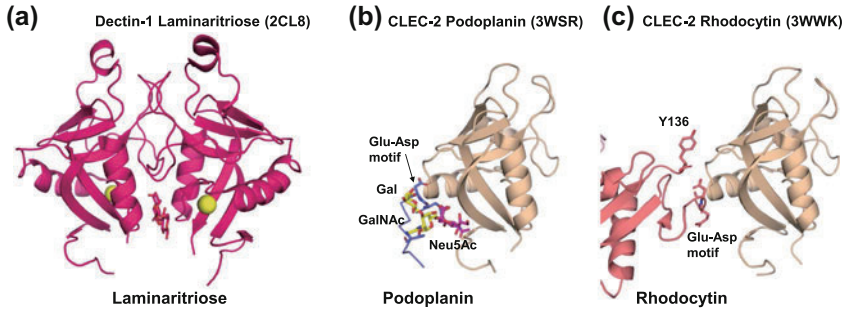

Fig. 7 Ca^{2+}-independent carbohydrate recognition of C-type lectin-like domain: **a** Dectin-1-laminaritoriose complex (*PDB code* 2CL8). **b** CLEC-2-*O*-glycosylated (Neu5Acα2-6[Galβ1-3] GalNAc-*O*-Thr52) podoplanin complex (*PDB code* 3WSR) and **c** CLEC-2-rhodocytin complex (*PDB code* 3WWK). Carbohydrate, Glu-Asp motif, and C-terminal Y136 are shown in stick models

Crystallographic analysis revealed that two consecutive acidic residues (Glu-Asp motif) as well as an α2-6 linked sialic acid residue attached on the *O*-glycan interact with the lateral face of CLEC-2 (Nagae et al. 2014). Four arginine residues of CLEC-2 interact with the sialic acid and the two acidic residues of podoplanin (Fig. 7b). Interestingly, snake venom rhodocytin also binds to CLEC-2, however the interaction mode is somewhat different. Although the Glu-Asp motif is conserved in rhodocytin, rhodocytin is not *O*-glycosylated. Instead, the carboxylate of the rhodocytin C-terminus contributes to an electrostatic interaction with the arginine residue of CLEC-2 (Fig. 7c).

4.4 Genetic Variants of C-Type Lectins

Specific sugar recognition is affected by changes in amino acid residues. Single-nucleotide polymorphisms (SNPs) and genetic variations are potentially involved in the susceptibility for developing disease and disease outcomes. Various SNPs and disease causative mutations of C-type lectins have been reported (Goyal et al. 2016). The effects of SNPs and species-dependent sugar binding are not well studied and are limited to a few examples. In human langerin, the W264R mutation was found in an individual who lacks Birbeck granules in the Langerhans cells (Verdijk et al. 2005). This mutation results in the loss of mannose-binding ability (Ward et al. 2006). W264 is located inside the protein, and thus this mutation destabilizes the local folding of langerin. At present several SNPs, A278 V, N288D, A300P, and K313I, in the human langerin C-type lectin domain are deposited in the SNP database (Ward et al. 2006; Feinberg et al. 2013). Of note, K313 is one of the two lysine residues which are critical for recognition of sulfated galactose (Fig. 2c). The affinity for sulfated galactose is dramatically reduced, instead, the affinity against terminal GlcNAc is increased (Feinberg et al. 2013).

Surfactant protein A (SP-A) consists of two isoforms, SP-A1 and SP-A2, encoded by separate genes. SP-A defends against invading pathogens in the lung. The missense mutations of SP-A2 C-type lectin domain result in idiopathic pulmonary fibrosis (IPF), a serious lung disease affecting older adults (Wang et al. 2009). These mutations, like F198S and G231 V, dramatically reduce the expression level of the protein probably due to the disruption of normal protein folding. In addition, the K223Q mutation in the C-type lectin domain is one of the SNPs which are significantly associated with tuberculosis (Malik et al. 2006). This replacement could affect the glycan recognition of SP-A2, though as yet the mechanism has not been revealed.

For SP-D, three SNPs, M11T, A160T, and S270T, have been reported (Leth-Larsen et al. 2005). These residues are located in the signal peptides of collagen-like and C-type lectin domains. The S270T mutant is located on the opposite side of the sugar binding site and the effect of the mutation on sugar binding is obscure. Another example is Dectin-1. The Y238X mutation of Dectin-1 is found in Africans and western Eurasians (Ferwerda et al. 2009). The Y238X

mutant is poorly expressed and lacks β-glucan activity. Y236 in mouse Dectin-1, corresponding to human Y238, is buried inside the C-type lectin domain. Thus, the mutation likely inhibits proper folding. Although the binding of β-glucan is significantly lower in Y238X patients, fungal phagocytosis and fungal killing are normal, suggesting the presence of alternative receptors for phagocytosis.

The species-dependent sugar recognition mechanism has also been investigated. Human and murine langerin share 66% amino acid similarity, but show different ligand preferences for bacterial polysaccharides (Hanske et al. 2017). A crystal structure of murine langerin shows that the different residues map to the secondary binding site, which possibly accounts for the different ligand specificities.

5 Functional Oligomerization of C-Type Lectin Domains

C-type lectin and lectin-like domains often form stable homo- or heterodimers that are critical for their physiological functions. For example, C-type lectin-like domains of NK receptors (Group 5) such as Ly49s and NKGs accept various ligands via homo or heterodimers (Li and Mariuzza 2014). The C-type lectin domain itself forms a monomer in solution. However, many sugar-binding C-type lectins such as collectin and DC receptor families form multimers via their stalk or coiled-coil regions. Biochemical studies of murine Dectin-1 suggests that monomeric C-type lectin-like domain cooperatively forms an oligomer upon β-glucan binding (Dulal et al. 2018).

Domain swapping is a mechanism for two or more protein molecules to form a dimer or higher oligomer by exchanging an identical structural element (Liu and Eisenberg 2002). Oligomerization by domain swapping is often found in snake venom C-type lectin-like proteins (Eble 2019). In these proteins, the long loop between β2 and β3 strands extends away from the core of the protein to form a domain-swapped dimer. Various snake venom C-type lectin-like proteins form ordered heterooligomers via domain-swapping. Interestingly, domain-swapped heterodimers, bitiscetin, botrocetin, and rhodocetin, functionally grab their target platelet receptors such as von Willebrand factor (vWF) A1 domain, GPIbα, GPVI, and α2β1 integrin via an extended surface formed by an extended loop region (Maita et al. 2003; Fukuda et al. 2005; Eble et al. 2017).

In mammalian C-type lectin receptors, domain-swapped dimers can form under crystallization conditions. Crystal structures of several C-type lectin receptors are reported as domain-swapped dimers in a ligand-free state, such as CRD-4 of macrophage mannose receptor (Feinberg et al. 2000), BDCA-2 (Nagae et al. 2014), and NKRp1a (Kolenko et al. 2011). These domain-swapped dimers are similar to those of snake venom C-type lectin-like proteins. An interesting point is that the functional states of BDCA-2 and NKRp1a are monomeric and the domain-swapped dimers are thought to be an inactive state.

Of note, the BDCA-2 C-type lectin domain forms a domain-swapped dimer under three different crystallization conditions (Nagae et al. 2014). Although 1 mM

calcium chloride was present during protein purification, no calcium ion was found in the calcium binding site. The side chain of E178, which is critical for calcium coordination, points away from the putative calcium binding site. This indicates that the domain-swapped BDCA-2 cannot accept a carbohydrate ligand. Subsequently, a crystal structure of BDCA-2 in complex with trisaccharide was reported. BDCA-2 is a monomer in the crystal and binds the sugar at the calcium binding site (Jegouzo et al. 2015).

In the case of NKRp1a, the extended loop points away from the central core and mediates formation of a domain-swapped dimer in the crystal (Kolenko et al. 2011). Although the refolding buffer contains a high concentration of calcium chloride, there is no calcium ion in the structure. In contrast, a solution structure determined by NMR is monomeric with the loop tightly anchored to the central region (Rozbesky et al. 2016). Calcium titration analysis suggests monomeric NKRp1a binds a calcium ion weakly with a dissociation constant in the mM range.

Although the physiological relevance of domain-swapped dimer formation is still obscure, the domain-swapped dimer is likely a metastable conformation. Formation of the domain-swapped dimer may be used as a temporary inactive state under certain conditions.

6 Conclusion and Future Perspective

C-type lectins accept various glycans via highly conserved binding sites. Although the primary binding site is the most conserved, there are differences in the secondary binding site that enable various types of glycans to bind. Furthermore, accumulating of 3D structural information demonstrates that C-type lectin-like domains also recognize sugar ligands in a calcium-independent manner. The relationship between SNP and sugar-binding activity has a direct bearing on the susceptibility for pathogens, and however, the mechanism is largely unknown. Structural analysis of C-type lectins from individuals is a promising avenue to our understanding of individual variations in the immune system.

References

Alenton RR, Koiwai K, Miyaguchi K, Kondo H, Hirono I (2017) Pathogen recognition of a novel C-type lectin from *Marsupenaeus japonicus* reveals the divergent sugar-binding specificity of QAP motif. Sci Rep 7:45818

Brown J, O'Callaghan CA, Marshall AS, Gilbert RJ, Siebold C, Gordon S, Brown GD, Jones EY (2007) Structure of the fungal β-glucan-binding immune receptor dectin-1: implications for function. Protein Sci 16:1042–1052

Chatwell L, Holla A, Kaufer BB, Skerra A (2008) The carbohydrate recognition domain of Langerin reveals high structural similarity with the one of DC-SIGN but an additional, calcium-independent sugar-binding site. Mol Immunol 45:1981–1994

Crouch E, Hartshorn K, Horlacher T, McDonald B, Smith K, Cafarella T, Seaton B, Seeberger PH, Head J (2009) Recognition of mannosylated ligands and influenza A virus by human surfactant protein D: contributions of an extended site and residue 343. Biochemistry 48:3335–3345

Cummings RD, McEver RP (2015) C-type lectins. In: Varki A, Cummings RD, Esko JD, Stanley P, Hart GW, Aebi M, Darvill AG, Kinoshita T, Packer NH, Prestegard JH, Schnaar RL, Seeberger PH (eds) Essentials of glycobiology. Cold Spring Harbor, NY, pp 435–452

Drickamer K (1992) Engineering galactose-binding activity into a C-type mannose-binding protein. Nature 360:183–186

Drickamer K, Taylor ME (2015) Recent insights into structures and functions of C-type lectins in the immune system. Curr Opin Struct Biol 34:26–34

Dulal HP, Adachi Y, Ohno N, Yamaguchi Y (2018) β-glucan-induced cooperative oligomerization of Dectin-1 C-type lectin-like domain. Glycobiology 28:612–623

Eble JA (2019) Structurally robust and functionally highly versatile-C-type lectin (-related) proteins in snake venoms. Toxins (Basel) 11:136

Eble JA, McDougall M, Orriss GL, Niland S, Johanningmeier B, Pohlentz G, Meier M, Karrasch S, Estevao-Costa MI, Martins Lima A, Stetefeld J (2017) Dramatic and concerted conformational changes enable rhodocetin to block α2β1 integrin selectively. PLoS Biol 15: e2001492

Feinberg H, Torgersen D, Drickamer K, Weis WI (2000a) Mechanism of pH-dependent *N*-acetylgalactosamine binding by a functional mimic of the hepatocyte asialoglycoprotein receptor. J Biol Chem 275:35176–35184

Feinberg H, Park-Snyder S, Kolatkar AR, Heise CT, Taylor ME, Weis WI (2000b) Structure of a C-type carbohydrate recognition domain from the macrophage mannose receptor. J Biol Chem 275:21539–21548

Feinberg H, Mitchell DA, Drickamer K, Weis WI (2001) Structural basis for selective recognition of oligosaccharides by DC-SIGN and DC-SIGNR. Science 294:2163–2166

Feinberg H, Taylor ME, Weis WI (2007a) Scavenger receptor C-type lectin binds to the leukocyte cell surface glycan Lewis(x) by a novel mechanism. J Biol Chem 282:17250–17258

Feinberg H, Castelli R, Drickamer K, Seeberger PH, Weis WI (2007b) Multiple modes of binding enhance the affinity of DC-SIGN for high mannose *N*-linked glycans found on viral glycoproteins. J Biol Chem 282:4202–4209

Feinberg H, Taylor ME, Razi N, McBride R, Knirel YA, Graham SA, Drickamer K, Weis WI (2011) Structural basis for langerin recognition of diverse pathogen and mammalian glycans through a single binding site. J Mol Biol 405:1027–1039

Feinberg H, Jegouzo SA, Rowntree TJ, Guan Y, Brash MA, Taylor ME, Weis WI, Drickamer K (2013a) Mechanism for recognition of an unusual mycobacterial glycolipid by the macrophage receptor mincle. J Biol Chem 288:28457–28465

Feinberg H, Rowntree TJ, Tan SL, Drickamer K, Weis WI, Taylor ME (2013b) Common polymorphisms in human langerin change specificity for glycan ligands. J Biol Chem 288:36762–36771

Feinberg H, Rambaruth ND, Jegouzo SA, Jacobsen KM, Djurhuus R, Poulsen TB, Weis WI, Taylor ME, Drickamer K (2016) Binding sites for acylated trehalose analogs of glycolipid ligands on an extended carbohydrate recognition domain of the macrophage receptor mincle. J Biol Chem 291:21222–21233

Feinberg H, Jegouzo SAF, Rex MJ, Drickamer K, Weis WI, Taylor ME (2017) Mechanism of pathogen recognition by human dectin-2. J Biol Chem 292:13402–13414

Ferwerda B, Ferwerda G, Plantinga TS, Willment JA, van Spriel AB, Venselaar H, Elbers CC, Johnson MD, Cambi A, Huysamen C, Jacobs L, Jansen T, Verheijen K, Masthoff L, Morre SA, Vriend G, Williams DL, Perfect JR, Joosten LA, Wijmenga C, van der Meer JW, Adema GJ, Kullberg BJ, Brown GD, Netea MG (2009) Human dectin-1 deficiency and mucocutaneous fungal infections. N Engl J Med 361:1760–1767

Fukuda K, Doggett T, Laurenzi IJ, Liddington RC, Diacovo TG (2005) The snake venom protein botrocetin acts as a biological brace to promote dysfunctional platelet aggregation. Nat Struct Mol Biol 12:152–159

Gourdine JP, Cioci G, Miguet L, Unverzagt C, Silva DV, Varrot A, Gautier C, Smith-Ravin EJ, Imberty A (2008) High affinity interaction between a bivalve C-type lectin and a biantennary complex-type N-glycan revealed by crystallography and microcalorimetry. J Biol Chem 283:30112–30120

Goyal S, Klassert TE, Slevogt H (2016) C-type lectin receptors in tuberculosis: what we know. Med Microbiol Immunol 205:513–535

Guo Y, Feinberg H, Conroy E, Mitchell DA, Alvarez R, Blixt O, Taylor ME, Weis WI, Drickamer K (2004) Structural basis for distinct ligand-binding and targeting properties of the receptors DC-SIGN and DC-SIGNR. Nat Struct Mol Biol 11:591–598

Hanske J, Schulze J, Aretz J, McBride R, Loll B, Schmidt H, Knirel Y, Rabsch W, Wahl MC, Paulson JC, Rademacher C (2017) Bacterial polysaccharide specificity of the pattern recognition receptor langerin is highly species-dependent. J Biol Chem 292:862–871

Hatakeyama T, Kamiya T, Kusunoki M, Nakamura-Tsuruta S, Hirabayashi J, Goda S, Unno H (2011) Galactose recognition by a tetrameric C-type lectin, CEL-IV, containing the EPN carbohydrate recognition motif. J Biol Chem 286:10305–10315

Ishikawa E, Ishikawa T, Morita YS, Toyonaga K, Yamada H, Takeuchi O, Kinoshita T, Akira S, Yoshikai Y, Yamasaki S (2009) Direct recognition of the mycobacterial glycolipid, trehalose dimycolate, by C-type lectin mincle. J Exp Med 206:2879–2888

Jegouzo SA, Feinberg H, Dungarwalla T, Drickamer K, Weis WI, Taylor ME (2015) A novel mechanism for binding of galactose-terminated glycans by the C-type carbohydrate recognition domain in blood dendritic cell antigen 2. J Biol Chem 290:16759–16771

Kansas GS (1996) Selectins and their ligands: current concepts and controversies. Blood 88:3259–3287

Kolenko P, Rozbesky D, Vanek O, Kopecky V Jr, Hofbauerova K, Novak P, Pompach P, Hasek J, Skalova T, Bezouska K, Dohnalek J (2011) Molecular architecture of mouse activating NKR-P1 receptors. J Struct Biol 175:434–441

Leth-Larsen R, Garred P, Jensenius H, Meschi J, Hartshorn K, Madsen J, Tornoe I, Madsen HO, Sorensen G, Crouch E, Holmskov U (2005) A common polymorphism in the SFTPD gene influences assembly, function, and concentration of surfactant protein D. J Immunol 174:1532–1538

Li Y, Mariuzza RA (2014) Structural basis for recognition of cellular and viral ligands by NK cell receptors. Front Immunol 5:123

Liu Y, Eisenberg D (2002) 3D domain swapping: as domains continue to swap. Protein Sci 11:1285–1299

Maita N, Nishio K, Nishimoto E, Matsui T, Shikamoto Y, Morita T, Sadler JE, Mizuno H (2003) Crystal structure of von Willebrand factor A1 domain complexed with snake venom, bitiscetin: insight into glycoprotein Ibalpha binding mechanism induced by snake venom proteins. J Biol Chem 278:37777–37781

Malik S, Greenwood CM, Eguale T, Kifle A, Beyene J, Habte A, Tadesse A, Gebrexabher H, Britton S, Schurr E (2006) Variants of the SFTPA1 and SFTPA2 genes and susceptibility to tuberculosis in Ethiopia. Hum Genet 118:752–759

Matsunaga I, Moody DB (2009) Mincle is a long sought receptor for mycobacterial cord factor. J Exp Med 206:2865–2868

Mehta-D'souza P, Klopocki AG, Oganesyan V, Terzyan S, Mather T, Li Z, Panicker SR, Zhu C, McEver RP (2017) Glycan bound to the selectin low affinity state engages Glu-88 to stabilize the high affinity state under force. J Biol Chem 292:2510–2518

Nagae M, Yamanaka K, Hanashima S, Ikeda A, Morita-Matsumoto K, Satoh T, Matsumoto N, Yamamoto K, Yamaguchi Y (2013) Recognition of bisecting N-acetylglucosamine: structural basis for asymmetric interaction with the mouse lectin dendritic cell inhibitory receptor 2. J Biol Chem 288:33598–33610

Nagae M, Morita-Matsumoto K, Kato M, Kaneko MK, Kato Y, Yamaguchi Y (2014a) A platform of C-type lectin-like receptor CLEC-2 for binding *O*-glycosylated podoplanin and nonglycosylated rhodocytin. Structure 22:1711–1721

Nagae M, Ikeda A, Kitago Y, Matsumoto N, Yamamoto K, Yamaguchi Y (2014b) Crystal structures of carbohydrate recognition domain of blood dendritic cell antigen-2 (BDCA2) reveal a common domain-swapped dimer. Proteins 82:1512–1518

Nagae M, Ikeda A, Hanashima S, Kojima T, Matsumoto N, Yamamoto K, Yamaguchi Y (2016) Crystal structure of human dendritic cell inhibitory receptor C-type lectin domain reveals the binding mode with *N*-glycan. FEBS Lett 590:1280–1288

Ng KK, Weis WI (1997) Structure of a selectin-like mutant of mannose-binding protein complexed with sialylated and sulfated Lewis(x) oligosaccharides. Biochemistry 36:979–988

Ng KK, Drickamer K, Weis WI (1996) Structural analysis of monosaccharide recognition by rat liver mannose-binding protein. J Biol Chem 271:663–674

Ng KK, Kolatkar AR, Park-Snyder S, Feinberg H, Clark DA, Drickamer K, Weis WI (2002) Orientation of bound ligands in mannose-binding proteins. Implications for multivalent ligand recognition. J Biol Chem 277:16088–16095

Palma AS, Feizi T, Zhang Y, Stoll MS, Lawson AM, Diaz-Rodriguez E, Campanero-Rhodes MA, Costa J, Gordon S, Brown GD, Chai W (2006) Ligands for the β-glucan receptor, Dectin-1, assigned using "designer" microarrays of oligosaccharide probes (neoglycolipids) generated from glucan polysaccharides. J Biol Chem 281:5771–5779

Poget SF, Legge GB, Proctor MR, Butler PJ, Bycroft M, Williams RL (1999) The structure of a tunicate C-type lectin from *Polyandrocarpa misakiensis* complexed with D-galactose. J Mol Biol 290:867–879

Preston RC, Jakob RP, Binder FP, Sager CP, Ernst B, Maier T (2016) E-selectin ligand complexes adopt an extended high-affinity conformation. J Mol Cell Biol 8:62–72

Riboldi E, Daniele R, Parola C, Inforzato A, Arnold PL, Bosisio D, Fremont DH, Bastone A, Colonna M, Sozzani S (2011) Human C-type lectin domain family 4, member C (CLEC4C/BDCA-2/CD303) is a receptor for asialo-galactosyl-oligosaccharides. J Biol Chem 286:35329–35333

Rozbesky D, Adamek D, Pospisilova E, Novak P, Chmelik J (2016) Solution structure of the lymphocyte receptor Nkrp1a reveals a distinct conformation of the long loop region as compared to in the crystal structure. Proteins 84:1304–1311

Sancho D, Reis e Sousa C (2013) Sensing of cell death by myeloid C-type lectin receptors. Curr Opin Immunol 25:46–52

Sanhueza CA, Baksh MM, Thuma B, Roy MD, Dutta S, Preville C, Chrunyk BA, Beaumont K, Dullea R, Ammirati M, Liu S, Gebhard D, Finley JE, Salatto CT, King-Ahmad A, Stock I, Atkinson K, Reidich B, Lin W, Kumar R, Tu M, Menhaji-Klotz E, Price DA, Liras S, Finn MG, Mascitti V (2017) Efficient liver targeting by polyvalent display of a compact ligand for the asialoglycoprotein receptor. J Am Chem Soc 139:3528–3536

Shrive AK, Tharia HA, Strong P, Kishore U, Burns I, Rizkallah PJ, Reid KB, Greenhough TJ (2003) High-resolution structural insights into ligand binding and immune cell recognition by human lung surfactant protein D. J Mol Biol 331:509–523

Silva-Martin N, Bartual SG, Ramirez-Aportela E, Chacon P, Park CG, Hermoso JA (2014) Structural basis for selective recognition of endogenous and microbial polysaccharides by macrophage receptor SIGN-R1. Structure 22:1595–1606

Somers WS, Tang J, Shaw GD, Camphausen RT (2000) Insights into the molecular basis of leukocyte tethering and rolling revealed by structures of P- and E-selectin bound to SLe^X and PSGL-1. Cell 103:467–479

Sutkeviciute I, Thepaut M, Sattin S, Berzi A, McGeagh J, Grudinin S, Weiser J, Le Roy A, Reina JJ, Rojo J, Clerici M, Bernardi A, Ebel C, Fieschi F (2014) Unique DC-SIGN clustering activity of a small glycomimetic: a lesson for ligand design. ACS Chem Biol 9:1377–1385

Swaminathan GJ, Myszka DG, Katsamba PS, Ohnuki LE, Gleich GJ, Acharya KR (2005) Eosinophil-granule major basic protein, a C-type lectin, binds heparin. Biochemistry 44:14152–14158

Toyonaga K, Torigoe S, Motomura Y, Kamichi T, Hayashi JM, Morita YS, Noguchi N, Chuma Y, Kiyohara H, Matsuo K, Tanaka H, Nakagawa Y, Sakuma T, Ohmuraya M, Yamamoto T, Umemura M, Matsuzaki G, Yoshikai Y, Yano I, Miyamoto T, Yamasaki S (2016) C-type lectin receptor DCAR recognizes mycobacterial phosphatidyl-inositol mannosides to promote a Th1 response during infection. Immunity 45:1245–1257

Unno H, Itakura S, Higuchi S, Goda S, Yamaguchi K, Hatakeyama T (2019) Novel Ca(2+)-independent carbohydrate recognition of the C-type lectins, SPL-1 and SPL-2, from the bivalve Saxidomus purpuratus. Protein Sci 28:766–778

van Eijk M, Rynkiewicz MJ, Khatri K, Leymarie N, Zaia J, White MR, Hartshorn KL, Cafarella TR, van Die I, Hessing M, Seaton BA, Haagsman HP (2018) Lectin-mediated binding and sialoglycans of porcine surfactant protein D synergistically neutralize influenza A virus. J Biol Chem 293:10646–10662

Varki A (2017) Biological roles of glycans. Glycobiology 27:3–49

Varki A, Cummings RD, Aebi M, Packer NH, Seeberger PH, Esko JD, Stanley P, Hart G, Darvill A, Kinoshita T, Prestegard JJ, Schnaar RL, Freeze HH, Marth JD, Bertozzi CR, Etzler ME, Frank M, Vliegenthart JF, Lütteke T, Perez S, Bolton E, Rudd P, Paulson J, Kanehisa M, Toukach P, Aoki-Kinoshita KF, Dell A, Narimatsu H, York W, Taniguchi N, Kornfeld S (2015) Symbol nomenclature for graphical representations of glycans. Glycobiology 25:1323–1324

Verdijk P, Dijkman R, Plasmeijer EI, Mulder AA, Zoutman WH, Mieke Mommaas A, Tensen CP (2005) A lack of birbeck granules in langerhans cells is associated with a naturally occurring point mutation in the human langerin gene. J Invest Dermatol 124:714–717

Walker JR, Nagar B, Young NM, Hirama T, Rini JM (2004) X-ray crystal structure of a galactose-specific C-type lectin possessing a novel decameric quaternary structure. Biochemistry 43:3783–3792

Wang Y, Kuan PJ, Xing C, Cronkhite JT, Torres F, Rosenblatt RL, DiMaio JM, Kinch LN, Grishin NV, Garcia CK (2009) Genetic defects in surfactant protein A2 are associated with pulmonary fibrosis and lung cancer. Am J Hum Genet 84:52–59

Ward EM, Stambach NS, Drickamer K, Taylor ME (2006) Polymorphisms in human langerin affect stability and sugar binding activity. J Biol Chem 281:15450–15456

Wedepohl S, Dernedde J, Vahedi-Faridi A, Tauber R, Saenger W, Bulut H (2017) Reducing Macro- and microheterogeneity of N-glycans enables the crystal structure of the lectin and EGF-like domains of human L-selectin to be solved at 1.9 Å resolution. ChemBioChem 18:1338–1345

Weis WI, Drickamer K, Hendrickson WA (1992) Structure of a C-type mannose-binding protein complexed with an oligosaccharide. Nature 360:127–134

Xia L, Ramachandran V, McDaniel JM, Nguyen KN, Cummings RD, McEver RP (2003) N-terminal residues in murine P-selectin glycoprotein ligand-1 required for binding to murine P-selectin. Blood 101:552–559

Zelensky AN, Gready JE (2005) The C-type lectin-like domain superfamily. FEBS J 272:6179–6217